GDAŃSK UNIVERSITY OF TECHNOLOGY

The author of the doctoral dissertation: DOMINIK DOBRZYNIEWSKI
Scientific discipline: CHEMICAL SCIENCES

DOCTORAL DISSERTATION

Title of doctoral dissertation: *Process control of the removal of odorous compounds from gas streams using instrumental or sensory techniques and evaluation of the effectiveness of different deodorization methods using gas sensor arrays (electronic noses)*

Title of doctoral dissertation (in Polish): *Kontrola procesowa usuwania związków uciążliwych zapachowo ze strumieni gazowych przy użyciu technik instrumentalnych lub sensorycznych oraz ocena skuteczności różnych metod dezodoryzacji z wykorzystaniem matryc czujników gazowych (elektronicznych nosów)*

Supervisor *signature*	Second supervisor - *signature*
Jacek Gębicki, Ph.D, D.Sc, University professor	
Auxiliary supervisor - *signature*	Cosupervisor - *signature*

Gdańsk, 2026

GDAŃSK UNIVERSITY OF TECHNOLOGY

STATEMENT

The author of the doctoral dissertation: DOMINIK DOBRZYNIEWSKI

I, the undersigned, declare that I am aware that in accordance with the provisions of Art. 27 (1) and (2) of the Act of 4th February 1994 on Copyright and Related Rights (Journal of Laws of 2021, item 1062), the university may use my doctoral dissertation entitled: *Process control of the removal of odorous compounds from gas streams using instrumental or sensory techniques and evaluation of the effectiveness of different deodorization methods using gas sensor arrays (electronic noses)* for scientific or didactic purposes.[1]

Gdańsk, ...

signature of the PhD student

Aware of criminal liability for violations of the Act of 4th February 1994 on Copyright and Related Rights and disciplinary actions set out in the Law on Higher Education and Science(Journal of Laws 2021, item 478), as well as civil liability, I declare, that the submitted doctoral dissertation is my own work.

I declare, that the submitted doctoral dissertation is my own work performed under and in cooperation with the supervision of *Jacek Gębicki, Ph.D, D.Sc, University professor*, ~~the second supervision of <name of the second supervisor>, the auxiliary supervision of <name of the auxiliary supervisor>, the cosupervision of <name of the cosupervisor>~~*.

This submitted doctoral dissertation has never before been the basis of an official procedure associated with the awarding of a PhD degree.

All the information contained in the above thesis which is derived from written and electronic sources is documented in a list of relevant literature in accordance with Art. 34 of the Copyright and Related Rights Act.

I confirm that this doctoral dissertation is identical to the attached electronic version.

Gdańsk, ...

signature of the PhD student

I, the undersigned, agree/~~do not agree~~* to include an electronic version of the above doctoral dissertation in the open, institutional, digital repository of Gdańsk University of Technology.

Gdańsk, ...

signature of the PhD student

[1] Art 27. 1. Educational institutions and entities referred to in art. 7 sec. 1 points 1, 2 and 4–8 of the Act of 20 July 2018 – Law on Higher Education and Science, may use the disseminated works in the original and in translation for the purposes of illustrating the content provided for didactic purposes or in order to conduct research activities, and to reproduce for this purpose disseminated minor works or fragments of larger works.

2. If the works are made available to the public in such a way that everyone can have access to them at the place and time selected by them, as referred to in para. 1, is allowed only for a limited group of people learning, teaching or conducting research, identified by the entities listed in paragraph 1.

GDAŃSK UNIVERSITY OF TECHNOLOGY

DESCRIPTION OF DOCTORAL DISSERTATION

The Author of the doctoral dissertation: DOMINIK DOBRZYNIEWSKI

Title of doctoral dissertation: *Process control of the removal of odorous compounds from gas streams using instrumental or sensory techniques and evaluation of the effectiveness of different deodorization methods using gas sensor arrays (electronic noses)*

Title of doctoral dissertation in Polish: *Kontrola procesowa usuwania związków uciążliwych zapachowo ze strumieni gazowych przy użyciu technik instrumentalnych lub sensorycznych oraz ocena skuteczności różnych metod dezodoryzacji z wykorzystaniem matryc czujników gazowych (elektronicznych nosów)*

Language of doctoral dissertation: ENGLISH

Supervisor: Jacek Gębicki, Ph.D, D.Sc, University professor

~~**Second supervisor**~~*:

~~**Auxiliary supervisior**~~*:

~~**Cosupervisior**~~*:

Date of doctoral defense:

Keywords of doctoral dissertation in Polish: substancje odorotwórcze, odory, związki uciążliwe zapachowo, dezodoryzacja, kontrola procesowa, olfaktometria terenowa, olfaktometria dynamiczna, składowiska odpadów, matryce czujników gzowych, elektroniczne nosy, sieć monitoringu odorów

Keywords of doctoral dissertation in English: odor-causing substances, odors, malodorous compounds, deodorization, process control, field olfactometry, dynamic olfactometry, landfills, gas sensor arrays, electronic noses, odor monitoring network

Summary of doctoral dissertation in Polish: Przedmiotem rozprawy doktorskiej jest opracowanie i walidacja instrumentalnych metod ciągłego monitorowania uciążliwości zapachowej oraz skuteczności procesów dezodoryzacji z wykorzystaniem matryc czujników gazowych. Badania przeprowadzono dwuetapowo: od skali laboratoryjnej po rzeczywiste warunki przemysłowe. W skali laboratoryjnej wykazano możliwość ilościowej kontroli efektywności oczyszczania strumieni gazowych z LZO w procesach absorpcji i biofiltracji (ze złożem zraszanym) z dokładnością porównywalną do chromatografii gazowej. W warunkach terenowych zintegrowano matrycę czujników gazowych z bezzałogowym statkiem powietrznym, co umożliwiło mapowanie stężeń zapachowych, identyfikację hotspotów na składowisku, szacowanie emisji zapachowej oraz modelowanie dyspersji smugi odorów. Zwieńczeniem prac było opracowanie instrumentalnego indeksu odorowej jakości powietrza łączącego stężenie zapachowe, intensywność zapachu i jego ton hedoniczny, a także wdrożenie pierwszej w Polsce wielopunktowej sieci monitoringu odorów. Sieć monitoringu zintegrowano z chmurową aplikacją gromadzenia danych oraz systemem wspomagania decyzji na terenie miejskiego zakładu gospodarki odpadami stałymi. Wielosezonowa walidacja operacyjna wykazała, że sieć monitoringu z ponad 90% trafnością przypisuje stan powietrza do właściwych klas uciążliwości zapachowej opracowanego indeksu. Praca dowodzi, że skalibrowane matryce czujników gazowych stanowią rzetelną i opłacalną alternatywę dla metod referencyjnych.

GDAŃSK UNIVERSITY OF TECHNOLOGY

Summary of doctoral dissertation in English: The subject of this doctoral dissertation is the development and validation of instrumental methods for the continuous monitoring of odor nuisance and the effectiveness of deodorization processes using gas sensor arrays. The research was conducted in two stages: from the laboratory scale to actual industrial conditions. At the laboratory scale, the ability to quantitatively assess the effectiveness of VOCs removal from gas streams in absorption and biofiltration (biotrickling filter) processes was demonstrated, with agreement comparable to that of gas chromatography. Under field conditions, a gas sensor array was integrated with an unmanned aerial vehicle, enabling the mapping of odor concentrations, the identification of hotspots at the landfill cell, the estimation of odor emissions, and the modeling of odor plume dispersion. The culmination of this thesis was the development of an instrumental odor air quality index combining odor concentration, odor intensity, and its hedonic tone, as well as the implementation of Poland's first multi-point odor monitoring network. The monitoring network was integrated with a cloud-based data collection application and a decision support system at a municipal solid waste treatment plant. Multi-season operational validation showed that the monitoring network assigns air quality to the appropriate odor nuisance classes of the developed index with over 90% accuracy. The study demonstrates that calibrated gas sensor arrays are a reliable and cost-effective alternative to reference methods.

Summary of doctoral dissertation in language, in which it was written**: -

Keywords of doctoral dissertation in language, in which it was written**: -

**delete where appropriate*

***applies to doctoral dissertations written in other languages, than Polish or English*

Acknowledgments

The preparation of this doctoral dissertation was not only the culmination of several years of academic work, but also a journey filled with challenges, doubts, inspiring encounters, and meaningful experiences. I would not have been able to complete it on my own, which is why I would like to wholeheartedly thank everyone who stood by me during this time.

First and foremost, I would like to express my heartfelt thanks to my supervisor, Jacek Gębicki, Ph.D, D.Sc, University professor, for his trust, academic guidance, patience, and all the valuable advice. Thank you for our conversations, which often allowed me to see the problem from a different perspective, for your constructive feedback, and for your support during times when the remaining path seemed particularly challenging. I greatly appreciate the opportunity to learn and grow under your guidance.

I would also like to thank my colleagues from the Department of Process Engineering and Chemical Technology for their daily cooperation, support, kind words, and all the conversations that enabled me not only to grow professionally but also to maintain perspective during the most intense periods of work.

I would like to extend my most heartfelt thanks to my beloved family. I want to thank Mom and Dad for always teaching me perseverance, a curiosity about the world, and the belief that it's worth taking on ambitious challenges. Thank you for your constant support, patience, and presence even when I wasn't sure myself whether I'd be able to reach my goal.

I would like to thank all my friends and close ones who, over the years, have asked after me, supported me, motivated me, and patiently waited for my "doctorate to finally be finished."

Every person who crossed my path along the way left a part of themselves in it. That is why I view the completion of this dissertation not only as a personal achievement, but also as a moment in which I think with immense gratitude of everyone who helped me get to this point.

Thank you.

The author would like to acknowledge the management of Waste Utilization Facility Ltd. in Gdańsk for their cooperation, providing access to their facility, for technical assistance, and for making it possible to perform the measurement at the active landfill cell and for enabling comprehensive measurements to be conducted throughout the plant site.

The author would like to acknowledge the management of Miejski Zakład Oczyszczania Ltd. in Pruszków for their cooperation, providing access to their facility, for technical assistance, and for making it possible to perform the measurement at the compost screening site.

The author would like to acknowledge Dacsystem LLC in Gdańsk for their invaluable support in the development of the odor air quality meters (model sensor BOX-3 XXXX), dedicated software application, and the integration of the IoT cloud infrastructure, which were essential for the real-time processing and visualization of the odor monitoring data.

Table of contents

Summary of doctoral dissertation in Polish 3
Summary of doctoral dissertation in English 4
Acknowledgments 5
Table of contents 6
List of designations and abbreviations 10
1. Introduction 11
1.1 Brief description of the research problem 11
1.2 Justification of the research problem in the context of the state of the art 11
2. Characterization of odorous substances 15
2.1 General information 15
2.2 Definition of odorants 15
2.3 Olfactory threshold 16
2.4 Odor nuisance 17
2.4.1 Definition and essence of the phenomenon 17
2.4.2 Factors shaping perception and the level of nuisance 17
2.4.3 Impact on health and quality of life 18
2.4.4 Objectivity parameters for the assessment of nuisance 18
2.5 Basic odor parameters (features) 19
2.5.1 Odor concentration 19
2.5.2 Odor intensity 20
2.5.3 Hedonic tone 21
2.6 Sources of odor nuisance substances 22
2.6.1 Odor emission from the industrial, food and agricultural sectors 23
2.6.2 Waste management facilities 23
2.7 Counteracting of odor nuisance substances – review of legal regulations 25
2.7.1 Worldwide odor regulations 25
2.7.2 Odor regulations in Poland 26
3. Characterization of deodorization techniques for contaminated gases 28
3.1 General information 28
3.2 Absorption processes 29
3.3 Biological gas treatment 30
3.3.1 Principles of biological gas treatment 30
3.3.2 Biofilters 31
3.3.3 Bioscrubers 33
3.3.4 Biotrickling filters 34
3.4 Odor compensation 35
3.5 Summary of the described deodorization methods 37
4. Methods of odor impact analysis 39
4.1 General information 39
4.2 Sensory techniques 40
4.2.1 Field olfactometry 40

4.2.2 Dynamic olfactometry ... 42
4.2.3 Parametric sensory measurements ... 45
4.2.4 Citizen science ... 46
4.3 Analytical techniques ... 47
4.3.1 Gas chromatography ... 48
4.3.2 Application of chromatographic techniques in odor nuisance control ... 50
4.4 Gas sensor array (electronic nose) ... 51
4.4.1 General principle of electronic nose operation ... 51
4.4.2 Gas sensors used in electronic noses ... 53
4.4.3 Data processing and identification system ... 58
4.5 Overview of the application potential of gas sensor arrays ... 62
4.5.1 Gas sensor arrays as a tool for analytical assessment of odor air quality ... 62
4.5.2 Gas sensor arrays as a tool for sensory assessment of odor air quality ... 63
4.5.3 Gas sensor arrays as a tool for monitoring deodorization processes ... 65
4.5.4 UAV-mounted gas sensor arrays for odor air quality control ... 66
4.6 Summary of the literature review and identification of research gaps ... 68
5. Research objectives and scopes ... 70
5.1 Main objective and research hypotheses ... 70
5.2 Scope and structure of the research ... 70
5.3 Methodological assumptions and integrity of the research concept ... 72
5.4 Elements of a scientific novelty ... 73
6. Assessment of the absorption efficiency of toluene vapors from a polluted air stream using a gas sensor array ... 74
6.1 Purpose of the study ... 74
6.2 Materials and methods ... 74
6.2.1 Absorption system and process parameters ... 74
6.2.2 Reference equipment (GC-FID analysis) ... 75
6.2.3 Gas sensor array development ... 75
6.2.4 Measurement procedure and sampling ... 77
6.2.5 Data analysis and mathematical modeling ... 77
6.3 Results and discussion ... 80
6.3.1 Characteristics of the absorption process and the predictive model ... 80
6.3.2 Monitoring the course and assessing the efficiency of toluene absorption ... 82
6.3.3 The influence of acetone on monitoring and assessing the process efficiency ... 83
6.4 Summary and conclusions ... 85
6.5 Publication basis of the chapter ... 86
7. Application of gas sensor array to evaluate removal efficiency of hydrophobic organic compounds in a biotrickling filter (BTF) ... 87
7.1 Purpose of the study ... 87
7.2 Materials and methods ... 87
7.2.1 Biofiltration unit ... 87
7.2.2 Reference equipment (GC-FID analysis) ... 88
7.2.3 Gas sensor array development ... 89

7.2.4 Measurement procedure and sampling ... 90
7.2.5 Data analysis and mathematical modeling ... 92
7.3 Results and discussion ... 95
7.3.1 Characteristics of the sensor array response ... 95
7.3.2 Development and characterization of predictive models ... 97
7.3.3 Monitoring the course and assessing the efficiency of the biofiltration process ... 100
7.4 Summary and conclusions ... 103
7.5 Publication basis of the chapter ... 105
8. Monitoring the absorption purification of biogas from a multicomponent mixture of pollutants using gas sensor array ... 106
8.1 Purpose of the study ... 106
8.2 Materials and methods ... 106
8.2.1 Absorption unit ... 106
8.2.2 Reference equipment (GC-FID) ... 107
8.2.3 Gas sensor array development ... 108
8.2.4 Measurement procedure and sampling ... 110
8.2.5 Data analysis and mathematical modeling ... 113
8.3 Results and discussion ... 118
8.3.1 Development and characterization of predictive models ... 118
8.3.2 Monitoring and assessing the efficiency of the model biogas absorption process ... 121
8.3.3 Evaluation of the agreement between sensor array results and the GC-FID ... 124
8.4 Summary and conclusions ... 132
8.5 Publication basis of the chapter ... 133
9. Identification and mapping of odor emission sources and modeling of odor plume dispersion using a gas sensor array ... 134
9.1 Purpose of the study ... 134
9.2 Materials and methods ... 134
9.2.1 Test site description ... 134
9.2.2 Gas sensor array development ... 135
9.2.3 UAV platform, sensing module, and measurement campaigns ... 136
9.2.4 Processing and spatial interpolation of UAV data ... 138
9.2.5 Reference equipment (Dynamic olfactometry) ... 139
9.2.6 Data analysis and mathematical modeling ... 141
9.2.7 Odor emission modeling ... 143
9.3 Results and discussion ... 144
9.3.1 Olfactometric characteristics of landfill cell ... 144
9.3.2 Spatial distribution of gaseous components over landfill cell ... 145
9.3.3 Calibration and parameterization of PLS regression models ... 147
9.3.4 Spatial mapping of odor concentrations and odor emissions ... 150
9.3.5 Comparative modeling of odor plume dispersion ... 152
9.4 Summary and conclusions ... 155
9.5 Publication basis of the chapter ... 156
10. Implementation of a gas sensor array for instrumental assessment of odor nuisance in field conditions ... 157

10.1 Purpose of the study ... 157
10.2 Materials and methods ... 157
10.2.1 Test site description ... 157
10.2.2 Reference equipment (Field olfactometry) ... 158
10.2.3 Gas sensor array development ... 159
10.2.4 Measurement procedure ... 160
10.2.5 Data analysis and mathematical modeling ... 162
10.3 Results and discussion ... 164
10.3.1 Development of predictive models of odor concentration ... 164
10.3.2 Evaluation and validation of odor concentration prediction models ... 167
10.3.3 Application of selected models for continuous odor monitoring ... 172
10.4 Summary and conclusions ... 175
10.5 Publication basis of the chapter ... 177
11. Development of Instrumental Odor Monitoring System Network (IOMSN) for continuous assessment of odor air quality at a MSWTP ... 178
11.1 Purpose of the study ... 178
11.2 Materials and methods ... 178
11.2.1 Test site description ... 178
11.2.2 Characteristics and structure of IOMSN ... 179
11.2.3 IOMSN calibration using field olfactometry ... 180
11.2.4 Statistical and exploratory data analysis ... 181
11.2.5 Hybrid predictive mathematical model of odor concentration ... 181
11.2.6 Predictive model validation under operational conditions ... 182
11.3 Results and discussion ... 183
11.3.1 Exploratory data analysis and sensor signal correlation ... 183
11.3.2 Calibration and parameterization of predictive models. ... 186
11.3.3 Long-term operational validation of the IOMSN under field conditions ... 189
11.3.4 Integration of IOMSN with the IoT cloud and the DSS ... 193
11.4 Summary and conclusions ... 195
11.5 Publication basis of the chapter ... 196
12. General conclusions and future research directions ... 197
12.1 Summary of the results and general conclusions ... 197
12.2 Limitations of the applied methods and solutions ... 197
12.3 Directions for future research and development prospects ... 198
References ... 200
List of Figures ... 215
List of Tables ... 219
Scientific achievements ... 220
Copyrights and permissions ... 226

List of designations and abbreviations

MSWTP	-	Municipal Solid Waste Treatment Plant
BAT	-	Best Available Techniques
GC	-	Gas Chromatography
DO	-	Dynamic Olfactometry
FO	-	Field Olfactometry
GC-O	-	Gas Chromatography - Olfactometry
VOC	-	Volatile Organic Compound
VIC	-	Volatile Inorganic Compound
ppm	-	parts per million
ppb	-	parts per billion
ppt	-	parts per trillion
OT	-	Olfactory Threshold
OU	-	Odor unit
EROM	-	European Reference Odour Mass
OAV	-	Odor Activity Value
VSC	-	Volatile Sulfur Compound
VTA	-	Volatile Fatty Acid
C_{OD}	-	Odor concentration
OI	-	Odor intensity
HT	-	Hedonic tone
BF	-	Biofilter
BTF	-	Biotrickling filter
BS	-	Bioscrubber
OER	-	Odor Emission Rate
CS	-	Citizen Science
GC-MS	-	Gas Chromatography Mass Spectrometry
MDGC	-	Multidimensional Gas Chromatography
GC-O	-	Gas Chromatography-Olfactometry
MOS	-	Metal Oxide Semiconductor
CP	-	Conductive Polymer
EC	-	Electrochemical (sensor)
NDIR	-	Non-dispersive Infrared Radiation
PID	-	Photoionization Detector
MLR	-	Multiple Linear Regression
PCA	-	Principal Component Analysis
PCR	-	Principal Component Regression
PLSR	-	Partial Least Squares Regression
ANN	-	Artificial Neural Network
UAV	-	Unmanned Aerial Vehicles
IOMSN	-	Instrumental Odor Monitoring System Network
DSS	-	Decision Support System
IoT	-	Internet of Things

1. Introduction

1.1 Brief description of the research problem

The research topic addressed in this doctoral dissertation concerns the potential usage of gas sensor arrays (so-called electronic noses) to monitor and control the deodorization processes of gaseous streams, and consequently to manage the odor air quality around any installations that operations involve the release of offensive odors (including various municipal, industrial, agricultural, and service-sector sources). Attempts were made to demonstrate the practicality, validity, usefulness, and application potential of such devices in the continuous monitoring of gas stream purification processes (removal of malodorous compounds) and the assessment of odor nuisance from technological processes carried out at solid waste recovery and processing plants. The conducted research served to demonstrate that gas sensor arrays may be viewed as a promising alternative to costly and time-consuming reference techniques used in odor nuisance assessment (for example gas chromatography as an instrumental technique and field or dynamic olfactometry as a sensory technique). For this to be the case, the results obtained using sensor arrays must show good agreement with those obtained by reference methods, indicating a comparable level of measurement quality.

1.2 Justification of the research problem in the context of the state of the art

The rapid development of civilization, driven by the industrial and agricultural sectors, has led to a steady increase in pollutant emissions into the biosphere (soils, waters, air). Among the wide range of gaseous substances emitted, odorous compounds pose a particular challenge. Due to their unpleasant nature, they drastically reduce quality of life and can cause health conditions in humans, such as mood disorders, fatigue or even depression [1–5]. Sometimes, however, the effects of exposure to substances that cause unpleasant odors are far more serious than a decline in overall physical and mental well-being. Long-term exposure to BTEX compounds (benzene, toluene, ethylbenzene, xylenes) causes irreversible changes in brain structure. Hydrogen sulfide (H_2S), when it affects the central nervous system at high concentrations, leads to paralysis of the olfactory nerve [3,6]. Highly reactive gases, such as ammonia or organic amines, exhibit corrosive properties, causing immediate damage to the mucous membranes of the upper respiratory tract and the eyes [6,7].

It is therefore essential to identify sources of odor emissions and monitor them continuously. Accurately locating specific emission sources and assessing their odor nuisance is complex process resulting primarily from the complexity of odor perception. This is because odor is not merely a function of chemical concentration, but depends on hedonic quality, intensity, frequency and duration, as well as unpredictable interactions between the components of the odorous gas mixture, such as synergism, neutralization or masking [8–10]. In chemical engineering practice, this means that eliminating a single odor-causing contaminant, might, paradoxically, increase the perceived nuisance of the entire odorous mixture.

Given the complexity of this issue and growing public awareness, the reduction of odor emissions is becoming a key component of environmental management at many industrial and municipal facilities where technological processes can be a source of odor nuisance. Increasingly stringent environmental regulations are forcing operators of such facilities to implement preventive technologies aimed at minimizing odor emissions and reducing the impact of odors on the surrounding area [5,11,12]. These include, among other things, the use of natural protective barriers, appropriate spatial planning of facilities, the hermetization of selected technological processes, and organizational measures to reduce the risk of odor emissions into the environment. These solutions are designed to reduce odor nuisance for residents of areas adjacent to facilities, from which complaints about unpleasant odors are frequently received [13]. Facilities are also required to implement solutions consistent with the BAT (Best Available Techniques) concept, which is not always possible, especially in the case of older installations designed and built according to earlier technological standards. Structural, spatial, and economic constraints can significantly hinder or even prevent the full implementation of moder solutions.

It implies that the implementation of preventive technologies is often limited by technical and economic considerations. In many cases, their use involves high investment costs or does not provide the expected efficiency relative to the expenses incurred. For this reason, deodorization technologies are widely used, enabling the reduction of concentrations of odor-causing compounds in exhaust gases. Deodorization does not prevent the formation of odorants, which arise, for example, in composting processes or as a result of putrefactive processes occurring in landfills, but it ensures high efficiency in their removal [14,15].

Selecting the appropriate deodorization method is a complex issue that depends on many factors related to the quality of emitted gases and the conditions prevailing in a given facility. Factors of primary importance include the quantity and nature of emitted substances, the exhaust gas flow rate and its variability, and the desired efficiency of the deodorization system [16–19]. Factors influencing the choice of installation include required space, compatibility with existing installation facilities, and the operating conditions of the given installation. Financial considerations also influence the choice of technology, including construction costs and subsequent operating expenses such as ongoing supplies, chemical resources, operating time, etc. Therefore, the choice of deodorization method is a compromise and a balance between the specific elimination of odorants, installation conditions, and financial profitability [11,17,20].

The effectiveness of deodorization processes requires regular monitoring of the quality of the treated gases. To this end, both instrumental (analytical) methods, such as gas chromatography (GC), and sensory techniques, including dynamic (DO) and field olfactometry (FO), are used [21,22]. Although these methods provide reliable results, their use involves high costs, is time-consuming, and requires sampling or the involvement of qualified assessors (panelist). Gas chromatography coupled with olfactometry (GC-O) is an attempt to combine the advantages of instrumental and sensory methods. This technique allows for the simultaneous analysis of the chemical composition and odor concentration of a gaseous mixtures, however, it still does not enable real-time monitoring [23,24].

In recent years, multi-sensor gas detection systems, known as electronic noses, have been attracting increasing interest. The popularity of these solutions stems primarily from their ability to automate the air quality monitoring process and perform continuous measurements [25–27]. In some industrial applications, monitoring of specific compounds, such as ammonia or hydrogen sulfide, can be performed using simple and relatively inexpensive selective sensors. However, this approach is not always sufficient, as odorous mixtures are complex systems often containing hundreds of different chemical substances [27]. An additional limitation is the occurrence of cross-selectivity, which can lead to signal interference and hinder the correct interpretation of results. Multi-sensor system using non-selective gas sensors are therefore an excellent alternative. In such solutions, the identification of odor mixtures is based on the analysis of the collective response of a set of sensors that react to a broad spectrum of chemical substances. However, the effective application of such systems requires the implementation of advanced data analysis methods, including chemometric and statistical tools as well as machine learning algorithms [28,29].

Advances in machine learning methods and chemometric tools have made it possible to use such systems for quantitative purposes as well [28,30]. After proper calibration using reference methods, gas sensor arrays can be used to estimate the concentrations of selected chemical compounds or odor levels, enabling automatic and continuous monitoring of air quality and the effectiveness of deodorization processes [26,29,31]. It should be emphasized that he term “electronic nose” is most commonly used in reference to qualitative analyses, whereas for quantitative determinations, the term “gas sensor array” is more appropriate, underlining the ability to determine numerical parameters such as chemical concentrations (ppm) or odor concentration (ou/m^3).

The construction and implementation of a fully functional electronic nose presents a significant engineering challenge, the success of which depend on the proper integration of multiple design phases. This process begins with a rigorous selection of sensors, proceeds through a phase of collecting training data during measurement campaigns using reference methods, and concludes with the implementation of advanced algorithms and mathematical models. Despite this challenges, gas sensor arrays show tremendous potential as a bridge technology, filling the gap between precise chromatographic analysis, subjective olfactometry, and simple selective sensors. Rather than viewing these techniques as competing with one another, they should be regarded as complementary, as each provides a different type of information – chemical or sensory. In modern environmental monitoring, particularly in the area of odor control, it is essential to strive for synergy among all available methods. This approach provides the most comprehensive picture of the samples being analyzed while minimizing the time required for analysis, which is essential in systems operating in continuous mode. Figure 1 summarizes the characteristics of individual instrumental and sensory techniques in terms of their ability to provide data and their potential for online monitoring.

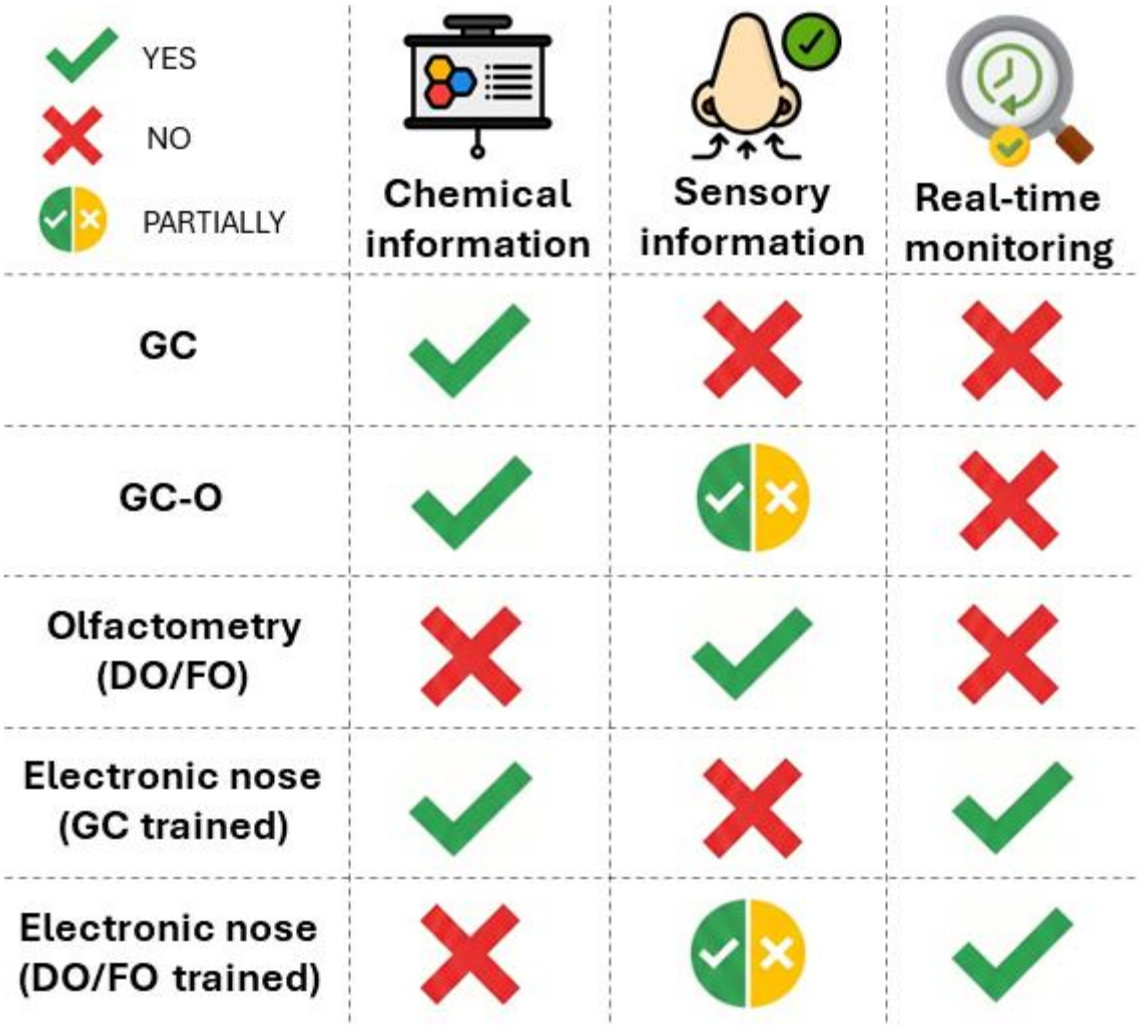


Figure 1. Methods of odor analysis and their characterization in providing chemical information, sensory information, and potential for real-time odor monitoring.

2. Characterization of odorous substances

2.1 General information

The sense of smell is considered one of the oldest and most complex of the five basic senses. Significant progress in understanding its mechanisms was made thanks to the discoveries by Richard Axel and Linda B. Buck regarding olfactory receptors and the organization of the olfactory system, for which they were awarded the 2004 Nobel Prize in Physiology or Medicine. These discoveries have helped elucidate the fundamental molecular mechanisms of odor recognition, however, many issues related to stimulus integration, the interpretation of odor mixtures, and the subjective perception of odor remain the subject of ongoing research [32]. From a physiological perspective, sense of smell is defined as a stimulus for olfactory cells that arises in the presence of specific chemical molecules and is transmitted in the form of electrical impulses directly to the brain [33,34]. Although humans possess an extraordinary ability to detect and distinguish between a vast number of substances, the way they perceive them and their detection thresholds vary from person to person [32,33]. In addition, the interpretation of a given odor signal is influenced by variable environmental conditions, such as temperature, humidity and pressure [33]. For this reason, it is necessary to clarify the concept of odor-generating substances (odorants). In common parlance, this term is mainly associated with unpleasant smell, however, in technical and environmental sciences, the definition of this term must be significantly broadened.

2.2 Definition of odorants

Malodorous substances, referred to in the technical literature as odorants, are volatile chemical compounds that evoke unpleasant olfactory sensations and are detected by olfactory receptors at very low concentrations [35]. As mentioned before, in physiological terms, smell is a sensation produced by the stimulation of olfactory receptors in the olfactory epithelium of the nose by electrical impulses [33,34]. Chemically, these substances are classified into two main groups:

- Volatile Organic Compounds (VOCs) – which include most carbon-containing compounds (with expectations such as carbon monoxide and carbon dioxide) that have high vapor pressure [36].
- Volatile Inorganic Compounds (VICs) – which include, among others, ammonia, hydrogen sulfide, sulfur dioxide and carbon disulfide.

Substances responsible for odor nuisance also include volatile organic acids, such as butyric, propionic, and valeric acids, as well as aldehydes, ketones, alcohols, phenols, and esters [32,34,37,38]. It should therefore be emphasized that not all odor-generating substances cause unpleasant olfactory sensations. Certain esters, aldehydes, and alcohols, commonly found in fruity and floral fragrances, have a pleasant scent [34,39]. Consequently, the term *odorants* refers to all substances capable of stimulating olfactory receptors, regardless of the nature of the olfactory sensation they create [32,34]. So, the scent is a sensory experience, and how it is

perceived depends on a person's individual sensitivity, the concentration of odorous substances, and environmental conditions (mostly temperature and humidity). Although some countries have regulations and guidelines regarding odor emissions and nuisances, their scope, methods of assessment, and permissible levels vary depending on the legal system in place. In many cases, the available legal instruments remain limited or do not provide a clear basis for effectively reducing odor emissions, even though such emissions are a frequent cause of complaints from residents [32,39,40].

2.3 Olfactory threshold

A distinction should be made between the concept of and odorant (a substance that triggers a stimulus) and odor – the olfactory sensation, most often associated with an unpleasant smell or stench. Scientific and technical analyses generally assume that odor nuisance results from the presence of substances containing specific functional groups, which the brain perceives as negative sensations [41].

The osmophores groups present in the molecule are responsible for the perception of a specific odor (pleasant or unpleasant) and its intensity. The composition of these groups determines the olfactory detection threshold (OT), which, depending on the molecular structure, can vary by as much as a millionfold – from parts per billion (ppb) to parts per million (ppm) [32,34,41]. Figure 2 shows examples of osmophores groups of selected chemical compounds along with their corresponding OT values. OT is defined as the minimum concentration (expressed in chemical units) at which an odor is detected by 50% of people in a representative sample group. These thresholds are often significantly lower than the detection limits of analytical methods [34,42].

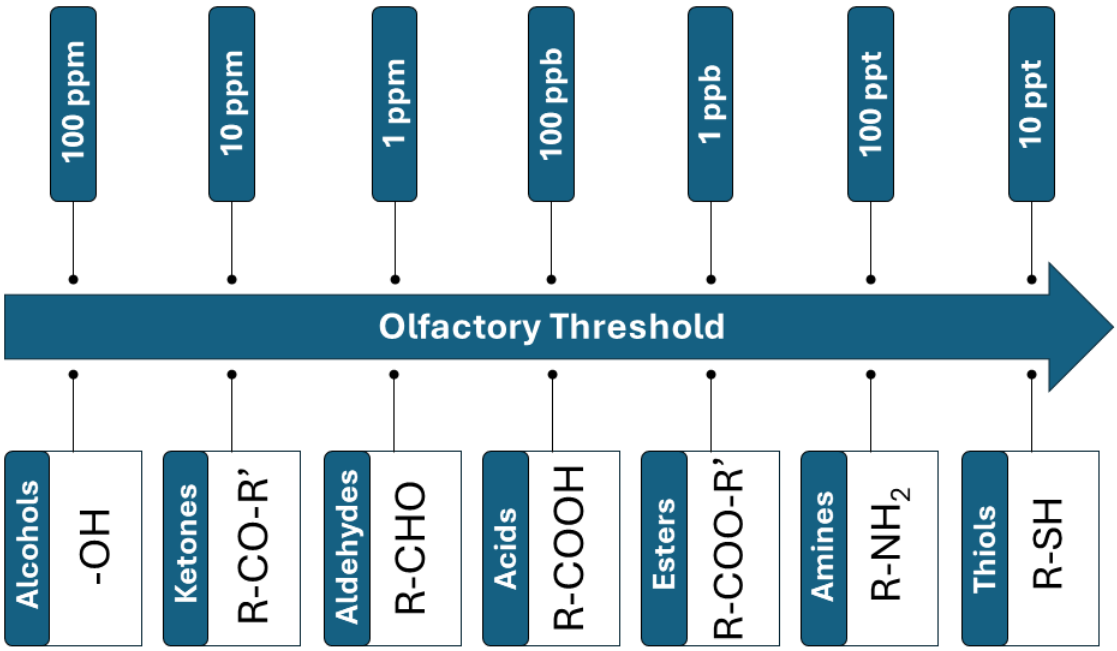


Figure 2. Examples of osmophore groups of chemical compounds with their corresponding olfactory thresholds [43,44].

A concept inextricably linked to the OT is the odor unit (ou), which is defined as the minimum amount of an odor-causing substances that, when dispersed in one cubic meter of clean air (at standard temperature and pressure), causes the detection limit to be reached. In order to standardize olfactometric measurements, the European standard (EN 13725) adopted the odor unit standard (EROM – European Reference Odor Mass), which was defined as the mass of 123 μg of n-butanol [35,39].

The introduction of such amount of standard odorant to one cubic meter of inert gas corresponds to the value of 1 ou/m^3 and is numerically equivalent to the olfactory threshold value for n-butanol. In practice, it is assumed that any other odor-generating substance or their mixture reaches its OT (the level of 1 ou/m^3) when it exhibits an odor with the strength identical to the above mentioned n-butanol standard.

$$OT = 123\ {}^{\mu g}/_{m^3} = 1\ {}^{ou}/_{m^3} \quad (1)$$

2.4 Odor nuisance

2.4.1 Definition and essence of the phenomenon

Odor nuisance is defined as discomfort caused by odorous substances or circumstances surrounding their presence that negatively affect the well-being of an individual or group of people [32,45,46]. It results from the subjective perception of unwanted odors. The literature distinguishes between odor annoyance - a reaction to immediate exposure, and odor nuisance – a cumulative effect resulting from repeated olfactory experiences over a longer period of time. It should also be emphasized that odor nuisance is primarily caused by the olfactory properties of odorants, which in most cases also possess toxic properties. While toxicity may even cause fatal consequences, the biological effects of the odor nuisance itself are usually limited to physiological changes resulting from a destructive impact on the human psyche.

2.4.2 Factors shaping perception and the level of nuisance

The nuisance is not simply and directly related to the concentration of the malodorous substance itself – it results from the interaction of many physical and personal factors [46,47]. Crucial variables that modify the perception of odor include:

- Personal factors – individual olfactory sensitivity, exposure history, mood and life situation (fatigue, sleep duration), age, health status and emotional attitude towards the source of the odor (fear of a decline in property value) modify the individual assessment of discomfort [32,39,48].
- Environmental condition – spatial development, architecture and the presence of other pollutants, noise, vibrations or dust accompanying the emission often intensify the perception of odors.
- Emission source properties and location - the proximity of facilities such sewage treatment plants, waste disposal sites or industrial plants (metallurgical, chemical) is the main determinant of the reported nuisance [46,48].

- Metrological and topographic conditions – the direction and speed of the wind determine the dispersion (spread) of the odor plume, while low wind speeds and high temperatures and humidity favor the accumulation of pollutants near the ground, which drastically increase the number of complaints from residents [32,46–49].

2.4.3 Impact on health and quality of life

Exposure to offensive odors causes a range of negative reactions, from irritation to serious health problems. These effects could be divided into:

- Emotional reactions – long term exposure leads to chronic stress, anxiety, frustration, tearfulness, depression, mood disorders and problems with concentration and insomnia [32,45].
- Physical (somatic) symptoms – the most commonly reported side effects include headaches, dizziness, nausea, vomiting, respiratory problems (difficulty breathing) and irritation of the mucous membranes of the eyes and throat (people with existing respiratory problems show significantly higher levels of odor irritation) [46].
- Behavioral change and mobility – in response to odor, people take defensive measures, such as closing windows, avoiding outdoor activities (gardening, recreation), and limiting social gatherings, extreme nuisance becomes a direct cause for the decision to move and abandon their place of residence [32,45,46,48].
- Reduced well-being – research shows a strong correlation between the absence of unpleasant odors and a sense of happiness and overall life satisfaction (odor nuisance is one of the strongest factors determining negative assessments of urban living comfort) [48,49].

2.4.4 Objectivity parameters for the assessment of nuisance

The perception of odor nuisance is intensified by synergism, i.e. the mutual strengthening of the odorous of various substances in the mixture. This makes the overall olfactory effect stronger than the sum of the individual component's effects. Two complementary sets of parameters are used to scientifically describe odor nuisance.

The first one is the FIDOL model, which is a key tool in assessing odour nuisance and form the basis for legal regulations in many countries [39]. This is a standard set of criteria, which includes:

- Frequency (F) – determines how often people are exposed to the odor.
- Intensity (I) – is the strength of the perceived stimulus or the concentration of the odor.
- Duration (D) – the time that the odor is noticeable during a single episode.
- Offensiveness (O) – subjective assessment of how unpleasant an odor is (so-called hedonic quality).
- Location (L) – the sensitivity of the place where the odor occurs, related to the use of the land (e.g. residential areas are more protected than industrial areas) [39,48].

The use of all five of these factors allows for a much more comprehensive assessment of the odor nuisance than simply measuring the concentration of the substances in the air. Another concept is hidden under the acronym CICOP, describing five main dimensions (features) that are used for the technical and scientific characterization of odor-generating gases. While the FIDOL model focuses on assessing odor nuisance in the environment, CICOP focuses on the measurable properties of the odorant itself [39,50]. The detailed explanation of each point is as follows:

- Concentration (C) – the minimum amount of a substance needed for it to be detected by a given portion of the population.
- Intensity (I) – the strength of odor perception, which increases logarithmically with increasing concentration (according to the Weber-Fechner law).
- Character (C) – describes what a given scent “smells like” using standard vocabulary (e.g., fishy, fruity, chemical).
- Offensiveness (O) – a measure of the pleasantness or unpleasantness of an odor at a specific concentration.
- Persistency (P) – the rate at which the intensity of an odor decreases as it is diluted in the atmosphere.

FIDOL is mainly used by regulatory authorities for managing odor conflicts and spatial planning, while CICOP is used in laboratories to precisely describe the physicochemical properties of samples.

2.5 Basic odor parameters (features)

Three dimensions are crucial for understanding the mechanism of odor nuisance: odor concentration (C_{OD}), odor intensity (OI), and hedonic tone (HT). C_{OD} quantifies the strength of the physical stimulus, OI measures the psychological magnitude of the sensation experienced, and the HT reflects the observer’s emotional relationship to the odor [10,51,52]. These parameters are closely interconnected by psychophysical relationships, and their precise definition is necessary for the objectivity of the assessment of the impact of odors on the environment.

2.5.1 Odor concentration

Odor concentration is defined as the number of European odor units per cubic meter of gas under standard conditions (ou_E/m^3). This parameter quantitatively describes the strength of an odor and is an objective measure based on the dilution of the sample [51]. As can be seen from equation 1, a concentration of 1 ou_E/m^3 corresponds to the stimulus caused by 123 μg of n-butanol evaporated in 1 m^3 of inert gas (this is so-called EROM) [10,50,53]. For measurement purposes, dynamic olfactometry (considered to be “golden standard”), field olfactometry or static olfactometry (e.g. the Japanese triangular bag method) are used. It involves repeatedly diluting the sample with a clean gas until 50% of the evaluation team (panel) can no longer distinguish the sample from clean air – this is olfactory threshold (OT).

Knowing the chemical concentration and OT of the given substance, in the tested sample, it is possible to determine its C_{OD}. For individual substances it is defined as the quotient of the odorant concertation (C) by the value of its OT (equation 2).

$$C_{OD} = \frac{C}{OT} \tag{2}$$

In the case of odorous gas mixtures, using the above formula is not possible due to the inability to determine the OT for the mixture. In this case, the C_{OD} is defined as the dilution rate of the tested sample with odorless air required to reach the OT by the odor evaluators (equation 3).

$$C_{od} = \frac{V_s + V_{air}}{V_{air}} \tag{3}$$

where:

V_s – sample volume,

V_{air} – dilution air volume.

The odor concentration can also be estimated analytically as the sum of the ratios of the chemical concentrations of individual compounds to their individual olfactory thresholds (equation 4). However, in the case of odorous gas mixtures, the measured odor concentration often differs from the calculated odor activity value (OAV) due to the synergy, masking or neutralization phenomena between the components [10,50].

$$OAV = \sum_{i=1}^{n} \left(\frac{C_i}{OT_i} \right) \tag{4}$$

where:

C_i – chemical concentration of i-th substance detected by analytical technique [ppm],

OT_i – olfactory threshold of i-th substance in the analysed sample [ppm].

2.5.2 Odor intensity

Odor intensity is the magnitude of the perceived odor sensation. It determines how strong the odor is to the observer. Unlike odor concentration, which is physical measure of stimulus, odor intensity measures the body's psychological response to that stimulus [54]. Categorical point scales are most often used to describe it, such as the 7-point scale according to the *VDI 3882 Blatt 1 – Olfactometry – Determination of odour intensity* standard, covering the range from 0 (no odor) to 6 (extremely strong odor) [32].

The relationship between odor concentration and odor intensity is not linear. It is described by fundamental psychophysical laws: the Weber-Fechner law, which assumes a logarithmic increase in sensation with concentration, and Stevens' power law. Studies show a very high correlation between odor concentration and odor intensity, which allows these parameters to be used interchangeably under certain field monitoring conditions [51].

The Weber-Fechner law can be applied to stimuli stimulating all the senses: sight, hearing, taste, touch and smell. The proportionality between the perceived strength of a stimulus (odor intensity) and the actual strength of the stimulus is described using a logarithmic relationship

(equation 5). This means that the intensity of human sensations increases as the logarithm of the increase in stimulus strength, not as rapidly as the increase in the stimulus itself.

$$OI = k_{WF} \cdot log \frac{C}{OT} \quad (5)$$

where:

C – chemical concentration of the substance detected by analytical technique [ppm],

OT – olfactory threshold of the substance in the analyzed sample [ppm],

k_{WF} – empirical coefficient determined for the analyzed substance.

Steven's law also describes the relationships between an increase in the intensity of an external stimulus and the perceived increase in the magnitude (strength) of the sensory experience evoked by that stimulus (equation 6). It is believed to somewhat replace the Weber-Fechner law because it covers a broader range of sensory experiences, down to the zero odor intensity.

$$OI = k_S \cdot C^n \quad (6)$$

where:

C – chemical concentration of the substance detected by analytical technique [ppm],

k_S – empirical coefficient determined for the analyzed substance,

n – empirical coefficient determined for the analyzed substance.

2.5.3 Hedonic tone

Hedonic tone (quality) describes the emotional character of an odor, so the degree of pleasure or displeasure it evokes [32,52,55]. It is normally measured on o 9-point scale according to *VDI 3882 Blatt 2 – Olfactometry – Determination of hedonic odour tone*, from -4 (extremely unpleasant) through 0 (neutral) to +4 (extremely pleasant) [32,55]. It is worth emphasizing that HT is not a constant characteristic of a given substance and can change dramatically with increasing concentration. Recent sources indicate the existence of so-called critical points at HT around $\pm$0.5 [55]. For instance, unpleasant odors such as dimethyl disulfide increase in aversiveness with increasing concentration. Pleasant odors (limonene) are rated positively at low concentrations, but after a certain concentration 9tipping point), their tone becomes negative [32,55].

It is the HT that is considered to be the strongest factor in determining the potential for odor nuisance, as negative odors trigger complaints from residents much more quickly than neutral or pleasant ones, even when the frequency of occurrence remains the same [10,53,55]. A complete sensory profile, combining odor concentration as a measure of the stimulus, odor intensity as the strength of the sensation and hedonic tone as an emotional response, is an essential basis for objective air quality management and resolving social conflicts related to odor emissions.

2.6 Sources of odor nuisance substances

The release of odors into the atmosphere has a twofold origin: it may result from processes occurring in nature itself or be a direct consequence of various human activities, so it might be of anthropogenic nature [40]. Natural emitters include primarily volcanic activity, forest and steppe fires, processes of microorganism decomposition of organic matter in marshy areas and erosion of minerals [35,40]. In such cases, ecosystem usually have mechanisms that allow for the cyclical exchange of elements and self-purification of the air, which limits their long-term odor nuisance. Figure 3 shows the main industrial sectors considered to be sources of odor emission. A brief characterisation of each, based on examples from scientific articles, is provided in the following sections.

Anthropogenic sources pose a significantly greater threat to the environment and health. Their specificity lies in the fact that the emitted compounds often exhibit toxic properties, and the scale of their emission and concentration in the air significantly exceed the natural regenerative capacity of the biosphere [56,57]. The main human activities generating odor nuisance can be divided into three key sectors:

- Industrial activities – including the chemical, petrochemical, pharmaceutical, metallurgical, pulp and paper, and food industries [56,57].
- Municipal waste management – where crucial sources are sewage treatment plants, sewer systems, landfills and composting plants [39,58].
- Agriculture and breeding – with particular emphasis on large-scale livestock farming, fermentation processes of natural fertilizers (manure, slurry) and the production of feed and meal [59].



Figure 3. The main sources of malodorous substance emissions in the environment.

2.6.1 Odor emission from the industrial, food and agricultural sectors

Although these sectors are not the main focus of this dissertation, they are a significant source of odorant emissions. The chemical industry, along with its branches such as pharmaceutical production, rubber production and fuel processing, is considered one of the main emitter of harmful odor into the atmosphere [35,56,57]. The processes and activities carried out release, among other things, ammonia, hydrogen sulfide, and BTEX (benzene, toluene, ethylbenzene, xylene) compounds into the atmosphere, which are the main sources of pollution from large industrial parks [60–62].

In the food industry and animal waste processing, the odor problem stems from the thermal decomposition of proteins and fats during disposal, drying, or roasting processes. The key markers here are trimethylamine (TMA), which imparts a characteristic fishy odor, and diacetyl-type compounds, which—even at very low concentrations—can amplify the perceived intensity of the odor through synergistic effects [63–66].

In agriculture and intensive animal husbandry (primarily poultry and swine farms), odors result from the anaerobic decomposition of manure and natural fertilizers. Volatile fatty acids (VTA e.g., butyric acid, isovaleric acid) and phenolic compounds are responsible for the “sour” and “sweat-like” odors. Sulfur compounds are also an important component. While hydrogen sulfide dominates on pig farms, dimethyl trisulfide (DMTS) and ammonia are the primary source of odor nuisance in poultry farming. The scale of these emissions is closely linked to the systems used for storing and disposing of slurry and manure [67–69].

2.6.2 Waste management facilities

This is the sector that generates the most interventions in Poland – according to GIOŚ data, complaints about municipal and waste management facilities accounted for 41.6% of all notifications [13].

Research conducted at one of the largest municipal waste landfills in China (Guangzhou) provided detailed data on the dynamics of odor emissions depending on the stage of operational work and the height of residential buildings [4]. Of the 145 compounds identified, oxygenated compounds constituted the largest group, accounting for over 73% of total emissions. Ethyl alcohol dominated this group. Benzene and xylenes were the most common aromatics (totaling approximately 78% of this fraction), and dichloromethane dominated among the halocarbons (nearly 50%). Scientist have demonstrated that, in addition to the distance of up to 6.8 km, the perceived odor is significantly influenced by the height of the residence and the geometry of the landfill. Resident of higher floors of high-rise buildings may experience a different frequency of odors than those on the ground floor, depending on the current height of the waste pile and the emission level. The use of temporary HDPE membrane covers has also been shown to reduce odor concentrations by nearly 50% compared to the active unloading area.

Cheng et al. [70] presented a study conducted in Shanghai, comparing odor emissions from two different disposal systems for the same municipal waste: a landfill operating under anaerobic conditions and a composting plant operating aerobically. The results showed that

composting plant generated significantly more odor nuisance – the average odor concentration was nearly twice as high as at the landfill. The most critical emission points were identified as the composting screening area and the landfill's active working area. The chemical composition of emitted gases varied depending on the technology: at the landfill, sulfides (mainly hydrogen sulfide and ethyl sulfide) and aromatics (benzene) dominated, while at the composting plant, the main components were ammonia and oxygenated compounds such as ethyl acetate and 1-butanol. In the case of the composting plant a unique, strong correlation was observed between the overall odor concentration and the content of halogenated compounds and sulfides.

Similar conclusions were presented by Schlegelmilch et al. [71]. Again scientists identified the main sources of odors from composting plant as the handling processes (delivery, shredding) especially the windrow turning and final screening stages. The composting waste gases were dominated by alcohols (ethanol), esters (ethyl acetate), ketones and aldehydes (acetone, butanone), and terpenes (alpha-pinene, limonene). The highest odor concentrations were released during the first 2-3 weeks of the composting cycle. Importantly, high ammonia concentrations (reaching up to 400 ppm) did not directly correlate with the total odor concentration, as other organic compounds have much lower detection thresholds and dominate odor perception. The authors emphasize that although odors from composting plant rarely cause direct health problems, due to negative psychological reactions among resident and the potential emission of bioaerosols, the use of advanced gas purification systems is essential.

The research described by Agus et al. [72] focused on identifying compounds responsible for the odor of municipal sewage, which may negatively affect the aesthetics of drinking water. Using GC-MS, olfactometry and flavor profile analysis (FPA), the researchers determined that the secondary treated wastewater was dominated by earthy, musty odors, accompanied by amine, sulfur, and fragrant notes. Geosmin, 2-methyllisoborneol (2-MIB), and 2,4,6-trichloroanisole (246TCA) were identified as the main sources of unpleasant odors. These compounds are present in wastewater at concentrations well above detection thresholds an are highly persistent. They remain detectable even after a 32-fold dilution of the sample or after advanced treatment processes such as reverse osmosis.

Further important data on sludge management are provided by the study described by Han et al. [73], conducted at a full-scale sewage sludge composting plant in Beijing. The composting hall was identified as the dominant source of emissions, accounting for over 91% of the total odor activity value (OAV) of the entire facility. In addition to ammonia, the following volatile sulfur compounds (VSCs) were identified in the plant chemical profile: DMDS, DMS, hydrogen sulfide (H_2S), and carbon disulfide (CS_2). Interestingly, methyl mercaptan (MT) was not detected at any of the locations studied. Although ammonia clearly outweighed the other substances quantitatively, dimethyl sulfide (DMS) and dimethyl disulfide (DMDS) demonstrated higher odor activity (OAV). This is due to the fact that the olfactory thresholds (OT) for these sulfur compounds are several orders of magnitude lower than for ammonia, which means that even low concentrations cause a very strong sensory response.

Gonzalez et al. [67] showed, based on 17 Italian wastewater treatment plants, that the main source of odor is the pre-treatment (mechanical) units, especially the primary settling tanks, and the odor nuisance decreases with each subsequent stage of the treatment cycle. In anaerobic digestion, the reactors are closed, so odors are released mainly during auxiliary operations: waste storage, batch preparation and digestate dewatering. The odor profile of the installation changes with the process stages (intensifying in the thermophilic phase), and the key odorants include VSC, ammonia and volatile organic acids. It was emphasized that odor control is currently the main challenge for the sustainable implementation of modern circular economy installations.

Research has also been conducted in Poland on odor nuisance generated by wastewater treatment plants. After analyzing two facilities, Czarnota et al. [13] demonstrated that the most emissive are mechanical treatment units (screens, grid chambers) and sludge management units (thickening and dewatering), especially if they operate in an open system. Hydrogen sulfide, ammonia and VOCs were identified as key odorants. Studies showed that H_2S concentrations in the analyzed treatment plants exceeded permissible standards many times over. In both facilities the highest H2S emissions were recorded above the sand traps and in the expansion chambers. Among the methods for counteracting odor nuisance, the high effectiveness of airtightness combined with air purification in biofilters or activated carbon was indicated. For surface sources where hermetization is not possible, the use of protective mats was recommended.

In summary, waste management facilities have the most complex and dynamic emissions profile among all the sectors analyzed. The predominance of sulfur compounds, ammonia, and volatile organic compounds, combined with the large surface area of surface sources (such as active landfills or composting sites), means that traditional, point-source measurement methods could be insufficient under these conditions. The extreme variability in odorant concentrations identified in the literature, which depends on technological processes and meteorological conditions, provides a direct justification for the implementation of continuous instrumental monitoring systems.

2.7 Counteracting of odor nuisance substances – review of legal regulations

The problem of odor nuisance is an international challenge and the approach to its regulation varies significantly depending on the chosen jurisdiction [39,74]. Although most countries classify odors as atmospheric pollutants, the majority of legal systems – including European Union Law – lac a single, comprehensive legal act that would regulate this issue in a profound manner [75,76]. Instead, a variety of emissions management models are used, ranging from rigid concentration standards, through technical guidelines, to procedures based on citizen complaints statistics [39,77].

2.7.1 Worldwide odor regulations

In Europe, the common foundation for member states is the Industrial Emission Directive (IED), which requires plants and facilities to use Best Available Techniques (BAT) to reduce odors, but rarely imposes specific numerical limits [75,78]. The exception are sectors such as

biological waste treatment, for which permissible odor concentrations ranges have been defined at EU level [75,78].

At the national level, the German model stands out, based on the concept of the “odor hour”. It is defined as the time during which an odor is detectable for at least 10% of the measurement period, which allows for the statistical designation of protected zones [39,47]. This allows for an objective determination of the permissible frequency of odor occurrence during the year depending on the intended use of the area [39,75,79]. In Great Britain, the benchmarking approach prevails, where thresholds values depend on the degree of unpleasantness of a given type of odor [39,75,78]. The introduce a division of odor sources into three offensive categories: the most bothersome – animal waste disposal (limit 1.5 ou_E/m^3), medium bothersome – animal breeding (limit 3.0 ou_E/m^3) and the least bothersome – breweries, coffee roasters (limit 6.0 ou_E/m^3).

In June 2023, the Italian ministry of the Environment adopted new national guidelines for the management of odor emissions from industrial plants. They introduce receptor sensitivity classes, where the permissible odor values at the recipient level range from 1 ou_E/m^3, for high-density residential areas, to 5 ou_E/m^3 for uninhabited areas [80]. In Flanders (Belgium), a popular method of assessing odor nuisance is the use of so-called sniffing teams (snuffelploegmetingen). They allow for direct determination of the odor plume range in the field, which is then used to calibrate dispersion models [39].

Outside Europe, Asian countries such as Japan and China are pioneers in odor regulation, where standards are enforced directly at the plant’s site boundary [39,74,75]. Since the early 1970s, Japan has been using system based on the odor index (determined by the triangular odor bag method), which regulates not only the concentration of specific chemical substances, but also the intensity of the odor as a mixture [39,75]. In the United States (e.g. Colorado, Connecticut), odors are typically not treated as contaminants at the federal level, and their control rests with local authorities, which often use field olfactometry to set dilution to thresholds (D/T) limits [39,75].

Many countries, including the Netherlands, Austria, and selected Canadian provinces, base odor protection on so-called setback distances. These are intended to prevent conflicts between intensive agriculture and residential development at the spatial planning stage [39,75,77]. Most of these systems use the FIDOL criteria to give resident’s subjective feelings a measurable legal framework [39,75,81]. The analysis of these international experiences constitutes an important point of reference for the polish system. In this case, in the absence of a dedicated act, protection relies primarily on indirect regulations and educational instruments, such as Odor Nuisance Prevention Code [74,77].

2.7.2 Odor regulations in Poland

The literature on the subject and reports of control bodies emphasize that odor are one of the most common causes of complaints about air quality submitted to environmental protection inspection bodies, accounting for more than half of all interventions in this area in Poland [74,77].

Despite the large scale of the problem, currently in the Polish legal system – similarly to the European union legal system – there is no single comprehensive legal act that would regulate the principles of combating odor nuisance.

In Poland, odor nuisance protection is based on indirect regulations, such as the Environmental Protection Law (Prawo Ochrony Środowiska), which allows authorities to impose obligations to limit negative environmental impacts. Another document, the Civil Code, regulates the issue of so-called “immissions”, or activities that disrupt the use of neighboring properties beyond reasonable limits [74,77]. There are also regulations specifying reference values for 167 substances in the air, including odorous substances (e.g. ammonia or hydrogen sulfide). However, there is no implementing regulation specifying permissible concentrations for odorous mixtures or methodology for measuring them [74,82].

Numerous legislative attempts were made, including in 2011, 2019 and 2021, but work on the so-called “odor law” was suspended, often under criticism from business circles (especially in the agricultural sector) fearing restrictions on freedom of operation [74]. The latest project (from 2021) focuses on the agricultural sector and assumes the introduction of minimum distances (e.g. 500m for farms 500 Livestock Unit, LU) [82,83]. Importantly, Polish administrative judiciary has evolved – while courts used to consider odor as an immeasurable substance, they now increasingly emphasise that the lack of legal standards does not exempt authorities from the obligation to examine odor nuisance when issuing environmental decisions [82].

The key tool for objectivizing the problem is dynamic olfactometry regulated by the EN 13725 standard (in Poland PN-EN 13725), which allows for the measurement of odor concentration in units of ou_E/m^3 with the participation of qualified teams of panelists [77,82,83]. Although this method is available and recognized worldwide, in Poland it still lacks universal legal recognition as an emission standard. The systematic deficiencies are supplemented by the Code for Counteracting Odor Nuisance (Kodeks Przeciwdzialania Uciążliwości Zapachowej) issued by the Ministry of the Environment in 2016. It serves an educational purpose, promoting good technical practices, although it is not a legally binding act [74,77,82].

3. Characterization of deodorization techniques for contaminated gases

3.1 General information

As discussed in the previous chapters, in light of the increasing number of complaints and growing public pressure, it is necessary to implement effective steps to reduce emissions of odorous substances into the atmosphere. These measures can be divided into two main categories: preventive technologies, which focus on eliminating or blocking emissions at the source, and methods for deodorizing contaminated gases. Although eliminating malodorous substances at the source – through modern technological solutions, the application of BAT principles, or the appropriate siting of facilities – is the most desirable approach, it often proves to be insufficient or economically unfeasible.

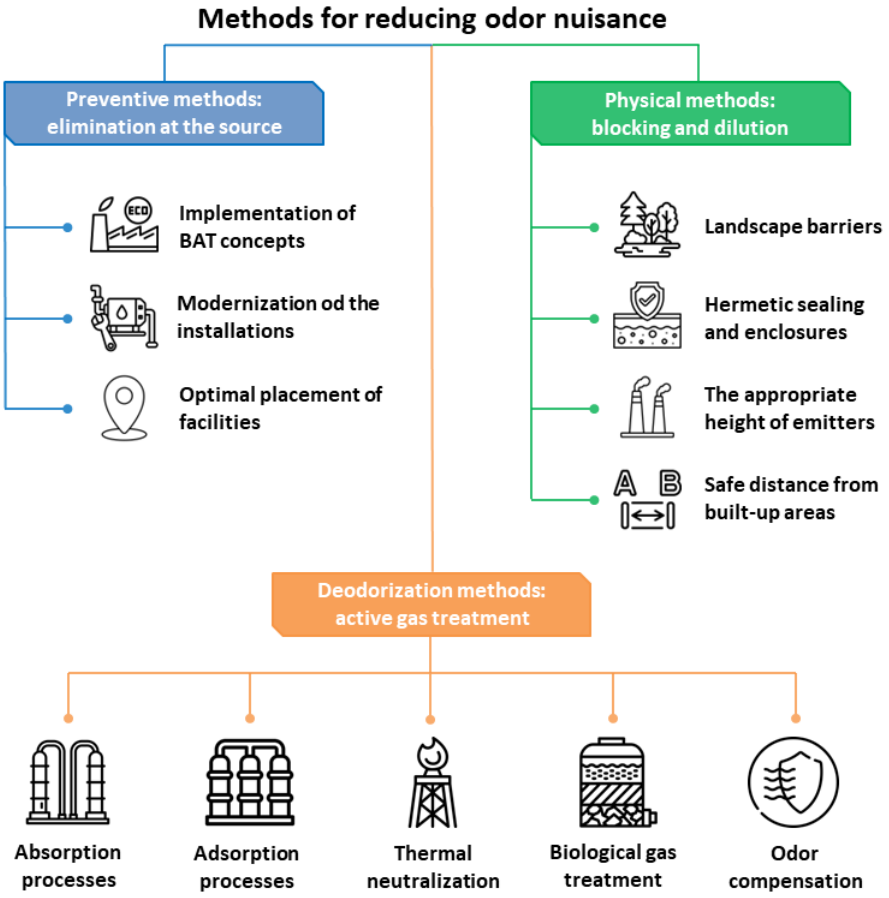


Figure 4. Classification of methods for reducing odorous gas pollution.

The primary objective of gas deodorization is to achieve the highest possible degree of decomposition of odorous substances, to convert them into completely odorless compounds, or to alter the odor profile of the treated gas stream (e.g., through masking or neutralization). These goals are achieved through a variety of technologies, the most popular of which include: absorption and adsorption processes, thermal neutralization (incineration), cold oxidation, biological gas treatment processes (biofiltration) and odor compensation [18,84]. Figure 4 shows a classification of methods for reducing odor nuisance.

Selecting a specific technology is an extremely complex process that requires not only extensive technical knowledge but also a thorough analysis of the gas's physicochemical properties, such as flow rate, temperature, humidity, and contaminant concentration [18,32,34,84]. The situation is further complicated by the fact that odorous gas streams are typically multicomponent mixtures consisting of hundreds of different chemical compounds. Due to this complexity and the low OT of many odorants, treatment systems must be highly efficient. In engineering practice, designing such installations requires constantly striking a balance between high efficiency and the investor's practical economic and spatial constraints. Often, the most optimal solution for a specific facility is not a single method, but a combination of several different treatment techniques [18,34].

One of the most critical factors determining the success of the entire project is the precise identification of all odor emission points, with particular attention paid to non-integrated sources. Misjudging the odor background and inaccurately identifying odor sources during design phase are the most common causes of disappointment during operation. As a result, systems that demonstrated excellent performance under laboratory conditions and during pilot-scale testing achieve significantly lower performance at the industrial scale [34,84]. Therefore, thorough preliminary studies and test in pilot installations are an essential step prior to selecting and implementing a specific deodorization method.

The subsequent part of the thesis characterizes the deodorization methods employed in the experimental studies (absorption and biofiltration processes), while the remaining methods are summarized in Table 1 outlining their key advantages and limitations.

3.2 Absorption processes

Absorption is a fundamental unit operation used in chemical and process engineering, involving, the capture of one or more components from the gas phase by a liquid phase in contact with it, known as the absorbent [85,86]. In gas stream purification processes, the objective is the selective removal of pollutants (CO_2, H_2S, NH_3, VOCs) by transporting them into the liquid phase. The reverse process is desorption (stripping), used to regenerate the absorbent by removing the absorbed components from it, which typically takes place under conditions of elevated temperature or reduced pressure [85–87].

The theoretical description of mass transfer from a gas to liquid is most often based on the two-film theory (Whitman), which assumes the existance of two thin layers 9films) on both sides of the interface: the gas side and the liquid side [86–89]. It is believed that all diffusion resistance is concentrated in these films, and that a state of equilibrium prevails at the phase contact surface itself [86–89].

The ability of an absorbent to absorb a given component is determined by equilibrium relationships. For dilute solutions, Henry's law is applied, according to which the partial pressure of a component above the solution is proportional to its molar fraction in the liquid. The proportionality factor is so-called Henry's constant [85,86,89]. The solubility of gases in liquids is

strongly dependent on temperature (it usually decreases as temperature increases) and pressure (it increases as the total pressure of the system increases) [85,86,90].

There are two main types of absorption: physical and chemical. In physical absorption, the substance simply dissolves in the absorbent. An example of this is the removal of acetone using water [87]. In chemisorption (chemical absorption), the dissolution of the substance is accompanied by a chemical reaction with the absorbent or its components [86,89]. The presence of a chemical reaction usually increases the mas transfer rate and the sorption capacity of the absorbent by converting gas molecules into ionic forms [91]. This rate is described by so-called enhancement factor (E), which defines how many times absorption with a reaction is faster than pure physical absorption [91].

For the removal of acidic gases, such as CO_2 or H_2S, solutions of amines (MEA, DEA, MDEA) or potassium carbonate are commonly used [88]. These reactions are exothermic, which causes the temperature inside the absorption column to rise, affecting the equilibrium conditions and the kinetics of the process [87,91]. This process is most often based on chemical absorption in packed columns, where these gases react with suitably selected solvent [91]. The choice between structured and random-bed packing is therefore critical for acidic gases. Structured packing ensures a more uniform liquid distribution and lower pressure drops, allowing for stable operation at high flow rates [86,89,91]. Random-bed packings (Pall rings, Berla saddles) are less expensive but more prone to gas channeling, which reduces the effective contact area and gas removal efficiency [89,91]. The removal of acidic gases is therefore a complex process in which the kinetics of the chemical reaction must be precisely balanced with the hydrodynamics of the column [88,89]. Figure 5 shows a diagram of the process of absorption-based gas deodorization.

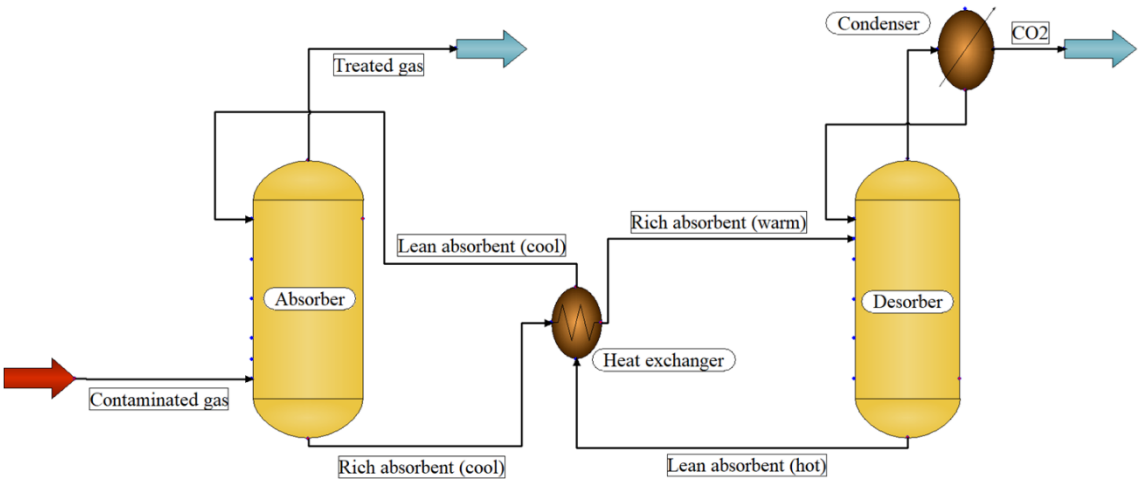


Figure 5. Process flow diagram of an absorptive gas deodorization system comprising an absorption and desorption column.

3.3 Biological gas treatment

3.3.1 Principles of biological gas treatment

Biological gas treatment is a technology that uses active microorganisms (mainly bacteria and fungi) to remove and degrade pollutants present in the air stream [92,93]. This process is

considered more sustainable and environmentally friendly compared to physiochemical methods. It typically does not require the use of harsh chemicals, occurs at ambient temperature (10-40℃) and under atmospheric pressure [93,94]. Biological methods are effective in removing a wide range of substances, including:

- VOCs - hydrocarbons, ethers, esters, alcohols, ketones, aldehydes and aromatic compounds (BTEX group) [92–94].
- Inorganic compounds – hydrogen sulfide and ammonia [92,94,95].
- Other malodorous compounds – mercaptans, sulfides and amines [94].

The fundamental mechanism of biodegradation is microbial oxidation. Microorganisms perceive pollutants as a source of carbon and energy necessary to growth. As a results of metabolic processes, pollutants are converted into new microbial biomass or non-toxic end products, such as carbon dioxide and water [92–94]. In the case of sulfur or nitrogen containing compounds, the oxidation products may include sulfates and nitrates [94,96]. The biofiltration is based on the complex interaction of physical and biological phenomena occurring at the interface between phases. The treatment process begins with the transfer of pollutants from the gas phase to the liquid phase, i.e., the moist layer surrounding the biofilm (absorption of contaminants) [94,97,98]. The key parameter is the solubility of the pollutants. Hydrophilic compounds are removed faster than hydrophobic compounds, which encounter greater resistance to mass transfer [93,97,99]. In addition to absorption in the liquid phase, adsorption might also occur directly on the filling material or on the surface of microbial cells (biosorption) [93,97,98].

Biofilm is a thin layer on the surface of the filter bed, which is an aggregate of microorganisms deposited on the surface of the filling material [93,97,99]. It consists of bacteria, fungi yeasts and protozoa [94,96]. An important component of biofilm is extracellular substances (EPS), primarily proteins and sugars, which form a gel matrix that protects cells and facilitates their aggregation [93,96,99,100]. The biofilm structure may also include channels that further the diffusion of oxygen and nutrients into its layers [96,97]. Inside biofilm, contaminants diffuse into the cells, where they undergo enzymatic processes. Biodegradation kinetics are often described by the Michael-Menten or Monod equation, which defined the dependence of the substrate consumption rate on its concentration [93]. For proper metabolism, the presence of nutrients (N, P, K, S, and trace elements) is essential, and these must be supplied externally or derived from the filling material. Most processes are aerobic, so oxygen availability is often a limiting factor in the rate of detoxification, especially in the case of thick biofilms [92–94,97]. Depending on the configuration and method of conducting the liquid phase (containing nutrients), three main types of devices are distinguished: biofilters (BF), biotrickling filters (BTF), and bioscrubbers (BS).

3.3.2 Biofilters

Biofilters are the oldest and simplest design for biological gas purification, used for decades in sewage treatment plants, waste disposal plants, and landfills. Polluted air passes through a porous bed containing active microorganisms that form a biofilm. The contaminant removal process takes place in several stages. First, substances transfer from the gas phase to

the moisture surrounding the bed or are adsorbed onto the packing material. Then, they diffuse into the biofilm, where they are metabolized by microorganisms into non-toxic products. The lack of a mobile liquid phase, because moisture is maintained by spraying the bed or humidifying inlet gas [93,94,99].

A typical biofiltration installation consists of a fan, a humidification unit, a biofilter reactor with a bed, and a drainage system. The important element of a conventional biofilter is the humidification unit (scrubber). Because there is no continuous liquid flow in a biofilter, the inlet gas must be humidified (to 95-99% relative humidity) in order to prevent drying of the bed and maintain biological activity [92,94,97]. The biofilter reactor is simply a tank filled with filter material (usually a layer about 1m thick), and the drainage system removes excess condensate and water from occasional sprinkling of the bed [92,97]. Two types of structures are used in industrial practice: open biofilters and closed biofilters. The former are concrete tanks placed outdoors, exposed to weather conditions (precipitation, temperature changes), which makes precise process control difficult. Closed biofilters are located in containers or halls, allowing for temperature stabilization and better control of purified gas emissions [94,97]. Figure 6 shows schematic diagram of a biofilter used for biological gas treatment.

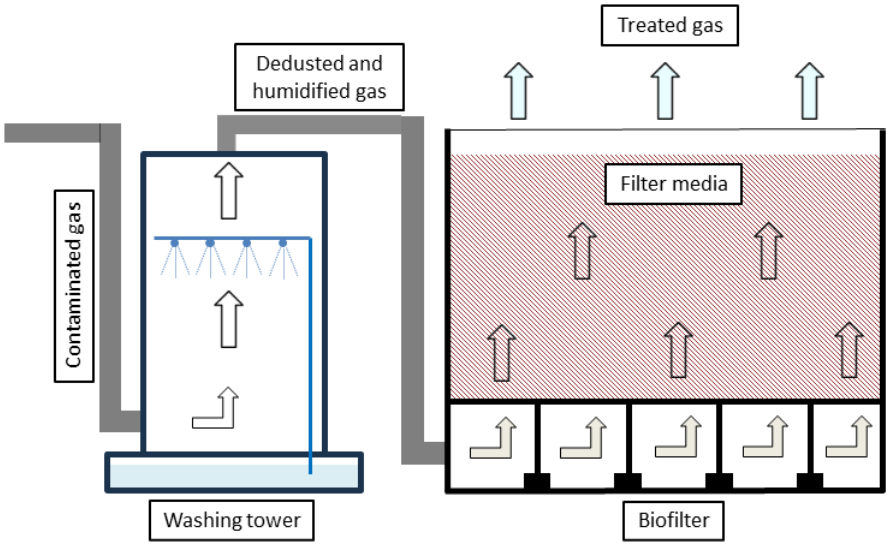


Figure 6. Schematic representation of a traditional biofilter used for biological waste gas treatment.

The packing material (filter bed) serves as the support medium for biofilm growth and provides nutrients required for microbial activity. The ideal filling should be characterized by high porosity (50-80%), large specific surface area and high water retention capacity [98]. The most commonly used materials are:

- Compost and peat – very effective due to their naturally high density and diversity of microorganisms and richness in minerals.
- Wood chips and bark – often used as additives to increase the porosity of the filter bed and prevent its excessive compaction.
- Inorganic materials (volcanic lava, expanded clay) – used less frequently, primarily to provide structural stability and reduce flow resistance.

Conventional biofilters are distinguished by low investment and operating costs and simple operation. Their significant advantage is the lack of production of secondary waste streams. This technology demonstrates very high efficiency in removing odors and low concentrations of VOCs. Despite these advantages, this solution has certain imitations, including the large space occupied by the installations and the difficult control of crucial process parameters, such as pH or humidity inside the filter bed. Additionally, the organic materials used are subject to natural degradation and clogging over time, which makes it necessary to replace the filling every few years [92–94,97,99].

3.3.3 Bioscrubers

A bioscrubber, also called a biological scrubber, is an advanced gas purification system that, unlike biofilter, separates the processes of physical absorption of pollutants from their biological degradation [97,99]. This device consists of two separate units: an absorption tower (scrubber) and a bioreactor with suspended biomass, usually in the form of activated sludge [17,75,97]. The absorption tower often contains a packing, e.g. Raschig or Pall rings, which increases the mass transfer surface, facilitating the passing of gases into the liquid. The bioreactor (aerated tank) functions similarly to the activated sludge tank in sewage treatment plants. Continuous aeration provides the oxygen necessary for aerobic mineralization of pollutants [17,97]. Another important element of the system is the separator (demister) located at the gas outlet from the tower. It serves to trap liquid droplets before releasing the purified air into the atmosphere.

Figure 7 presents flow scheme of a bioscrubber used for waste gas treatment. First, the contaminated gas enters the absorption tower, where it contacts the spray liquid in a countercurrent system. The contaminants pass from gas phase to the liquid phase. The contaminant-laden liquid is pumped to a separate bioreactor, where microorganisms suspended in a mineral salt solution metabolize the dissolved compounds. The purified liquid is returned to the top of the absorption tower, thus completing the cycle (recirculation).

Due to the need to dissolve contaminants in water before they degrade, bioscrubbers are primarily dedicated to removing compounds that are highly soluble in it. They effectively remove alcohols, aldehydes, ketones and inorganic compounds (hydrogen sulfide and ammonia) [94,97]. In the case of poorly soluble compounds, the performance of bioscrubbers can be improved by adding organic solvents (e.g. silicone oil) to the liquid phase in two-phase system [97].

Bioscrubbers are characterized by high operational stability and precise control of process parameters, such as pH and nutrient dosing. This allows for the effective treatment of gases with high pollutant concentrations (up to 5 g/m^3) [94,97–99]. Their significant advantage is the small area occupied by the installation and the lack of problems with clogging of the filling bed by biomass, which as mentioned before, is a common drawback of traditional biofilters [17,94,99]. On the other hand, this technology is associated with higher investment costs and complicated construction and operation. The main disadvantages include the production of excess sludge and

wastewater that requires further management, as well as the limitation of capacity only to substances that are easily soluble in water [94,97,99].

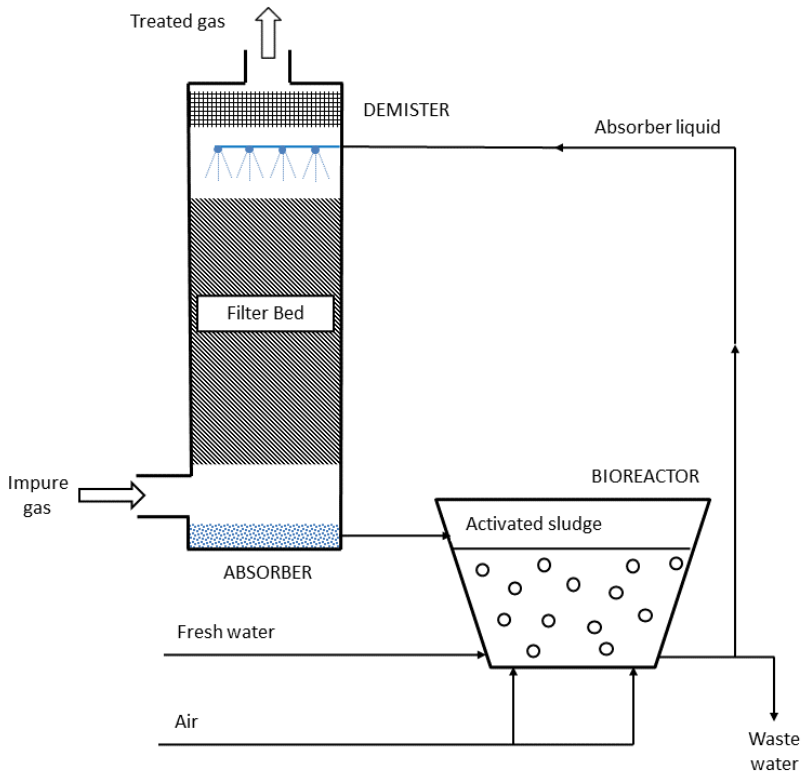


Figure 7. Process flow diagram of a bioscrubber consisting of an absorption column and a bioreactor.

3.3.4 Biotrickling filters

Biotrickling filtration is a gas purification technology that combines the features of a conventional biofilter and a bioscrubber [92,93]. The process involves passing contaminated gas through a filter bed with a chemically inert material on which a biofilm is deposited [93,94]. The key feature that distinguishes BTF from BF is the presence of a mobile liquid phase. The filter bed is continuously or intermittently sprayed with a mineral nutrient (salt solution) [93,94,97]. The contaminants removal mechanism is identical to that of previous types of biological gas treatment installations (absorption-diffusion-biodegradation). However, a typical BTF is designed as a vertical column, and the main structural elements of the installation also include inert packing, a trickling (spraying) system and a recirculation system.

Synthetic or inorganic materials are used as filling materials, such as plastic rings (e.g. Pall rings), ceramics, volcanic lava or polyurethane foam [93,94,97,99,100]. These materials must have a large surface area, high porosity and resistance to crushing and compensation. Additionally, they require microbial inoculation. Nozzles placed above the bed trickle the spray liquid. The liquid is then collected at the bottom of the reactor and transferred to the nutrient tank, from where it is returned to the top of the column by means of a pump (recirculation) [17,100]. To optimize mass transfer, a countercurrent system is most often used. Since the spray liquid is supplied from the top of the column, the contaminated gas is introduced from the bottom. Figure 8 shows an example diagram of BTF installation.

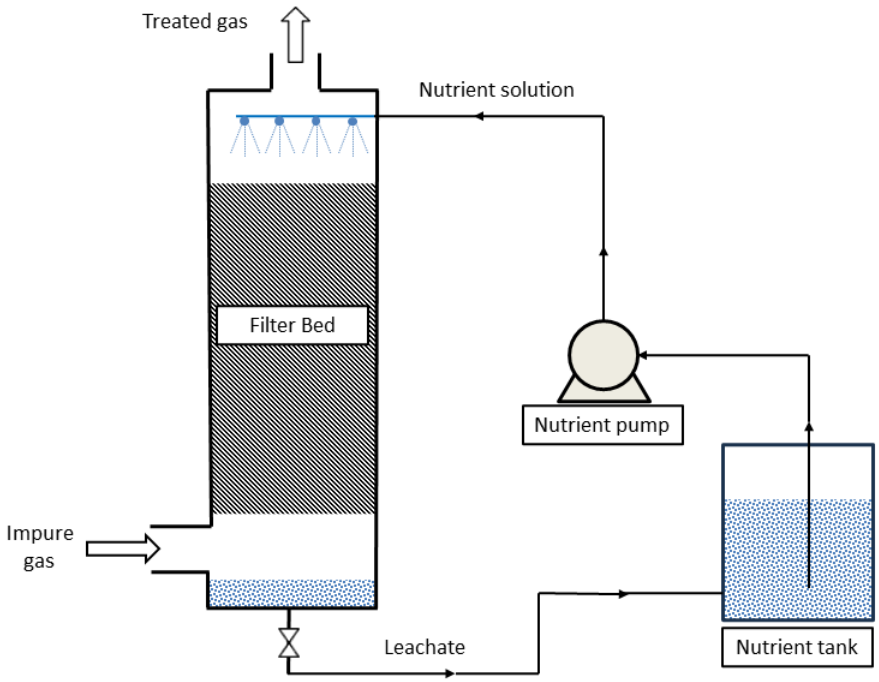


Figure 8. Process flow diagram of a biotrickling filter (BTF).

BTFs are extremely effective in removing a wide range of substances. Due to their constant contact with water, these reactors are excellent at handling alcohols, ketones and aldehydes [97,99]. These installations are standard in biodesulfurization processes (removal of H_2S from biogas, even at very high concentrations up to 12,000 ppm) and removal of ammonia and nitrogen oxides [101,102]. They also enable the removal of VOCs that are poorly soluble in water (e.g. toluene, styrene), often using additives that improve mass transport, e.g. biosurfactants [93,94,99,100].

BTF technology offers high efficiency and compact dimensions compared to traditional biofilters. The liquid phase allows for precise control of operating parameters such as pH, temperature and nutrient dosing [17,101]. BTFs are particularly recommended for removing contaminants that degradation leads to the formation of acidic products, because the trickling liquid continuously neutralizes and washes them away [97,101]. The main limitations include the risk of filter bed clogging due to excess biomass growth, which may lead to increased flow resistance (pressure drop) [98,99]. BTFs also generate a secondary wastewater stream (spent nutrient) and is associated with higher investment costs and more complicated operation than a traditional BF [17,94,97].

3.4 Odor compensation

Odor barriers and spraying (misting) systems constitute a distinct category of methods that differ significantly from traditional gas deodorization technologies. These systems, often referred to as fog walls or anti-odor/osmogenic barriers, are used to reduce odor nuisance emitted by industrial facilities such as wastewater treatment plants, landfills and composting facilities

[18,103]. Their primary purpose is to introduce substances into the gas stream or directly into the environment that alter the nature of the odor (masking) or permanently eliminate it (neutralization).

Odor masking works by replacing an unpleasant odor with a pleasant one through the introduction of a stronger scent that blocks the perception of the foul smell. However, this does not remove the pollutants themselves from the air [18,104]. Odor neutralization (counteraction) is a more advanced process in which the active ingredients of the anti-odor preparation undergo chemical reactions (oxidation-reduction, acid-base) with odor molecules. This leads to a change in the structure of the odor molecule, weakening its bonds or converting it into an odorless form [105]. For example, hydrogen sulfide might react with the anti-odor preparation to form sulfate ions and water [105,106]. The types of anti-odor preparations can be divided into three main groups. The most commonly used are natural plant extracts (essential oils) such as eucalyptus, lemon, pine, tea tree and coconut oils [18,105]. Second group is plant-based deodorants such as crystal-like materials derived from herbs that release volatile compounds which react with odors, exhibiting antibacterial and odor-neutralizing properties [106]. Surfactants, as the third group, they can be used as physical barriers (e.g. foam on slurry) that limit the release of ammonia and facilitate the action of odor-degrading bacteria [11,105].

Traditional technologies are termed end-of-pipe methods [103,107]. Anti-odor barriers and misting systems differ from the methods discussed above in several important ways. First and foremost, they are used predominantly for diffuse emissions. Unlike traditional methods, misting systems are ideal for surface and volume sources that cannot be easily sealed and enclosed [103]. Examples include compost piles, open sludge tanks and the working face of a landfill. They are also characterized by the absence of complex infrastructure. These methods do not require the construction of exhaust installations, the hermetization of facilities, or the construction of tall emission stacks [105]. The system consists mainly of pressure pipes and nozzles, making it easy to install and mobile. The equipment may be moved depending on the current source of odors. A photo of misting (spraying) system and the mist canon is shown in Figure 9.

From a technical standpoint, spraying systems utilize an atomization mechanism. Instead of passing gas through a sorption bed, these systems atomize a liquid to create a mist with droplet sizes of 0.04 mm or smaller [105]. Microdroplets have a large surface area and high kinetic energy, which allows them to capture and counteract odor molecules directly in the air [16,105]. They thus provide immediate deodorization as soon as they are activated, whereas biological systems, for example, require time for the microorganisms to adapt [18,103,107]. In fact, these systems generally have lower capital costs, although operating costs depend on the price of the anti-odor preparations used and can by relatively high. This depends on how often the odor source is sprayed with the preparation and on its concentration [18,103].

The main limitation of spraying systems compared to traditional methods is their dependence on weather conditions [104]. Strong winds can blow the mist away from the odor nuisance area, which drastically reduces the effectiveness of the external barrier. Therefore, precise dosing and careful selection of nozzle locations are crucial [18,104]. Unfortunately,

anti-odor preparations are quite controversial among residents of areas plagued by odor nuisance. Firstly, they can mask so-called warning odors that signal the presence of toxic substances [18]. Secondly, anti-odor products lack thorough verification. Many commercially available preparations do not have chemical safety certifications, and their mechanism of action is not always fully understood. They also cause what is known as secondary nuisance. If uses in excessive dose, the preparation's scent itself (e.g., pine) can become a source of complaints from residents [18,103]. In summary, misting systems and odor barriers are effective supplementary tools, particularly for diffuse emissions. However, their use requires precise dosing and consideration of specific local metrological conditions.



Figure 9. Odor emission reduction system based on aerosol misting technology (spraying installation and mist cannon).

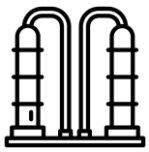
3.5 Summary of the described deodorization methods

Selecting the optimal deodorization technology is not a simple process and does not allow for a clear ranking of methods from best to worse. Although from an ecological and social perspective, complete emission prevention remains the most beneficial solution, in industrial practice, continuous improvement of gas treatment systems becomes crucial. The decision to select a specific solution must be preceded by a thorough analysis of the gas stream's chemical composition and physical properties. Then a comparison of this data with the technical advantages and disadvantages of the available methods (Table 1). In the design process, engineers are rarely guided solely by efficiency. Budget constraints and available installation space are equally important. Due to the complexity of pollutants mixtures, it often turns out that the most effective and economical approach is to use hybrid systems, combining several different

techniques. The choice is based on a number of criteria, such as emission intensity, type of odorants, applicable legal standards and social aspects, including a history of complaints from local residents.

An essential element of the investment preparation is the use of scientific literature and conducting tests in pilot installations. This allows for the achievement of the required efficiency on an industrial scale. However, it is important to underline that even the most advanced system may fail to meet expectations if all emission sources are not properly identified. Particularly problematic are so-called unintegrated emissions, which can drastically reduce actual treatment efficiency compared to results obtained in laboratory conditions. In summary, effective deodorization is the result of finding a compromise between technological efficiency and economic viability. Each case requires an individual approach, sound engineering knowledge and precisely tailored technology to the specific needs of the facility.

Table 1. Summary of the advantages and disadvantages of deodorization methods.

Deodorization method	Advantages	Disadvantages
 Absorption processes	Low investment and operating costs Simple system design Easy and safe to operate No dust removal from treated gas High efficiency Easy coupling with other methods Desorption of absorbed compounds	Generation of secondary waste Difficulty regenerating the absorbent Possible secondary emission of absorbed substances Corrosion of the installation Problems with disposal and storage of the resulting waste
 Adsorption processes	High efficiency Removal of contaminants present in concentrations of several ppb Easy of coupling with other methods Possibility of bed desorption Desorption of absrbed compounds	Adsorbent are sensitive to solid contaminants Requires pre-treatment and dedusting of gases Numerous adsorbent poisons Desorption requires large flows of regeneration gases
 Thermal neutralization	Can be use with any type of gas Recovering reaction heat Catalysts allows for reduced energy consumption and fuel savings Very high efficiency No secondary waste Simple system design	High investment and operating costs High concentration of flammable substances is required High risk of system corrosion High catalysts costs Generation of by-products (CO, NOx)
 Biological gas treatment	No secondary waste High effectiveness Low investment and operating costs Complete neutralization of odorants by microbes Good for gases with low pollutants concentrations	Contaminants must be water-soluble Sensitivity of microbes to changing conditions Need to control filter bed activity Large surface for the installation Need to control excessive biomass growth
 Odor compensation	Low installation complexity Low investment costs Wide variety of anti-odor preparations Effective for temporary odor nuisance prevention Immediate results	Can only be used at low odor concentrations Complex process mechanism Effectiveness dependent on atmospheric conditions Possibility of masking compounds toxic to humans

4. Methods of odor impact analysis

4.1 General information

Effective combating odor nuisance requires the use of precise analysis methods that allow for an objective assessment of its impact on the environment. Odor analysis measurements techniques enable the treated air to be characterized qualitatively and quantitatively. They are used to identify key odorants emitted from a given plant, monitor odor nuisance countermeasure processes undertaken, and even model the dispersion of malodorous substances. Modern techniques of odor impact analysis might be divided into two main groups: instrumental (analytical) methods and sensory methods. Each of this approaches provides different information and has specific advantages and limitations [38,50,108]. Since the former focuses on individual odorants and the latter on the overall olfactory sensation using them separately is absolutely justified, as it is conditioned by the specifically defined objectives of the measurements campaigns.

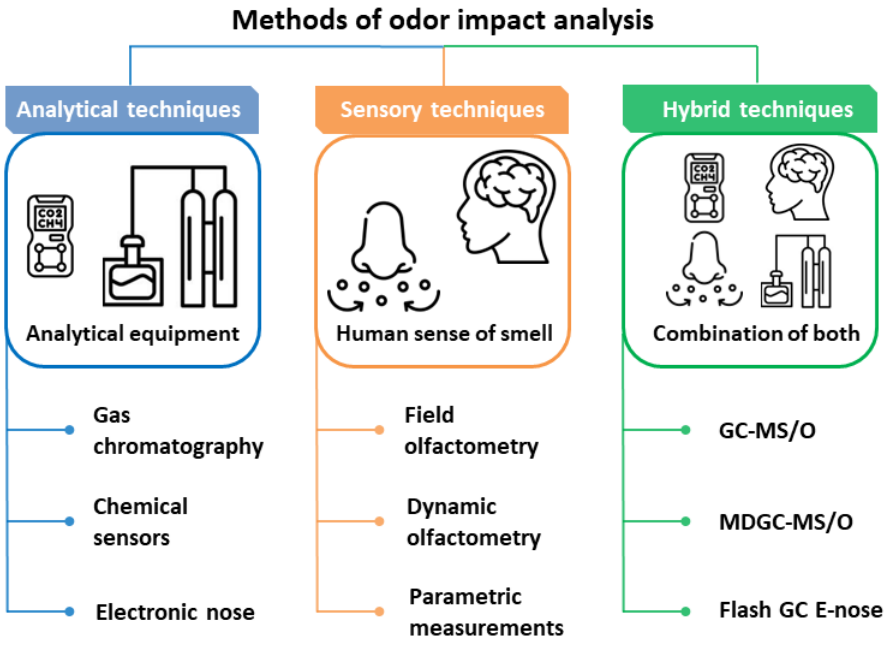


Figure 10. General structure of the division of measurement methods used in the assessment of odor nuisance.

Sensory methods utilize the human nose as a detector, allowing for direct assessment of odor perception, its strength, and character. This approach is considered the most reliable in assessing odor nuisance perceived by humans [10,21]. Analytical methods use research equipment to identify the chemical composition of gas mixtures and determine the concentrations of individual odorants. They provide objective and repeatable data that are essential for the design of gas purification systems and the control of technological processes [21,108]. The general structure of the division of measurements methods used in the assessment of odor nuisance is illustrated in the Figure 10.

The choice of the appropriate method depends on the specific nature of the problem, the type of emission source, and the expected results [25,38,108]. It should be emphasized that analytical methods do not always directly correlate with human odor perception. This is due to the phenomenon of synergy, masking or low OTs of some compounds, which may be lower that detection limits of the instruments [10,38,50,108]. For this reason, modern analytics strives to use an integrated approach, combining sensory and instrumental techniques (e.g., Gas Chromatography-Olfactometry, GC-O). This would allow to obtain a comprehensive picture of odor nuisance (taking into account their chemical concentrations, olfactory thresholds, odor intensity and hedonic tone) and to develop effective strategies to reduce it [22,25,38,50].

4.2 Sensory techniques

For sensory measurements, the human sense of smell is used as a detector. Using dynamic or field olfactometry, it is possible to determine odor concentrations expressed in odor units per cubic meter (ou/m^3), while parametric measurements are used to project odor intensity, odor character, and hedonic quality [109,110]. The main limitations of these methods are related to the subjective nature of the measurements made, which depends on the encumbrances of the human sense of smell and the psycho-physical state of the panelist.

Emotional state, fatigue, olfactory adaptation, individual threshold of perception, all these and many other factors make these methods less accurate and repeatable than analytical ones. However, with their application, it has been proven, for example, that both excessive exposure to low concentrations of an odor theoretically considered pleasant, and short exposure to high concentrations of this type of odor may be irritating to human sense of smell [109]. Citizen science (parametric measurements) is also playing an increasingly important role, engaging residents in the process of monitoring odor nuisance using various types of surveys and mobile applications [38,108].

4.2.1 Field olfactometry

Field olfactometry (FO) is a sensory method used to determine odor concentration directly in the field (in-situ), without the need to collect samples. Unlike dynamic olfactometry (DO), which is mainly used to investigate odor emission at the source and requires laboratory tests, FO allows for the quantitative assessment of odors in ambient air, directly at the place where they occur, e.g. at the plant boundary or at a potential receptor point [111,112].

Portable devices called field olfactometers are used for measurements. The most common on the market and described in the literature is the Nasale Ranger (St. Croix Sensory, USA) olfactometer. This device is equipped with two carbon filters and a dilution to threshold (D/T) dial, ranging from 2 to 500 D/T values. The operator (assessor) places the device mask on the nose and breathes at specific rate, gradually changing the mixing ratio of ambient and filtered air. In the first step of the analysis, only pure air is inhaled. Then, after about a minute, the valve setting is changed gradually increasing the volume of air bypassing the activated carbon filter.

This causes an increase in the concentration of odorant active substances in the inhaled air. The analysis continues until the assessor smells the odor for the first time.

The result of field olfactometry measurement is the numerical value of the dilution to olfactory threshold (D/T) ratio read from the dilution dial on the front of the olfactometer. This parameter should be interpreted as the number of dilutions needed to make the odor of contaminated air undetectable for 50% of the evaluation team members [22,38,50]. It must then be correlated with odor concentration expressed in ou/m^3, although FO itself is not covered by the EN 13725 standard [109,112]. However, The D/T values correspond, after conversion, to the Z_{ITE} value (individual estimation of the dilution to threshold) defined in EN 13725 standard. Z_{ITE} has to be calculated for each team member separately according to the relationships:

$$Z_{YES} = (D/T)_{YES} + 1 \tag{7}$$

$$Z_{NO} = (D/T)_{NO} + 1 \tag{8}$$

$$Z_{ITE} = \sqrt{Z_{YES} \cdot Z_{NO}} \tag{9}$$

where Z_{YES}/Z_{NO} is the dilution rate on which the odor was perceptible/undetectable. By calculating the geometric mean for the estimated individual Z_{ITE} values of all team members, the odor concentration is determined:

$$C_{od} = \sqrt[n]{\prod_{i=1}^{n} Z_{ITE,n}} \tag{10}$$

where n is the number of assessors.

This method is widely used in monitoring odor nuisance of various object, such as: municipal installations (landfills, sewage treatment plants and sewer systems), agriculture and industry (livestock farms, biogas plants, poultry farms, rendering plants), identification of emission sources, verification of resident's complaints and validation of mathematical model of odor spreading [38,111–113]. The practical application of field olfactometry to asses odor nuisance using the Nasal Ranger device is shown in Figure 11. The figure shows the assessor during the procedure of determining the D/T ratio.

An alternative to the Nasal Ranger is the Scentroid SM-100 field olfactometer (and its intelligent version SM-110), which offers a different technological approach to the preparation of the gas mixture [113,114]. While the Nasal Ranger relies on passive filtration of ambient air through activated carbon, the Scentroid SM-100 uses external source of compressed clean air from a cylinder. This solution allows for the maintenance of positive pressure in the Teflon mask, which more effectively isolates the assessor from background odors and prevent the ingress of ambient air from the side. This device has a much wider measuring range (D/T from 2 to even 30 000) and higher reading resolution, offering 15 dilution levels compared to 11 positions available in the Nasal Ranger [113–115]. The main operational limitation of this alternative is the need to transport a compressed air cylinder, the capacity of which directly limits the duration of the field inspections [114].



Figure 11. In-situ odor concentration measurement using the Nasal Ranger portable olfactometer.

FO offers a number of significant advantages, including the elimination of degradation or adsorption of substances on the walls of sampling (transport) bags. This methos is considered highly cost-effective and less labor-intensive compared to traditional DO, offering immediate results that allow for the rapid identification of emission sources and the validation of dispersion models [10,50,112]. Moreover, field devices show higher sensitivity at low odor concentrations (close to the OT values), which is difficult to achieve in laboratory conditions.

On the other hand, one of the drawback is its high subjectivity and the difficulty in maintaining full objectivity by the assessor, who, when seeing the emission source, may be subjected to visual suggestion [109]. The results are strongly dependent on uncontrolled atmospheric factors, such as wind speed and direction, humidity and barometric pressure. The operator himself is exposed to olfactory fatigue (adaptation) and saturation of receptors with the ambient odor [10,22,38]. Another limitation is the difficulty in distinguishing the odor of the tested source from background odors and the fact that this method has not yet been fully standardized on a European scale.

4.2.2 Dynamic olfactometry

Dynamic olfactometry (DO) is the only standardized method for determining the odor concentration of gaseous samples. In Europe, this process is strictly regulated by the standard EN 13725 *Air quality. Determination of odour concentration by dynamic olfactometry* (in Poland

PN-EN 13725). The latest update of this standard comes from 2022 (EN 13725:2022), replacing the 2012 standard [21,32,50]. It follows that DO has a strictly defined requirements for: sampling methods, e.g. from point sources, surface air or waste gases, ways of dynamic dilution of the tested gas stream, selection of people forming the evaluation panel and methods of interpretation of the obtained results.

DO is used primarily for the quantitative characterization of odor emission sources, which allows for verification of compliance with emission standards and limits specified in integrated permits. It is also a key tool in assessing the effectiveness of deodorization systems, such as biofilters or chemical scrubbers, by comparing odor concentrations at the inlet and outlet of the treatment installation [103]. The obtained results, after combining them with the gas volume flow, allow for the determination of the odor emission rate (OER). This is a necessary input parameter for mathematical atmospheric dispersion models used to predict the extent of odor nuisance in the vicinity of the plants [38,50,103].

The sampling procedure must ensure their representativeness and stability of chemical composition, which is crucial for the reliability of the result [22,116]. Samples are collected statically into bags made of inert and low-permeability materials such as Nalophan, Tedlar or Teflon (PTFE), which minimizes the risk of adsorption and chemical reactions on the walls [10,22,116,117]. It is possible to sample from both point sources (hall exhaust vent, tank vent pipe, roof fan) and surface sources (sewage lagoon, compost pile, landfill, open settling pond). For a point source, the emission parameters must be determined, e.g. emitter high, outlet diameter, gas velocity, temperature, volume flow and odor concentration. For a surface-active source (emission driven by gas flow), the air flow through the surface is usually more important, while for a surface-inactive source (emission occurs mainly by evaporation, diffusion and wind action), the surface, metrological conditions and the method of sampling are critical factors [32,116,117].

The most commonly used sampling technique is the lung sampler. This involves placing a sampling bag in a rigid, airtight container from which air is sucked out, indirectly filling the bag without the gas coming into contact with the measuring pump [116,118]. Figure 12 shows how to collect samples from two basic types of emission sources: point and surface. For point source, a sample is collected from a single, geometrically defined emitter, whereas for surface sources, it is necessary to limit the known emission area using a measurement chamber or other sampling system. In the case of hot or humid gases, it is necessary to pre-dilute the sample already at the sampling stage to avoid condensation of water vapor in the bag [22,32]. EN 13725 standard allows analysis up to 30 hours after collection, however, due to the rapid degradation of many odorants (e.g., sulfur compounds), it is recommended to shorten this time to 6-14 hours [32,116].

Measurements are performed using dynamic olfactometer, which is a device for precisely mixing an odor sample with neutral air purified by activated carbon [38,109,119]. The procedure involves presenting the panel with a series of increasing concentrations (decreasing dilutions) of the sample, usually in geometric progression. Two main response methods are used: yes/no, where the proband signals the detection of the odor itself, and forced choice, where the proband

must indicate the specific port from which the odor is emitted [109,120]. The standard gas flow rate in the nasal mask is 20 l/min and is controlled by precisely calibrated flow meters. The odor concentration, expressed in European Odor Units (ou_E/m^3), is numerically equal to the dilution factor at which 50% of the panel begins to detect odor and is calculated as the geometric mean of the individual thresholds [32,109,110,113,114,117].



Figure 12. Methods of sampling odor gases from point and surface sources for determining odor concentration by dynamic olfactometry.

The selection of the panel members (probands) is subject to rigorous statistical criteria to ensure that the team constitutes a representative group with average olfactory sensitivity [110,121]. Candidates are tested using a certified reference gas (n-butanol) and their individual detection threshold must be within a defined range of 20 to 80 ppb [25,38]. Furthermore, the standard deviation of their responses must be less than 2.3 ppb to ensure repeatability. The panel usually consists of 4 to 8 people who must adhere to a “code of conduct” before the test. They cannot smoke, use perfume, chew a gum or consume aromatic foods (e.g., coffee or garlic) for at least one hour before the session [32,113,122]. Panelists with symptoms of respiratory infection are strictly excluded from the measurements.

The main advantage of dynamic olfactometry is its direct link to human perception. This allows for the assessment of odor as a whole, taking into account synergistic and masking phenomena that chemical analysis cannot capture. It is the only method that is fully standardized and legally recognized in most EU countries as an objective basis for determining odor annoyance. The most important drawbacks include the lack of continuous monitoring and the high costs and labor-intensity of analyses. This method provides only quantitative data, without giving

information about the qualitative nature or hedonic tone of odors. Furthermore, its sensitivity is limited at very low concentrations found in ambient air, making it less suitable for direct measurements in built-up areas [110,123].

4.2.3 Parametric sensory measurements

Parametric sensory measurements are methods that allow for quick and relatively cheap odor assessment without the need for advanced laboratory equipment. Their goal is to describe odor as sensory experience, allowing for a direct link between emission and actual human perceptions of odor nuisance [22,110]. The basis for the modern assessment of odor nuisance is a set of parameters often summarized by the acronyms FIDOL (Frequency, Intensity, Duration, Offensiveness, Location) or CICOP (Concentration, Intensity, Character, Offensiveness, Persistence - see chapters 2.4 and 2.5) [50,124,125].

As mentioned in previous chapters, odor intensity (OI) and its hedonic tone (HT) are measured using point (categorical) scales in accordance with the VDI 3882 Blatt 1 or VDI 3882 Blatt 2 standards [125,126]. This approach allows trained panelists to assess odor strength in the case of OI. However, for HT, the most difficult task is separating the strength of the stimulus from its actual unpleasantness. This is the most subjective parameter, strongly dependent on a given person's experiences, memory and context [22,50,109,127].

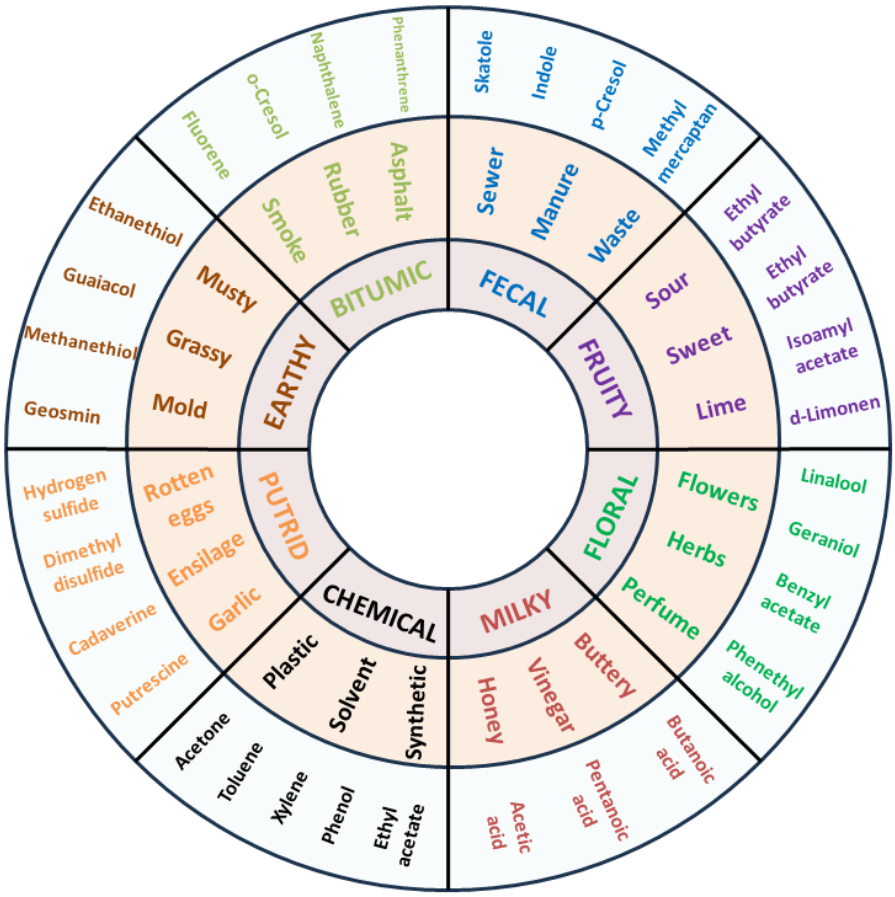


Figure 13. A classification of odor in the form of an *odor wheel*, including the main odor groups and their descriptors.

Odor character is used to identify the type of odor by assigning specific descriptors to it (e.g., rotten eggs, fruity, fecal). To objectify assessments, so-called “odor wheels” (Figure 13) are used, which systematize terminology for specific industries, such as sewage or waste management [10,110,126]. The goal is to facilitate the identification of the emission source when multiple facilities are present in a single area. Frequency and Duration are parameters that determine how often and for how long a given odor is present in the air. In field studies, these are typically assessed on 10-minute cycles, recording the presence of odor at 10-seconds intervals [124,125]. This data allows for the determination of so-called “odor hours”, the time during which an odor exceeds a specific nuisance threshold annually [50,127,128]. Modern research aims to combine the above parameters into one indicator, such as the Odour Air Quality Index (OAQI). OAQI aggregates data on concentration, frequency intensity and hedonic quality using empirical weights. The results allows for air quality to be classified on a 5-point scale, from “very good” (0-20) to “very bad” (81-100) [124,125]. The parametric approach is considered complementary to chemical analytics because it takes into account a phenomena of synergy and masking of odors, which cannot be fully interpreted by instruments alone.

4.2.4 Citizen science

Citizen science (CS) aims to increase knowledge and generate large data sets by promoting public participation and cooperation in scientific research. In odor analysis, this approach uses the human nose as the best available sensor, allowing for the mapping of odor nuisance at their location (at the receptor) in real time. Program participants (volunteers, residents) act as “sentinels”, identifying odor episodes that standard measurement methods fail to capture [129,130]. Citizen reports are based on a set of parameters defined by the FIDOL or CICOP concepts. Participants also often use odor wheels to help assign a specific descriptor to an odor [129–131].

Contemporary odor detection projects rely on digital technologies that facilitate the collection of data from large number of people. The most popular tools include mobile applications such as *OdorCollect,* (D-NOSES project), *Smell Pittsburgh, Corlu KODER,* and *Odor.net* [129–132]. They allow for quick geolocation of the report and description of the odor parameters. Traditional odor diaries are also used. Residents systematically record the duration, type and degree of odor nuisance [133]. Workshops and sensory walks (smell walks) are becoming increasingly popular. These serve to train participants, calibrate their sensitivity and collaboratively identify emission sources [129,133]. Table 2 lists some of the latest CS projects and application examples.

For CS to be considered a reliable data source, incoming reports have to be verified. One approach its metrological validation, which involves checking reports for consistency with wind direction and speed. This serves to eliminate complaints from areas outside the potential odor plume dispersion zone and resulting from citizen misconduct. Another approach requires the use of machine learning. Mathematical algorithm are trained on citizen data to predict future odor episodes based on process and weather parameters [129,130,132,133].

Table 2. Latest projects and application examples of citizen science in odor nuisance monitoring.

Location	Subject of the study	CS tools	Main research objectives	Ref.
Thessaloniki, Greece	Refinery, Municipal sewage Port Truck traffic	*OdourCollect* application Odor diaries Smell walks	Odor nuisance mapping Metrological validation of reports	[133]
Southern Italy (urban area)	Sewer system Sewage treatment plant Waste facility	Dedicated mobile application (*CS APP*)	Real-time monitoring Automatic report validation algorithm	[130]
Pittsburgh, USA	Odor episodes of industrial and anthropogenic origin	*Smell Pittsburgh* mobile application	Using resident reports to train ML models that predict odor nuisance	[132]
Plock, Poland	Refinery Sewage treatment plant Landfill (MTB installation0	Proprietary online survey Analysis of 10-year register of residents' complaints	Surveys and GIS data Impact on the quality of life of residents Identification of main emitters	[134]
Corlu, Turkey	Five organized industrial zones	*Corlu KODER* mobile application Complaint management platform	Correlation of residents observations with weather parameters and backward trajectory models	[131]

The primary factor in favor of developing CS for odor monitoring is the cost-effectiveness of such solution. Building a network of observers is significantly less expensive than installing a dense network of professional sensors or meters. Due to the often high level of citizen involvement, it is possible to obtain high-resolution spatial and temporal data. Furthermore, such pro-social activities increase the transparency of the facility, which builds trust and helps manage conflicts surrounding odor nuisance facilities. A limiting factor is certainly the lack of uniform legal regulations and models for collecting citizen data at the international level, as well as the high level of subjectivity of the reports received. They may be subject to errors resulting from individual characteristics (age, gender), experiences and psychological attitudes of participants. Moreover, the need to geolocate reports raises challenges related to the protection of participants personal data [129,132,134].

4.3 Analytical techniques

Instrumental analysis of odor nuisance is frequently used to monitor odor air quality. Unlike sensory techniques, analytical methods are also used to objectively and qualitatively determine the composition of malodorous compounds gas mixtures [21,110]. Therefore, they enable complementary qualitative and quantitative analysis. While, olfactometry provides only quantitative results, expressed in odor units, chromatographic techniques identify both specific substances and their chemical concentrations [109,135].

Analytical approach to odor emission control ensures the repeatability and accuracy of research, thanks to the use of high quality laboratory equipment. This eliminates the subjectivity inherent in odor assessments associated with sensory techniques. This allows for the optimization of monitoring and deodorization systems and provides the high standard of the obtained results.

On the other hand, there is the problem of translating chemical concentrations into the olfactory sensations that a given process or installation will evoke in humans. Low chemical concentrations do not necessarily mean the absence of odor nuisance. Limit of detection (LOD) of a device can also pose a problem, as they are often higher than the actual OTs of chemical compounds [136].

Bearing in mind that various interactions occur between odors, it might be concluded that analytical techniques, while offering undeniable benefits, also have certain limitations. However, the wide range of available techniques makes it possible to tailor the measurement methodology to a specific plant, emission source or sample type. Apart from classical chromatographic techniques, chemical sensors and gas sensor arrays (electronic noses), this group also includes fluorescence spectroscopy, differential optical absorption spectroscopy and the calorimetric tests [109,110].

4.3.1 Gas chromatography

Gas chromatography (GC) is the best analytical tool for monitoring the fate of individual odor-causing compounds, from their formation to potential neutralization or degradation [50,110]. Even in its simplest, one-dimensional form (single detector), it provides very high sensitivity and, above all, ensures repeatable analyses. Using the appropriate detector also enables the selective determination of compounds belonging to different chemical groups responsible for odor nuisance. An advanced form of this analytical technique involves coupling it with mass spectrometry (GC-MS), which acts as a precise detector. After ionizing and breaking down the molecules of the analyzed substances, their mass-to-charge ratio is determined, creating a mass spectrum unique to a given odor mixture.

From the perspective of odor nuisance, the LOD of chromatographic detectors poses the most serious limitations. As mentioned earlier, it often happens that the OTs of the substances are lower that the device's LOD. In such cases, the chromatogram is characterized by the absence of a specific peak despite a detectable odor. This is known as so called *odor gap* [21,109,136]. One way to address this phenomenon is preconcentration. This involves concentrating collected samples using various preparation techniques: thermal desorption (TD), solid-phase microextraction (SPME) or dynamic headspace (HS) [21,109,110,136,137].

The situation is completely opposite when co-elution occurs – chromatographic peaks overlap. This indicates that the matrix of the sample being analyzed is so complex and rich that classic one-dimensional GC may be insufficient. This most often occurs in environmental samples from sewage treatment plants, landfills or breeding farms. The solution to this problem is multidimensional gas chromatography (MDGC). It uses two columns of different polarities connected in series. This allows for the removal of a specific, unresolved fragment and its reseparation on a second column, drastically increasing the resolution [50,109,136]. Another approach involves the use of comprehensive two-dimensional gas chromatography (GCxGC). In this case, the entire sample is separated on two columns, allowing the identification of hundreds of compounds in a single analysis [138,139]. This technique, combined with time-of-flight mass

spectrometry (TOF-MS), enables the detection of trace odorants previously masked by dominant matrix components [21,139,140].

Knowing the composition of a gas mixture still does not allow it to be associated with the odor nuisance caused by it. Correlation between the instrumental and sensory characteristics of odor can be presented using carious indices. One of them is the odor activity value (OAV). This index is defined as the ration of the concentration of a given odorant to its OT (equation 4) [135,138,141,142]. Compounds with an OAV greater than one are considered to have a potential contribution to the overall odor of the mixture. By considering all substances present in the mixture, the overall OAV is determined as the sum of the OAVs values of the individual substances. The OAV is often used to build mathematical models to predict the total odor concentration (ou_E/m^3) [21,135].

Additional challenges with chromatographic detection include cost and time, sample instability, and the lack of analysis of odor interaction. Time consuming is associated with the need to collect samples, transport them to the laboratory and potentially concentrate them, which increases the analysis costs [109,138]. At each of this stages, sample matrix distortion may occur. This can be caused by compound degradation in the hot chromatograph injector, adsorption on polymer bag particles or simply poor sampling procedures [135,136]. Furthermore, odorants are analyzed separately, preventing the evaluation of synergistic phenomena, masking or neutralization of odors that occur in real mixtures [21,110]. This is where gas chromatography coupled with olfactometry (GC-O) comes into play, which is a key development of classical chemical analysis in odor research.

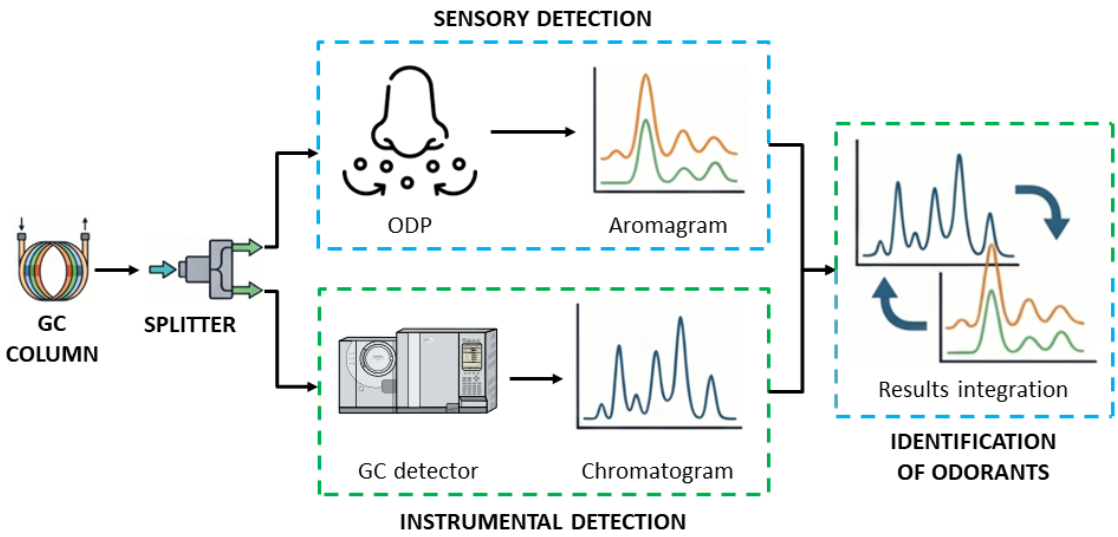


Figure 14. Simplified schematic diagram of the GC-O system for identifying odorants.

GC-O aims to combine the qualitative and quantitative chromatographic analysis of a sample with the sensory impressions it generates. After separating the gas mixture on a chromatographic column, the gas stream enters a flow splitter, which divides it into two parallel paths. The first path (instrumental detection) terminates with a physicochemical detector, most often a mass spectrometer (GC-MS/O) or flame ionization detector (FID). At the end of the second

path (sensory detection) is the so-called olfactometric detection point (ODP) [143,144]. The sensory line is heated to prevent condensation of compounds. Figure 14 shows the GC-O analysis scheme.

In the ODP, a trained panelist performs a real-time sensory evaluation, recording the odor's duration, odor character and intensity. To prevent drying of the panelist's nasal mucosa during long analysis, humidified auxiliary air is supplied to the port [136,138,144]. This is important because the quality of the results obtained largely depends on the comfort of the assessors. The assessor records the odor intensity and duration in real time. This is known as the intensity method (e.g., OSME), which produces a graph, so-called Aromagram, resembling a classic chromatogram. The peak height corresponds to the maximum intensity of the odor, and its width to the duration of the stimulus [109,110,138,144].

4.3.2 Application of chromatographic techniques in odor nuisance control

Available instrumental techniques are effectively used in a variety of areas related to odor monitoring, encompassing both municipal emission and industrial and agricultural processes. Advanced systems such as GC-MS and GC-O enable precise identification of odorants and understanding their individual contribution to overall odor perception. Table 3 presents selected examples of the application of chromatographic techniques in research and operational practice, taking into account the variety of monitored facilities, such as sewage treatment plants, landfills, and livestock farms.

Table 3. Selected applications of GC methods in the analysis of odorous emissions from various sources.

Research object	Methodology	Application / Main conclusions	Ref.
Drinking water (odor episode study)	GC-MS/O	The human nose was more sensitive than the GC-MS, geosmin was detected at 0.5 ng/L	[145]
Animal husbandry (livestock buildings)	SPME-MDGC-MS/O	Identification and ranking of priority odorants in dust and air	[146]
Construction products (with linseed oil)	TD-GC-MS/O	Comparison or identified and previously unknown odors	[147]
Sewage sludge (stabilization processes)	GC-MS/O	2,4,6-Trichloroanisole (TCA) has been identified as a key odorant in sediments	[148]
Food industry (cheese, coffee production)	GC-MS/O	Determining the odor profile of wastewater and products and their nuisance	[149]
Municipal waste landfills	TD-GC-MS/O	Identification of odor markers necessary for nuisance monitoring	[150]
Emission modeling (concentration forecasting)	GC/MS-O	Incorporating sensory data improved the accuracy of predictive models	[37]
Pu-Erh tea aroma	GC/MS-O	Identification of key odorants and the mechanisms of their formation	[151]
Biosolids (sewage sludge)	GCxGC-TOF-MS	High-resolution VOC identification in sludge aging processes	[152]
Mandarin juice	MDGC-MS/O	Precise identification of compounds responsible for undesirable odors	[153]
Municipal sewage treatment plant (technological stages)	GC-IMS	GC-IMS has been shown to effectively complement GC-MS in detecting compounds with low OTs	[140]

Research object	Methodology	Application / Main conclusions	Ref.
Bitumen and asphalts (from 13 refineries)	GC-MS	Predicting odor emissions based on chemical concentrations using AI algorithms	[154]
Sewage treatment plants (odor persistence)	TD-GC-MS	Determination of degradation kinetics and half-life of odorants	[155]
Chicken manure (composting process)	GC-MS	Identification of organic compounds conversion pathways and characterization of gas emissions during composting	[156]
Flooring products (with bitumen)	TD-GC-MS/O	Identification of groups of compounds responsible for odor nuisance, it has been shown that high MS signal does not always indicate a strong odor	[144]

4.4 Gas sensor array (electronic nose)

4.4.1 General principle of electronic nose operation

The electronic nose (e-nose) is an analytical device designed to mimic the structure and function of the human sense of smell and to reflect the complex processes that make up olfactory perception. The original application concepts of e-noses were based on holistic analysis of odorous gas mixtures. The technology aims to recognize the global character of an odor, identifying it as a whole without having to separate gases into individual substances. This requires the use of a range of electrical and electronic components and chemical gas sensors in combination with statistical signal processing and mathematical modeling techniques. By using several non-selective gas sensors, that rages of operation overlap, it is possible to obtain a so-called *fingerprint* of a given odor mixture [157–159]. This is unique data pattern generated by a sensor array for a specific odor. It allows, among other thigs, for quick attribution of odors to specific sources [160], verification of product authenticity [160,161], and medical diagnosis by detecting disease markers [159].

The principle of operation of e-noses directly replicates all the processes occurring during smelling in the biological olfactory system. Each stage, tissue and receptor has its electronic or mathematical counterpart. Although e-nose technology has been improved and developed over the last few years, it still does not match the human sense of smell in terms of detection range [25,159,162–164]. In the case of olfaction, odor molecules reach the olfactory epithelium, where they interact with receptors, generating nerve impulses. These impulses are then transmitted to the olfactory bulb and then to the brain, which interprets the signal based on previous experiences [25,165,166]. In e-nose, this process follows the pattern of sampling-detection-signal processing-recognition. So technically, the device structure may be divided into four subsystems, each corresponding to a different mechanism involved in odor recognition process. Figure 15 schematically presents an analogy between the operation of human olfactory system and the electronic nose.

The first subsystem is sampling system that acts as a human nasal cavity and reflects the smelling mechanism. It consists of a diaphragm pump that generates flow, tubes, valves and flow meters that control the timing and rate of gas injection into sensor chamber. Filters are also

often used to purify the carrier air (reference gas), used to restore the sensors to their baseline state after measurement [157,160,161,164]. In environmental monitoring using e-noses, passive methods are commonly used, in which gaseous samples reach the device by freely spreading into the atmosphere. Regardless of whether the system operates in active or diffusion based mode, all components in contact with the gas must be chemically inert to prevent unwanted interaction of the analytes with the system's surface [157,167]. Because factors such as humidity and temperature critically affect measurements precision and can change the odor fingerprint profile, these parameters need to be constantly monitored [168,169].

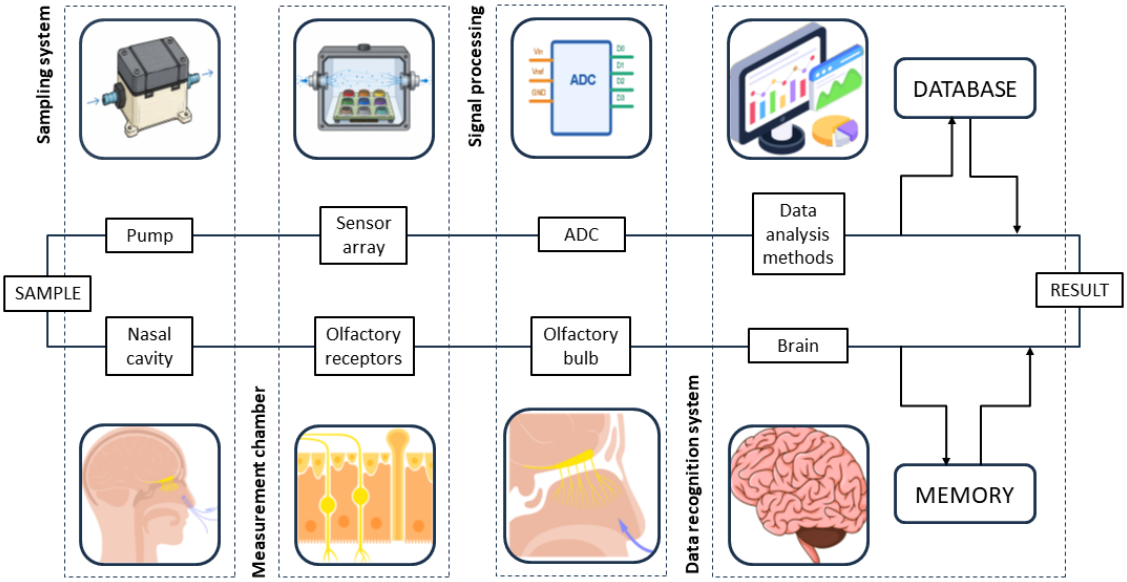


Figure 15. Schematic comparison of the mechanism of odor perception in the human olfactory system and the process of odor analysis by e-nose.

The detection system (sensors chamber) mimics the functions of the olfactory epithelium and consists of an array of several or a dozen sensors. The most commonly used sensors are non-selective or partially selective, which causes their signals to overlap, generating a multidimensional array response (aroma fingerprint) [158,170]. This mechanism is an analogy to human perception, where millions of olfactory receptors respond simultaneously to incoming aromas, creating complex patterns. Based on the output signal from the sensor array, it assigns the sample to a specific pattern from the database [158,163,165]. In terms of sensitivity, modern electronic sensors detect substances at the ppb level, although those in the ppm range are more common. However, this still does not compare to the human sense of smell, which, thanks to its vast number of receptors, might reach detection thresholds in the ppt range [169–171]. A significant advantage of e-noses is the ability to detect substances that are completely odorless to humans, such as carbon monoxide or explosive markers [157,169]. An additional benefit is the modular configuration of the array, allowing for easy replacement of individual sensors and adapting device to various tasks. In order to ensure a stable working environment for the sensors, cooling systems, sample dilution or system stabilizing the microclimate in the chamber are used without interfering with the structure of the sample itself [164,172,173].

The next system is the data acquisition (signal identification) system, which acts as a linker between chemical analysis (sensors) and mathematical signal processing. Its main task is to amplify, average, filter and digitize signals to convert chemical information into an antically useful form [157,173]. For humans, the odor stimulus equivalent to the output signal from the matrix is transmitted by nerve receptors to the olfactory bulb and then to the brain, where the information it carries is recognized. In the case of sensor array technology, signal processing is carried out using electronic devices in the form of transducers (conductivity, piezoelectric, optical, etc.). The electrical signals (voltage or current) obtained in this way are converted into a digital form (using an analog-to-digital converter), understandable by the processor and software [157,160,163,174]. Further signal processing, after conversion, requires statistical analysis methods, the most commonly used of which are discriminant analysis, multidimensional scaling, and correspondence analysis. These steps are crucial for the final results, as minimizing signal distortions significantly simplifies the qualitative or quantitative analysis of samples performed by the final e-nose subsystem.

The brain (olfactory cortex) is represented by a data recognition system equipped with pattern discrimination algorithms that classify odors based on a stored library of aromas. It is a computing unit (usually a computer or microprocessor) that analyzes the digital data it receives [159,163–165]. Biologically, this is a complex process in which, in addition to distinguishing the odor character, it is also possible to determine its intensity, hedonic quality, duration of the stimulus, and even recall the emotion that accompanied a particular odor when first encountering it [175]. In the case of electronic nose, it is necessary to use statistical methods and mathematical algorithms that compare the odor profile of the sample with the pattern available in the database. This process is divided into several key steps, the first of which is preprocessing. This includes normalizing and scaling signals to eliminate the effects such as humidity or sensor drift. The most relevant information is then extracted from the sensor response curves (feature extraction), which allows the data to be simplified into numerical from [157–159]. The final stage is pattern recognition, which lead to the identification of the odor. Methods of clustering or classification are used for this purpose, but research being conducted to develop e-nose technology toward adapting it for quantitative determination of odorants as well (predicting methods) [158,175].

4.4.2 Gas sensors used in electronic noses

Chemical gas sensors are the most important element in the e-nose design, as they serve as the biological equivalent of olfactory receptors. They are miniaturized measurement systems (transducers) that, regardless of their operating principle, contain an active layer that reacts with gas (odor) molecules [159,173,176]. Their task is to generate a measurable signal, such as a change in resistance, voltage, current or vibration frequency, by transforming physicochemical or chemical interactions occurring on the sensing layer [26,176,177].

For e-noses, arrays are formed that can consist of several different types of sensors. The type and characteristics of the sensors used in the matrix determine its analytical capabilities. These matrices must respond to odorants molecules, sometimes occurring in very low

concentrations, and in addition are often exposed to direct weather conditions. For these reasons, in order for a sensor to be used effectively in an artificial olfactory system, it should have a number of specific features:

- Limit of detection (LOD) – preferably at the ppt or at least ppb level to try to match the olfactory receptors [166,173].
- Cross-selectivity – they should be partially non-selective (respond to many different compounds) to create unique odor patterns [31,178].
- Reversibility – quick return of the signal to the baseline after inert gas flushing [174,178].
- Response time – short time to generate a signal after contact with an odor [160,173].
- Stability – minimizing the impact of humidity and temperature on the signal [172].

Considering the design and mechanism of converting chemical information into electrical one (transduction), the sensors most commonly used to construct arrays might be divided into the following classes:

- Chemoresistance (conductometric) – changes in the electrical resistance.
- Electrochemical – changes in current flow (amperometric) or electrical potential (potentiometric).
- Gravimetric (piezoelectric) – changes in the mass of the active layer (adsorption of odorants) cause changes in the vibration frequency.
- Optical – changes in light parameters (absorbance, fluorescence, refractive index).
- Bionic (biological) – active layer made of biomaterial (olfactory receptors, proteins, cells).
- MOSFET – field-effect transistors in which gas interaction with a catalytic gate changes the device parameters (threshold voltage, drain current, gate potential etc.).

The subsequent part of the thesis characterizes the gas sensors employed in the experimental studies (MOS, EC, NDIR, PID). The construction and main operating principles of the gas sensors used in the devices constructed for the research underlying this dissertation are described below.

Conductometric sensors measure changes in the electrical resistance of an active layer upon contact with gas molecules. The active layer can be composed of semiconducting metal oxides or conductive polymers. This material is placed between electrodes, allowing the change in its resistance to be recorded as a measurement signal. The most common group of chemoresistive sensors are metal oxide semiconductors (MOS). A typical MOS sensor consists of a substrate (ceramic element), electrodes, heating element and sensing layer (Figure 16). Depending on the semiconducting metal oxide used, a distinction is made between n-type MOS sensors (zinc oxide, titanium oxide) that respond to gases of reducing nature, and p-type (nickel and cobalt oxide) that generate a response to the presence of gases of an oxidizing character [26,178–180]. The heater maintains the sensor at elevated temperature, typically in the range of about 100℃ to 500℃, at which it exhibits optimal sensitivity.

The operating principle of MOS sensors is based on adsorption processes and chemical reactions occurring on the surface of the sensitive layer. In clean air, oxygen molecules adsorb

onto the sensing material surface, extracting electrons from the conduction band creating negatively charged oxygen species [26,170,180]. This phenomenon creates a charge carrier-depleted layer. This results in a specific base resistance of the sensor, which serves as a reference point for further measurements. When the gas mixture is introduced, odor molecules interact with the adsorbed oxygen, which lead to a change in the number of free charge carriers. In the case of reducing gases, electrons can be transferred back to the semiconductor. For n-type materials, this reduces the potential barrier, increases conductivity, and decreases resistance (oxidizing gases have the opposite effect) [177,180,181].

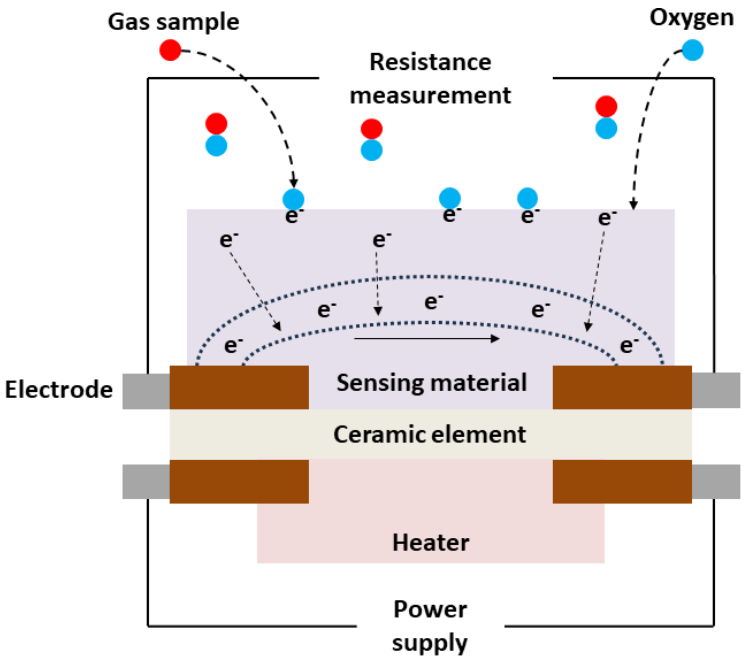


Figure 16. Schematic representation of the structure and operating principle of a MOS-type sensor.

The operational stability of MOS sensors is influenced by many factors, including the composition and morphology of the active layer, material doping, temperature, humidity and the use of auxiliary components such as filters. The response may be strongly dependent on humidity, and the sensing layer can be poisoned by certain volatile sulfur compounds or fatty acids. An additional complication is the need to operate at elevated temperatures, which increases power consumption [176,182]. Despite these limitations, MOS sensors are the most commonly used components in electronic nose arrays. This is due to their small dimensions, relatively low cost, good availability, and well-understood manufacturing technologies.

Electrochemical (EC) sensors, particularly amperometric, constitute an important group of sensors used in e-noses. The typical structure of such sensors (Figure 17) comprises an arrangement of three electrodes immersed in a suitable electrolyte (solid or liquid):

- Sensing (working) electrode – usually made of noble metal (platinum, gold) [167,170,178] and interacts with the odor molecule.
- Counter (auxiliary) electrode – closing the electrical circuit.
- Reference electrode – with a constant potential, serves to eliminate interference resulting from side reactions, which increases the precision of the measurement [166,167].

The operating principle of electrochemical sensors is based on measuring the current generated during the oxidation or reduction (redox) reaction of gas molecules on the surface of a working electrode. VOCs reach the electrode surface through a special diffusion barrier, and the generated current signal is proportional to the substance's concentrations [25,167,170,178]. The are characterized by low power consumption because they can operate at room temperature without the need for heating elements. This ensures a long operating life, which directly translates into signal stability and durability, making them ideal for battery-powered devices [160,182]. Additionally, their great advantage is that signal does not depend on humidity, which makes them extremely useful, especially in portable and environmental applications [25,182]. On the other hand, EC sensors are largely selective towards specific chemical compounds. While e-noses rely on cross-sensitivity, EC sensors are designed to detect specific substances, such as ammonia, hydrogen sulfide, sulfur oxides and nitrogen oxides [158,160,182]. Nevertheless, they are used in artificial olfactory devices, often as part of the hybrid systems, enriching the measurements data with valuable information regarding the concentration of toxic odor maker.

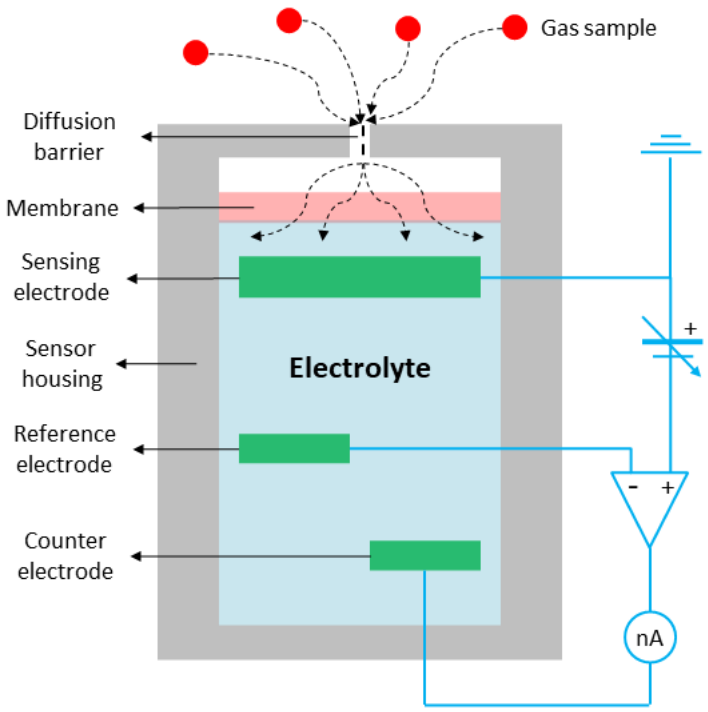


Figure 17. Schematic representation of the structure and operating principle of an EC gas sensor.

Optical sensor constitute another group of sensors used in e-noses. A typical optical system consists of a light source, measuring chamber or gas flow path, a sensitive layer and a light detector [162,167,182]. Their operation is not based directly on measuring changes in the electrical parameters of the active layer, as is the case with chemoresistive sensors, but on recording changes in the properties of electromagnetic radiation after its interaction with the analyzed gas. Depending on the design, detection may be related to changes in absorbance, fluorescence, luminescence, refractive index or polarization [31,167,176].

One of the most commonly used solutions are non-dispersive infrared sensors (NDIR), in which the source emits IR radiation passing through a chamber filled with the tested gas mixture.

The molecules of the gas being analyzed absorb radiation at a characteristic wavelength, and the reduction in the intensity of the light reaching the detector serves as the basis for determining the presence or concentration of a given compound. This method is particularly effective in detecting methane, carbon dioxide and carbon monoxide [162,176]. Such a system typically uses an optical filter that allows the selected range of radiation to pass through, and a detector, e.g., photon, pyroelectric, thermistor or thermoelectric, responsible for converting the radiation energy into a measurable signal [158,176] .

The main advantages of optical sensors include high sensitivity and selectivity, operational stability and lower signal susceptibility to humidity and temperature changes than in the case of many conductivity sensors. However, limitations include greater structural complexity, relatively high cost, higher power consumption and greater miniaturization difficulties, which may hinder their use in small, portable electronic noses [165,171,173,176,177].

In addition to classic optical sensors, photoionization detectors (PID) can also be used in electronic noses. These advanced analytical devices represent a bridge between optical and ionization techniques. They use UV radiation to ionize the gas molecules being tested, and measurement information is obtained from the ionic current. PID cannot identify a specific compound in a mixture because it is a non-selective sensor. However, it provides information on the total concentration of all detectable volatile organic compounds (TVOC) [162,173]. Therefore, it enriches the digital aroma fingerprint with data in the global concentration of ionizable substances. Consequently, in electronic nose technology, the PID sensor is often used as an element performing a complementary function in hybrid systems [167,170,173]. Figure 18 shows the construction and operating principle of a PID sensor.

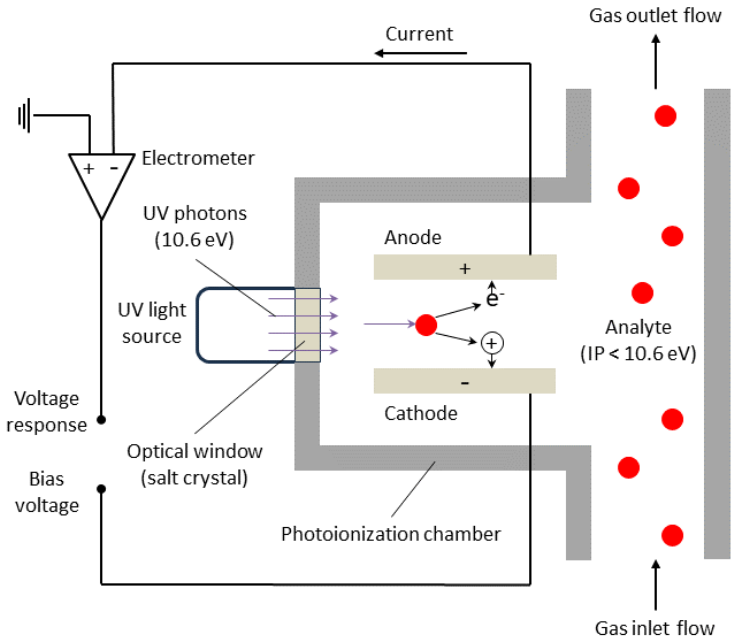


Figure 18. Schematic representation of the structure and operating principle of a photoionization detector.

The basic requirement for measurements using this type of sensor is that the substance must have an ionization potential lower than or equal to the energy emitted by the UV lamp

[25,167,173]. The detection mechanism is based on the photoionization of gas molecules using ultraviolet radiation generated by a high-energy lamp. Depending on the energy of the UV lamps used, the range of substances detected varies:

- 9.5 eV UV lamp – allows the detection aromatic compounds (benzene, amines).
- 10.6 eV UV lamp – the most commonly used, enables the detection of ammonia, acetone, ethanol and many other organic compound.
- 11.7 eV UV lamp – the widest detection range, acetylene, methanol and formaldehyde.

When analyte molecules enter the measuring chamber, photons strike them, causing an electron to be ejected and creating a positively charged ion. The resulting ions and electrons are attracted to the detector electrodes, generating an electric current measured by the electrometer [26,31,173]. The crucial advantages of PID detectors include their insensitivity to changes in air humidity, prompt regeneration and resistance to electromagnetic interference. They also feature rapid response times and the ability to operate at very low concentration levels (from ppb to ppm) [162,173]. Their main disadvantages include the need for frequent calibration, high cost and limited portability due to the delicate optical components [160,162,173].

4.4.3 Data processing and identification system

The learning and training process is the absolute foundation of electronic noses. Its purpose is to develop a specific rule, usually in the form of an algorithm or mathematical model, that allows for precise assessment of tested samples, both qualitatively and quantitatively. In the case of odor classification, the system compares signals with patterns stored in the database, while quantitative analyses use predictive models to calculate the concentrations of individual substances. Due to the vast number of variables generated by sensors, data processing, multidimensionality reduction and feature extraction are a crucial steps. All these stages make up the data identification system, the individual components of which are shown in Figure 19.

The first phase of data curation (management) is data preprocessing. This can be achieved through noise reduction and baseline correction (subtracting a defined level from the actual signal) or through normalization and standardization [166,174,183,184]. The latter processes unify the signal ranges, giving them a mean of zero and a standard deviation of one, facilitating direct comparison. This is particularly valuable for the subsequent use of artificial neural networks (ANNs) [162].

The next step is reducing the multidimensionality of the data, which is closely linked to the extraction of key signal features [174,185,186]. These procedures are essential to shorten computational time and increase the certainty of obtaining accurate results. While techniques such as independent component correction (ICC) and orthogonal signal correction (OSC) are used, the most popular choice remains principal component analysis (PCA) [166,183,185]. PCA works by examining the distribution of data variation and determining new, mutually perpendicular directions in space. This process involves rotating the coordinate system to maximize the variance of subsequent coordinates, called principal components (PCs). This allows for most of the variability to be explained by the initial factors. Furthermore, the analysis is simplified by the

extraction of signal parameters, which allows for the reduction of random errors and the assessment of sensor response speed. Most often, the signal is described by: amplitude (maximum or minimum), ratio or difference of the steady-state signal relative to the baseline, derivatives (primary, secondary) or fractional difference, and more advanced methods, e.g. curve fitting or signal analysis over time [158,184–189].

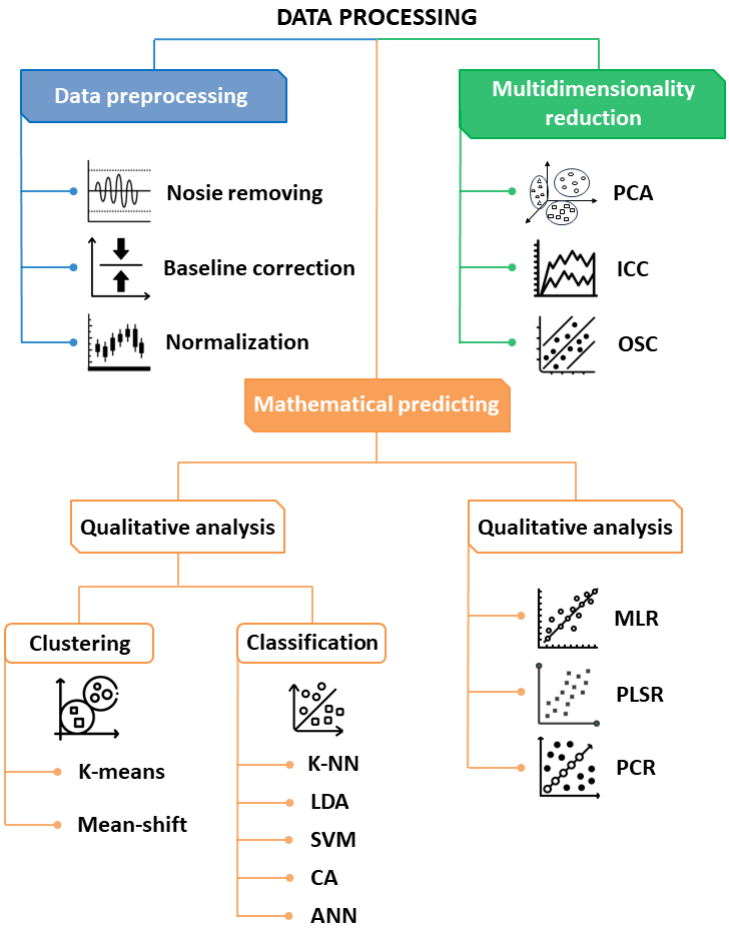


Figure 19. Structure of data processing and identification obtained from e-noses.

In the process of qualitative sample recognition using the electronic nose, after the multidimensionality reduction stage, clustering and classification processes are of key importance [174,183,188]. Clustering involves the systematic division of odors into classes and smaller subunits according to strictly defined rules. Classification, on the other hand, assigns unknown samples to specific groups based on their similarity to objects already classified there. The field of data science utilizes numerous statistical methods to accomplish these tasks. Mathematically, both approaches rely on determining the distance between points in space, which, defined in various ways, provides a measure of their relatedness. The principle is that the smaller the distance between points representing data samples, the greater their degree of similarity [166,174,188].

It's worth emphasizing that PCA goes beyond dimensionality reduction, representing a technique that straddles the boundaries of clustering and classification. Among standard cluster analysis methods, the K-means and Mean-shift algorithms occupy a key place [166,185,186,190].

Their task is to isolate groups of points that constitute subsets of the data generated by the sensor array. Elements within a single cluster share common characteristics, such as distance from each other, location in the same data space, or similar statistical distributions. This is because non-selective sensors in the array are simultaneously stimulated by specific VOCs. An example is the K-means algorithm, also known as the centroid method, which creates k clusters, aiming to maximize the similarity within the clusters while maximizing the differences between them. A significant limitation of these techniques is the need to pre-define the number of clusters [166,186]. This number can be arbitrary and often requires adjustments during the research or reliance on prior knowledge, which can prolong the analysis process [185].

The most commonly used classification techniques include k-nearest neighbors (k-NN), linear discriminant analysis (LDA), nonlinear support vector machines (SVM), canonical analysis (CA), and artificial neural networks (ANN) [158,162,183,185,188–190]. These methods belong to the supervised learning group, which requires operating on training and test datasets. During the training phase, the algorithm modifies input parameters to create a coherent logical model. The developed mathematical model is then used to predict results for test data, allowing for statistical verification of its precision and consistency with reference results. The key advantage of supervised methods, distinguishing them from cluster analysis, is the ability to generate a confusion matrix – a tool necessary to objectively measure the efficiency and effectiveness of the algorithm [189].

For example, to classify an unknown sample using the k-NN algorithm, the system analyzes the degree of similarity between the new observation vector and the confusion matrix containing the training data. This is done using mathematical distance measures such as the Euclidean or Manhattan distance [166,189]. The algorithm selects the k closest vectors from the training set and, based on the majority rule, assigns the tested sample to the group with the most representatives in the selected neighborhood. The main weakness of this method is its susceptibility to errors when classes are unequal in size - a larger group has a greater chance of "capturing" a new observation [183,185]. In turn, ANNs, due to their structure inspired by the human brain, are ideal for processing complex signals from gas sensors. Their learning involves precisely calibrating weights and activation thresholds, most often using a backpropagation algorithm. Although ANNs can handle nonlinear dependencies without parameter estimation errors, their structure remains implicit and difficult to interpret. Furthermore, this model is susceptible to overfitting and locking on local extremes, which can limit its effectiveness in predicting new data [185,191–193].

In addition to classification and clustering methods, supervised regression methods are also crucial. They are primarily used when the analysis aims not only to identify the sample type but also to quantify a selected parameter, such as the concentration of a chemical compound being analyzed, odor intensity, or sample contamination level. The most commonly used methods of this type include multiple linear regression (MLR), principal component regression (PCR), and partial least squares regression (PLSR) [185,191–195].

MLR is one of the basic statistical methods for describing the relationship between a set of independent variables and a dependent variable. In the case of e-nose data, the independent variables are most often the responses of individual sensors or features determined from their signals, while the dependent variable might be, for example, the concentration of the analyzed substance. The MLR model assumes that the relationship between these quantities is linear. Furthermore, this method requires meeting certain assumptions, such as the absence of strong collinearity between predictors, constant residual variance, independence of observations, and an appropriate distribution of model errors [192–196]. In practice, MLR can be limited by the large number of correlated variables, which is often found in sensor data and can lead to decreased model stability and overfitting to the training data.

PCR is an extension of the regression approach, which, prior to modeling, performs dimensionality reduction of the data using principal component analysis (PCA). Instead of directly using the original signals or sensor features, the regression model employs principal components, which are new variables that are linear combinations of the input variables. These components describe as much of the variability contained in the dataset as possible while simultaneously limiting the number of predictors. This allows PCR to reduce the impact of measurement noise, remove features with little informative value, and mitigate multicollinearity. After determining the appropriate number of principal components, a regression model is constructed, in which these components serve as explanatory variables [193–195,197]. This approach reduces the risk of overfitting, particularly when the number of variables describing the samples is large relative to the number of available observations.

PLSR is a method similar to PCR, but it differs in the way new latent variables are determined. In PLSR, model factors are constructed not only based on the variance of the independent variables but also on their relationship to the dependent variable. This means that this method seeks combinations of input features that best describe both the structure of the measurement data and the variability of the quantitative parameter being analyzed. Therefore, PLSR is particularly useful in analyzing multidimensional, highly correlated data containing a large number of features, which is typical of measurements performed with electronic noses. This method often produces more stable predictive models than classical linear regression, especially when the input data are complex and not all variables have direct analytical significance [192–195,197,198].

Undoubtedly, the challenges of processing data generated by gas sensor array can by looked out for on two levels. The first is the method, number and characteristics of the samples used in the training process. It is often the case that laboratory scale studies produce decently high concordance rates of class matches or mathematical models that quantitatively predict the composition of analyzed samples with high accuracy. In laboratory tests, it is possible to use wide range of concentrations of the substances to be determined, ensure stable conditions for sensors, and additionally get rid of substances that interfere with measurements. In real conditions, odor mixtures are characterized by high complexity and it is difficult to predict their composition even by constructing a gas sensor array for a specific process. The natural solution would seem to be

to increase the number of sensors, but this would increase the cost of the device and make it more difficult to select appropriate machine learning algorithms (by increasing the dataset), which has to be pointed as the second level of many challenges connected with data processing [199].

4.5 Overview of the application potential of gas sensor arrays

Gas sensor arrays appear to be a good alternative to both instrumental and sensory methods. The use of appropriate training, calibration and validation offers the possibility of teaching electronic noses to recognize and classify different groups of VOCs, to predict the odor concentration of a gas mixture or the chemical concentrations of its individual components. Some literature examples demonstrating the use of gas sensor arrays in these types of tasks are presented below.

4.5.1 Gas sensor arrays as a tool for analytical assessment of odor air quality

In e-nose research, analytical techniques play a fundamental role in objectively characterizing the chemical composition of odor mixtures. This allows for the precise identification of pollutant markers responsible for odor nuisance. Odor fingerprint analysis is becoming more accurate, which translates into optimized sensor selection for selectivity and the monitoring of technological processes and the effectiveness of exhaust gas treatment systems. A review of studies in which analytical techniques were used as a reference method in e-nose monitoring is presented in Table 4.

Table 4. A review of studies on the use of e-noses in monitoring odor air quality, in which instrumental techniques were used as reference or complementary methods.

Scope of research	Monitoring device	Reference technique	Data processing	Ref.
Odor emission monitoring from a compost pile	Lab-made e-nose with 7 MOS sensors	GC-MS	PCA CA	[200]
Determination of the compost maturity on the basis of VOCs emitted from the compost pile	Commercially available e-nose PEN3 (Airsense Analytics GmbH, Germany) with 10 MOS sensors	GC-MS	PCA PLSR Factor Analysis	[201]
Monitoring of air quality in terms of odor emissions in urban areas	E-nose prototype with 6 MOS sensors	TD-GC-MS	PCA PLSR	[202]
Early warning mechanism for anaerobic digestion process failures in the event of organic overload (laboratory scale)	Commercially available e-nose PEN2 (Airsense Analytics GmbH, Germany) with 10 MOS sensors	GC-MS	PCA	[203]
Identification and quantification of VOCs emitted during composting of municipal waste	Commercially available e-nose PEN3 (Airsense Analytics GmbH, Germany) with 10 MOS sensors	GC-MS	PCA PLSR	[204]
Monitoring odor air quality and odor emissions in urban areas	Self-made e-nose with 6 MEMS sensors	Gas analyzer	K-means PLSR	[205]
Development energy efficient device using photoactivation instead of traditional heating	2 different μLED sensors integrated on one platform	Gas analyzer	CNN	[206]
Development of an effective monitoring and decision support system to improve odor detection in a waste management facility	E-nose prototypes with 10 MOS and 32 CP sensors	GC-MS/O	PCA LDA	[207]

Scope of research	Monitoring device	Reference technique	Data processing	Ref.
Development and validation of a system for continuous measurement of odor emission in real time in a MWWTP	E-nose prototype seedOA with 13 MOS sensors	GC-MS	ANN	[208]
Construction and evaluation of the effectiveness of two complementary multisensory systems, e-nose and VE-tongue, for monitoring odors in water and wastewater	Self-made e-nose with 6 MOS sensors	TD-GC-MS SPME-GC-MS	PCA SVM	[209]
Assessment of the feasibility of using an e-nose to distinguish the processing conditions of alkaline (lime) stabilized sewage sludge	Commercially available e-nose PEN3 (Airsense Analytics GmbH, Germany) with 10 MOS sensors	GC-MS	PCA LDA	[210]
Comparative evaluation of two odor measurements methods (GC-MS and e-nose) used to identity and characterize emissions from MWWTP	E-nose prototype seedOA with 12 MOS and 2 EC sensors	GC-MS	PLSR LDA	[211]
Implementation of an e-nose system for continuous, real-time monitoring of odor emissions at the inlet to a sewage treatment plant	Commercially available e-nose Rubix WT1 with 4 MOS, 3 EC and 1 PID sensors	GC-MS Citizens science	PCA SVM	[212]

4.5.2 Gas sensor arrays as a tool for sensory assessment of odor air quality

Research on the use of gas sensor arrays in correlation with sensory techniques focuses mainly on the implementation of dynamic olfactometry (compliant with the EN 13725 standard) as the main reference method for the quantitative determination of odor concentration (ou_E/m^3). Using the human sense of smell as a detector allows for the effective training of artificial intelligence algorithms, such as neural networks (ANN) or support vector regression (SVR), to predict odor intensity continuously and objectively. Additionally, sensory methods including residents reports and field tests (field olfactometry, sniffing team) are a key tool for validating classification models, allowing the definition of normal operating regions and warning thresholds in the vicinity of industrial and municipal plants. A detailed overview of studies using sensory techniques as a reference for e-noses is presented in Table 5.

Table 5. A review of studies on the use of e-noses in monitoring odor air quality, in which sensory techniques were used as reference or complementary methods.

Scope of research	Monitoring device	Reference technique	Data analysis	Ref.
Monitoring odor emission from compost piles at various stages of maturity	Lab-made e-nose (7 MOS sensors)	Dynamic olfactometry	PCA	[213]
Development of fast, reliable and cost-effective technique for measuring the odor concentration emitted from tailings ponds on pig farms	Commercially available e-nose AromaScan A32S with 32 CP sensors	Dynamic olfactometry	PCA ANN	[214]
Development of an odor prediction model and assessment of the possibility of using e-nose for continuous monitoring of odor concentration inside the broiler house	E-nose prototype (24 MOS sensors)	Dynamic olfactometry	PCA PLSR	[215]

Scope of research	Monitoring device	Reference technique	Data analysis	Ref.
Measuring odor concentration from sewage treatment plant and examining the correlation between sensor response, DO results and H_2S concentration	Commercially available e-nose Neotronics NOSE (model D) with 12 CP sensors	Dynamic olfactometry	CA	[216]
Continuous monitoring of environmental odors directly at the receptor points	E-nose prototype EOS835 (6 MOS sensors)	Dynamic olfactometry	PCA k-NN	[217]
Assessment of odor emissions in the vicinity of landfills and estimation of odor nuisance zones in real time	Self-made e-nose (8 MOS sensors)	Dynamic olfactometry	CA MLR	[218]
Assessing the ability of recognition models to classify odors three years after their initial calibration	Lab-made e-nose (12 MOS sensors)	Parametric measurements	PCA ANN	[219]
Evaluation and comparison of the classification capabilities of two types of e-noses in the study of the odor air quality in the vicinity of a MSWPT	Commercially available e-nose HERACLES II E-nose prototype with 4 MOS, 2 EC and 1 PID sensor	Field olfactometry	PCA k-NN LDA	[220]
Continuous monitoring of odors in the vicinity of the composting plant and verification of resident's complaints about odor nuisance	E-nose prototype EOS 3 and EOS 9 (6 MOS sensors)	Dynamic olfactometry	k-NN Confusion matrix	[221]
Continuous classification and quantification of odorous emissions in complex industrial plants	E-nose prototype with 14 MOS and 1 PID sensors	Dynamic olfactometry	LDA	[222]
Implementation and comparison parametric and non-parametric prediction techniques to develop an effective model for quantitative odor determination	E-nose prototype seedOA (13 MOS sensors)	Dynamic olfactometry	ANN MLR PLSR	[223]
Development and validation of a two-stage model for real-time quantitative odor determination at the landfill boundary	Commercially available e-nose WT1 (Ellona) with 4 MOS and 2 EC sensors Commercially available e-nose EOS 507F (SACMI) with 6 MOS sensors	Dynamic olfactometry	PCA k-NN PLSR	[224]
Implementation and validation of two systems for continuous monitoring of odor emissions at the faceline of a waste treatment plant	Commercially available e-nose WT1 (Ellona) with 4 MOS and 2 EC sensors	Dynamic olfactometry	PCA SVR SVM	[225]
Evaluation and verification of the ability of the e-nose to quantify odor concentrations in real time at the landfill faceline	Commercially available e-nose Rubix WT1 with 4 MOS and 2 EC sensors	Dynamic olfactometry	PCA k-NN	[226]
Implementation of a system for continuous measurement of odor concentration in real time as the inlet to the scrubber in a sewage treatment plant	Commercially available e-nose WT1 (Ellona) with 4 MOS and 3 EC and 1 PID sensors	Dynamic olfactometry	PCA SVR	[227]
Comparison of two different regression models (linear and non-linear) for real-time quantification od odor concentration	Commercially available e-nose WT1 (Ellona) with 4 MOS and 3 EC and 1 PID sensors	Dynamic olfactometry	PCA PLSR SVR	[228]

4.5.3 Gas sensor arrays as a tool for monitoring deodorization processes

Odorant containing gas treatment techniques are particularly needed in the case of municipal services, industry and poultry and cattle farming. They ensure the reduction of odor nuisance and the amount of odor emitted per time unit (odor flux). However, it is necessary to monitor the effectiveness of such processes, preferably with systems that allow for continuous control. Such capabilities are provided by properly trained, calibrated and validated gas sensor arrays. Table 6 shows some of the most recent examples of the application of e-noses to control deodorization processes.

Table 6. A review of studies on the use of e-noses in monitoring deodorization processes.

Deodorization method	**Process control**	**Scope of research**	**Data analysis**	**Ref.**
Biofiltration (BTF) Membrane filtration	MultiRAE portable multi gas detector	Determining the effect of bed parameters and membrane type on the simultaneous removal of a mixture of VOCs, NH_3 and H_2S	Descriptive Statistics	[15]
Absorption (scrubber)	Commercial WT1 e-nose and DO	Estimating the odor concentration at the scrubber inlet	SVR	[229]
Biofiltration (BTF)	E-nose prototype with 5 MOS, 2 EC sensors and 1 PID GC-FID	Monitoring of BTF performance and response to disturbances (ethanol starvation)	MLR	[230]
Biofiltration (BTF)	E-nose prototype with 5 MOS, 2 EC and 1 PID sensors GC-FID	Assessment of the device's capabilities for estimating changes in odor intensity and butanol concentration	ANN	[231]
Biofiltration (BTF)	E-nose prototype with 8 MOS sensors GC-FID	Online monitoring of n-butanol removal in a transient state (from start-up for 12 hours until parameters stabilize)	MLR PCR PLSR	[232]
Biofiltration (BF)	E-nose prototype with 8 MOS sensors GC-FID	Monitoring and estimating the biofiltration efficiency of air polluted with a mixture of n-hexane, acetone and toluene	Liner logarithmic models	[233]
Absorption (scrubber)	E-nose NetPID Plus with EC, MOS and PID sensors and DO	Continuous monitoring of odor concentration at the inlet and outlet of a wet scrubber at a MSWTP	Non-linear models	[234]
Biofiltration (BF)	Commercial e-nose PEN 3	Reduction of VOCs emitted during composting of kitchen and garden waste	PCA	[235]
Biofiltration (BF)	Commercial e-nose PEN 3 and GC-MS	Assessment of α-piene removal efficiency depending on the type of compost used	PCA PLSR	[236]
Biofiltration (BTF)	E-nose prototype with 8 MOS sensors GC-FID	Assessment of the e-nose suitability for real-time monitoring of BTF performance	MLR	[237]
Biofiltration (BF)	Commercial e-nose AromaScan A32S	Evaluation of the suitability of the e-nose for monitoring the efficiency of odor removal in the operational conditions of a pig farm	PCA ANN PLSR	[238]
Biofiltration (BF) Spray tower (ST)	Commercial e-nose PEN 3.5 (with 10 MOS sensors) GC-MS PTR-TOF-MS	Waste gas treatment from a wastewater treatment plant in a textile dyeing plant	PCA	[239]

4.5.4 UAV-mounted gas sensor arrays for odor air quality control

In recent years drones or unmanned aerial vehicles (UAVs) have been rapidly transforming industries through their advanced capabilities and versatility related to environmental monitoring and industrial safety. Drones come in different configuration, each suited for specific tasks. Among them quadcopters are particularly favored for their maneuverability and stability, making them ideal for detailed inspections and measurements in complex environments. Fixed-wing drones are also employed, especially for covering larger areas during inspections [240]. For example, drones outfitted with thermal imaging cameras can detect heat leaks from industrial processes, while high-resolution RGB cameras facilitate visual inspections [241–243]. Additionally, UAVs equipped with GPS and internal measurement units (IMUs) ensure precise navigation and stable flight, allowing for accurate data collection and mapping of emissions [244,245].

The development of UAVs technology and advanced gas detection systems has enabled the creation of mobile monitoring platforms. This innovative technology integrates real-time gas detection capabilities of sensor arrays with the mobility of drones. Operators can control drones remotely, issuing commands from distance up to 1 km, which enhances operational flexibility and safety during inspections. This enables comprehensive assessments of harmful gases emissions, making the deployment of drone-mounted gas sensor arrays an appealing alternative for achieving precise and objective monitoring. In particular, they demonstrate the ability to quickly identify and analyze these emissions, which is crucial in mitigating their environmental impact and ensuring compliance with regulatory standards [240,244,246]. When mounted on drones, these arrays make it possible, among other things, to:

- Quick and precise emissions mapping – drones can travel over vast areas of industrial plants, collecting data in real time and creating maps of individual gas concentrations.
- Identification of emission sources – with the ability to precisely locate points with the highest concentrations and identify gas leaks or abnormal emissions, specific emission sources can be pinpointed, making it easier to take corrective action.
- Monitoring hard-to-reach areas – UAVs can reach areas inaccessible to traditional measurement methods, such as tall chimneys or enclosed spaces, what reduces the risk of accidents that could occur if human inspectors were to enter hazardous environments.

The use of gas sensor arrays attached to drones represents a significant advancement in environmental monitoring and industrial safety. First and foremost, from an environmental perspective, precise monitoring of emissions allows abnormalities to be detected more quickly and corrective action to be taken, minimizing the negative impact on the environment [247,248]. Moreover, it ensure the transparency of industrial plants because regular monitoring and sharing of measurement results builds public trust and show the plant's commitment to environmental protection. Companies must document their emissions and the effectiveness of control measures, often utilizing dispersion modeling and chemical characterization techniques to assess odor impacts. The real-time data provided by drones enhances compliance efforts, offering insights into the dispersion of odors and allowing for timely interventions to mitigate adverse effects on

surrounding communities. In addition, the rapid identification of sources of offensive odors enables effective response to complaints from local communities, which improves relations between the plant and residents. In other words, by utilizing drone-mounted gas sensor arrays, researchers and environmental consultants can improve the detection and mapping of odor emissions. This innovative approach allows for comprehensive assessments of odor dispersion patterns, facilitating targeted interventions to mitigate their impact on surrounding communities.

Recent studies have demonstrated the effectiveness of gas sensor arrays attached to drones in monitoring and mapping odor emissions from industrial plants. Such attempts to apply this technology have already been made by various research teams and examples of the implementation has been shown in Table 7.

Table 7. Deployment of UAV-mounted gas sensor arrays for industrial odor air quality monitoring.

Facility	UAV type	Monitoring device	Scope of research	Ref.
WWTP	Rotorcraft DJI Matrice 600 Pro	Gas sensor array (16 MOS sensors)	Mapping odors in real sewage treatment plant conditions	[244]
WWTP	Rotary-wing DJI M600	E-nose RHINOS with 16 MOS, 4EC and 1 NDIR sensors	Development of a system capable of quantitatively predicting odor concentration in real time	[245]
Urban areas	Hexacopter multirotor	Gas sensor array with 4 EC sensors	Development of a lightweight system for monitoring air pollution in hard-to-reach urban places	[249]
MSWTP	Quadrocopter DJI M350	Laser methane detector (Laser Falcon)	Testing an innovative mass balance method for estimating fugitive methane emissions	[250]
Landfills	Quadrocopter ALG-EOS	Gas sensor array with 5 MOS sensors	Development of a low-cost method for monitoring methane and carbon dioxide emission	[251]
Industrial areas	Quadrocopter DJI M100	Sniffer 4D system (CH_4, CO_2, CO, SO_2, NO_2)	Using a drone as a rapid mapping system to characterize greenhouse gas emission patterns	[252]
Breeding zones	Multirotor DJI Mavic Air 2	Gas sensor array with 4 MEMS sensors	Implementation of an intelligent, low-cost system for remote monitoring of air quality	[253]
WWTP	Quadrocopter DJI M300	U10 sensor (laser absorption spectroscopy)	Monitoring and quantification of methane emissions at the level of individual facilities	[254]
Coal mine	Multirotor DJI Inspire 1	Active AirCore technology (CH_4, CO_2, CO)	Quantification of methane emissions from point sources such as mine shafts	[255]
Landfill	Hexacopter DJI M600 Pro	ABB GLA133-GPC Analyzer (CH_4)	Evaluation of a mass balance method for quantifying methane emissions	[256]
Oil sites	Quadrocopter DJI Inspire 1 V2.0	Gas sensor array with 1 MOS and 1 NDIR sensors	Implementation of a drone-based system capable of real-time methane monitoring	[257]
National Forest Park	Small quadrocopter	Gas sensor array with 2 NDIR sensors	Development of an autonomous, lightweight system for precise pollution mapping	[258]
Industrial Park	Gyroplane Huanying No. 1	Multi-gas device BRD Mx6	Development of a method for effective monitoring of air pollution and its early detection	[259]
Industrial areas	Quadrocopter	Gas sensor array with CO_2 sensors	Monitoring air quality at a designated location, enabling the detection of pollutants at a specific height	[260]

4.6 Summary of the literature review and identification of research gaps

The literature review conducted showed a wide range of applications of gas sensor arrays in monitoring odorous air quality, technological processes and pollutant emissions. Previous studies have included the use of both instrumental techniques, particularly gas chromatography, and sensory methods as reference techniques for calibrating and validating sensor systems. Solutions enabling continuous prediction of odor concentrations and array application in real industrial and municipal facilities were also described.

In the field of monitoring deodorization processes, the literature confirms the feasibility of using gas sensor arrays in absorption, biofiltration, and trickling biofiltration processes. However, the solutions used differ in the range of compounds analyzed, the configuration of the sensor systems, and the method of assessing agreement with reference methods. Therefore, a significant research problem remains determining the extent to which sensor arrays can provide reliable quantitative monitoring of various deodorization processes under variable process conditions, including absorption processes using new, more environmentally friendly absorbing liquids (e.g., deep eutectic liquids). In the case of trickling biofilters (BTFs), despite previous applications of sensor systems to monitor their performance, the number of studies on simultaneous quantitative monitoring of several hydrophobic volatile organic compounds under variable process inlet load conditions remains limited.

In relation to the instrumental assessment of odor nuisance, the possibility of predicting the odor concentration and conducting continuous monitoring based on calibration with olfactometric methods was demonstrated. However, the method of converting sensory data into information reflecting not only the odor concentration but also its significance from the point of view of human perception still requires further development. Another significant challenge is the transfer of predictive models developed for single devices to multi-point systems operating long-term in variable field conditions, with the possibility of ongoing interpretation of spatial and temporal variability of odor nuisance.

Most publications still describe installations consisting of just two or less devices, typically arranged in a relationship: one at the plant boundary (faceline) and one at the nearest recipient (receptor). In the author's opinion the simplest odor monitoring network should consist of at least three devices providing real-time observation. Despite the author's best efforts, only two significant cases were found that met this assumption. One of them is odor monitoring system presented by Nicolas et al. [261]. FIDOR – a network of five identical gas sensor arrays (with 6 MOS sensors) designed for continuous, real time odor monitoring around composting plant. Second, the most extensive contemporary example, where a network of 15 devices placed strategically around a feed production plant in Germany was implemented, was presented by Mifsud et al. [262]. The network enabled precise mapping of as many as 12 different emission sources.

The low number of multi-device systems is likely due to the lack of standardization, calibrations costs and data complexity. Field procedures for Instrumental Odor Monitoring System (IOMS) are still not fully standardized, making large installations difficult to legally validate. Each

device in the network must be individually trained using for example expensive dynamic olfactometry, which with 10-15 devices generates significant costs. The large number of devices requires advanced cloud infrastructure (loT) and real time data processing systems, which is still perceived as an engineering challenge. IOMS technology is undoubtedly becoming more intelligent and weather-resistant, but in industrial and research practice, systems consisting of more than two devices are still rare and novel.

Furthermore the development of UAV platforms equipped with gas sensors has enabled spatial mapping of pollutant concentrations, localization of areas of increased emission and quantitative determination of selected gases. The literature also describes the use of UAVs to predict odor concentrations and determine methane emissions from landfills. However, the use of georeferenced multi-sensor data for spatial assessment of odor emissions from surface sources, identification of local zones of increased emission and further use of these data in modeling odor propagation remains a less well-researched issue. Another important development direction is the use of mobile UAV platforms to quickly identify local zones of potential danger associated with increased concentrations of toxic gaseous components, such as hydrogen sulphide, especially in the immediate vicinity of point elements of landfill infrastructure, e.g. degassing wells.

The identified research gaps therefore indicate the need for further research on gas sensor arrays, not only in terms of their ability to record responses to the presence of pollutants, but above all, in their reliable use in quantitative monitoring of deodorization processes, spatial assessment of odor emissions, and continuous, multi-point monitoring of odor nuisance in real industrial conditions. These problems formed the basis for formulating the main objective and research hypotheses of this dissertation.

5. Research objectives and scopes

5.1 Main objective and research hypotheses

The main objective of the doctoral dissertation was to demonstrate the potential of using appropriately designed and calibrated gas sensor arrays as rapid, relatively low-cost tools for monitoring deodorization processes and odor nuisance. It was assumed that, after proper calibration against reference techniques, the sensor arrays could provide results of sufficient quality for process and environmental applications, and that a significant advantage would be the ability to conduct measurements directly at the site of the phenomenon under study, without the need to collect and transport samples to a laboratory. To achieve the main objective of this thesis, the following research hypotheses were formulated:

1. Properly designed and calibrated gas sensor arrays can be used for quantitative monitoring of deodorization processes, including absorption processes, such as those using green solvents, and biological treatment of gas streams in biotrickling filters (BTF), enabling the determination of the concentrations of components in gas mixtures and the evaluation of process efficiency with a level of accuracy comparable to that of gas chromatography.
2. The integration of a gas sensor array with an unmanned aerial vehicle (UAV) enables the spatial identification and quantitative assessment of odor emissions and selected gaseous compounds from surface sources, including the localization of zones of increased emissions associated with degassing wells, and the data obtained can be used to assess total emissions and the spatial dispersion of odors.
3. Gas sensor arrays properly calibrated against olfactometric techniques can be used for continuous instrumental assessment of odorous air quality by determining odor concentration and classifying the results into categories that account for odor intensity and hedonic tone, and the integration of several such devices into a measurement network enables a spatial and temporal assessment of odor nuisance under real-world conditions at a waste management facility.

5.2 Scope and structure of the research

The first research hypothesis was tested based on studies covering various gas stream deodorization processes: absorption processes, including those using deep eutectic solvents (DES), and BTF biofiltration. The studies, results, and conclusions regarding absorption treatment of odorous gas mixtures are presented in chapters 6 and 8, respectively, while the studies on the biological process conducted at BTF are presented in chapter 7. The research presented in this chapters differed in the composition of the treated mixtures, the configuration of the sensor arrays, and the process conditions, however, they all addressed a common set of research objectives:

i. Conducting and characterizing deodorization processes using absorption and BTF biofiltration for gas streams containing selected volatile organic compounds (VOCs).

ii. Design and calibration of gas sensor arrays tailored to the properties of the mixtures being analyzed and the conditions of specific processes, using gas chromatography with flame ionization detector (GC-FID) as the reference technique.
iii. Development of mathematical predictive models that enable the determination of the concentrations of components in gas mixtures based on the multidimensional response of sensor arrays.
iv. Validation of the performance of sensor arrays and predictive models under variable process conditions, including, among other things, changes in mixture composition, process inlet load, and the type of absorption fluid used.
v. An assessment of the suitability of gas sensor arrays for monitoring the efficiency of deodorization processes based on a statistical comparison of results obtained from them with those obtained using GC-FID, and a determination of their potential for use as a faster and less expensive measurement tool.

The second research hypothesis was tested at an active section of a municipal landfill cell using an unmanned aerial vehicle (UAV) equipped with a gas sensor array. The results of the study are presented in chapter 9. The following research objectives were formulated as part of the investigation of the second hypothesis:

i. Conducting spatial measurements of selected gas components above the surface of the active landfill cell using a UAV equipped with a gas sensor array.
ii. Development and calibration of predictive models that enable the correlation of multidimensional sensor signals with odor parameters determined using dynamic olfactometry as the reference technique.
iii. Development of a spatial representation of gas concentrations and odor emissions based on georeferenced measurement data obtained during UAV flights.
iv. Identification of areas with increased odor emissions and estimation of total emissions from the active section of the landfill cell, with particular emphasis on areas associated with degassing wells.
v. An assessment of the suitability of data obtained from the UAV-sensor array system for modeling odor dispersion, by comparing the dispersion modeling results with a variant using data obtained via the reference method.

The verification of the third research hypothesis was conducted in two stages, involving the development and validation of a single gas sensor array for the instrumental assessment of odorous air quality, followed by the expansion of this solution into a multipoint measurement network operating under municipal waste treatment plant conditions. The research results are presented in chapters 10 and 11. As part of the investigation of the third hypothesis, the following research tasks were formulated:

i. Development, calibration, and validation of predictive models for determining odor concentration based on multidimensional signals from a gas sensor array, using field olfactometry as the reference technique.

ii. Determining the relationship between odor concentration, odor intensity, and hedonic tone, and using these parameters for the instrumental classification of odor air quality.
iii. An assessment of the feasibility of continuously monitoring changes in odorous air quality under field conditions using a single gas sensor array.
iv. Expanding the developed solution into a multipoint network of gas sensor arrays and calibrating it under varying seasonal and location-specific conditions at the MSWTP.
v. Long term validation of the odor monitoring network's performance under operational conditions, including an assessment of model stability and the ability to identify spatial and temporal changes in odor nuisance, including short term odor episodes.
vi. Integration of sensor array networks with the IoT infrastructure and the decision support system (DSS) to enable real time visualization and interpretation of data and to support the management of odor nuisance on the plant premises.

5.3 Methodological assumptions and integrity of the research concept

Due to the diverse nature of the analyzed processes, gas mixtures, and measurement conditions, gas sensor arrays with different configurations were used in subsequent stages of the research. The selection of the type and number of sensors was tailored in each case to the properties of the analyzed pollutants, the characteristics of the measurement environment, and the requirements of the specific application. A common element of all the developed systems, however, was a methodology that included multisensory measurement of the sensor array's response, calibration against a reference technique, development of a predictive model, and its validation. Thus, the focus of the research was not on a single universal hardware configuration, but rather on the possibility of using appropriately designed gas sensor arrays for various tasks related to monitoring deodorization processes and odor nuisance.

A similar principle was applied in the selection of mathematical data processing methods and predictive models. In subsequent stages of the research, various predictive models were used, selected based on the nature of the problem being analyzed, the data structure, and the purpose of the analysis. For the quantitative determination of concentrations of individual compounds or simpler mixtures, regression models were used that allowed for a direct correlation between sensor signals and the concentration of the analyzed component. In more complex measurement environment, methods were used to limit the influence of signal collinearity and reduce the dimensionality of the data. In contrast, in studies on odor perception, models were used that also took into account the psychophysical nature of human responses to odor stimuli. The change in the models used was therefore not due to a lack of methodological consistency, but rather to their deliberate adaptation to the specific nature of subsequent research tasks.

Detailed configurations of the individual gas sensor arrays, the methods used to prepare and process signals, the mathematical models employed, and the procedures for their calibration and validation are presented in the relevant chapters of the dissertation devoted to the individual stages of the research. This subsection outlines only the overarching methodological assumptions common to the entire thesis.

5.4 Elements of a scientific novelty

The research gaps identified in the literature review formed the basis for defining the dissertation's scientific novelty. The original contribution of the work concerns three main areas corresponding to the formulated research hypotheses.

With regard to the first research hypothesis, the starting point was the previous applications of gas sensor arrays for monitoring deodorization processes, as described in the theoretical section and summarized in Table 6. These included, among others, absorption, biofiltration, and BTF processes, as well as the determination of individual compounds and mixtures of volatile organic compounds. The novelty of this study thus lay in further expanding the potential applications of gas sensor arrays for determining the concentrations of components in gas mixtures and evaluating process efficiency, while simultaneously increasing the complexity of the analyzed systems and the scope of validation relative to gas chromatography.

For the second research hypothesis, the reference point was the previous applications of unmanned aerial vehicles equipped with gas sensor arrays for air quality monitoring, as summarized in the theoretical section and Table 7. These included, among other things, mapping pollutant concentrations, identifying areas of elevated emissions, and predicting odor concentrations using olfactometry as a reference technique. The original contribution, however, involved developing this approach toward the spatial localization of odor emissions from a heterogeneous surface source. A unique aspect of the study was the transition from mapping gas concentrations or odor concentrations to developing spatial odor emission maps, which made it possible to identify local areas of increased emissions and estimate the total emissions from the active section of the landfill. A further development involved using emissions estimated based on UAV measurements as input data for odor dispersion modeling and comparing the results obtained with a variant based on emissions determined using the reference method. This made it possible to verify the developed approach both in terms of the source’s characteristics and its predicted spatial odor impact.

The third research hypothesis was to build upon previous applications of gas sensor arrays for monitoring odor air quality. As presented in the theoretical section (Table 4 and Table 5), it has already been demonstrated that such systems can be calibrated against sensory techniques and used to predict odor concentration. The original contribution of this work included developing the approach from a single sensor array, enabling the assessment of odor air quality taking into account parameters related to odor perception, to a multi-point network operating in real industrial conditions. An important element of the novelty was the development of hybrid predictive models combining the analysis of multidimensional sensory signals with the psychophysical description of odor perception, multi-season calibration and long-term validation of the network operation in various location and chemical conditions. In addition, the integration of the results with the IoT infrastructure and a decision support system enabling the ongoing assessment of the spatial and temporal variability of odor nuisance.

6. Assessment of the absorption efficiency of toluene vapors from a polluted air stream using a gas sensor array

6.1 Purpose of the study

The aim of this stage of the research was to demonstrate the usefulness of the designed gas sensor array as a cheap and fast analytical tool for monitoring the efficiency of the toluene vapor absorption process from the air stream. This study was to confirm that the constructed device could be a real alternative to traditional chromatographic methods (GC-FID) in the control of the deodorization processes. The gas sensor array was used to monitor toluene concentration during dynamic absorption, and the developed predictive model was verified after introducing acetone as an additional component of the mixture, without changing its previous calibration. This made it possible to assess the robustness of the sensor system and the predictive model against changes in the gas stream composition and the presence of an interfering substance.

6.2 Materials and methods

6.2.1 Absorption system and process parameters

The research task was to monitor the effectiveness of the deodorization process of the air stream from toluene vapors. As a purification technique, absorption processes were used, which seem justified from engineering and technical reasons and the poor biodegradability of toluene. It was decided to use this compound as a contamination of the gas stream to be purified because, in addition to the low olfactory threshold, inhalation of its vapors has a negative impact on the human body, in particular the respiratory, reproductive and immune systems. This poses a great risk because this substance is commonly used in varnishing, engraving or perfumery, and additionally it occurs naturally in crude oil and tolu tree. This means that it could be emitted into the atmosphere during processes such as fuel production or composting carried out in municipal treatment plants.

The study was conducted using a test laboratory setup based on the dynamic pollutant generation system, in which purified air was directed into a bubbler (barbotte) with liquid toluene (Figure 20). The air flow through the bubbler was precisely controlled using a mass flow controller (MFC 1) and maintained at 5.0 $mL \cdot min^{-1}$. The saturated gas stream obtained in this way was then diluted with pure air from a zero air generator (controlled by MFC 2), which allowed for the preparation of mixtures with toluene concentrations within the range of 5 to 80 ppm. This range was selected to correspond to the concentrations found in the vicinity of actual emission sources, such as composting facilities and landfills. The contaminated air stream prepares in this manner was fed into the absorption column at a flow rate of 100 $mL \cdot min^{-1}$. The absorbent used was a commercially available absorption liquid for nonpolar compounds (Genosorb® 1843, Clariant, USA) designed for the removal of aromatic hydrocarbons. This product is a dark liquid with a very faint odor, a molar mass of 270 $g \cdot mol^{-1}$, a boiling point exceeding 250°C, and a density of 0.91 $g \cdot cm^{-3}$ and viscosity of 6-8 $mm^2 \cdot s^{-1}$ at 20°C.

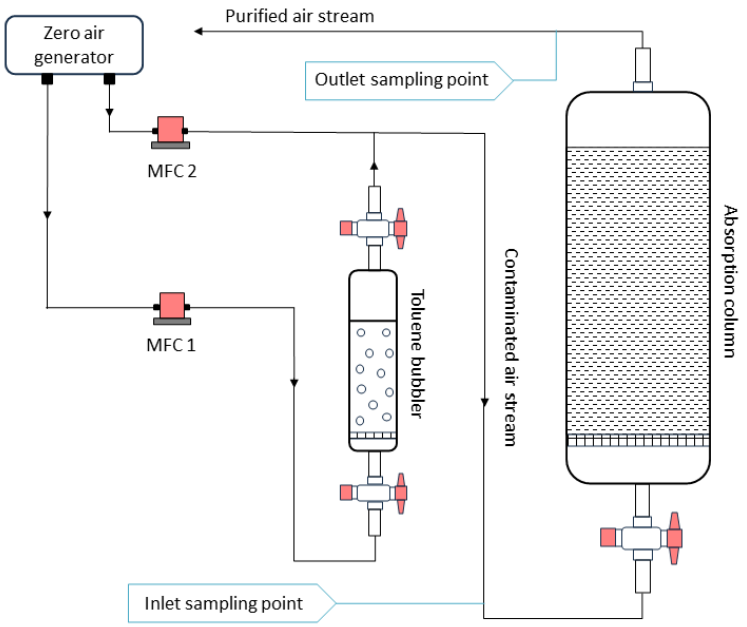


Figure 20. Schematic diagram of the measurement setup for monitoring the absorption of toluene vapor. Adapted from [263], licensed by CC BY 4.0.

6.2.2 Reference equipment (GC-FID analysis)

Gas chromatography coupled with a flame ionization detector (GC-FID) served as a reference technique for the quantitative determination of toluene in the samples. Table 8 presents the detailed operating parameters of the device used in the study. The calibration procedure began with the preparation of ten standard gas mixtures in TEDLAR bags, each with a known concentration of toluene. These mixtures were used to determine the calibration curve using the external standard method (absolute calibration), with each sample analyzed three times. The same gas samples were introduced into the constructed gas sensor array, and the resulting signals were used as a training dataset in the learning process.

Table 8. Parameters of the chromatographic analysis used for the quantitative determination of toluene.

System	Varian CP-3800 (Varian Analytical Instruments, USA)
Detector	Flame Ionization Detector (FID)
Capillary column	DB-624 (60 m x 0.32 mm x 1.8 μm, Agilent Technologies, USA)
Carrier gas	Nitrogen
Carrier gas flow	3.5 mL·min^{-1}
Injector temperature	150°C
Oven temperature	150°C
Detector temperature	250°C
Split ratio	10
Injection volume	0.5 mL

6.2.3 Gas sensor array development

The prototype gas sensor array consisted of five commercially available sensors. The detection system included four MOS sensors from Figaro Engineering Inc. (Mino, Osaka, Japan) and one photoionization detector (PID) from Alphasense Metek (Great Notley, Braintree, United Kingdom). The individual sensors were selected to enable the detection of a wide range of

substances. TGS2600 (S1) and TGS2602 (S3) sensors are designed for general air pollutants, the TGS2603 (S2) responds to VOCs and odorous gases, the TGS823 (S4) is sensitive to organic solvent vapors, and the PID-A12 detector (S5) detects VOCs with an ionization potential below 10.6 eV. More detailed characteristics of the sensors used are presented in Table 9. Each sensor was housed in an isolated measuring cell made of polytetrafluoroethylene (PTFE). The choice of PTFE as the construction material was crucial, as this material does not adsorb contaminants, thereby eliminating the risk of results being skewed by remnants of substances from preceding analyses. The configuration of the circuits and electrical connections was implemented in compliance with the technical documentation and guidelines provided by the manufacturers.

Table 9. Parameters of gas sensors used for monitoring the absorption of toluene vapor from the air stream.

Model	Producer	Sensing principle	Target gases	Signal conditioning
TGS2600	Figaro Engineering Inc. (Mino, Osaka, Japan)	MOS type	Air contaminants (hydrogen, ethanol)	Voltage divider
TGS2603	Figaro Engineering Inc. (Mino, Osaka, Japan)	MOS type	Air contaminants (trimethylamine, methyl mercaptan)	Voltage divider
TGS2602	Figaro Engineering Inc. (Mino, Osaka, Japan)	MOS type	Air contaminants (VOCs, ammonia, H_2S)	Voltage divider
TGS823	Figaro Engineering Inc. (Mino, Osaka, Japan)	MOS type	Organic solvents	Voltage divider
PID-A12	Alphasense Metek (Great Notley, Braintree, United Kingdom)	UV type	VOCs with ionization potentials < 10.6 eV	Integrated amplifier

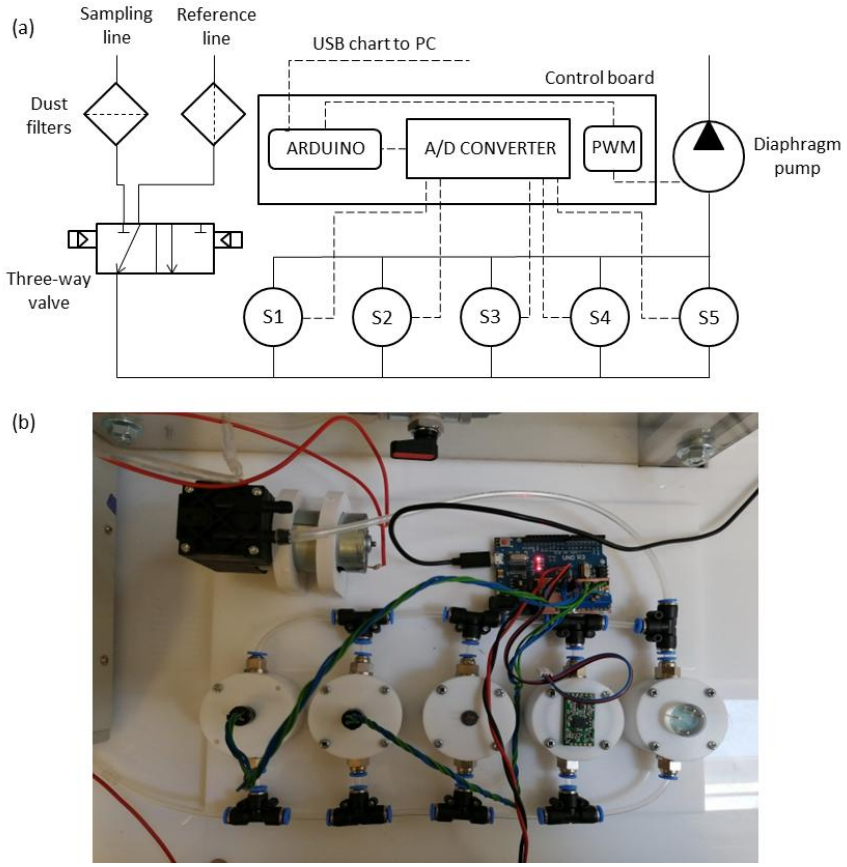


Figure 21. Structure of the pneumatic system (a) and general view of the gas sensor array prototype (b). Adapted from [263], licensed by CC BY 4.0.

The pneumatic system of the sensor array consisted of two pathways: a reference line and a measurement line. Switching between them was accomplished using a three-way valve. The reference line supplied clean air, which allowed the sensors to return to their default parameters (baseline) before subsequent measurements. Through the measurement line, gas samples were drawn into the array by a diaphragm pump, with interchangeable dust filters installed at the intake ports of both lines. The system operated in stop-flow mode, in which the sample passage time through the sensor chambers and the residence time were both 40 seconds. After this time had elapsed, the system was purged with clean air until the next analysis began. The structure of the pneumatic system and a general view of the constructed gas sensor array prototype are shown in Figure 21.

6.2.4 Measurement procedure and sampling

The process was divided into three stages. In the first stage, the breakthrough time of toluene and acetone on the applied absorbent was determined, and the obtained concentrations and signals from the sensors were used in the matrix training process. Machine learning also used samples prepared on the gas mixture generator to increase the number of calibration points.

On the basis of the obtained results, the MLR model was created, predicting toluene concentrations based on the collected signals from the sensors. The matrix trained in this way was used in the second stage of the process, which consisted of passing only toluene through the prepared installation, and in the third stage, in which a mixture of both compounds was flowing through the system. Stage two was to test the applicability of the constructed matrix with the MLR model, as an alternative to chromatographic techniques, for the purpose of monitoring absorption deodorization of the air stream.

The third stage, on the other hand, was to verify the selectivity of the developed model against toluene in the presence of other polluting compounds. Acetone was chosen because, first of all, it is used in similar industrial sectors to toluene, and its presence has also been confirmed in the literature in compost gases. The simultaneous presence of both compounds in gases emitted from municipal facilities is very likely to happen. Secondly, acetone is a polar solvent, so it quickly broke through the absorbent used (about ten times faster than toluene), so its concentration during the third stage of the process could be considered almost constant.

The absorption process was carried out continuously until the absorption liquid was completely saturated, as indicated by the equalization of concentrations at the inlet and outlet of the system. Gas samples were collected at approximately five-hour intervals into special TEDLAR bags, allowing for parallel analysis using two methods. The efficiency of the air stream purification was evaluated based on the determined absorption coefficient (A), defined as the ratio of the pollutant concentration at the outlet to the concentration at the column inlet.

6.2.5 Data analysis and mathematical modeling

The analysis of all collected measurement data and the necessary statistical calculations were conducted employing RStudio Desktop software (v. 1.0.143). The first step in analyzing the

results from the gas sensor array was signal feature extraction. The output signal (independent variable) from each sensor was defined as the difference between the maximum response value recorded during the measurement phase (S_{max}) and the baseline value (S_0) determined for pure synthetic air (Eq. 11).

$$\Delta S = S_{max} - S_0 \tag{11}$$

The calibration of the gas sensor array was performed with the use of multiple linear regression (MLR). As a part of the analysis, a calibration model was developed in which toluene concentration served as the dependent variable, while the signals recorded by individual sensors acted as independent variables. This model made it possible to quantitatively characterize the relationship between the sensor array response and the analyte concentrations. In other words, the mathematical model predicted toluene concentrations based on the recorded sensor signals.

The MLR model assumes a linear relationship between the output variable and a set of input variables. For the i-th observation, this relationship could be described as the sum of the weighted sensor responses, a constant term (intercept, θ_0), and a residual term (r_i), which represents the portion of the variance not explained by the model (Eq. 12).

$$C_i = \theta_0 S_{i,0} + \theta_1 S_{i,1} + \theta_2 S_{i,2} + \cdots + \theta_k S_{i,j} + r_i \tag{12}$$

where C_i is the reference value of the analyte concentration for the i-th observation $(i = 1,2 \ldots n)$, θ_k the regression coefficient assigned to the j-th sensor signal $(j = 1,2 \ldots k)$, $S_{i,j}$ the output of the j-th sensor for the i-th observation, n the number of observations used to build or evaluate the model, k the number of input variables (the number of sensor signals). During prediction, the deterministic part of the equation is used, and the residual term is ignored. The predicted concentration might therefore be expressed according to Eq.13:

$$\hat{C}_i = \theta_0 S_{i,0} + \theta_1 S_{i,1} + \theta_2 S_{i,2} + \cdots + \theta_k S_{i,k} \tag{13}$$

The model residual defines the difference between the reference value and the predicted value. This relationship allows the observed value to be expressed as the sum of the model's prediction and the fit error (Eq.14):

$$C_i = \hat{C}_i + r_i \quad or \quad r_i = C_i - \hat{C}_i \tag{14}$$

After writing out the equation for subsequent measurements, a set of equations is obtained in which each line corresponds to a single sample used in the model calibration or validation process:

$$\begin{aligned} C_1 &= \theta_0 S_{1,0} + \theta_1 S_{1,1} + \theta_2 S_{1,2} + \cdots + \theta_k S_{1,k} + r_1 \\ C_2 &= \theta_0 S_{2,0} + \theta_1 S_{2,1} + \theta_2 S_{2,2} + \cdots + \theta_k S_{2,k} + r_2 \\ &\vdots \\ C_n &= \theta_0 S_{n,0} + \theta_1 S_{n,1} + \theta_2 S_{n,2} + \cdots + \theta_k S_{n,k} + r_n \end{aligned} \tag{15}$$

When there are more observations and input variables, a matrix notation is more convenient:

$$\begin{bmatrix} C_1 \\ \vdots \\ C_n \end{bmatrix} = \begin{bmatrix} S_{1,0} & S_{1,1} & \cdots & S_{1,k} \\ \vdots & \vdots & \ddots & \vdots \\ S_{n,0} & S_{n,1} & \cdots & S_{n,k} \end{bmatrix} \begin{bmatrix} \theta_0 \\ \vdots \\ \theta_k \end{bmatrix} + \begin{bmatrix} r_1 \\ \vdots \\ r_n \end{bmatrix} \quad (16)$$

For a matrix defined in this way, the model might be written as:

$$\boldsymbol{C} = \boldsymbol{S}\theta + \boldsymbol{R} \quad (17)$$

In the above expression, $\boldsymbol{C}$ denotes an $n \times 1$ vector of reference values, $\boldsymbol{S}$ is an $n \times (k+1)$ input data matrix, θ is $(k+1) \times 1$ vector of model parameters, and $\boldsymbol{R}$ stands for $n \times 1$ vector of residuals. The vector of values predicted by the models is described by the following equation:

$$\widehat{\boldsymbol{C}} = \boldsymbol{S}\theta \quad (18)$$

The model parameters are estimated to minimize the discrepancies between the reference values and the values calculated by the model. In the classical least-squares approach, this means minimizing the sum of the squares of the residuals. If the matrix $\boldsymbol{S}$ is full-rank, the estimator of the parameter vector may be written as:

$$\widehat{\boldsymbol{\theta}} = (\boldsymbol{S}^T\boldsymbol{S})^{-1}\boldsymbol{S}^T\boldsymbol{C} \quad (19)$$

The MLR model developed in this way made it possible to convert a multidimensional output signal from gas sensor array into a value corresponding to the predicted toluene concentration. The advantage of this method is its clear mathematical form and the ability to interpret the model coefficients in relation to individual sensor signals. However, the MLR describes only linear relationships, and its effectiveness depends on the quality of the training data, the range of concentrations analyzed, and the degree of interdependence among the input variables.

The efficiency of the absorption process was evaluated based on the relative concentration of toluene in the effluent stream (A). So called absorptivity, was defined as the ratio of toluene concentration measured at the system outlet (C_{out}) to its concentration measured at the system inlet (C_{in}). This parameter served as a measure of the fraction of toluene not removed during the absorption process, and lower values corresponded to higher efficiency in purifying the gas stream.

$$A = \frac{C_{out}}{C_{in}} \quad (20)$$

To verify the accuracy of the readings from the trained and calibrated gas sensor array against the reference method (GC-FID), the absolute error and the root mean square error (RMSE) were determined. RMSE is commonly used to quantitatively assess the discrepancy between the values predicted by the model and the actual or reference values, and thus to determine how close the model fits the experimental data. In this study, RMSE was used as a measure of agreement between the results obtained using a model developed based on the responses of a gas sensor array and the values determined by the gas chromatography. This parameter was calculated as the square root of the arithmetic mean of the squares of the differences between the reference values (x_i) and the values predicted by the model (y_i).

$$RMSE = \sqrt{\frac{\sum_{i=1}^{n}(x_i - y_i)^2}{n}} \quad (21)$$

In general, lower RMSE values indicate fewer deviations of the predictions from the reference values, and thus a better fit of the model to the measured data. This parameter was therefore one of the criteria used to assess the model accuracy and its suitability for quantitatively predicting the analyzed variables. However, when interpreting the obtained RMSE values, the fact that this parameter is relative and should be considered in relation to the unit of the analyzed variable and the range of input data values was taken into account.

6.3 Results and discussion

6.3.1 Characteristics of the absorption process and the predictive model

Before assessing the feasibility of using gas sensor array for quantitative monitoring of absorption process, the behavior of individual components of the tested gas stream in contact with the applied absorbent was analyzed. In the first stage of the study, breakthrough curves for toluene and acetone were determined for Genosorb® 1843 (Figure 22). The obtained results demonstrated distinctly different affinities of the two compounds for the absorbent.

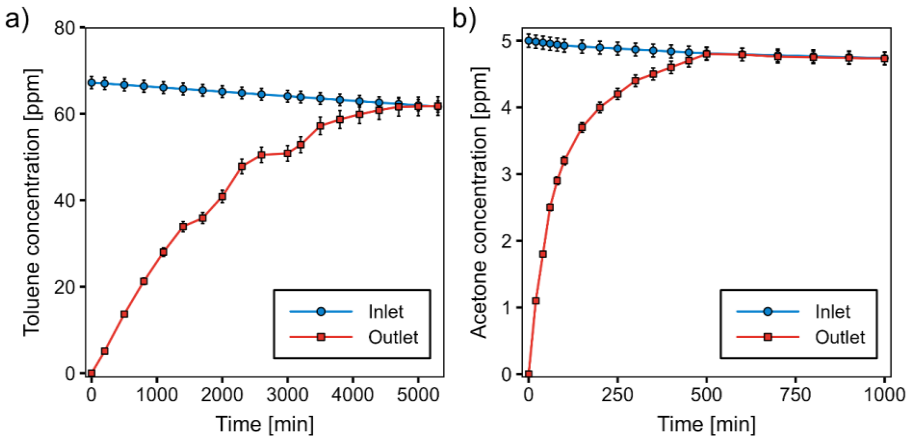


Figure 22. Breakthrough curves of toluene (a) and acetone (b) during the absorption process. Points represent the mean values of the three replicate chromatographic analyses, and error bars indicate standard deviation (±SD). Adapted from [263], licensed by CC BY 4.0.

In the case of toluene, full breakthrough occurred after approximately 5,000 minutes of process operation, while for acetone, this time was approximately ten times shorter. This large difference caused the composition of the gas stream at the outlet of the absorption column to change over time when both compounds were present. Acetone appeared in the outlet stream much earlier than toluene, which remained effectively retained in the absorbent for a longer period. The observed difference in the absorption process of both compounds was of significant importance from the point of view of further evaluation of the sensor system. The introduction of acetone not only changed the concentration of the additional component of the mixture, but also dynamically changed its composition at the outlet of the absorption column. These conditions

constituted a more demanding measurement case and enabled the assessment of the developed model's resistance to the presence of the interfering compound.

To quantitatively determine toluene concentration, a multiple linear regression (MLR) model was used, in which the independent variables were the signals generated by individual sensors, and reference concentration values were obtained using the GC-FID method. The model developed based on the calibration data had a coefficient of determination of R^2 = 0.986, indicating a very good fit to the calibration data (Figure 23). The significance of individual variables in the MLR model was assessed based on the Student's t-test for regression coefficients, assuming the significance level α = 0.05. Variables for which regression coefficients were not statistically significant (p > 0.05) were eliminated from the model. As a result of the selection, the signals of sensors S1 and S3 were rejected, while the responses of sensors S2, S4 and S5 were retained in the final model. For these variables, the p values were 0.0247, 0.0483 and 0.0012, respectively, which confirmed their statistically significant contribution to the model. This result indicates that increasing the number of array elements does not automatically lead to an improvement in prediction quality, and that the actual information contribution of individual sensors is more important.

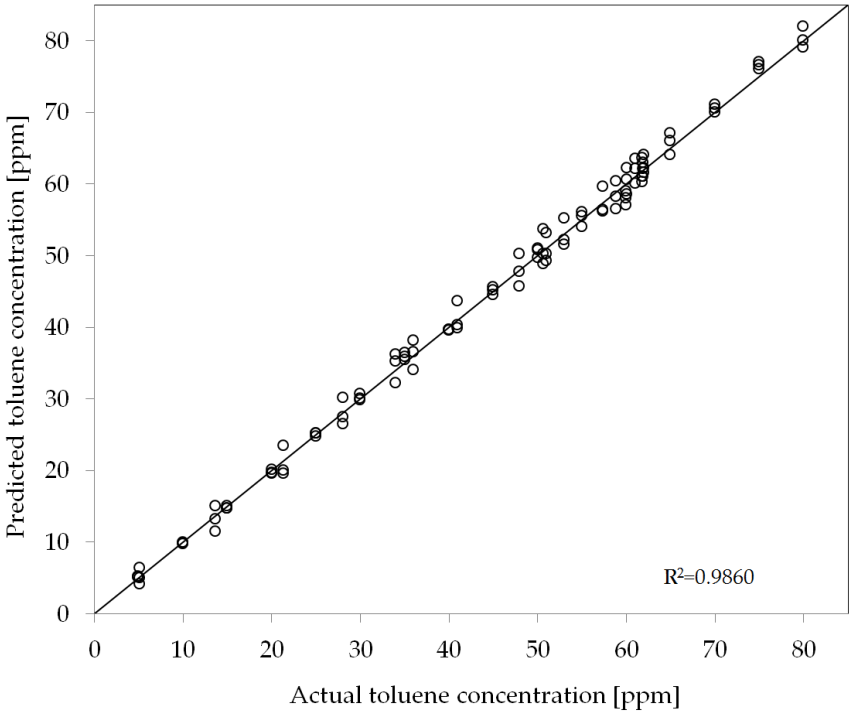


Figure 23. MLR calibration chart: toluene concentration determined by the model relative to GC-FID reference values. Reproduced from [263], licensed by CC BY 4.0.

After model calibration, the key step in its evaluation was its verification under dynamic absorption process conditions. Unlike the evaluation of the calibration fit alone, this allowed for verification of whether the relationship determined during the calibration stage retained its utility during actual concentration changes at the inlet and outlet of the absorption column, and subsequently also after the introduction of an additional component, acetone, into the gas stream. The results of this verification are presented in the following sections.

6.3.2 Monitoring the course and assessing the efficiency of toluene absorption

The toluene concentration was determined at subsequent time points both at the inlet and outlet of the system, using in parallel the GC-FID reference method and a gas sensor array with a developed prediction model. The aim of this stage was to check whether the sensor array response allows for a quantitative representation of concentration changes occurring during the process and whether the obtained results can be used to assess its effectiveness.

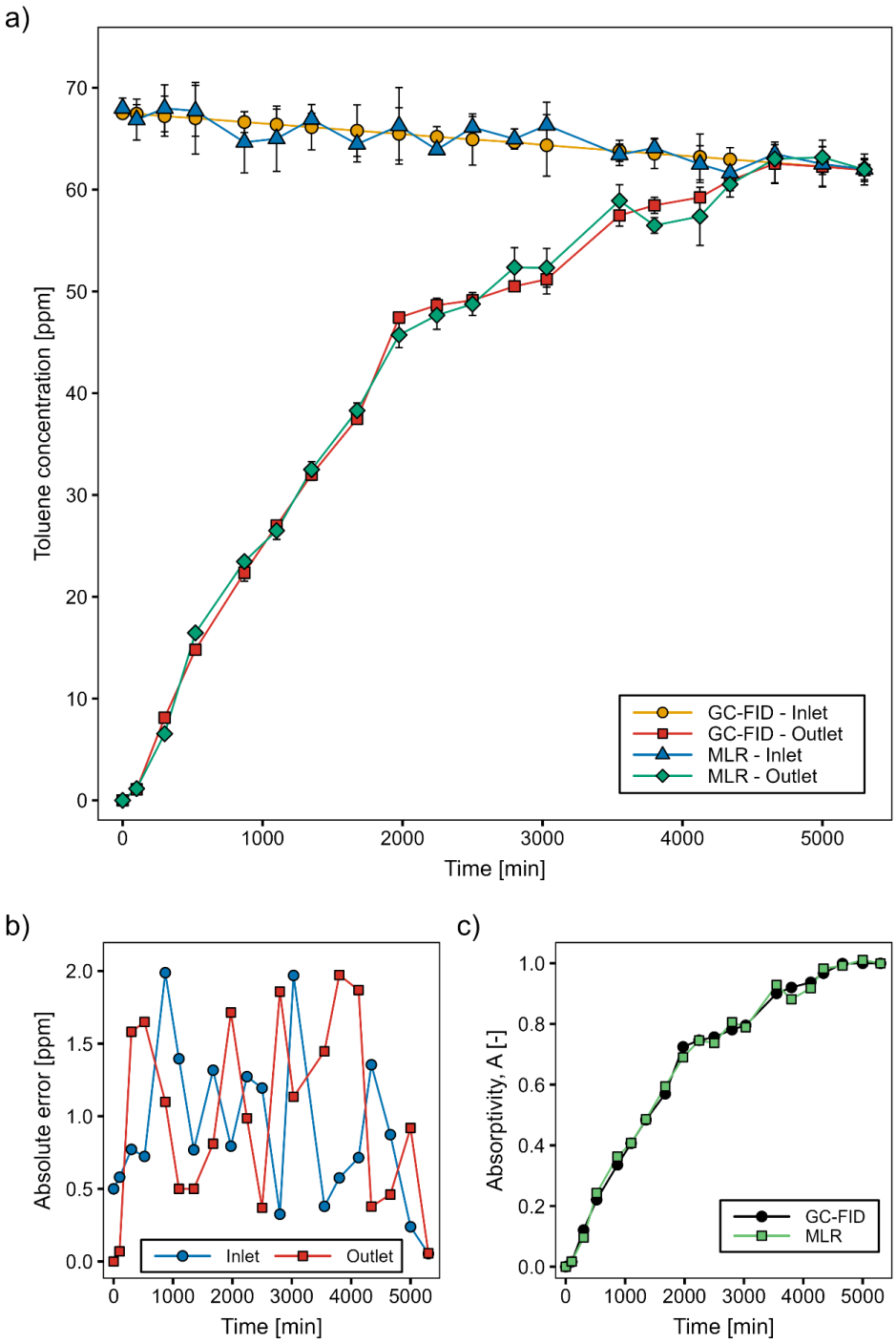


Figure 24. Monitoring of the toluene absorption process: (a) inlet and outlet concentrations determined by GC-FID and MLR model; (b) absolute prediction errors; (c) absorptivity values determined from GC-FID and MLR results. Concentration values in panel (a) represent means of three replicate analyses, and error bars indicate standard deviations (±SD). Adapted from [288], licensed under CC BY 4.0.

In the initial phase of the process, the toluene concentration in the outlet stream was close to zero, while at the inlet it remained at approximately 70 ppm. As the absorption continued, a gradual increase in the toluene concentration was observed at the outlet of the absorption column, associated with the progressive saturation of the absorbent. In the final phase of the process, the inlet and outlet concentrations converged. The sensor array, along with the MLR model, reproduced both relatively small changes in the inlet concentration and much larger changes occurring in the outlet stream (Figure 24a).

The agreement between the sensor array results and the reference results was assessed quantitatively (Figure 24b). The RMSE values reported for this stage of the study were 1.3 ppm for the inlet stream and 1.6 ppm for the outlet stream. The analysis of absolute errors at individual time points showed that their values for both streams varied throughout the process, reaching a maximum of approximately 2.0 ppm. There was no systematic increase in error with progressive absorbent saturation. The agreement of the results for the outlet stream was of particular importance, because the changes in C_{out} reflected the progressive saturation of the absorbent and the change in toluene removal efficiency.

From the perspective of using the sensor array for process monitoring, it was important not only to be able to determine toluene concentration, but also to use these results to assess changes occurring in the absorption column. For this purpose, parameter absorptivity (*A*) was determined based on the inlet and outlet concentration values (Figure 24c). In the initial phase of the process, its value was close to zero, which corresponded to almost complete retention of toluene in the absorbent. As Genosorb® 1843 became more saturated, the coefficient *A* gradually increased, reaching values close to unity by the end of the experiment. Its curve determined from the sensor array results was similar to that obtained from the GC-FID data. The RMSE between the two methods was 0.019, corresponding to 1.9%. This means that the information obtained from the array could be used not only to quantify toluene concentration but also to map changes in a parameter directly describing the absorption process.

The obtained results confirmed the feasibility of using a calibrated gas sensor array to quantitatively monitor toluene absorption and assess changes in process efficiency relative to the GC-FID reference method. However, these studies were conducted for a relatively simple stream containing toluene as the main component analyzed. The next step was to verify whether the developed model would remain useful after changing the gas mixture composition and introducing acetone as an additional interfering compound.

6.3.3 The influence of acetone on monitoring and assessing the process efficiency

The next stage of the research involved evaluating the performance of the developed MLR model under conditions of altered gas stream composition. Acetone at a concentration of approximately 5 ppm was introduced into the toluene containing stream. The same MLR model was used in the research, without recalibration. This allowed for an assessment of the developed solution's susceptibility to changes in gas mixture composition and the presence of an additional compound that could affect the sensor response. The course of changes in toluene concentration

determined by the GC-FID method and predicted based on the response of the sensor array is shown in Figure 25a. As in the acetone free variant, the toluene concentration at the outlet of the absorption column was close to zero in the initial phase of the process, then increased with progressive saturation of the absorbent. The MLR model reproduced both the changes in the inlet concentration and the increase in outlet concentration. However, in the presence of acetone, larger local differences were observed between the model results and the GC-FID determinations than in the toluene-only process.

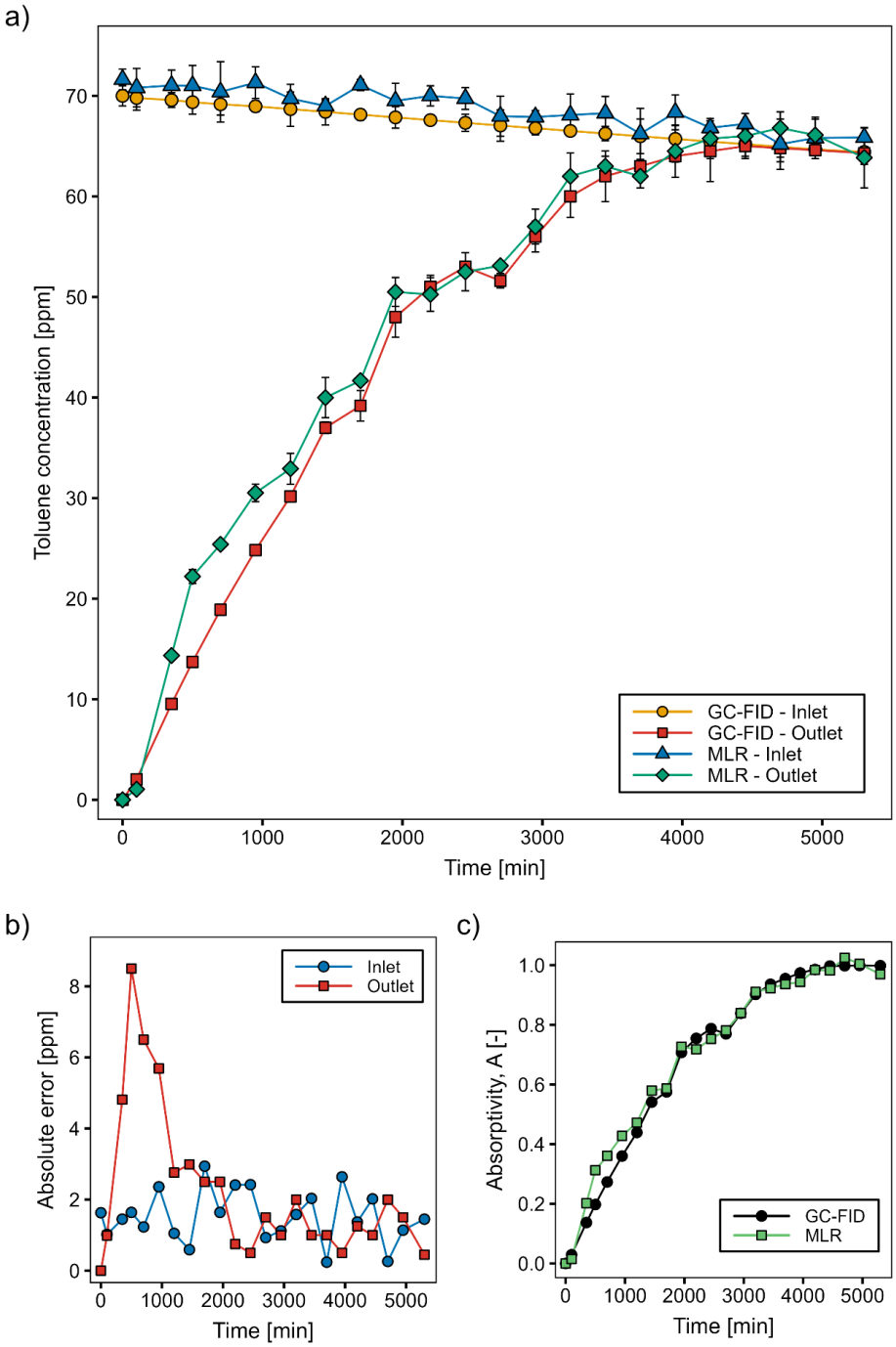


Figure 25. Monitoring of toluene absorption in the presence of acetone: (a) inlet and outlet concentrations determined by GC-FID and MLR model; (b) absolute prediction errors; (c) absorptivity values determined from GC-FID and MLR results. Concentration values in panel (a) represent means of three replicate analyses, and error bars indicate standard deviations (±SD). Adapted from [288], licensed under CC BY 4.0.

Quantitative evaluation of the agreement between the two methods showed RMSE of 1.7 ppm for the inlet stream and 3.1 ppm for the outlet stream. The higher error for the outlet stream was primarily due to a transient increase in the differences between the GC-FID and MLR results early in the process. As shown in Figure 25b, the maximum absolute error for the outlet stream occurred after approximately 500 min and amounted to 8.5 ppm. At subsequent points, its value decreased: after 700 min it was approximately 6.5 ppm, after 950 min approximately 5.7 ppm, and from 1200 min onwards it did not exceed approximately 3 ppm. For the inlet stream, the maximum absolute error was significantly smaller and amounted to approximately 2.9 ppm.

The peak error for the outlet stream occurred during the period corresponding to acetone breakthrough through the absorption liquid. During this time, the composition of the gas leaving the absorber changed rapidly, presenting more challenging conditions for the model previously developed for toluene determination. However, the increase in error was transient - as the exhaust stream composition stabilized, the differences between the GC-FID and MLR results decreased significantly. This result indicates that the presence of the interfering compound affected the prediction accuracy primarily during the period of dynamic change in the mixture composition, without causing a permanent loss of the model's ability to represent the process.

The influence of the observed differences on the possibility of assessing the process was also verified on the basis of the absorptivity (*A*) parameter (Figure 25c). The values determined from GC-FID and MLR results followed a similar pattern throughout the experiment. The coefficient *A* increased from values close to zero in the initial absorption phase to values close to one in the final part of the process, reflecting the progressive saturation of the absorbent. The RMSE between the coefficients determined from both methods was 0.041, corresponding to approximately 4.1%. The obtained results indicate that the introduction of acetone decreased the accuracy of toluene concentration determination compared to the variant without the interfering compound, especially during the period of rapid change in the outlet stream composition. Despite this, MLR model (without recalibration), was able to reproduce changes in toluene concentration and the course of the process.

6.4 Summary and conclusions

The conducted studies allowed to characterize the toluene absorption process and verify the feasibility of using a gas sensor array for quantitative monitoring of this process. Based on the GC-FID reference results, the MLR predictive model was developed and calibrated, which was then used to determine the toluene concentration at the inlet and outlet of the absorption system. The obtained results showed that the sensor array responses can be used not only to determine the pollutant concentration, but also to determine changes in the course and efficiency of the absorption process. A significant element of the validation was to verify the model's performance after changing the gas stream composition by introducing acetone as an interfering compound. The presence of the additional component caused a temporary increase in prediction errors, particularly during periods of dynamic changes in the outlet stream composition, but did not lead

to a permanent loss of the model's ability to represent the process. This allowed to verify the model's suitability even under conditions deviating from the basic calibration conditions.

The obtained results are part of a broader research direction on the quantitative determination of VOCs using gas sensor arrays and multidimensional data analysis methods. Wolfrum et al. [264] demonstrated the ability to detect, distinguish, and quantify VOCs using a commercial MOS sensor array and PLS models, conducting studies in the concentration range of 0.01–0.30 ppm. Szczurek et al. [265] used a commercial Figaro sensor array together with MLR model to recognize and quantify the components of binary VOC mixtures. One of the analyzed groups included mixtures in which toluene was the dominant component. Singh et al. [266], in turn, studied mixtures containing, among others, toluene and acetone, and found a clear effect of co-occurring VOCs on sensor responses. Despite the interference, the use of machine learning methods enabled quantitative prediction of the concentrations of individual components, and the best regression model achieved R^2 >0.99.

Direct comparison of prediction error values reported in the cited studies with the results obtained in this chapter is not justified. These studies were conducted for different concentration ranges, gas mixture compositions, sensor array configurations, and modeling methods. However, it is reasonable to compare the direction of the observed dependencies: the possibility of quantitative use of appropriately calibrated gas sensor array and the deterioration of the prediction quality due to the presence of interfering components. The cited studies did not directly address the absorption deodorization process. In the research presented in this chapter, the sensor array approach was extended to the dynamic absorption process, in which the results obtained using a predictive model were compared to GC-FID measurements and then also used to assess changes in gas stream treatment efficiency. The results of chapter 6 constitute the first stage of verification of the assumptions of the first research hypothesis, including the characterization of the process, development and calibration of the predictive model, its validation against the reference method and verification of the operation under conditions of changed mixture composition. In the next chapter, the scope of research was extended to the biological deodorization process carried out in a biotrickling filter (BTF), which enabled the assessment of the usefulness of the sensor array in a system with a different mechanism of pollutant removal and more complex process dynamics.

6.5 Publication basis of the chapter

This chapter is based in part on research previously published in:

Dobrzyniewski D., Szulczyński B., Gębicki J. (2022). Application of a Gas Sensor Array to Effectiveness Monitoring of Air Contaminated with Toluene Vapors Absorption Process. *Journal of Ecological Engineering,* 23(10), pp. 269-282. doi: 10.12911/22998993/152427.

The article is distributed under the Creative Commons Attribution 4.0 International License (CC BY 4.0). The material has been revised, adapted, and expanded for the purpose of this doctoral dissertation. The findings are discussed in the context of the main research objective of the thesis.

7. Application of gas sensor array to evaluate removal efficiency of hydrophobic organic compounds in a biotrickling filter (BTF)

7.1 Purpose of the study

The aim of this study was to determine the feasibility of using a proprietary gas sensor array as an alternative device for quantitatively monitoring the BTF efficiency of a mixture containing hydrophobic VOCs. The research was conducted on an air stream containing n-hexane and cyclohexane vapors, and GC-FID was used as the reference technique. Scope of the research was expanded to include the biological deodorization process. A different gas sensor array configuration was used, and its performance was verified at various inlet loads (IL). An additional element of the original contribution was the comparison of MLR and PCR models, which allowed for an assessment of how the method of processing the array's multidimensional response affected the estimation of the concentrations of both components.

7.2 Materials and methods

7.2.1 Biofiltration unit

A contaminated air stream with a specified composition was prepared in a dynamic generation system using the bubbling (barbotage) method. This process involved passing the dehumidified and filtered air (from the zero air generator (LAT LTD, Katowice, Poland)) through glass vessels containing the liquid chemicals under study, which allowed the gas bubbles to become saturated with n-hexane and cyclohexane vapors. Precise dosing and control of the flow rates of individual components, as well as the entire feed rate, were ensured through the use of electronic mass flow controllers (MFCs). The test setup included a laboratory scale biotrickling filter (BTF) designed for the biological treatment of a gas stream to remove VOCs. The bioreactor was made of poly(methyl methacrylate) (PMMA, acrylic glass) in the form of a one-section column with an internal diameter of 0.08 m. A detailed block diagram, including the gas mixture generation system, is shown in Figure 26. The biofilter was filled with a hybrid material with total height of 0.68 m and an operating volume, calculated based on the column's geometry, of 2.5 dm^3. The filling consisted of alternating discs of polyurethane foam (Murano Feniks, Wejherowo, Poland) with and a mixture of peat and perlite (Compo Sana, Compo GmbH, Munster, Germany) with ceramic Raschig rings (BROWIN, Łódź, Poland).

The composition of the filter bed was selected to simultaneously ensure biological activity, appropriate hydrodynamic conditions, and the mechanical stability of the system. The perlite-peat fraction was characterized by a dry material porosity of 90%, a wet material porosity ranging from 25-30%, and a bulk density of 176 $kg \cdot m^{-3}$. It served as a source of a natural, diverse population of microorganisms capable of initiating the biodegradation of organic pollutants. Raschig rings (porosity: 58%, bulk density: 946 $kg \cdot m^{-3}$, material density: 2250 $kg \cdot m^{-3}$) increased the heterogeneity of the packing structure and facilitated the uniform distribution of the liquid and gas phase within the column.

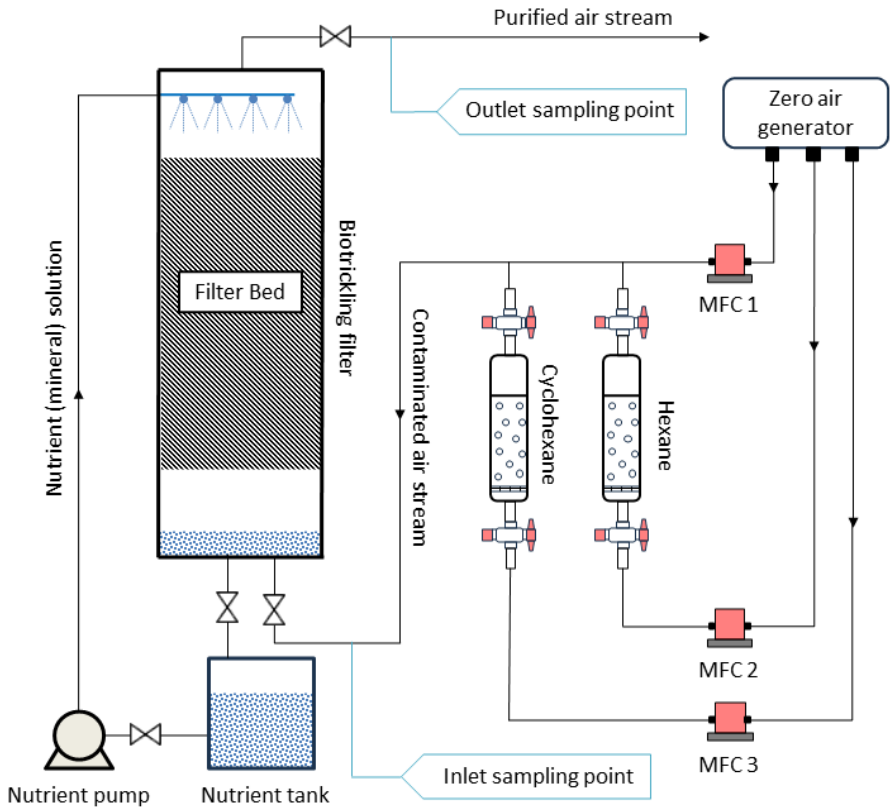


Figure 26. Laboratory set-up for monitoring the biofiltration of n-hexane and cyclohexane in a BTF. Adapted from [267], licensed by CC BY-SA 4.0.

Polyurethane foam discs (PPI: 10, porosity: 97%, bulk density: 25 kg·m^{-3}) provided a durable support structure that promoted biomass immobilization and biofilm formation. Its use limited the impact of gradual peat loss or degradation on the BTF operational parameters, enabling the system to maintain stable performance with acceptable gas flow resistance and pressure drop. The polyurethane foam discs used in this study were sourced from previous air biofiltration processes. The were therefore already colonized by certain microbial cultures, which made it possible to skip the lengthy activation phase (start-up period). The conditions necessary to maintain the metabolic activity of the biofilm were assured by repeatedly irrigating the bed with a mineral solution containing $Na_2HPO_4 \cdot 2H_2O$, KH_2PO_4, NaCl and NH_4Cl. Sprinkling was performed in an intermittent mode, with the liquid flow activated for 0.5 min during each one-hour operating cycle. The flow rate of the mineral solution through the column was 0.2 dm^3·min^{-1}.

7.2.2 Reference equipment (GC-FID analysis)

GC-FID was used as the reference method for determining the concentrations of n-hexane and cyclohexane in air streams undergoing biofiltration. The analyses were performed using the same equipment (Varian CP-3800, Varian Analytical Instruments, USA) and under the same chromatographic conditions as those used for determining toluene concentrations in the studies on absorption-based air purification. The chromatographic apparatus and conditions, as listed in Table 8, are described in detail in chapter 6.2.2. Due to the change in the compounds being analyzed, appropriate n-hexane and cyclohexane standards were used, on the basis of

which separate calibration curves were prepared. The calibration ranges were adjusted to the concentrations encountered in the conducted studies. The remaining elements of the analytical procedure were left unchanged.

7.2.3 Gas sensor array development

A multisensory measurement system comprising seven commercial gas sensors was developed for the evaluation of the biofiltration process of n-hexane and cyclohexane. The sensor array configuration was optimized to provide the broadest possible response to the presence of volatile gas phase components in the test laboratory setup. The selection criteria was primarily based on the sensor's detection ranges, their sensitivity to VOCs, and ability to operate at concentrations corresponding to the conditions of the biofiltration process.

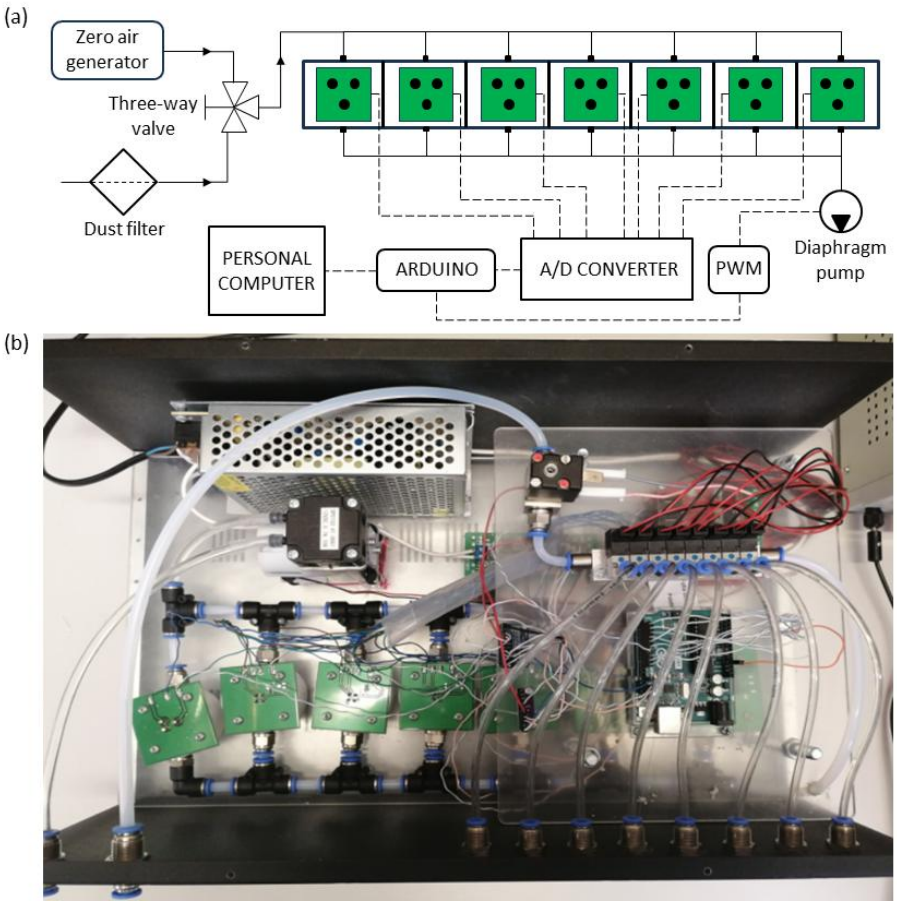


Figure 27. Structure of the pneumatic system (a) and general view of the gas sensor array prototype (b) used in the biofiltration process. Adapted from [267], licensed by CC BY-SA 4.0.

As in the toluene absorption process, the gas sensor array was based on four MOS sensors from Figaro Engineering Inc. (Mino, Osaka, Japan) and a PID manufactured by Alphasense Metek (Great Notley, Braintree, United Kingdom). The models used were TGS2600 (S1), TGS2602 (S2), TGS2603 (S3), TGS823 (S4) and PID-A12 (S5), whose specifications were given in Table 9. The system was also equipped with TGS8100 (S6) and a temperature and relative humidity sensors SHT25 manufactured by Sensirion AG (Stäfa, Switzerland). The TGS8100 is a broadband air pollution sensor, while temperature and humidity were monitored

due to the expected significant changes in these parameters between the inlet and outlet of the biofiltration installation. These changes might affect the resistance of the active layers in MOS sensors, their baseline signal level, and the stability of the measurements response. The constructed gas sensor arrays and flow path configurations are presented in Figure 27.

The individual measuring components were reinstalled in separate chambers made of polytetrafluoroethylene. The use of PTFE minimized the possibility of undesirable interactions between the chamber material and the components of the gas sample. The low surface activity and chemical resistance of this material reduced the likelihood of adsorption of the analyzed compounds, their subsequent desorption, and the accumulation of contaminants within the measurement path. This solution was designed to minimize the memory effect and improve the repeatability of subsequent measurement cycles. The sample was transported through the system using a diaphragm pump. The pump's flow rate was controlled using pulse width modulation (PWM), which made it possible to maintain a gas flow rate of 50 mL·min^{-1}.

7.2.4 Measurement procedure and sampling

The biofiltration process of a mixture of n-hexane and cyclohexane was conducted in continuous mode for 30 days, dividing the experiment into three main stages, each lasting 10 days. The purpose of this regimen was to verify the biological stability of the bed and the predictive effectiveness of mathematical models of the sensor array under various reactor loading conditions. Basic process parameters, such as the empty bed residence time (EBRT = 60 s) and the total gas flow rate ($\dot{Q}$ = 2.5 dm^3·min^{-1}), were kept constant throughout the entire duration of the experiments. This allowed for the analysis of the effect of a single independent variable - the inlet loading (IL) - whose values were modified in successive phases of the experiment by adjusting the concentrations of analytes in the feed stream. The process was monitored through daily gas sampling in accordance with a 30-day measurement cycle. A summary of the set of parameters for each stage of the BTF operation is presented in Table 10.

Table 10. Operating parameters of the BTF system during each stage of the experiment.

		Research stage		
Parameter	**Unit**	**Phase I**	**Phase II**	**Phase III**
Duration	days	10 (days 1-10)	10 (days 11-20)	10 (days 21-30)
EBRT	s	60	60	60
Gas flow rate ($\dot{Q}$)	dm^3·min^{-1}	2.5	2.5	2.5
IL of n-hexane	g·m^{-3}·h^{-1}	~ 20-25	~ 50-60	~ 80-90
IL of cyclohexane	g·m^{-3}·h^{-1}	~ 15-20	~ 55-65	~ 25-35

The use of this measurement regimen made it possible to test the system across a wide range of concentrations: from optimal conditions (Stage I), through high-load conditions (Stage II for n-hexane and Stage III for cyclohexane), to the maximum removal efficiency testing phase (Stage III for n-hexane and Stage II for cyclohexane). All changes in IL were monitored in real time, which allowed for the validation of sensory models across the entire operating range. The process efficiency was determined based on the difference in contaminant concentrations in the gas stream before and after passing through the biologically active bed. For this purpose, samples

were collected at the reactor inlet and outlet and stored in bags made of Tedlar film. Quantitative analysis was performed immediately after sample collection using GC-FID. The same gas samples, collected in TEDLAR bags, were used for both chromatographic and gas sensor array analysis. The results obtained by the GC-FID method were compared in parallel with the readings from a gas sensor array developed specifically for this study. This approach made it possible to directly correlate the sensor's electrical signals with the actual concentrations of n-hexane and cyclohexane determined by chromatography.

The gas sensor responses was recorded in a cyclic stop-flow mode. One measurement cycle consisted of a dynamic filling stage of the sensor cells and a static exposure stage of the sensors. In the first stage, the gas sample was introduced into the chambers for 60 s. During this time, the flow forced by a diaphragm pump ensured air exchange inside the chambers and contact between the active layers of the sensors and the sample. After the flow stage was completed, the pump was turned off, and the sample was left in the chambers for another 40 seconds. Stopping the flow eliminated disturbances resulting from hydrodynamic changes and allowed the responses of individual elements to stabilize. Signals were recorded after the static exposure period, when changes in sensor readings were minimal and the system was approaching quasi-steady-state conditions. Before each analytical run, the measurement line was conditioned with blank air. The system was purged until the sensor signals decreased and returned to near their initial baseline level. This procedure minimized the influence of sample residues from the previous cycle and reduced the risk of response overlap between consecutive measurements.

In order to convert the multidimensional signal from the sensor array into specific analyte concentration values, a two-step process was required: laboratory calibration and validation under process conditions. The calibration process was carried out prior to the start of the 30-day research process, using specially prepared gas mixtures with known concentrations. The mixtures were generated using the system shown in Figure 28.

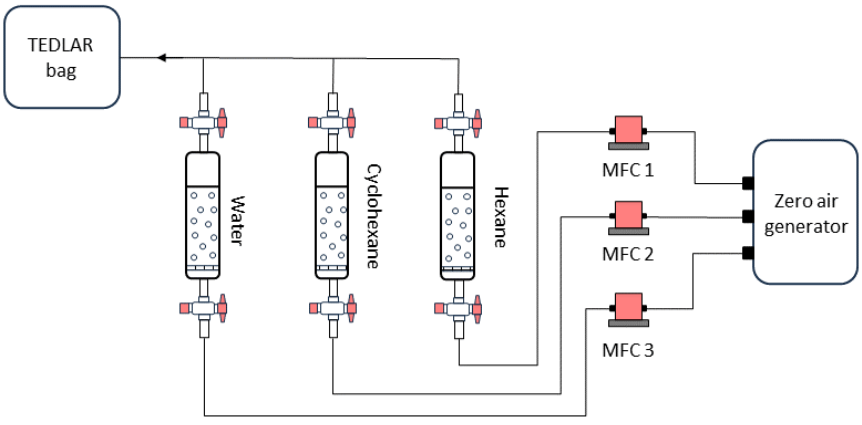


Figure 28. Structure of a generator for gas calibration mixtures with a sample humidification section. Adapted from [267], licensed by CC BY-SA 4.0.

During the sensor array calibration, the effect of humidity on the sensor signals was deliberately taken into account. To this end, the system generating the calibration mixtures was retrofitted with an additional water bubbler, which made it possible to train the models to operate

under high humidity conditions typical for biofilters. Calibration was performed for n-hexane and cyclohexane in the range of 50 to 500 ppm. The actual concentrations in the calibration mixtures were determined using GC-FID. The analysis of each calibration sample was repeated three times to ensure the stability of the model. Two regression techniques were used to develop the predictive algorithms: MLR and PCR. The models were validated using actual samples collected directly from the inlet and outlet of the biofilter during a 30-day study.

7.2.5 Data analysis and mathematical modeling

The analysis of all collected measurement data and the necessary statistical calculations were conducted employing RStudio Desktop software (v. 1.0.143). In order to quantitatively reflect the multidimensional electrical responses recorded by a gas sensor array as concentrations of the analyzed VOCs a procedure was applied that involved the extraction of diagnostic signal parameters and the construction of regression models. The input variables for the models were two variants of the response representation for individual sensors:

- ΔS_i – the change in the signal from the i-th sensor, calculated as the difference between the maximum response value recorded under steady state conditions $(S_{max,i})$, and the baseline value recorded during the sensor's exposure to clean air $(S_{0,i})$.

$$\Delta S_i = S_{max,i} - S_{0,i} \tag{22}$$

- $S_{r,i}$ – the relative response of the i-th sensor, representing a normalized measure of the signal change against its corresponding baseline level.

$$S_{r,i} = \frac{S_{max,i}}{S_{0,i}} \tag{23}$$

The resulting data matrices were used to calibrate and validate two statistical modeling methods: MLR and PCR. The theoretical foundations and estimation procedure for the MLR were presented in the previous chapter (6.2.5). The reminder of the analysis was devoted to the formal characterization of the PCR model and its application to predicting analyte concentrations. PCR is a two-step modeling method in which the original set of intercorrelated explanatory variables is replaced by a set of orthogonal latent variables, referred to as principal components (PCs). These components are linear combinations of the input variables and are ranked in descending order according to their contribution to explaining the total variance of the data. The procedure for constructing a predictive model includes the following steps:

- Principal Component Analysis (PCA) – the sensor response matrix is transformed into principal component space, this transformation yields uncorrelated predictors, reduces the impact of multicollinearity, and allows for dimensionality reduction by retaining only those components that describe a significant portion of the variability observed in the measurement dataset.
- Regression model estimation – a multiple regression model is fitted to the selected subset of principal components, the predictors in the model are the principal component scores, while the dependent variable is the concentration of the target compound.

The general matrix form of the regression equation can be written as:

$$\boldsymbol{Y} = \boldsymbol{T\beta} + \boldsymbol{\zeta} \tag{24}$$

where $\boldsymbol{Y}$ denotes the vector or matrix of observed values of the dependent variable, $\boldsymbol{T}$ is the matrix of principal component scores, $\boldsymbol{\beta}$ is the vector of regression coefficients, and $\boldsymbol{\zeta}$ is the vector of random components. The matrix $\boldsymbol{T}$ is not given directly, but is obtained by transforming the matrices of the original variables. The estimation of the PCR model, therefore, proceeds in several stages. Let $\boldsymbol{S} = [S_{i,j}]$ be a data matrix comprising *n* observations and *k* explanatory variables. First, for each column, the empirical mean $\boldsymbol{z_j}$ is calculated, and the resulting values are compiled into a vector of means z in accordance with equation (25):

$$\boldsymbol{S} = \begin{bmatrix} S_{1,1} & \cdots & S_{1,k} \\ \vdots & \ddots & \vdots \\ S_{n,1} & \cdots & S_{n,k} \end{bmatrix} \rightarrow \boldsymbol{z_j} = \frac{1}{n}\sum_{i=1}^{n} \boldsymbol{S}_{i,j} \tag{25}$$

Next, the data are centered by subtracting the mean vector from each row of matrix $\boldsymbol{S}$. This yields the matrix $\boldsymbol{B}$, where *m* is n-element vector of ones. This allows for the subsequent inclusion of a constant term in the regression model. The covariance matrix $\boldsymbol{C}$ is determined based on matrix $\boldsymbol{B}$. The operator "*" denotes the Hermitian conjugate, which for real data reduces to the transpose:

$$\boldsymbol{B} = \boldsymbol{S} - \boldsymbol{mz}^T \rightarrow \boldsymbol{C} = \frac{1}{n-1}\boldsymbol{B}^*\boldsymbol{B} \tag{26}$$

The next step is analyzing the eigenvalues of matrix $\boldsymbol{C}$. Its eigenvectors form matrix $\boldsymbol{V}$ and define an orthogonal basis for the space of variables. The corresponding eigenvalues, collected in the diagonal matrix $\boldsymbol{D}$, indicate the contribution of individual directions to the total variance of the data:

$$\boldsymbol{D} = \boldsymbol{CVV}^{-1} \tag{27}$$

After selecting *k* principal components, the centered data are projected onto a basis formed by the corresponding eigenvectors. This yields the output matrix $\boldsymbol{T}$, whose columns are new, uncorrelated predictors. Applying linear regression to these and substituting $\boldsymbol{T}$ into equation (24) leads to the final matrix form of the PCR model:

$$\boldsymbol{T} = \boldsymbol{BV} \rightarrow \boldsymbol{Y} = \boldsymbol{T\beta} + \boldsymbol{\zeta} \tag{28}$$

The relationship given by Equation (28) can be expanded for a single observation. If the predicted value is denoted by *C* in the applied analysis, then the i-th element of the forecast vector corresponds to a linear combination of the results of that observation for the selected principal components. The general form of the PCR prediction is then as follows:

$$\hat{C}_i = \beta_0 + \beta_1 PC_1 + \beta_2 PC_2 + \cdots + \beta_k PC_{i,k} \tag{29}$$

where:

$\hat{C}_i$ – the predicted concentration of the analyte for the i-th observation,

β_0 – the intercept of the regression model,

β_k – the regression coefficient associated with the k-th principal component,

$PC_{i,k}$ – the predicted value of the k-th principal component for the i-th observation,

i – the number of principal components included in the model.

Equation (29) is therefore a scalar expansion of the relationship (24). Principal component analysis provides new, uncorrelated predictors, and linear regression determines their impact on the predicted value of the dependent variable. The Student's t-test played a key role in the process of optimizing the regression models, as it was used to rigorously assess the statistical significance of individual explanatory variables. Thanks to an iterative approach based on test statistics, signals from those sensors that did not make a substantive contribution to the prediction of n-hexane or cyclohexane concentrations were eliminated from the final equations. The use of this test significantly reduced the likelihood that the obtained correlations were incidental, which directly translated into higher mathematical reliability of the algorithms. The RMSE (chapter 6.2.5) was used to quantitatively assess prediction errors and verify the degree of fit of the models to the reference data.

The use of PCR in monitoring the biofiltration process was intended to reduce model instability resulting from strong correlations among sensor signals and to minimize the risk of overfitting. In classical MLR regression, adding additional predictors does not reduce the coefficient of determination R^2 for the calibration set. Therefore, an apparent improvement in the fit does not necessarily lead to an increase in the model's predictive ability for new observations. In the PCR method, the number of PCs is limited to a subset representing the dominant structure of data variability. This approach can increase the model's resistance to measurement noise, improve the stability of the estimated coefficients, and enhance the reliability of long-term concentration predictions under operational conditions of the biofilter system.

In order to reliably evaluate the performance of a BTF in the process of purifying air of n-hexane and cyclohexane vapors, a set of standard engineering parameters was used to quantitatively describe the process dynamics. Process data, such as the bed volume (V = 2.5 dm^3) and gas flow rate ($\dot{Q}$ = 2.5 $dm^3 \cdot min^{-1}$), were used in the calculations. The key parameters were calculated according to the following methodological approach:

- Removal efficiency (RE) – this parameter specifies the percentage efficiency of the process, it was determined based on the difference between the concentration of the substance at the BTF inlet (C_{in}) and its concentration in the treated stream (C_{out}).

$$RE = \frac{C_{in} - C_{out}}{C_{in}} \cdot 100\% \quad [\%] \tag{30}$$

- Elimination Capacity (EC) - this indicator provides information on the mass of pollutants that has been permanently removed by a unit volume of the filter bed within one hour, it measures the actual biological activity of the microorganisms colonizing the filter media.

$$EC = \frac{\dot{Q} \cdot (C_{in} - C_{out})}{V} \quad [gm^{-3}h^{-1}] \tag{31}$$

- Inlet Loading (IL) - defines the mass of contaminant introduced into a unit volume of the biofilter per unit of time, during the experiment, this parameter was systematically modified (in three stages), which allowed for an investigation of the system's stability under conditions of varying analyte concentrations.

$$IL = \frac{\dot{Q} \cdot C_{in}}{V} \quad [gm^{-3}h^{-1}] \tag{32}$$

- Empty Bed Residence Time (EBRT) – defines contact time between the gas phase and the filter material, it was calculated as the quotient of the bed volume and the flow rate of the gas mixture (for conditions of the described experiment it is a constant value of 60 s).

$$EBRT = \frac{V}{\dot{Q}} \quad [min] \tag{33}$$

7.3 Results and discussion

7.3.1 Characteristics of the sensor array response

Before developing predictive models, the response of individual array sensors to changes in cyclohexane and n-hexane concentrations was analyzed. The response of each sensor was described using two signal characteristics, designated ΔS and S_r. This made it possible to assess whether individual signal processing methods provide comparable information on changes in analyte concentration and whether these relationships are sufficiently regular to be used in quantitative modeling.

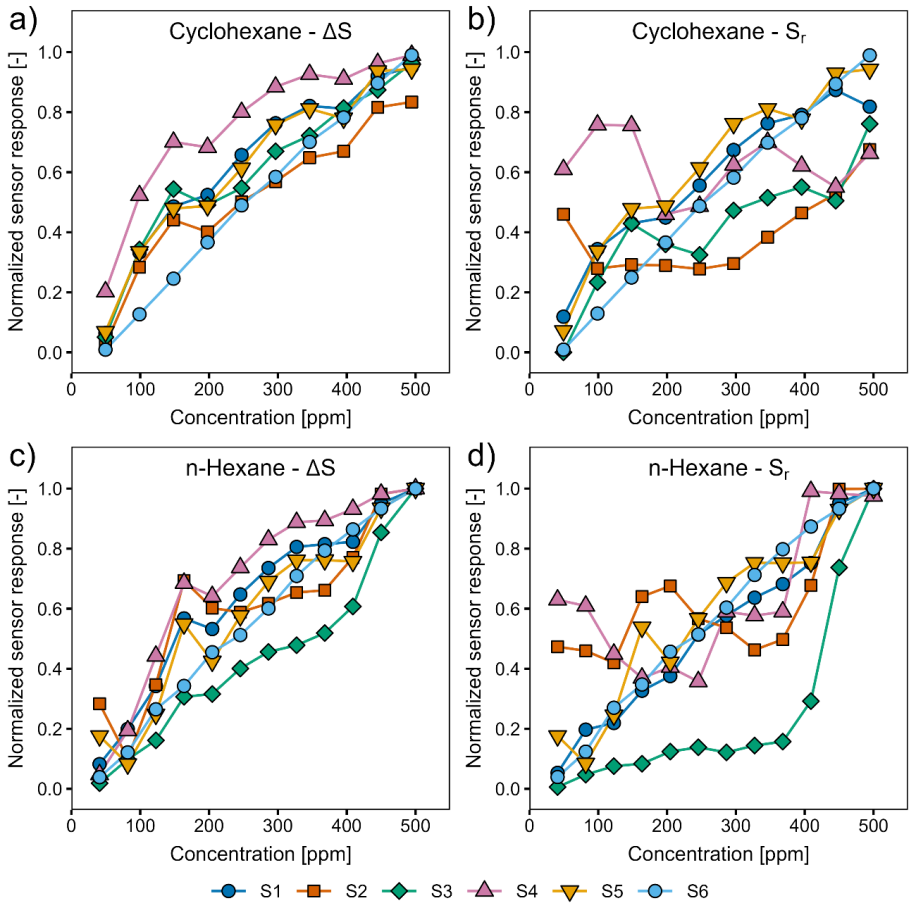


Figure 29. Normalized responses of the gas sensor array to increasing concentrations of cyclohexane: (a) ΔS and (b) S_r, and n-hexane: (c) ΔS and (d) S_r. Points represent mean sensor responses at individual calibration concentrations, while lines connect consecutive concentration levels. Responses were normalized separately for each sensor signal using min–max scaling.

Figure 29 shows the changes in the normalized responses of individual sensors as a function of the concentration of both compounds tested. Min - max normalization was performed separately for each signal characteristic, solely to enable their common presentation despite differences in signal values and ranges. Normalized values do not therefore directly reflect the absolute sensitivity of individual sensors, but allow for comparison of the direction and nature of changes in their response with increasing concentration. For both compounds, a more regular pattern of changes was observed in the case of ΔS characteristics. The responses of most sensors increased with increasing concentration across the entire analyzed range, with the dynamics of these changes dependent on both the type of sensor and the compound being determined. The S_r characteristics showed greater variability. In addition to signals that varied regularly, there were responses characterized by local changes in direction or a significantly weaker dependence on concentration.

To quantitatively assess the relationships, Pearson linear correlation coefficients were determined between compound concentration and individual matrix signal characteristics. Temperature (T) and relative humidity (RH) were also analyzed, as potential explanatory variables in the construction of predictive models. The results are presented in Figure 30.

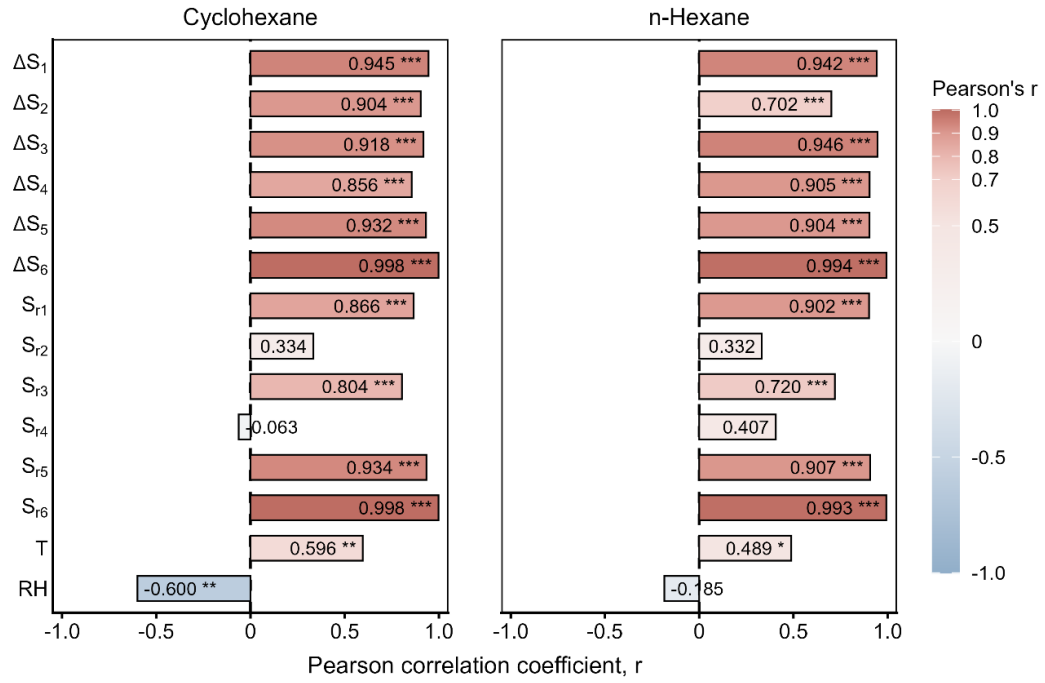


Figure 30. Pearson correlation coefficients between calibration concentration and sensor response characteristics (ΔS and S_r), temperature (T), and relative humidity (RH) for cyclohexane and n-hexane. Bar length and colour represent the magnitude and direction of Pearson's correlation coefficient (r). Asterisks indicate statistical significance after Benjamini–Hochberg correction (* $0.01 \leq p_{BH} < 0.05$, ** $0.001 p_{BH} < 0.01$, *** $p_{BH} < 0.001$).

For cyclohexane, the *r* coefficient values for the characteristics ΔS_1 - ΔS_6 were in the range of 0.856–0.998, while for n-hexane in the range of 0.702–0.994. This indicates a strong positive linear dependence of most ΔS characteristics on the concentration of the tested compounds. The highest values were obtained for ΔS_6, for which *r* was 0.998 for cyclohexane and 0.994 for n-hexane. Greater variation was found for the characteristics of S_r. For cyclohexane,

r values ranged from −0.063 for S_{r4} to 0.998 for S_{r6}, while for n-hexane they ranged from 0.332 for S_{r2} to 0.993 for S_{r6}. This means that not all methods of describing the responses of individual sensors were equally linearly related to the change in concentration. For some of the S_r characteristics, a strong positive relationship was found for both analyzed compounds (S_{r1}, S_{r5}, S_{r6}). A different nature of the relationships was found for environmental parameters. The temperature - concentration correlation coefficient was 0.596 for cyclohexane and 0.489 for n-hexane, respectively. For relative humidity, the values obtained were −0.600 and −0.185, respectively. These results indicated covariation of measurement conditions and concentration in the calibration sets and justified the inclusion of temperature and humidity as potential predictors during model construction.

It is important to note, however, that the correlation coefficient between a single signal and concentration was not a direct criterion for its inclusion in the final model. Pearson correlation describes relationship between each variable and concentration considered separately, whereas in a multivariate model, the significance of a predictor also depends on the information provided by the other variables. Consequently, signals strongly correlated with concentration could contain partially redundant information, while variables with weaker individual correlation could contribute complementary information. Observed variation in response characteristics and the coexistence of multiple signals strongly associated with concentration change formed the basis for the application of multivariate methods. Two approaches were subsequently employed: MLR, which allows for the direct use of selected input variables, and PCR, in which the information contained in interdependent predictors was represented using mutually orthogonal PCs. Characteristics of the developed models and assessment of their fit are presented in the next section.

7.3.2 Development and characterization of predictive models

In the case of MLR models, sensor response characteristics ΔS and S_r, as well as temperature and relative humidity, were considered as potential explanatory variables. Variables for the final model were selected iteratively, and the significance of regression coefficients was assessed using Student's t-test. Consequently, not all signal characteristics were retained in the final equations. For cyclohexane, the signals from the TGS2602 and TGS2603 sensors were deemed insignificant, while in the n-hexane model, variables related to the TGS823 sensor were eliminated. Temperature and relative humidity, however, were statistically significant elements of the developed models. This confirms the observation from the previous section that a high individual correlation between signal and concentration did not necessarily mean its inclusion in the multivariate model. The significance of individual predictors stemmed not only from their direct dependence on concentration, but also from the information they contributed after taking into account other variables.

In PCR, the interdependent variables describing the matrix response were replaced by PCs, which are mutually orthogonal combinations of the input variables. This transformation helps reduce problems resulting from signal collinearity, which is particularly important in the case of a sensor array, where individual elements may respond simultaneously to the same analyte. The

developed PCR models utilized seven principal components. Although the first component accounted for the dominant portion of the variability in the input dataset, subsequent components retained the orthogonal information contained in the array responses. It should be emphasized that the proportion of variance explained by the PCA components relates to the variability of the predictors, not directly to their ability to predict analyte concentration. Therefore, the usefulness of the final PCR models was assessed based on their prediction quality and then verified on samples from the biofiltration process.

The quality of the model fit to the calibration data was first assessed based on the relationship between the reference concentrations determined by GC-FID and the concentrations predicted by the models. The results are presented in Figure 31. For all developed models, high values of the coefficient of determination were obtained, exceeding 0.93. For cyclohexane, R^2 was 0.963 for MLR and 0.989 for PCR, while for n-hexane it was 0.932 and 0.990, respectively. In both cases, the PCR model was characterized by a higher R^2 value than the MLR model, and the points corresponding to the PCR predictions were more clustered near the relationship corresponding to 1:1 agreement with the reference method.

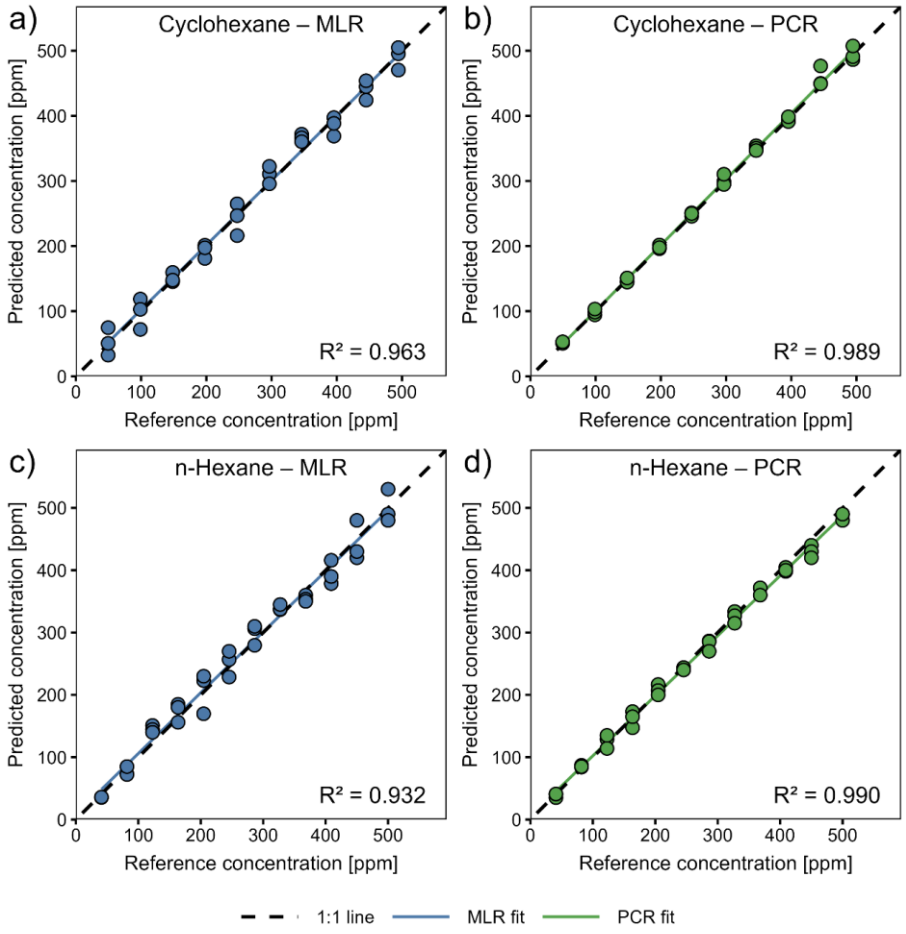


Figure 31. Calibration plots of the gas sensor array predictive models for cyclohexane: (a) MLR and (b) PCR, and n-hexane: (c) MLR and (d) PCR. Points represent concentrations predicted by the models versus reference GC-FID values. Solid lines indicate linear fits, while dashed lines represent the 1:1 agreement line. Adapted from [267], licensed by CC BY-SA 4.0.

However, the R^2 value alone is not sufficient to fully assess the quality of the prediction. Therefore, the analysis was expanded to include the mean square error of calibration (RMSEC), the mean absolute error (MAE), and the model bias, defined as the average difference between the predicted and reference concentrations. These indices were calculated based on the data used to develop the calibration plots and are summarized in Table 11. The greatest improvement in calibration parameters after PCR was observed for cyclohexane. The RMSEC decreased from 16.19 ppm for MLR to 7.59 ppm for PCR, while the MAE decreased from 12.68 to 4.84 ppm. For n-hexane, the PCR model also showed a smaller error. RMSEC decreased from 18.92 to 10.11 ppm, and the MAE from 16.83 to 7.67 ppm. The bias values were relatively small compared to the calibration range, although a negative bias of −3.85 ppm was obtained for the n-hexane PCR.

Table 11. Calibration performance metrics of MLR and PCR models for cyclohexane and n-hexane.

Compound	Model	R^2 [-]	RMSEC [ppm]	MAE [ppm]	Bias [ppm]
Cyclohexane	MLR	0.963	16.19	12.68	+0.93
	PCR	0.989	7.59	4.84	+2.49
n-Hexane	MLR	0.932	18.92	16.83	+1.85
	PCR	0.990	10.11	7.67	-3.85

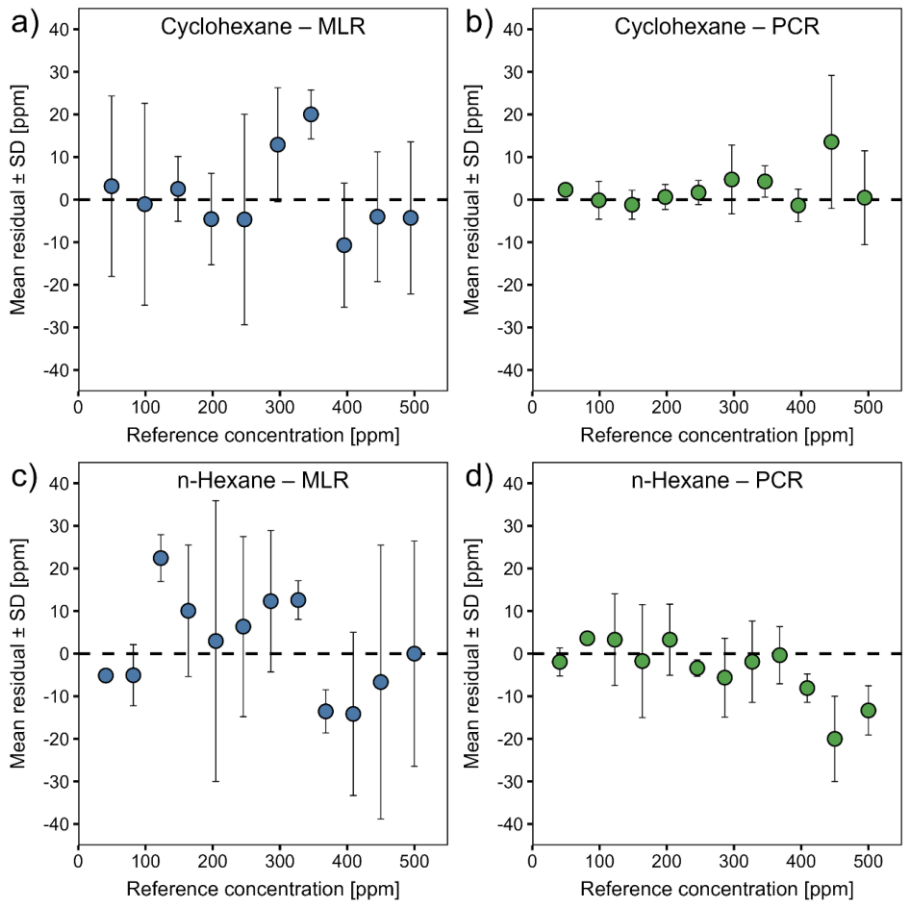


Figure 32. Mean residuals of calibration model predictions for cyclohexane: (a) MLR and (b) PCR, and n-hexane: (c) MLR and (d) PCR. Points represent mean residuals, while error bars indicate ±SD for repeated measurements. The dashed horizontal line denotes zero residual.

The results indicate a generally better fit of the PCR models to the calibration dataset, but the assessment of their quality also required checking the error structure in individual parts of the

measurement range. For this purpose, the model residuals (e_i), defined as the difference between the concentration predicted by the model and the reference concentration, were analyzed. Figure 32 shows the mean values of the residuals for subsequent calibration levels along with the standard deviations resulting from repeated measurements. Analysis of the residual distribution confirmed the differences seen in the calibration charts. For cyclohexane, the PCR model residuals were generally more concentrated around the zero value than for MLR, consistent with the lower RMSEC and MAE values. For the MLR model, larger deviations, both positive and negative, were observed in different parts of the calibration range. For n-hexane, PCR also reduced the overall error magnitude, but the distribution of residuals indicated some concentration dependence of the error. At the highest calibration levels, the PCR model tended to underestimate the concentration. This is an important observation because it demonstrates that a high R^2 value does not rule out the presence of local, systematic model biases. Therefore, analysis of residuals is an important complement to classical goodness-of-fit measures.

The combined analysis of the coefficients of determination, calibration errors and residual distributions indicates that both approaches allowed for quantitative representation of the relationship between the multivariate gas sensor array response and the concentration of cyclohexane and n-hexane. Under calibration conditions, PCR provided lower prediction errors, particularly for cyclohexane. However, at this stage, this did not yet determine the model's superiority in the actual biofiltration process. The final assessment of the models' suitability required their verification on samples taken from the BTF inlet and outlet under conditions of variable inlet load, as presented in the next subsection.

7.3.3 Monitoring the course and assessing the efficiency of the biofiltration process

The next stage of the research was to assess the feasibility of using the developed predictive models to monitor biofiltration under varying process load conditions. Applying successive levels of IL allowed to simultaneously characterize the biofilter's response to changes in the amount of pollutant input and verify whether the models using sensor array signals correctly represent the resulting differences in VOCs removal efficiency (RE). Figure 33 compares the RE determined using the GC-FID reference method with the values determined using the PCR and MLR models. Changes in the IL are also presented. This allows the sensor measurement results to be considered not only as subsequent concentration predictions, but primarily in relation to the actual changes occurring during the biofiltration process.

For cyclohexane, the stage I corresponding to the lowest IL of 13.20 - 18.50 g m^{-3} h^{-1}. It was characterized by the highest RE, in the range of approximately 61 - 71%. Increasing IL to 57.42 - 63.19 g m^{-3} h^{-1} (stage II) was associated with a significant decrease in RE and represented the conditions under which cyclohexane RE was the lowest. For further reduction of IL to 28.74 - 36.48 g m^{-3} h^{-1} (stage III), a temporary increase in RE was observed, followed by its stabilization at a level of approximately 42 - 51%. The course of changes therefore indicates that the biofilter response to load changes was not always immediate, and achieving a new level of efficiency may have required a period of adaptation of the biological system to the changed operating conditions.

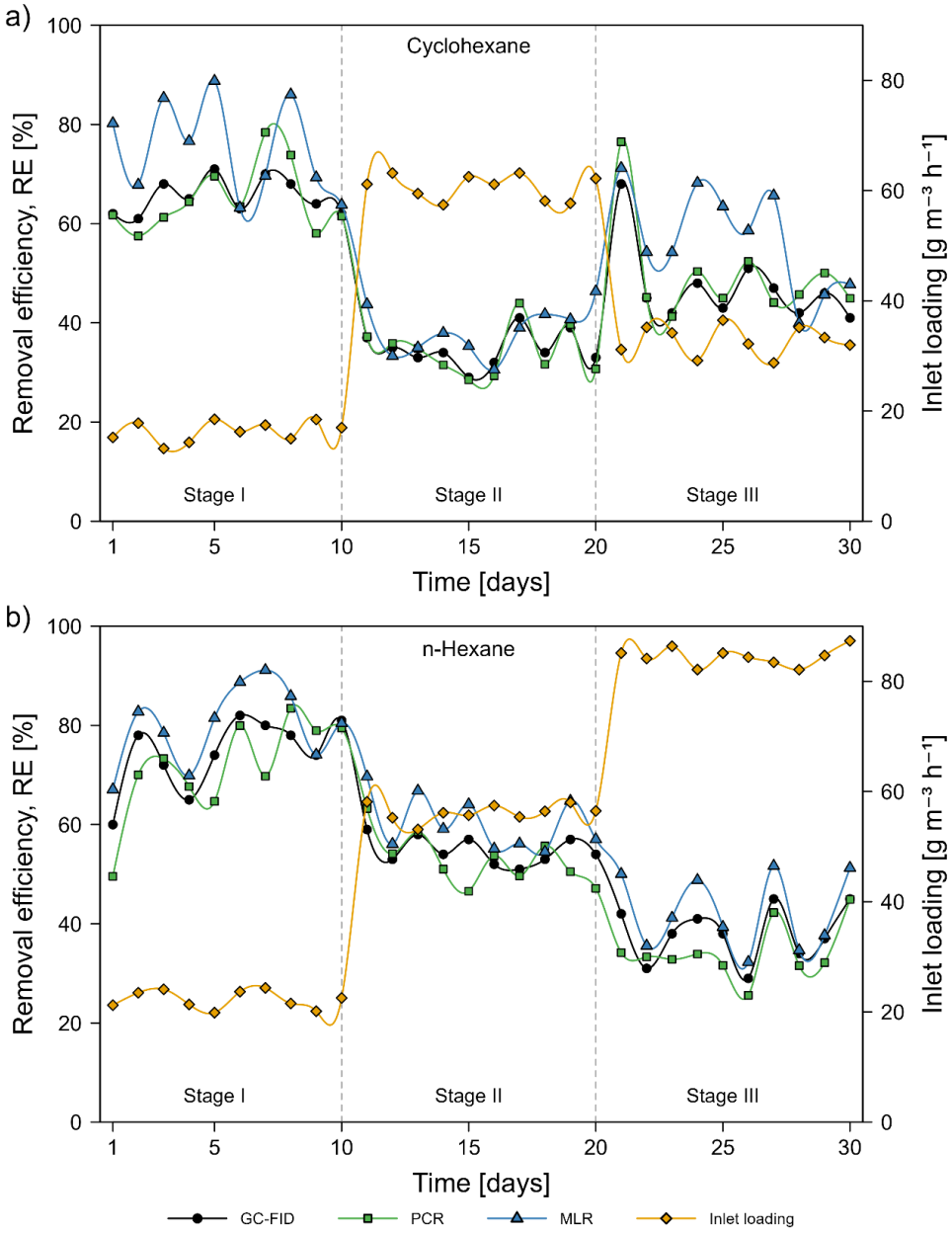


Figure 33. Changes in removal efficiency (RE) and inlet loading (IL) during the biotrickling filtration of cyclohexane (a) and n-hexane (b). RE values were determined using the reference GC-FID method and predicted by the gas sensor array with PCR and MLR models. Inlet loading is presented on the secondary y-axis. Dashed vertical lines indicate the boundaries between the three process stages.

For n-hexane, the relationship between IL and RE was even more regular. At a loading of 19.87 - 24.36 g m^{-3} h^{-1} (stage I), the highest RE values of about 70 - 80% were obtained. Increasing IL to 53.12 - 58.12 g m^{-3} h^{-1} (stage II) resulted in a reduction of removal efficiency to 51 - 59%, while at the highest applied loading of 82.11 - 87.34 g m^{-3} h^{-1} (stage III) RE decreased to about 29 - 41%. In the entire studied range, the increase in the amount of n-hexane fed to the biofilter was therefore associated with a gradual decrease in the share of the pollutant removed from the gas stream. However, evaluating a process solely based on RE does not fully reflect its ability to remove contaminants. Therefore, the elimination efficiency (EC) was also analyzed, which describes the amount of a compound removed per unit of bed volume and time. Unlike RE,

this parameter depends on both the degree of contaminant removal and its IL. Consequently, a decrease in the percentage removal efficiency with an increase in IL does not necessarily mean a proportional decrease in the amount of compound actually eliminated in the biofilter.

The maximum EC value was approximately 30 g m^{-3} h^{-1} for cyclohexane and 40 g m^{-3} h^{-1} for n-hexane, both in stages with the highest IL. These results show that with increasing loading, the biofilter was able to eliminate more VOCs per unit of bed volume, despite a simultaneous decrease in RE value. Considering RE together with IL and EC allows for a more comprehensive description of the BTF behavior. RE determines the relative efficiency of gas stream purification, while EC characterizes the actual capacity of the bed to remove the incoming contaminant load. Therefore, under the analyzed conditions, the limit for increasing the load was not the complete loss of VOC biodegradability, but rather the gradual reduction in the proportion of the compound that could be removed during contact with the bed. Comparison of the results for both compounds also indicates that the relationship between IL, RE, and EC was compound-specific. N-hexane achieved a higher maximum EC than cyclohexane, however, a direct comparison of the biodegradability of both compounds based solely on this is not justified, as the experiments employed different inlet loading ranges. Therefore, the obtained values should be interpreted primarily as a characteristic of BTF performance under the process conditions employed, rather than as a direct measure of the relative biodegradability of both VOCs.

From the perspective of the main goal of the conducted research, it was then important to determine whether the described process changes could be correctly tracked using the gas sensor array. The curves presented in Figure 33 indicate that the RE values determined using the PCR and MLR models generally reproduced the direction of changes observed using the GC-FID reference method. This applied both to periods of relatively stable biofilter operation and to changes accompanying transitions between individual IL levels. Thus, the array response enabled not only the determination of the concentration of the analyzed compounds but also the tracking of changes in the parameter directly used to assess the effectiveness of the process.

However, the differences between the GC-FID results and the predicted values visible in the figure indicate that the accuracy of the two models was not the same. Especially in the case of cyclohexane, the MLR model more often overestimated the RE values relative to the chromatographic results, while the PCR derived curve remained much closer to the reference values. For n-hexane, the differences between the models were smaller, although again in this case, MLR tended to predict values slightly higher than those determined by GC-FID. Therefore, the assessment of visual consistency of the waveforms was supplemented with an RMSE parameter analysis (Table 12).

For cyclohexane, significantly better agreement with the reference results was achieved using the PCR model. The RMSE for the entire process was 3.542%, while for MLR it reached 10.597%. The advantage of PCR was also visible in each of the analyzed stages. The smallest error for this model, equal to 1.944%, was obtained at the largest IL range. These results are consistent with the better representation of RE changes by the PCR model, observed in Figure 33. In the case of n-hexane, the difference between the models was much smaller. The

RMSE for the entire process was 5.954% for MLR and 5.494% for PCR, indicating similar prediction quality for both methods. However, PCR achieved smaller errors in the second and third stages, while in the first stage, the RMSE values of both models were practically identical.

Table 12. RMSE values between the removal efficiency (RE) determined by the GC-FID method and the values determined by the MLR and PCR models in individual biofiltration stages and for the entire process.

Compound	Model	RMSE [%]			
		Stage I	Stage II	Stage II	Entire process
Cyclohexane	MLR	12.363	5.950	12.192	10.597
	PCR	4.447	1.944	3.717	3.542
n-Hexane	MLR	6.524	6.206	5.028	5.954
	PCR	6.587	4.885	4.827	5.494

An interesting relationship was also observed between the magnitude of model errors and process conditions. The lowest RMSE generally occurred in stages corresponding to higher IL values, and thus higher concentrations of the analyzed compounds in the gas stream. For cyclohexane, the minimum error occurred in stage II, while for n-hexane, the lowest values were obtained in stage III. It can be assumed that as the VOC concentration increased, the sensor signals were within the more favorable range of their measurement characteristics, while at low concentrations, the sensor responses were closer to the lower limit of the quantitation range. This resulted in a greater relative prediction uncertainty precisely in the conditions of the lowest process load. The obtained results show that the developed models allowed for quantitative representation of changes in BTF efficiency occurring under the influence of changes in IL. Good agreement with the GC-FID method was achieved for the PCR model applied to cyclohexane, while for n-hexane, both models provided similar accuracy. A combined analysis of the RE, IL and EC parameters, and RMSE values confirms the feasibility of using the gas sensor array not only for determining the concentrations of the studied VOCs, but also for quantitative monitoring of changes in the efficiency of the biological deodorization process under varying conditions.

7.4 Summary and conclusions

The obtained results regarding biofiltration were consistent with the trends described for biological removal of hydrophobic VOCs. For both compounds analyzed, increasing the IL led to a decrease in the percentage RE, with the maximum RE being approximately 40 g m^{-3} h^{-1} for n-hexane and 30 g m^{-3} h^{-1} for cyclohexane. A similar relationship for n-hexane was observed by Yu et al. [268], who noted a decrease in the average RE from 92.6 to 63.8% when the loading increased from 15.67 to 61.59 g m^{-3} h^{-1}. The results of Cheng et al. [269] also indicate that the n-hexane removal efficiency can be increased by improving the transport of the hydrophobic compound to the biological phase, e.g., using surfactants.

In the case of cyclohexane, Salamanca et al. [270] obtained RE of 80 - 99% and EC of up to approximately 38 g C m^{-3} h^{-1}, while at the highest tested concentration the RE decreased to approximately 40%. Direct comparison of EC values in this case requires caution because the authors expressed it as a mass of carbon. Comparing these results with this research indicates that RE and EC values are strongly dependent on process conditions, filling type,

microorganisms, and mass transfer intensification. Therefore, for further analysis, it was more important not to achieve a specific maximum RE or EC value, but to obtain controlled changes in process efficiency, which could be used to verify the sensor array's ability to quantitatively monitor them.

The primary goal of this research stage, however, was not to optimize the BTF process itself, but to assess the feasibility of its quantitative monitoring using a gas sensor array. The developed calibration models were characterized by high coefficients of determination, ranging from 0.932 to 0.990, while their validation during biofiltration demonstrated RMSE for the entire process of 5.954% for MLR and 5.494% for PCR for n-hexane, and 10.597% and 3.542%, respectively, for cyclohexane. These results indicate that evaluating the model solely based on calibration parameters would be insufficient, as its actual usefulness is determined only by its compliance with the reference method under variable process conditions.

Quantitative results obtained in other studies allow to place the achieved modeling quality against the background of previous applications of sensor arrays. Rybarczyk et al. [237], using a MOS sensor array to determine cyclohexane during BTF operation, obtained an MLR model with R^2 = 0.91 after removing statistically insignificant variables. In own studies, for the same compound, the coefficient of determination was 0.963 for MLR and 0.989 for PCR, which indicates a very good ability of the developed models to represent the relationship between the array response and the cyclohexane concentration. Due to differences in arrays design, concentration ranges, and experimental conditions, the R^2 values should not be considered a direct ranking of the two systems, but they do show that the obtained calibration quality is at least within the range of results reported for similar electronic nose applications.

Even more important is the comparison of different modeling methods. Szulczyński et al. [232,233], monitoring n-butanol biofiltration using an eight-sensor electronic nose, obtained RMSE values of 7.5 ppm for MLR, 12.8 ppm for PCR, and 5.4 ppm for PLSR. Therefore, PLSR was the best, while PCR had the largest error. In own studies the relationship was different: for cyclohexane PCR gave a much smaller error than MLR (3.542 vs. 10.597% RE), while for n-hexane the difference was small (5.494 vs. 5.954% RE). The RMSE numerical values from that study should not be directly compared with the RMSE obtained in own studies, as the former were expressed in ppm concentration, while the latter were expressed in percentage points of RE. However, the comparison is important from the perspective of the relative effectiveness of the models and shows that there is no single regression model that provides the best results regardless of the compound analyzed or the array used.

The significance of this conclusion is strengthened by the fact that in the studies by Szulczyński et al. [232] the greatest discrepancies during the actual biofiltration occurred for PCR and were related to the presence of water vapor in the gas leaving the bed, which was not included in the calibration samples. In own studies, temperature and relative humidity were included in the models, and both variables were found to be statistically significant. This result indicates that when using sensor arrays for BTF monitoring, incorporating environmental variables can be

crucial to maintaining the quality of predictions after switching from controlled calibration mixtures to process-derived samples.

With respect to the tasks assigned to the first research hypothesis, the conducted stage involved characterizing the biological deodorization process, calibrating the matrix against GC-FID, developing quantitative models, and verifying their performance under varying process load. It was particularly important to confirm the quality of the models not only using the determination coefficients obtained during calibration, but also by assessing the errors relative to GC-FID during the actual biofiltration. The results of this stage thus provide direct support for the part of the hypothesis relating to the biological treatment of gas streams. They indicate that the ability to quantitatively monitor the process results from a combination of appropriate sensor selection, calibration, modeling, and validation under varying operating conditions.

The obtained results confirmed the applicability of this approach to biological deodorization. In the next stage of the research, the scope of its verification was expanded to include a process with a different contaminant removal mechanism, i.e., the absorption of model biogas components, also conducted using green solvents. The greater complexity of the purified gas stream composition and the use of different absorbent systems allowed for further evaluation of the potential for quantitative use of sensor array responses and data analysis methods under more complex process conditions.

7.5 Publication basis of the chapter

This chapter is based in part on research previously published in:

Dobrzyniewski D., Szulczyński B., Rybarczyk P., Gębicki J. (2023). Process control of air stream deodorization from vapors of VOCs using a gas sensor matrix conducted in the biotrickling filter (BTF). *Archives of Environmental Protection,* 49(2), pp. 85-94. doi: 10.24425/aep.2023.145900.

The article is distributed under the Creative Commons Attribution-ShareAlike 4.0 International License (CC BY-SA 4.0). The material has been revised, adapted, and expanded for the purpose of this doctoral dissertation. The findings are discussed in the context of the main research objective of the thesis.

8. Monitoring the absorption purification of biogas from a multicomponent mixture of pollutants using gas sensor array

8.1 Purpose of the study

The aim of this stage of the research was to evaluate the effectiveness of monitoring the absorption treatment process of a model biogas using a gas sensor array as a fast and low-cost alternative to conventional gas chromatography. The study focused on the removal of key organic pollutants (VOCs) - acetone, toluene, and cyclohexane, which negatively affect the calorific value of biogas and the durability of cogeneration systems. A key innovation was the use of an expanded procedure for assessing the agreement between the two methods, encompassing not only correlation and prediction error but also Passing–Bablok regression, the CUSUM test, and Bland–Altman analysis. Furthermore, a set of criteria was proposed for a comprehensive assessment of the agreement between the sensor-based method and the reference method. An additional contribution was the application of a baseline correction dependent on the type of absorbent liquid, which helped limit the influence of the absorbent on the sensor response and reduce the number of required predictive models.

8.2 Materials and methods

8.2.1 Absorption unit

An experimental evaluation of the ability of sorption liquids to remove VOCs was conducted in a flow-through absorption system operating under dynamic conditions (Figure 34). Contact between the gas phase and the absorbent occurred in a barbotage column, where the gas stream was introduced directly into the liquid phase and dispersed as bubbles. This experimental setup ensured a large interfacial contact area and enabled observation of changes in separation efficiency over time. The test conditions were set up to generate gas streams with a specific concentration of pollutants, maintain stable process conditions, and simultaneously analyze gas composition before and after contact with the absorbent.

Acetone, toluene, and cyclohexane (Sigma-Aldrich, St. Louis, MO, USA, with a declared purity of at least 99.5%) were selected as contaminants (odorous compounds), representing VOCs that differ in polarity and affinity for the liquid phase. In the studies, air was used as the carrier gas, into which the vapors of individual analytes were introduced, so that their concentration at the system inlet was about 2000 mg m^{-3}. All measurement series were conducted at room temperature under consistent hydrodynamic conditions. The gas flow rate was set at 50 mL min^{-1}, while the volume of the absorption liquid in the column was 50 mL.

Two absorption liquids with different chemical properties were used in the study. The reference material was the commercial absorbent Genosorb® 1843 (Clariant, USA), which was used as a reference medium to evaluate the effectiveness of an alternative sorption liquid. The second medium was a deep eutectic solvent (DES) prepared from octanoic acid (OA, purity ≥ 99%, Sigma-Aldrich, St. Louis, MO, USA) and nonanoic acid (NA, purity ≥ 97%, Sigma-Aldrich,

St. Louis, MO, USA). The components were combined in a 1:1 molar ratio and heated to 70°C while stirring until a homogeneous, clear liquid phase was obtained. The DES prepared in this manner was then used directly in the absorption experiments. A summary of the basic physicochemical parameters of both absorption liquids is presented in Table 13.

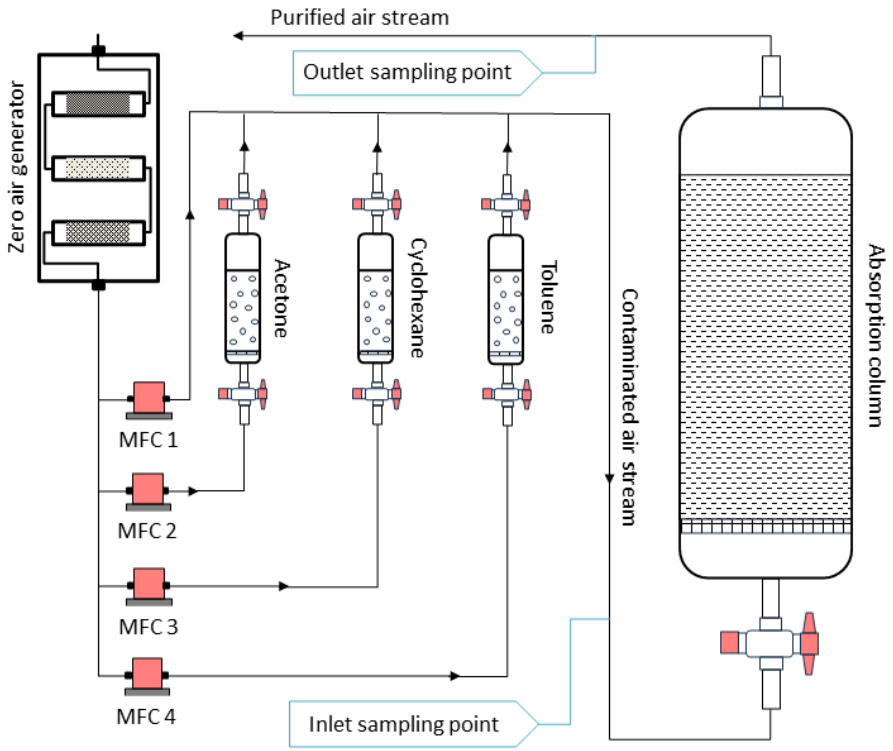


Figure 34. A test setup for the quantitative determination of acetone, toluene, and cyclohexane in a model biogas purification process. Adapted from [271], © 2024 Elsevier Ltd.

Table 13. Selected physicochemical properties of absorbents used to remove acetone, toluene, and cyclohexane from a model biogas stream.

Parameter	Unit	Genosorb® 1843 (G)	DES (OA:NA 1:1)
Absorbent type	-	Commercial organic solvent	Green, ecological solvent
Density at 20℃	$g \cdot cm^{-3}$	1.02 – 1.04	0.91
Viscosity at 20℃	$mm^2 \cdot s^{-1}$	7.80	6.36
Melting point	℃	-23.0	-1.4

8.2.2 Reference equipment (GC-FID)

Quantitative analysis of acetone, toluene, and cyclohexane concentrations in a model gas stream was performed using GC-FID, which served as the reference technique for evaluating the absorption process. The analyses were performed using a Varian CP-3800 gas chromatograph (Varian Analytical Instruments, USA). The same instrument configuration and unchanged chromatographic separation conditions were used as in the experiments described earlier in chapters 6.2.2 and 7.2.2. A detailed description of the analytical procedure is therefore presented in the previous section of this work, while the most important operating parameters of the system, relevant to this series of measurements, are summarized in Table 8. GC-FID analysis was performed on gas samples taken from the process stream, before the absorption column, and

after passing through the absorbent. The measured values were then used to quantify the disappearance of each volatile compound, estimate concentration profiles, and plot breakthrough curves. Furthermore, the GC-FID results served as a reference for the signals collected by the gas sensor array, enabling calibration and validation of the predictive models.

8.2.3 Gas sensor array development

A modular gas sensor array was used for the purposes of this study. The system was designed to simultaneously record the responses of multiple sensors with different sensitivities and operating principles. This approach provides a multidimensional description of the gas sample, based on the signals from individual detection elements. The device contains a pneumatic section, switchable sensor inserts, a control unit for operating the elements, and an electronic acquisition unit. They were assembled in a common housing enclosure with the front panel. It has ports for gases, a power switch, a connection interface, and LEDs indicating the state of the entire setup. Modular design allows replacing sensors or changing the array configuration without rebuilding the entire system. The constructed gas sensor array and measurement line configurations (reference and measurement lines) are presented in Figure 35.

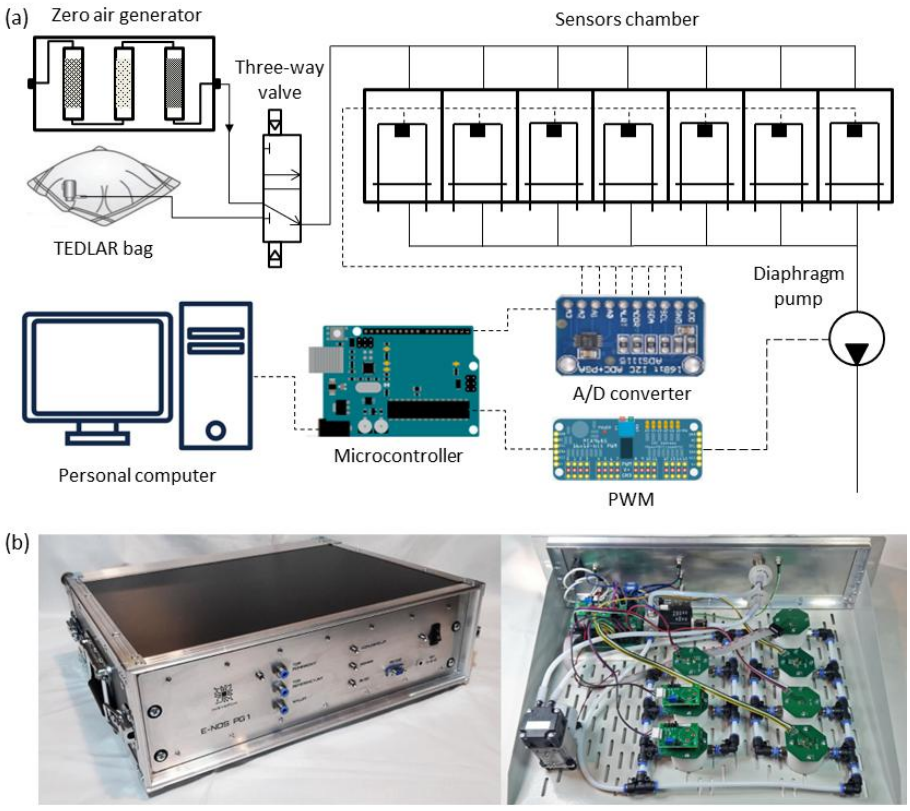


Figure 35. Structure of the pneumatic system (a) and general view of the gas sensor array prototype (b) used in the model biogas absorption process. Adapted from [271], © 2024 Elsevier Ltd.

The pneumatic system was responsible for delivering a gas stream to the sensor chambers in a precise and repeatable manner. This system had two isolated inputs: a reference input, supplied with purified air, and a measurement input that transported the tested sample. After passing through the matrix, the gas stream was discharged through a common outlet. The

connection to the device was made using bulkhead quick-connect fittings adapted to 4/6 mm PTFE tubing. Replaceable dust filters were placed upstream of the switching valve, on both gas inlets. Their function was to limit the ingress of particulate matter into the sensor chambers and the pump, reducing the risk of contamination of the measuring elements and tubing.

The gas source was selected using a two-position YSV321-DP solenoid valve. Reference line was connected to a normally open channel, while the measurement line was connected to a normally closed channel. In the default configuration, the reference gas flowed through the matrix. Each time the valve was turned on and left in this mode, sample gas flowed through the matrix. This reduced the risk of accidentally leaving test gas in the pneumatic system and causing overexposure, and also allowing the sensors to quickly return to baseline. Gas flow downstream of the valve was split into several independent streams using a splitter, one for each chamber. This allowed the sensors to have direct contact with the sample and limited the influence of one sensor on the operating conditions of the next, for example, by locally heating the sample or changing its flow. After leaving the chambers, the individual streams were recombined.

The sample flow was forced by a DP102-X2 diaphragm pump at the matrix outlet. Both the pump and the valve were powered by 12 V. The pump output was regulated by PWM, with a duty cycle ranging from 0% to 100%, allowing the flow rate to vary according to experimental conditions, chamber volume, and desired dynamic gas exchange performance. At very low duty-cycle PWM, the pump was sluggish to start, and it showed some increase in gas flow pulses during operation at low speed.

Similar to the monitoring of biofiltration purification processes (chapter 7), the array was equipped with five Figaro MOS sensors: TGS2600, TGS2602, TGS2603, TGS823, and TGS8100, a PID-A12 photoionization detector, and the SHT25 digital temperature and relative humidity sensor. Ultimately, the system comprised six channels dedicated to the detection of gaseous components and one channel for recording environmental conditions.

Each MOS sensor operated with a load resistor, creating a voltage divider. The reference elements were placed directly on the sensor module boards. Measuring the divider voltage allowed for determining the sensor resistance and then observing its changes relative to the value recorded in the gas samples. The relationship between sensor resistance and substance concentration is non-linear, so the analysis might use raw signals, resistance values, relative resistance changes, or parameters determined through individual calibration. Unlike MOS sensors, the PID signal's relationship to concentration is approximately linear. However, the conversion factor depends on the type of substance being analyzed, so correct concentration determination requires calibration for the specific gas or the use of an appropriate response factor. The SHT25 sensor communicates with the control unit via an I2C bus and provides temperature and relative humidity data. Recording these parameters is important because the responses of semiconductor sensors may depend not only on the sample composition but also on the current environmental conditions. Data from the SHT25 can therefore be used as additional variables to describe the measurement process and for subsequent signal processing.

The electronic circuit consisted of two modules operating in tandem. The former regulated the powering and switching of the actuators, such as the gas valve, pump, and indicator lights, while the latter collected data from the sensors, communicated with the computer, and followed the control instructions. The computing part consisted of the STM32F103RET6 ARM Cortex-M3 controller, orchestrating the entire measurement, valve control, pump control, and periodic sensor collection. The data acquisition portion uses an external 12-bit analog-to-digital converter to acquire precise analog measurements and an external high-accuracy ADS1256 module.

Measurement values were updated at one-second intervals. Data was transmitted either upon request from the master program or automatically in continuous mode. Communication with the computer was achieved via a UART interface operating in the RS232 standard. The device was controlled via ASCII text commands. The software enabled, among other things, changing the active gas channel, adjusting the pump's PWM signal, selecting the data transfer method, and defining the format of the presented results.

The use of software control of the valve and pump enables the preparation of a repeatable measurement sequence. After turning on the device, the reference path was active, while the pump remained off until the appropriate command was received. After the sensor warm-up phase was completed, the reference gas flow could be initiated and baseline values recorded. Once the valve is in the measurement position, the signals corresponding to the matrix's response to the sample being tested are recorded. After the measurement is complete, the reference gas is switched back to return the signals to their original values. The device's status can be monitored via LEDs. These LEDs indicate whether the power is on, whether the first complete set of measurements has been taken, whether the sampling line is open, whether a command has been received, or whether a communication error has occurred. This allowed the experiment to be monitored without having to look at the computer monitor.

8.2.4 Measurement procedure and sampling

The fundamental step before measuring process samples was preparing gas mixtures of known composition to calibrate the gas chromatograph and the sensor array. In both cases, calibration samples were prepared in TEDLAR bags, enabling the collection and short-term storage of gas mixtures. The method of preparing the mixtures was adapted to the type of measurement system. In chromatography, separate standards were prepared for each compound being analyzed, whereas during sensor array calibration, mixtures containing all analyzed contaminants were used. The gas chromatograph was calibrated using the external standard method. Independent series of standard samples were prepared for acetone, cyclohexane, and toluene, ranging in concentration from 0.5 to 2500 mg m^{-3}. Depending on the required concentration, the amount of liquid analyte fed to the mixture generation system (Figure 36) was adjusted accordingly. The volume of liquid dispensed ranged from 1 to 20 µL and was adjusted to achieve the required concentration in the gas phase after complete evaporation of the compound and dilution with a specified volume of air. Zero air was used to fill the bags, and its

volume was controlled using a mass flow controller (RED-Y GSC-B9SS-B23, Vögtlin Instruments GmbH, Muttenz, Switzerland).

Preparing each mixture required performing successive calculations based on the physicochemical properties of the given compound. First, its molar mass (M_i, g mol^{-1}) and density (ρ_i, kg m^{-3}) were considered, and then, based on a given volume of liquid (V_i, µL), its mass (m_i, g) and number of moles (n_i, moles) were determined. The next step was to determine the volume occupied by the analyte after entering the gas phase ($V_{gas,i}$, m^3). Knowing the volume of the evaporated substance and the amount of air introduced into the bag (V_{air}, dm^3), the volumetric concentration of the compound in the prepared standard was determined (C_i, ppm v/v). The C_i values were then converted to mg m^{-3}:

$$C_i = \frac{V_{gas,i}}{V_{air} \cdot 10^{-3}} \cdot 10^6 \quad [mg/m^3] \tag{34}$$

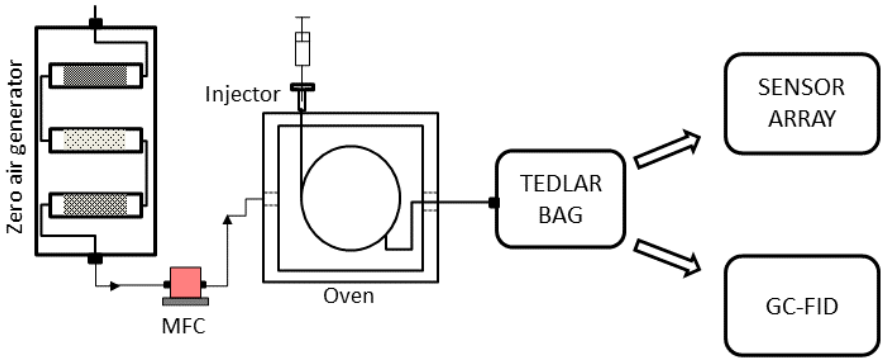


Figure 36. Schematic diagram of the system for preparing calibration gas mixtures. Adapted from [271], © 2024 Elsevier Ltd.

Thanks to this procedure, the actual analyte concentration in the mixture was determined directly by the amount of liquid intended for evaporation and the volume of diluent gas used. Samples prepared in this manner were subjected to chromatographic analysis, and calibration curves were determined based on these results. Measurements were repeated three times for each calibration gas mixture.

Sensor array calibration was based on similarly prepared reference mixtures, but the calibration sample had a more complex composition. Instead of preparing separate bags for acetone, cyclohexane, and toluene, a single TEDLAR bag was prepared containing all three compounds simultaneously at predetermined concentrations. First, the target concentration of each component was determined ($C_{odor,i}$, mg m^{-3} and then converted to ppm v/v). After determining the total mixture volume (V_m, dm^3), the amount of the appropriate gas standard to be transferred to the collective TEDLAR bag was calculated:

$$V_{odor,i} = \frac{C_{odor,i} \cdot V_m}{C_i} \quad [dm^3] \tag{35}$$

where C_i is the concentration of impurity substance in the reference mixture after evaporation (ppm v/v). After determining the volumes of all three components, the amount of zero air required to achieve the desired final volume was determined. This amount was equal to the difference between the total volume of the mixture and the sum of the volumes of the introduced standards:

$$V_0 = V_m - \sum_{i=1}^{n} V_{odor,i} \quad [dm^3] \tag{36}$$

The sample thus prepared was simultaneously analyzed by chromatography and by a gas sensor array. Chromatography provided reference values for individual components, while the sensors recorded the multidimensional response of the entire mixture. Combining both types of data enabled assigning specific sets of sensor signals to the actual concentrations of acetone, cyclohexane, and toluene. Only this prepared set provided the proper basis for calibrating the sensor system and for its subsequent use in evaluating samples from the absorption process.

A particularly important element of sensor array preparation was baseline correction. Sensor response depended not only on the presence of the compounds being assayed but could also be modified by the measurement environment, including the absorbent used in the purification process. Therefore, calibration performed solely against synthetic air did not provide sufficient background compensation in process measurements. Therefore, it was necessary to determine the baseline signal separately for the conditions corresponding to the absorbent used. To determine this background, synthetic air was passed through a vessel containing the tested absorbent and then directed to the sensor system (Figure 37). The signal recorded under these conditions reflected the influence of the absorbent and the entire measurement path in the absence of specific contaminants. This value was taken as the baseline $S_{0,i}$ for a given sensor.

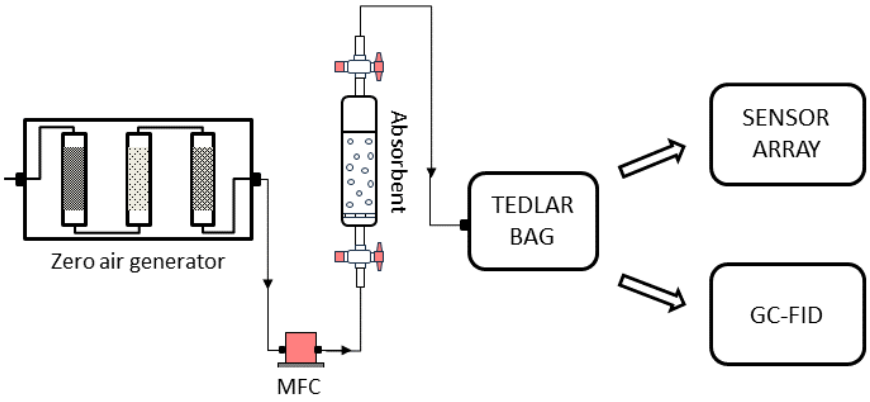


Figure 37. Schematic of the measurement setup used to determine the effect of the absorbent on sensor signals and to determine the corrected baseline. Adapted from [271], © 2024 Elsevier Ltd.

During the actual sample measurement, a fixed response value $S_{max,i}$ was determined. The signal used for further analysis was not the raw value, but the difference between the sample response and the corresponding background:

$$\Delta S_i = S_{max,i} - S_{0,i} \tag{37}$$

The term $S_{0,i}$ had two meanings related to the operating state: during calibration, it referred to a signal generated with synthetic air. During the analysis of working samples, it was found that, in relation to the measurement matrix (i.e., a specific sorbent). This meant that the ΔS_i signal primarily described the change in sensor response associated with the presence of the volatile pollutants being determined, and the influence of the process background was subtracted to the greatest extent possible before further data processing. Baseline correction was

consistently applied to both the calibration data and the signals from actual absorption samples. This had significant practical implications, as it minimized problems associated with absorbent-induced analyte concentration changes. At the same time, the corrected sensor response can be interpreted under similar operating conditions, regardless of background variations, without the need to develop a separate calibration for each operating background variant.

8.2.5 Data analysis and mathematical modeling

After baseline correction, the collected observations were treated as input data for training and learning a gas sensor array. The input variables were the corrected responses of the array elements, which included five MOS sensors, a PID photoionization detector, and SHT25 temperature and humidity sensor. The dependent variable was the concentration of a specific analyte determined using the reference method. Separate predictive relationships were generated for each of the three compounds. The data were separated into training and test data. The training dataset was used to estimate the model parameters (calibration phase), while the test dataset was used to verify the predictive validity of the created relationship for the observations on which it was not fitted (validation phase). Two regression models were used to quantify the relationship between the matrix response and contaminant concentration: MLR and PCR. In the MLR model, analyte concentration was determined directly as a linear function of the set of sensory signals. PCR used a PCA step in which the original, interdependent input variables were transformed into a system of orthogonal PCs, and regression was applied only then. Both approaches yielded predicted concentration values for each observation. The mathematical foundations of these models were described in sections 6.2.5 (MLR) and 7.2.5 (PCR).

Not all available collected sensor signals necessarily contributed significant information to a given model. The significance of individual explanatory variables was assessed using the Student's t-statistic for regression coefficients. For each coefficient, it was tested whether its value was statistically different from zero, indicating whether the corresponding variable made a measurable contribution to explaining concentration changes after accounting for the other predictors. The assumed significance level was $\alpha = 0.01$. A p-value lower than the assumed significance level ($p \ll \alpha$) constituted the basis for rejecting the null hypothesis of the lack of significance of the given predictor. Data analysis, processing, and statistical calculations were performed using RStudio Desktop (v. 1.0.143) and SigmaPlot (Version 15, Systat Software, USA). Using these programs, predictive modeling was carried out by selecting the appropriate explanatory variables, precisely determining the fit parameter for the devised algorithms, and carefully validating the results. From statistical treatment by which the matrix readings have been compared with the GC–FID reference values in such a way that a neutral estimation for agreements or discrepancies.

The statistical procedure should be viewed as consisting of two complementary tasks: assessing the calibration quality of the gas sensor array and validating the predictive models against the GC-FID reference technique. All formal criteria used for the purpose of statistical analysis are briefly summarized in Table 14.

Table 14. Summary of parameters and statistical criteria used to assess the quality of calibration and validation of the gas sensor array.

Analysis stage	Parameter	Symbol	Description	Acceptance criterion
Calibration	Student's t-test	t	Assessment of the significance of model parameters	p-value greater than significance level
	Residual Standard Error	RSE	Measure of the model's misfit to the training data	Value minimization
	Coefficient of multiple determination	R^2	Percentage of explained variance	Striving to unity
	Corrected coefficient of multiple determination	R^2_{adj}	Percentage of explained variance, adjusted for the number of variables	Striving to unity
	Akaike information criterion	AIC	Statistical evaluation of information loss by the model	Model selection indicator (lower is better)
	Relative reliability coefficient	R_r	Relative probability of model fit	Value maximizing
Validation	Root mean square error	RMSE	Mean error relative to the reference method	Value ≤ 10%
	Cumulative sum linearity test	CUSUM	Assessment of the randomness of the distribution of residuals relative to the regression line	p-value greater than significance level
	Passing-Bablok regression	P-B	Test for the absence of the systematic errors (constant and proportional)	Linear parameters consistency
	Bland-Altman analysis	B-A	Assessment of systematic, random and practical error of methods	No significant trend (close to zero)

A multi-criteria approach describing various features of the models fit during the calibration stage of the gas sensor array allow to avoid their overfitting. The first indicator used was the standard error of estimation (RSE). It determines the magnitude of deviations of the model's predicted values $(\hat{y}_i)$ from the actual values (y_i), taking into account the degrees of freedom. This parameter retains the unit of the dependent variable, and its interpretation requires reference to the range of determined values (analyte concentrations). The following relationship was used to calculate the RSE values for the individual models created:

$$RSE = \sqrt{\frac{\sum_{i=1}^{n}(y_i - \hat{y}_i)^2}{n - (k+1)}} \quad [mg/m^3] \tag{38}$$

Where: n is the number of observations and k is the number of explanatory variables in the model. The next step was to determine the coefficients of multiple determination (R squared statistics). The basic version of this parameter (R^2) determines the proportion of the variability of the dependent variable that is correctly represented by the predictive model. However, it does not take into account the sample size or the number of predictors. Therefore, an adjusted value of the coefficient of determination (R^2_{adj}) was also determined, taking into account these two variables. This allowed for the elimination of the phenomenon of an apparent improvement in the

model's predictive capabilities resulting solely from increasing the size of the dataset. Both parameters were calculated according to the following relationships:

$$R^2 = 1 - \frac{RSS}{TSS} = 1 - \frac{\sum_{i=1}^{n}(y_i - \hat{y}_i)}{\sum_{i=1}^{n}(y_i - \bar{y})} \quad [-] \tag{39}$$

$$\mathrm{R}^2_{\mathrm{adj}} = \mathrm{R}^2 - \frac{\mathrm{k}(1 - \mathrm{R}^2)}{\mathrm{n} - (\mathrm{k} + 1)} \quad [-] \tag{40}$$

Where: $\bar{y}$ is the mean value of the dependent variable, TSS is the total sum of squares and RSS is the residual sum of squares. The subsequent parameter was AIC, that is the Akaike information criterion. As a relative criterion, it does not allow for a definitive determination of whether a given model is correct. However, when comparing multiple models created on the same dataset and for the same dependent variable, its accurate interpretation allows for ranking the models according to increasing or decreasing predictive ability. A limitation is the need for a validated training dataset. An incorrectly prepared dataset will not result in incorrect values of this parameter. AIC values for individual models were calculated according to the equation:

$$AIC = n \bullet ln\frac{RSS}{n} + 2(k + 1) \ [-] \tag{41}$$

The final parameter determined during the quality assessment of the predictive calibration models was the model's relative reliability coefficient (R_r). This is determined based on the AIC value relative to the model with the lowest AIC value, which is theoretically the best model (among models describing the same prediction problem). The best model has a value of this parameter equal to unity, while the others range from zero to one. The lower the R_r value, the lower the model's reliability (strength of support) relative to the model considered the best.

$$R_r = e^{\frac{AIC_{min} - AIC_i}{2}} \quad [-] \tag{42}$$

All prepared calibration models were used to analyze samples from the absorption purification process of the model biogas. They were used to determine the concentrations of individual pollutants (acetone, toluene, cyclohexane) at the inlet (C_{in}) and outlet (C_{out}) of the system. Based on the determined concentrations, the efficiency of the treatment process was calculated using the absorptivity parameter:

$$A_i = \frac{C_{out,i}}{C_{in,i}} \tag{43}$$

The aim of the validation procedure of the predictive models was to analyze the regression consistency, linearity of correlations between methods and to verify the occurrence of possible random and systematic errors and their magnitude. The first parameter used was the RMSE. Its mathematical foundations are presented in section 6.2.5. The measurement results were paired appropriately (SM-MLR vs GC and SM-PCR vs GC), which allowed for the determination of the direct discrepancy between the sensor matrix (SM) and gas chromatography (GC) results. The results were presented as a percentage scale, with the RMSE of no more than 10% being considered as the acceptance criterion. The strength of the linear correlation between such paired results was characterized using the coefficient of determination R^2. Unlike its role in

the calibration stage, this time it did not provide information about the portion of the result variability accounted for by the model. The adopted quality level of prediction models for this parameter was set at $R^2 \geq 0.95$. Neither of this parameters (RMSE and R^2) provide information about the nature of the error. They only indicate its magnitude and the linearity of the relationship between the methods results. Therefore, Passing-Bablok regression and Bland-Altman analysis were performed to supplement the information provided by these parameters.

Passing–Bablok regression was used to assess the agreement between the GC-FID results and the sensor matrice (SM) results. Agreement between the methods was assessed relative to the identity line (y=x), which corresponds to the situation where both methods provide the same values. The regression model was described by the equation:

$$y = a + bx \tag{44}$$

Where: a is the intercept (intersection of the regression line) and b is the slope of the regression line. Since the interpretation of regression parameters a and b assumes a linear relationship between the methods, the linear nature of the relationship between the results of the compared methods was first assessed using the CUSUM test. This was used to assess whether the deviations of the observed values from the regression line were random or exhibited a systematic pattern indicating nonlinearity of the relationship. A significance level of $\alpha = 0.05$ was adopted. A p-value ≥ 0.05 was interpreted as no basis for rejecting the assumption of a linear relationship, which allowed for further interpretation of the Passing–Bablok regression parameters. A p-value < 0.05, on the other hand, indicated a significant departure from linearity and limited the validity of describing the relationships between the methods solely using the intercept a and slope coefficient b.

The P-B analysis assumed a comparable nature of the error distribution of both methods, but normality of distribution was not a necessary condition. If the linear nature of the relationship was confirmed, the 95% confidence intervals (95% CI) were determined for both parameters. Value of parameter a was used to assess the presence of a constant bias between the methods. The absence of significant constant bias was considered to be a situation in which the 95% CI for a encompassed the value 0. This meant there was no basis for observing a constant bias between the results of one method and the other. Coefficient b was used to assess the proportional bias. In the case of perfect agreement between methods, its value is 1. Absence of significant proportional bias was considered to be the case when the 95% CI for b encompassed the unity. Simultaneous fulfillment of both criteria, i.e., the CI for a encompassing the value 0 and the confidence interval for b encompassing the value 1, was interpreted as the absence of significant evidence of constant and proportional bias between the compared methods. Therefore, the regression equation was considered statistically consistent with the line of identity (y=x).

Bland–Altman analysis was used to complement the CUSUM linearity test and P-B regression. Unlike analyses based on the relationship between two variables, the B-A approach focuses on differences within individual measurement pairs. This allows for the determination of both the average shift in the results of one method relative to the other and the range of variability of these differences across the entire measurement interval. For each pair of results, the

difference between the methods and the mean value of the pair were determined. Assuming that $y_{SM,i}$ denotes the SM method result and $x_{GC,i}$ the GC-FID result, calculations were performed according to the following equations:

$$d_i = y_{SM,i} - x_{GC,i} \tag{45}$$

$$m_i = \frac{y_{SM,i} - x_{GC,i}}{2} \tag{46}$$

In the B-A plot, m_i values were plotted on the horizontal axis, and the corresponding d_i differences were plotted on the vertical axis. This presentation allowed for the assessment of whether the differences between methods were randomly distributed around zero or whether they exhibited a systematic shift or dependence on the level of the measured quantity. The basic measure in the B-A analysis was the mean difference, referred to as bias $(\bar{d})$. This parameter describes the average shift in the results of one method relative to the other and was calculated as the arithmetic mean of all differences between pairs of measurements:

$$bias = \bar{d} = \frac{\sum_{i=1}^{n} d_i}{n} \tag{47}$$

The interpretation of the bias sign depended on the subtraction order adopted. A positive value indicated that the SM method provided, on average, higher results than GC method, while a negative value indicated an average underestimation of the results relative to the reference method. A bias close to zero indicated a small average shift between the methods. The statistical assessment was supplemented by a practical acceptability criterion: a deviation of no more than 10% of the adopted reference value was considered acceptable. Bias value alone is not sufficient to fully assess the agreement, as a small mean difference can coexist with a large scatter of results for individual samples. Therefore, the standard deviation of differences (SD_d) was also determined, which characterizes the degree of dispersion of d_i values around the mean bias:

$$SD_d = \sqrt{\frac{\sum_{i=1}^{n}\left(d_i - \bar{d}\right)^2}{n-1}} \tag{48}$$

Based on bias and standard deviation, 95% limits of agreement (LoA) were determined. Assuming an approximately normal distribution of differences, these limits were defined as:

$$lower\ LoA = \bar{d} - 1.96 \cdot SD_d \tag{49}$$

$$upper\ LoA = \bar{d} + 1.96 \cdot SD_d \tag{50}$$

The LoAs define the interval within which approximately 95% of the differences between the results of the compared methods are expected. Their interpretation considered not only the number of points within the interval but also its width. Narrow limits indicate small variability in the differences, while a wide range may indicate limited practical agreement, even when the mean bias remains close to zero. B-A plot was also visually analyzed for the pattern of point distribution. The presence of a trend in differences with increasing mean level of the measured quantity, change in dispersion across the range, and the occurrence of individual observations outside the limits of agreement were assessed. A systematic increase or decrease in d_i values with increasing

m_i could indicate a level-dependent error, while a widening scatter of points could suggest heterogeneity in the variance of the differences. The assessment of agreement was not based solely on a single bias value but considered the entire pattern of differences between methods.

The combined use of these methods allowed for the separation of several aspects of the comparison. CUSUM addressed the question of the linear nature of the relationship, P-B regression addressed the presence of a systematic constant or proportional error, and B-A analysis determined whether the actual differences between the results of the two methods were sufficiently small and stable across the entire measurement range. This reduces the risk of equating high correlation with true agreement between the two measurement methods.

8.3 Results and discussion

8.3.1 Development and characterization of predictive models

For all compounds analyzed, the developed MLR and PCR models enabled quantitative determination of concentrations based on the gas sensor array responses. The obtained parameter values characterizing the model quality are summarized in Table 15. Comparison of both modeling methods showed that in each case, the PCR models obtained more favorable parameter values. They were characterized by lower RSE and AIC values and higher R^2 and R^2_{adj} values than the corresponding MLR models. The largest differences between the MLR and PCR models were found for acetone. The value of R^2 increased from 0.917 for MLR to 0.942 for PCR, while R^2_{adj} increased from 0.889 to 0.934, respectively. At the same time, the use of PCR was associated with a decrease in RSE from 44.09 to 36.46 and AIC from 61.47 to 58.19. In the case of cyclohexane, the differences between the models were smaller: the values of R^2 were 0.921 and 0.936 for MLR and PCR, respectively, and the RSE was 38.23 and 34.91. For toluene, more favorable results were also obtained for PCR, for which R^2 was 0.923 compared to 0.906 for MLR, while the RSE decreased from 54.61 to 46.37.

Table 15. Statistical parameters of MLR and PCR calibration models developed to predict acetone, cyclohexane and toluene concentrations. Reproduced from [271], © 2024 Elsevier Ltd.

Chemical compound	Model	RSE	R^2	R^2_{adj}	AIC	R_r
Acetone	MLR	44.09	0.917	0.889	61.47	0.194
	PCR	36.46	0.942	0.934	58.19	-
Cyclohexane	MLR	38.23	0.921	0.895	60.35	0.631
	PCR	34.91	0.936	0.913	59.43	-
Toluene	MLR	54.61	0.906	0.881	61.66	0.487
	PCR	46.37	0.923	0.903	60.22	-

Comparison of AIC values led to similar conclusions. In each case, a lower value of this parameter was obtained for PCR. Differences between the models were also reflected in the relative reliability R_r. For the MLR model developed for acetone, it was 0.194, for cyclohexane 0.631, and for toluene 0.487 compared to the corresponding PCR models. The smallest difference between the modeling variants was therefore found for cyclohexane, while the most pronounced advantage of PCR was observed for acetone. The relationships between the

reference concentrations determined by the GC-FID method and the values predicted by the individual models are shown in Figure 38. For all compounds analyzed, a clear relationship was observed between the reference values and the concentrations determined using the gas sensor array. Measurement points were distributed adjacent to the line representing a 1:1 relationship, with the degree of their dispersion depending on the compound analyzed and the model used. The R^2 values presented in the figure confirm the results presented in Table 15 and indicate a slightly better representation of the calibration data by the PCR models than MLR models.

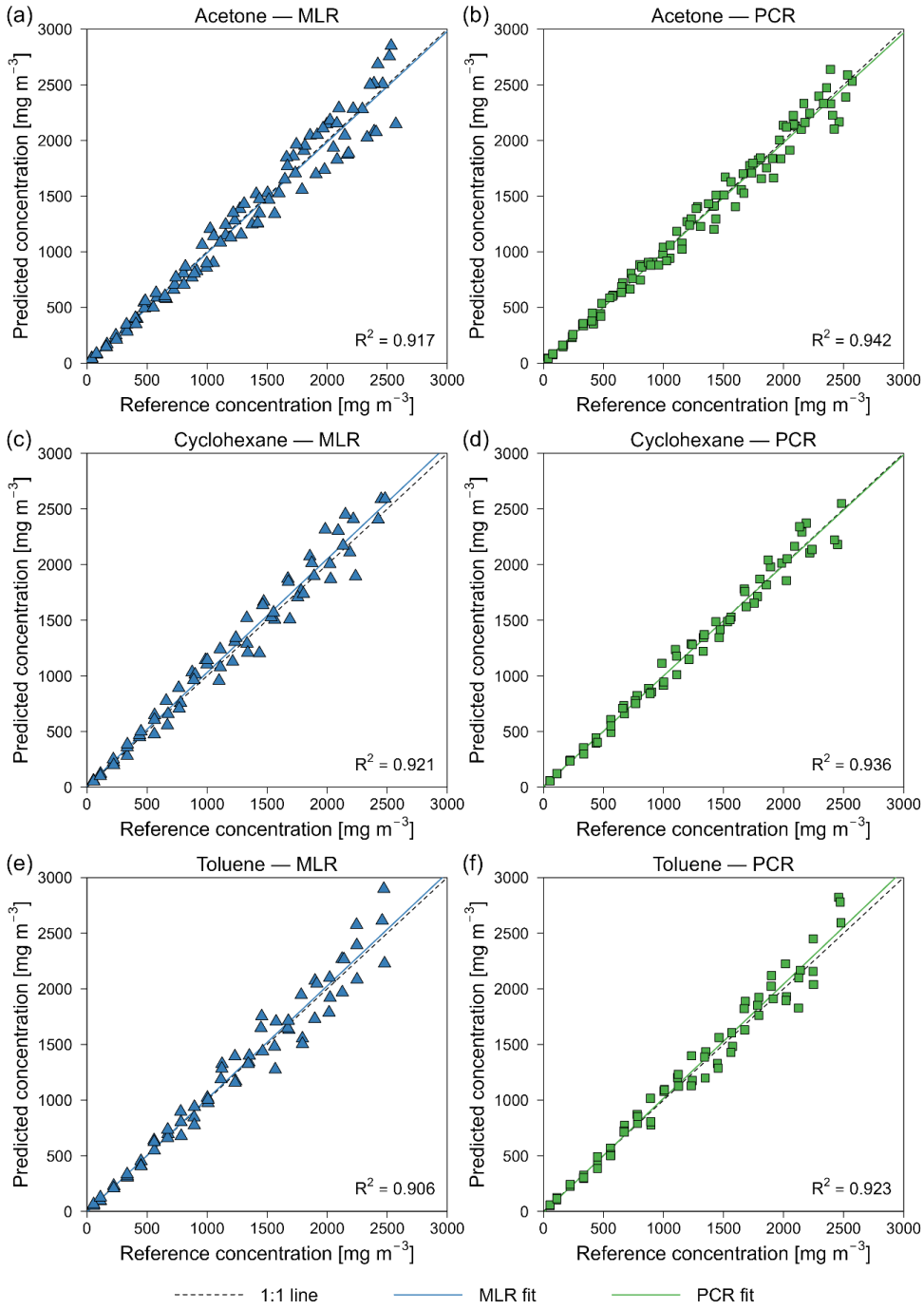


Figure 38. Comparison of reference concentrations determined by GC-FID with concentrations predicted using MLR and PCR models for acetone (a, b), cyclohexane (c, d), and toluene (e, f). The dashed line represents perfect agreement between reference and predicted values (1:1), while solid lines indicate linear fits for the respective models. Adapted from [271], © 2024 Elsevier Ltd.

The differences between the reference and predicted values were not uniform across the entire analyzed measurement range. Larger deviations occurred primarily at higher concentrations of the compounds tested. This phenomenon may be related to the response characteristics of the sensors used and the gradual shift of some of them beyond the linear relationship between the signal and the analyte concentration. This effect was also identified as a likely cause of the increasing discrepancies at high concentrations and the relatively high RSE values. A visual comparison of the reference and predicted values alone did not allow for a complete assessment of the distribution of errors within the calibration range. Therefore, the results were supplemented with a residual analysis, presented in Figure 39. Residuals were determined as the difference between the model predicted concentration and the corresponding reference value, with positive values indicating an overestimation of the concentration and negative values indicating an underestimation.

The distribution of residues indicated that for all analyzed compounds, the differences between the predicted and reference values were concentrated around the zero value, particularly at lower concentrations. However, with increasing concentration, an increase in the scatter of residues was observed, the nature of which depended on the analyzed compound and the model used.

For acetone, a clear increase in both positive and negative deviations was observed at the top of the calibration range, especially for the MLR model. For cyclohexane, the distribution of residues was more uniform around the baseline, and the use of PCR led to a significant reduction in the extreme deviations compared to the MLR. For toluene, as for acetone, the largest differences between the predicted and reference values occurred at higher concentrations, with both significant positive and negative values observed for the MLR. The PCR model reduced some of this scatter, but the increased scatter remained visible at the upper concentration range.

Among the analyzed cases, the most consistent distribution of residuals was observed for the cyclohexane PCR model, while the largest individual deviations occurred for the acetone and toluene models at the upper end of the calibration range. Therefore, residual analysis complemented the assessment based on the coefficients of determination, enabling the identification of both differences between the models and the dependence of the prediction quality on the type of compound and its concentration range.

The combined analysis of statistical parameters, the relationship between reference and predicted concentrations, and the residual distribution indicates the more favorable properties of the PCR models at the calibration stage. For all three compounds, PCR was characterized by lower RSE and AIC values and higher R^2 and R^2_{adj}. However, this did not provide a basis for assuming that PCR would always be more accurate when monitoring the absorption process. The practical usefulness of the models was determined by their ability to represent concentration changes in process samples, in which the array response could be additionally influenced by the process conditions and the absorbent used. Therefore, both model variants were used in the subsequent study to monitor the absorption process of the model biogas and determine the removal efficiency of individual pollutants.

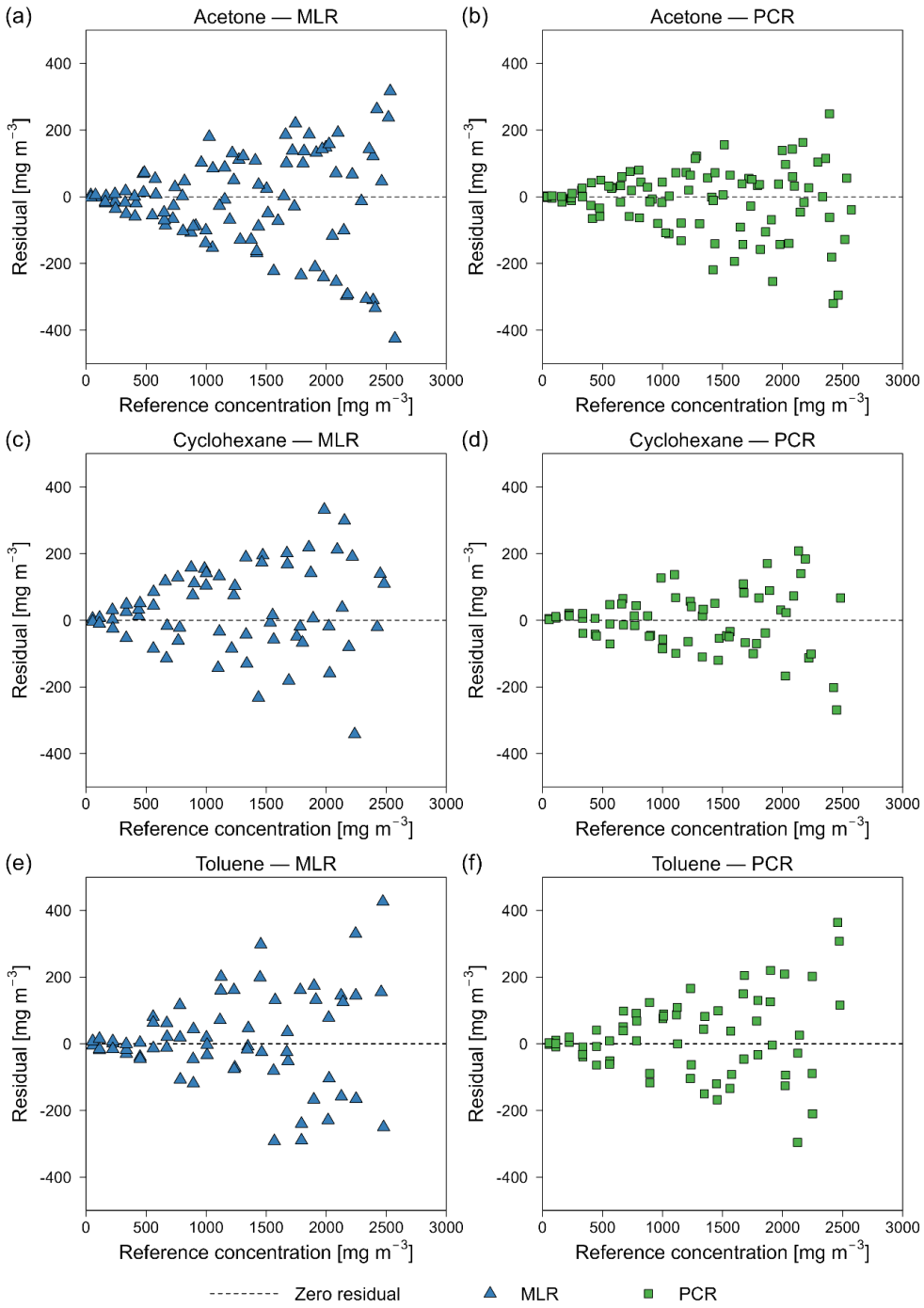


Figure 39. Distribution of residuals for MLR and PCR calibration models developed for acetone (a, b), cyclohexane (c, d), and toluene (e, f). Residuals were calculated as the difference between predicted and reference concentrations. The dashed horizontal line indicates zero residual.

8.3.2 Monitoring and assessing the efficiency of the model biogas absorption process

The developed predictive models were then used to monitor the actual absorption process using two absorption liquids: commercial Genosorb and a 1:1 OA:NA mixture. This allowed to assess the performance of the sensor array under conditions of time-varying gas stream composition and to verify whether the concentrations determined based on the MLR and PCR models could reproduce the process observed using the GC-FID reference method. Figure 40 shows the changes in absorptivity parameter (*A*) for acetone, cyclohexane and toluene,

determined independently on the basis of chromatographic results and the sensor array response.

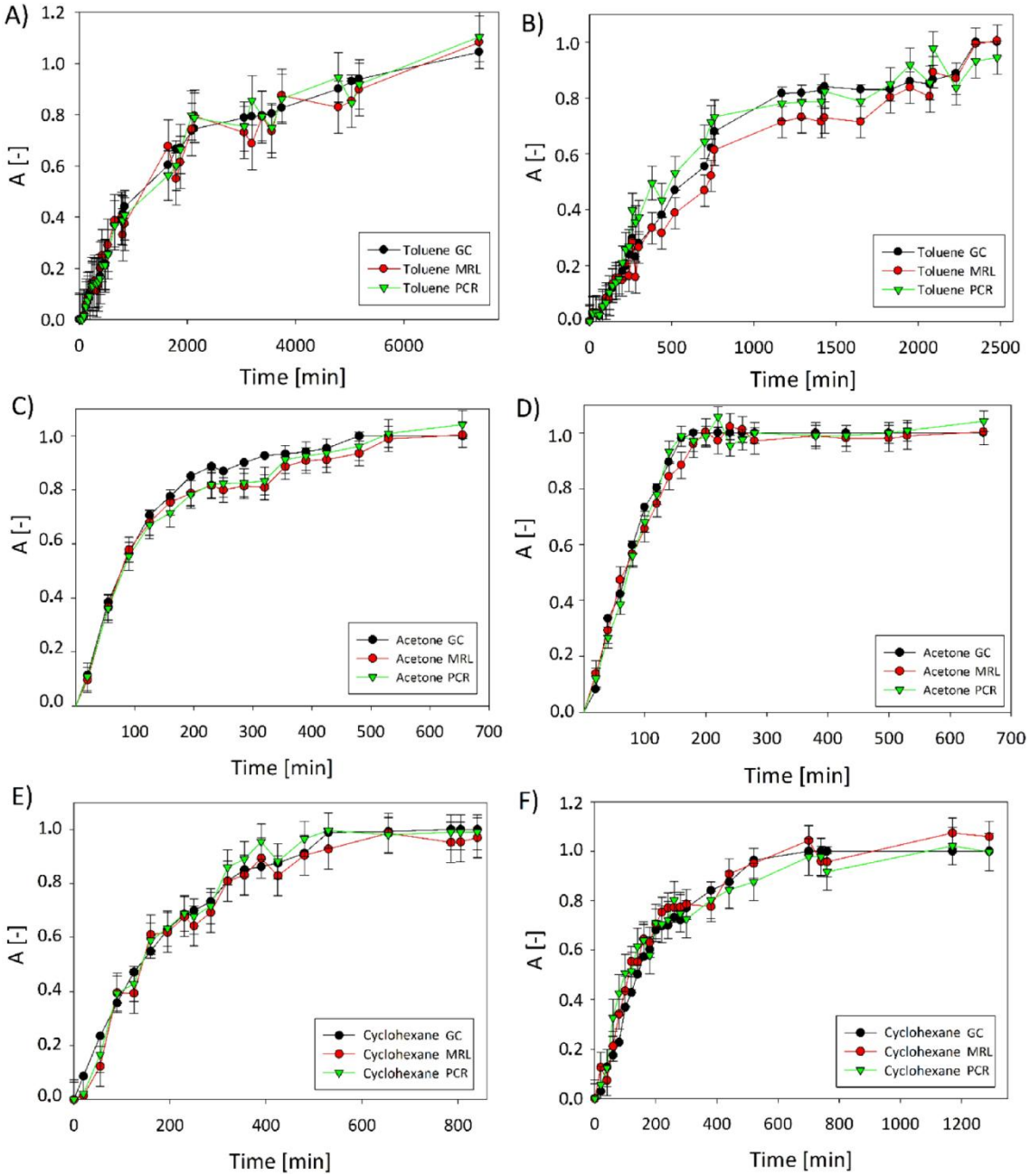


Figure 40. Evolution of absorptivity during model biogas purification monitored by GC-FID and the gas sensor array with MLR and PCR models. Toluene: (a, b), acetone: (c, d), cyclohexane: (e, f). Genosorb: (a, c, e), OA:NA (1:1): (b, d, f). Reproduced from [271], © 2024 Elsevier Ltd.

The curves indicated a clear differentiation in the behavior of the tested compounds depending on the absorbent used. The greatest differences between the absorption liquids occurred in the case of toluene. For Genosorb, the removal process of this compound maintained high efficiency for approximately 7500 min, while for OA:NA (1:1), this time was approximately 2500 min. This difference was also reflected in the absorption capacity, which was 5.14 mg g^{-1} and 2.84 mg g^{-1}, respectively.

Significantly lower absorption capacities were obtained for the remaining components of the model biogas. In the case of acetone, they were 0.56 mg g^{-1} for Genosorb and 0.24 mg g^{-1} for OA:NA (1:1), with the absorption course for both liquids lasting approximately 650 min. For cyclohexane, the absorption capacity was 0.61 mg g^{-1} and 0.46 mg g^{-1}, respectively, while the process time varied significantly and was approximately 840 min for Genosorb and approximately 1290 min for OA:NA (1:1). In comparison with toluene, for which Genosorb showed both the highest absorption capacity (5.14 mg g^{-1}) and the longest effective process time, these results indicate a strong dependence of the absorption process on the type of the compound being removed and the absorption liquid used.

The differences in absorption patterns and the resulting capacities may be attributed to the different nature of interactions between the compounds and the absorbing liquids. In the case of toluene, π–π and van der Waals interactions played a significant role, while the increased effectiveness of Genosorb may be attributed to the presence of longer alkyl chains and more favorable mass transfer conditions. The physical properties of the absorbents, including their viscosity, which determines the transport of components between the gas and liquid phases, may also have influenced the process. For acetone, the ability to form hydrogen bonds with the absorbent's carboxyl groups was important, while in the case of nonpolar cyclohexane, dispersion and hydrophobic interactions dominated. The different chemical nature of the analyzed VOCs resulted in different affinities for the two absorbing liquids. These differences were reflected both in the achieved absorption capacities and in maintaining high process efficiency.

Quantitative comparison of the sensor array results with GC-FID (Table 16) confirmed that for most of the analyzed variants, the differences between the methods remained small. The lowest RMSE value, 3.69%, was obtained for acetone absorbed in OA:NA (1:1) using the PCR model. For Genosorb, the lowest error values were also observed for acetone: 5.17% for MLR and 4.64% for PCR.

Table 16. RMSE values for process monitoring results using MLR and PCR models versus GC-FID. Adopted from [271], © 2024 Elsevier Ltd.

Compound	Absorbent	RMSE [%]	
		MLR	PCR
Toluene	Genosorb	10.26	9.65
	OA:NA (1:1)	5.62	6.03
Acetone	Genosorb	5.17	4.64
	OA:NA (1:1)	4.72	3.69
Cyclohexane	Genosorb	7.39	6.52
	OA:NA (1:1)	6.05	7.50

The largest deviations from the chromatographic method occurred during toluene absorption in Genosorb. The RMSE was 10.26% for MLR and 9.65% for PCR. Thus, the MLR variant slightly exceeded the accepted 10% threshold, while the remaining results were below or very close to this value. This does not change the overall picture of good agreement between the runs, but indicates that the prediction accuracy depended on both the compound analyzed and the process conditions. It is also important to note that the advantage of the PCR model observed at the calibration stage was not uniform across all process experiments. For Genosorb, PCR

provided lower RMSE values for all three compounds, while in the case of OA:NA (1:1), lower RMSE for cyclohexane and toluene was obtained using MLR. The largest difference between the models was observed for cyclohexane absorbed in OA:NA (1:1) and amounted to 1.45 percentage points. This result indicates that the assessment of model suitability should not be based solely on parameters obtained during calibration, but also on its performance under variable conditions of the actual process.

The obtained results show that the gas sensor array, combined with the predictive models, enabled the reproduction of changes in absorption efficiency for both tested liquids and for compounds characterized by significantly different removal dynamics. However, RMSE alone does not provide a complete basis for establishing the equivalence of both measurement methods. Therefore an extended assessment of the agreement between the sensor array and GC-FID results was performed using P-B regression, the CUSUM test, and B-A analysis.

8.3.3 Evaluation of the agreement between sensor array results and the GC-FID

P-B regression and B-A analysis were performed separately for acetone, cyclohexane and toluene, for MLR and PCR models and for two absorption liquids: Genosorb and OA:NA (1:1). The first one allowed for the assessment of the occurrence of constant and proportional differences between the compared methods, while the B-A analysis allowed for a direct assessment of the size and dispersion of differences between paired results. In the case of the process conducted using Genosorb, the relationship between the gas sensor array results and GC-FID determinations was strong for all analyzed compounds (Figure 41). The coefficients of determination R^2 ranged from 0.973 to 0.996. High values of R^2 confirm a strong linear relationship between the results obtained using both methods, but are not sufficient to establish their full agreement. For this reason, the position of the P-B regression line relative to the 1:1 identity line, as well as the values of the intercept *A* and the slope *B*, were also analyzed.

The largest deviation from the 1:1 relationship for Genosorb was observed for acetone (Figure 41a, b). For the MLR model, the obtained intercept $A = -0.314$ and slope $B = 1.354$ were obtained, whereas for PCR, these values were -0.186 and 1.198, respectively. Graphically, this was manifested by a smaller deviation of the P-B line from the identity line after applying the PCR model. At the same time, the 95% CI for the intercept included the value of zero, therefore the observed shifts cannot be considered unequivocal evidence of a constant error between the methods. Much better agreement was obtained for cyclohexane (Figure 41c, d). Particularly favorable parameters were obtained for the MLR model, for which $A = -0.030$, and $B = 1.001$. Both values were very close to the parameters expected for perfect agreement between the methods (0 and 1, respectively). For the PCR model, the slope was slightly higher and amounted to 1.122, but its confidence interval included the value of 1 (no clear indication of the presence of a proportional error).

The closest to ideal P-B parameters for Genosorb were obtained for toluene using the PCR model (Figure 41e, f). The intercept was only 0.002, while the slope was 0.993. This is reflected in the almost complete overlap of the P-B regression line with the 1:1 line in the

corresponding panel of the graph. The CI for both parameters encompassed the 0 and 1, respectively, indicating very small differences of both a constant and proportional nature.

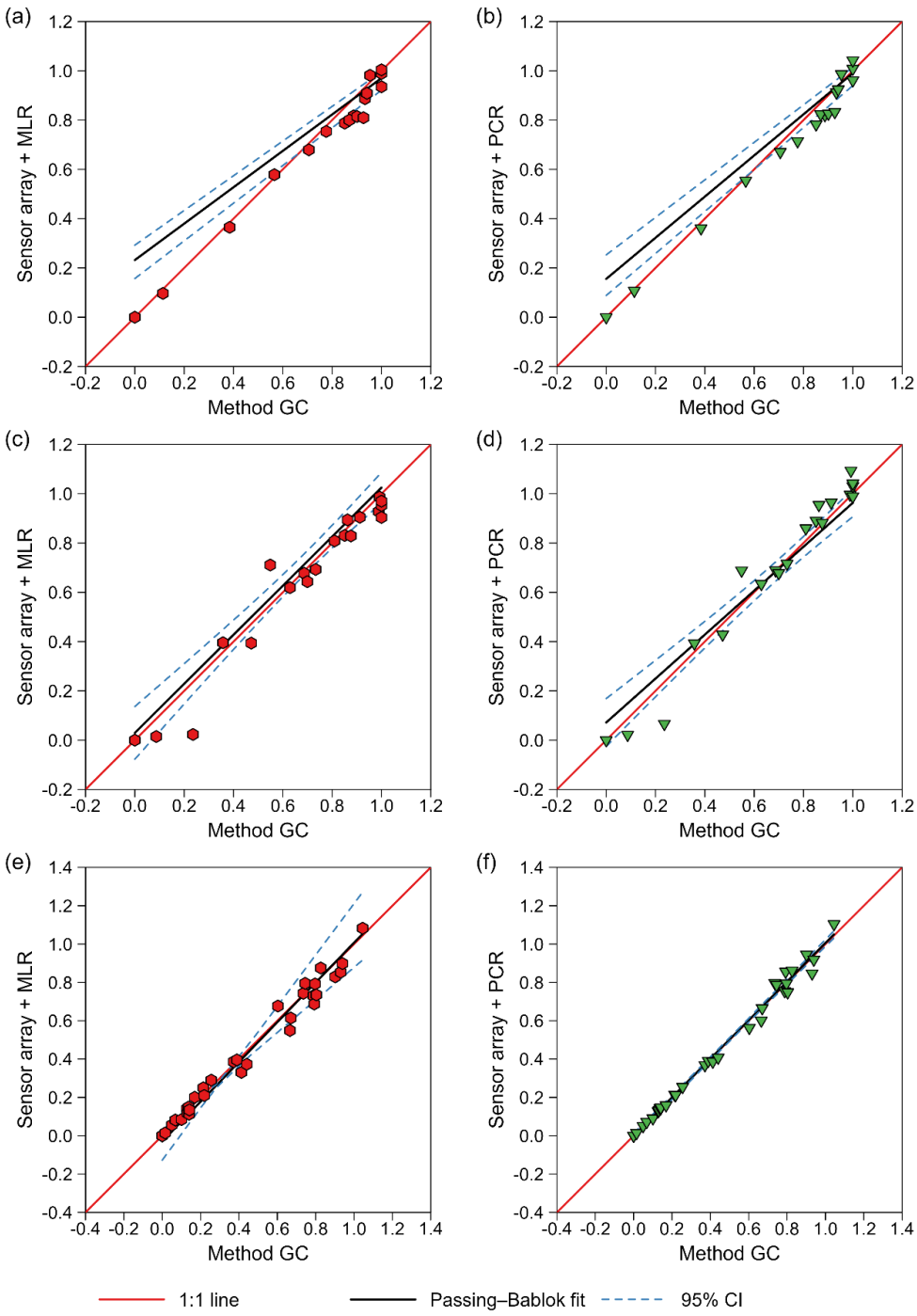


Figure 41. P-B comparison of GC and gas sensor array results obtained using MLR and PCR models for acetone (a, b), cyclohexane (c, d) , and toluene (e, f) removal with Genosorb. Black line - regression fit, red line - identity line, blue dashed lines - 95% confidence limits. Adopted from [271], © 2024 Elsevier Ltd.

For the OA:NA (1:1) absorbent, the methods agreement was more diverse and depended to a greater extent on the type of the analyzed compound and the prediction model used (Figure 42). Despite very high R^2 values, ranging from 0.979 to 0.995, in several cases more pronounced deviations of the regression parameters from the values corresponding to the 1:1 ratio were observed. In the case of acetone (Figure 42a, b), both models yielded positive intercept

values and slopes less than one. For MLR, the parameters were A = 0.150 and B = 0.874. The confidence interval for the intercept did not include zero, while the interval for the slope did not include one, indicating the possibility of a constant difference. For PCR, the obtained values were A = 0.095 and B = 0.905. In this case, the confidence interval for the intercept did not include zero, and the interval for the slope did not include one. Despite the very high coefficient of determination R^2 = 0.995, this result indicates that a strong correlation was not equivalent to full agreement between the methods.

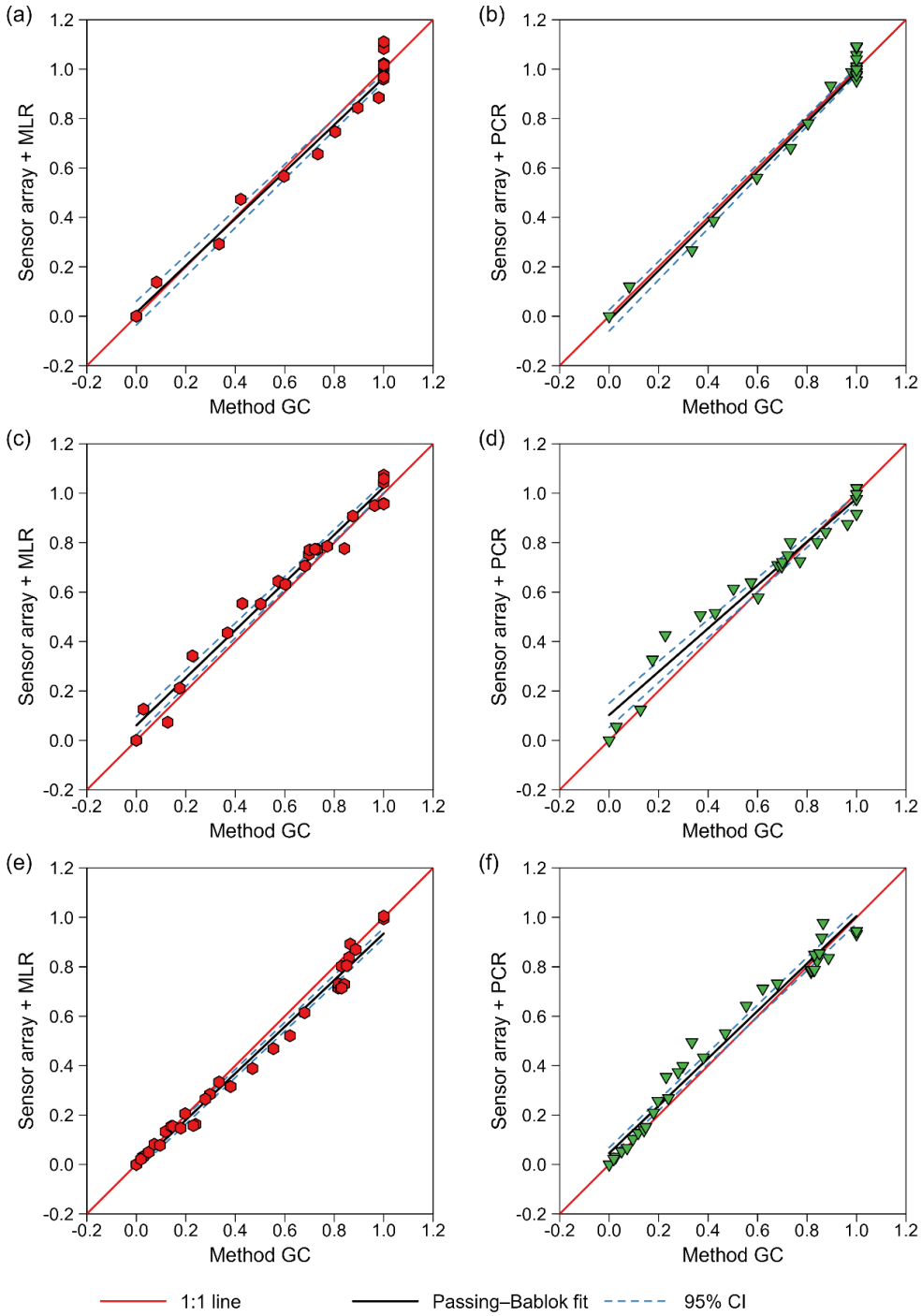


Figure 42. P-B comparison of GC and gas sensor array results obtained using MLR and PCR models for acetone (a, b), cyclohexane (c, d), and toluene (e, f) removal with OA:NA (1:1). Black line - regression fit, red line - identity line, blue dashed lines - 95% confidence limits. Adopted from [271], © 2024 Elsevier Ltd.

Even more pronounced differences were found for cyclohexane (Figure 42c, d). In the MLR model, the value $A = -0.087$ indicated a shift between methods, while the slope $B = 1.060$ remained relatively close to unity. For PCR, the differences were more pronounced: $A = -0.223$ and $B = 1.263$, with confidence intervals not encompassing 0 and 1, respectively. This result indicates the simultaneous presence of constant and proportional differences. This relationship was also visible graphically as a greater separation of the Passing-Bablok regression line and the identity line. For toluene, the deviations were smaller (Figure 42e, f). The MLR model had a virtually zero intercept $A \approx 0$ while the slope of 1.051 was slightly greater than unity. Importantly, the lower bound of its 95% CI was 1.002, indicating a small proportional difference. For PCR, the intercept was $A = -0.025$, and the slope coefficient was 1.035. In this case, the CI for the slope encompassed 1, while the interval for the intercept did not encompass zero, indicating primarily a small systematic shift between the methods.

Table 17. P-B regression parameters for the comparison of sensor array and GC-FID results during absorption experiments.

Compound	Absorbent	Model	R^2	Intercept A (95% CI)	Slope B (95% CI)	CUSUM P
Acetone	Genosorb	MLR	0.973	-0.314 (-0.534 to 0.188)	1.354 (0.812 to 1.632)	0.23
		PCR	0.981	-0.1863 (-0.426 to 0.165)	1.198 (-0.081 to 0.081)	0.07
	OA:NA (1:1)	MLR	0.993	0.150 (0.021 to 0.402)	0.874 (0.585 to 1.017)	0.39
		PCR	0.995	0.095 (0.048 to 0.237)	0.905 (0.730 to 0.968)	0.39
Cyclohexane	Genosorb	MLR	0.977	-0.030 (-0.168 to 0.090)	1.005 (0.855 to 1.174)	0.66
		PCR	0.986	-0.081 (-0.198 to 0.026)	1.122 (0.993 to 1.277)	0.97
	OA:NA (1:1)	MLR	0.988	-0.087 (-0.158 to -0.026)	1.060 (0.974 to 1.167)	0.72
		PCR	0.979	-0.223 (-0.338 to -0.090)	1.263 (1.094 to 1.4371)	0.42
Toluene	Genosorb	MLR	0.987	0.029 (-0.007 to 0.093)	0.964 (0.775 to 1.248)	0.34
		PCR	0.996	0.002 (-0.014 to 0.008)	0.993 (0.956 to 1.050)	0.63
	OA:NA (1:1)	MLR	0.993	0.00004 (-0.006 to 0.019)	1.051 (1.002 to 1.118)	0.19
		PCR	0.987	-0.024 (-0.048 to -0.001)	1.035 (0.932 to 1.080)	0.05

An additional element of the P-B regression verification was the CUSUM test, used to assess any deviations from the linear relationship between the gas sensor array and

GC-FID results. For Genosorb, the *P* values ranged from 0.07 to 0.97, while for OA:NA (1:1) they ranged from 0.05 to 0.72. In the vast majority of analyzed cases, the *P* values were therefore higher than 0.05, which did not indicate a significant deviation from linearity. The lowest value was obtained for toluene analyzed using the PCR model during absorption in OA:NA (1:1), for which $P = 0.05$. This result is at the borderline of the typically used significance level and should therefore be interpreted with caution. In the remaining cases, the CUSUM test did not provide grounds to question the linear relationship, which supports the use of the P-B regression to compare both methods. The complete summary of P-B regression parameters for all analyzed compounds, absorbents and prediction models, along with 95% CI and CUSUM test results, is presented in Table 17.

P-B regression provided information on the nature of the relationship between the results obtained using the gas sensor array and the GC-FID method, while B-A analysis allowed for a direct assessment of the magnitude and dispersion of differences between the paired results of both methods. The axis of differences was defined as *sensor array − GC*, so a negative bias value indicated a tendency to obtain lower results using the gas sensor array than the GC-FID method, while a positive value indicated the opposite tendency. The assessment of agreement was based primarily on the mean difference (bias), the standard deviation (SD) of the differences, and the limits of agreement, defined as a bias of ± 1.96 SD. For Genosorb, the mean differences between the results of both methods were relatively small for all analyzed compounds, but their dispersion was dependent on both the type of compound and the prediction model used (Figure 43).

In the case of acetone (Figure 43a, b), negative bias values of -0.035 for MLR and -0.028 for PCR were obtained for both models. This indicates a slight tendency for the sensor array to obtain lower values than GC-FID. The use of PCR reduced the absolute bias value and slightly limited the variability of the differences. The SD decreased from 0.039 to 0.038. At the same time, the limits of agreement narrowed slightly, from -0.112 to 0.041 for MLR to -0.103 to 0.046 for PCR. The difference between the models was therefore small, but PCR demonstrated a slightly more favorable agreement profile. For cyclohexane (Figure 43c, d), the bias was -0.028 for MLR and 0.014 for PCR. PCR not only reduced the absolute value of the mean difference but also changed its direction from negative to positive. Simultaneously, the SD decreased from 0.070 to 0.065. The limits of agreement were -0.165 to 0.109 for MLR and -0.114 to 0.142 for PCR, respectively. The results therefore indicate a slight improvement in overall agreement after PCR, although in both cases the spread of differences was larger than for acetone.

The most favorable result for Genosorb was obtained for toluene (Figure 43e, f), especially after applying the PCR model. For MLR, the bias was -0.013, with an SD of 0.047 and limits of agreement ranging from -0.104 to 0.078. After applying PCR, the mean difference decreased to only -0.002, a value very close to zero. At the same time, the SD decreased to 0.033, and the limits of agreement narrowed from -0.066 to 0.063. This means that for toluene, the PCR model provided not only minimal shift relative to GC-FID but also the lowest variability of differences among all combinations analyzed for Genosorb. Comparison of all three compounds indicates that the use of PCR for Genosorb generally led to a reduction in the absolute

bias and a reduction in the scatter of differences. This effect was particularly pronounced for toluene, while for acetone the differences between MLR and PCR remained relatively small.

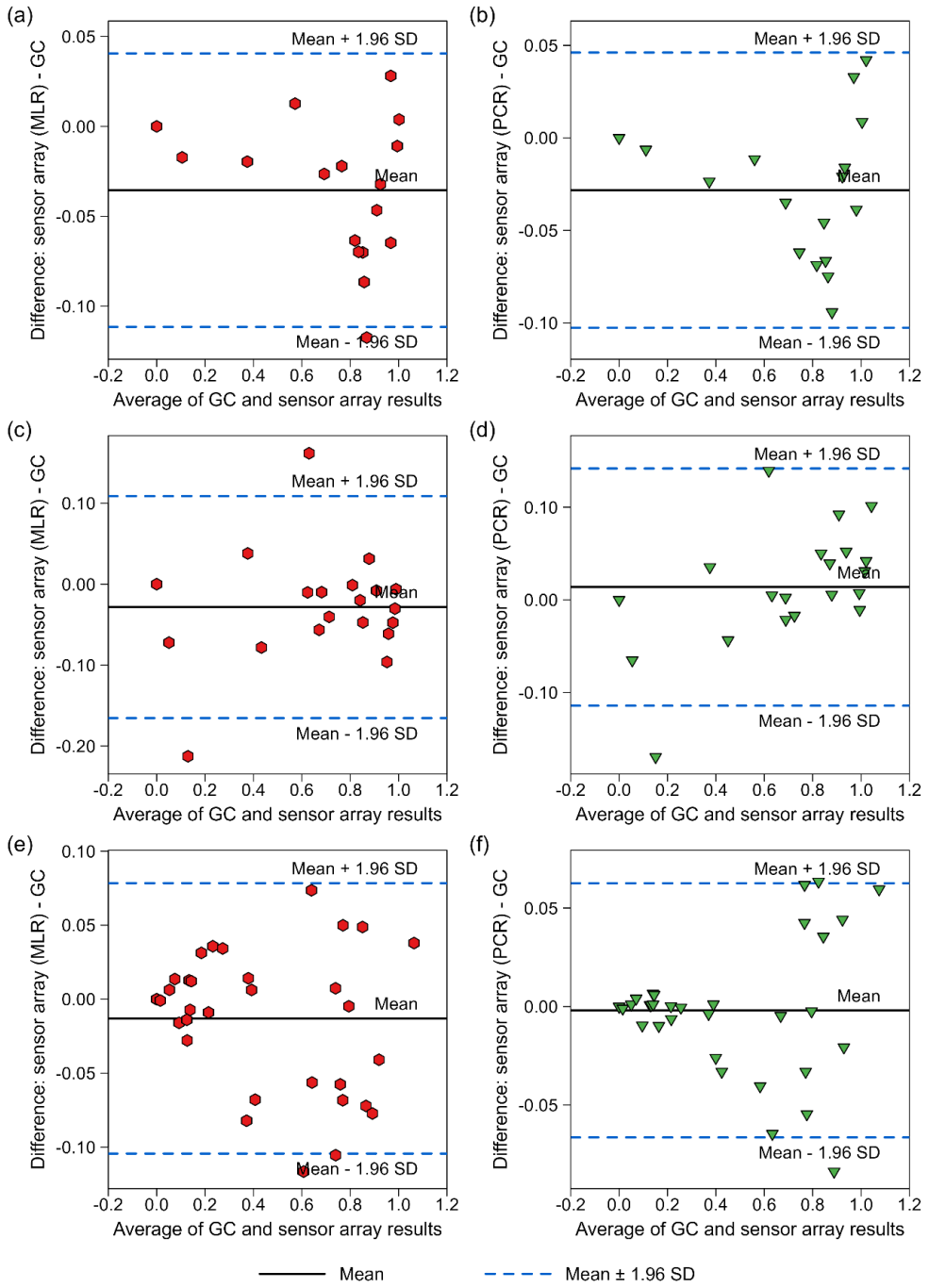


Figure 43. Bland-Altman comparison of GC and gas sensor array results obtained using MLR and PCR models for acetone (a, b), cyclohexane (c, d), and toluene (e, f) removal with Genosorb. Solid line - mean difference, dashed lines - mean ± 1.96 SD. Adopted from [271], © 2024 Elsevier Ltd.

In the case of the OA:NA (1:1) absorbent, the nature of the agreement was more diverse, and the use of PCR did not lead to a uniform improvement of all B-A parameters (Figure 44). For acetone (Figure 44a, b), the MLR model was characterized by a mean difference practically equal to zero (bias = −0.001), with an SD of 0.059 and limits of agreement of −0.116 to 0.114. This indicates a lack of a clear mean shift between the methods, with a relatively large scatter of individual differences. For the PCR model, the bias was −0.012, while the SD decreased to 0.036,

and the limits of agreement narrowed to −0.083 to 0.058. PCR did not produce a smaller bias than MLR, but it was characterized by a much smaller spread of results. For cyclohexane (Figure 44c, d), the bias was 0.035 for MLR and 0.024 for PCR. Thus, the use of PCR reduced the mean shift from zero, but at the same time the SD increased from 0.051 to 0.072. Consequently, the limits of agreement widened from −0.064 to 0.134 for MLR to −0.118 to 0.166 for PCR. This is a particularly significant result because it demonstrates that reducing bias does not necessarily equate to improving overall method agreement. In this case, PCR reduced the mean shift but increased the variability of the differences between individual measurements.

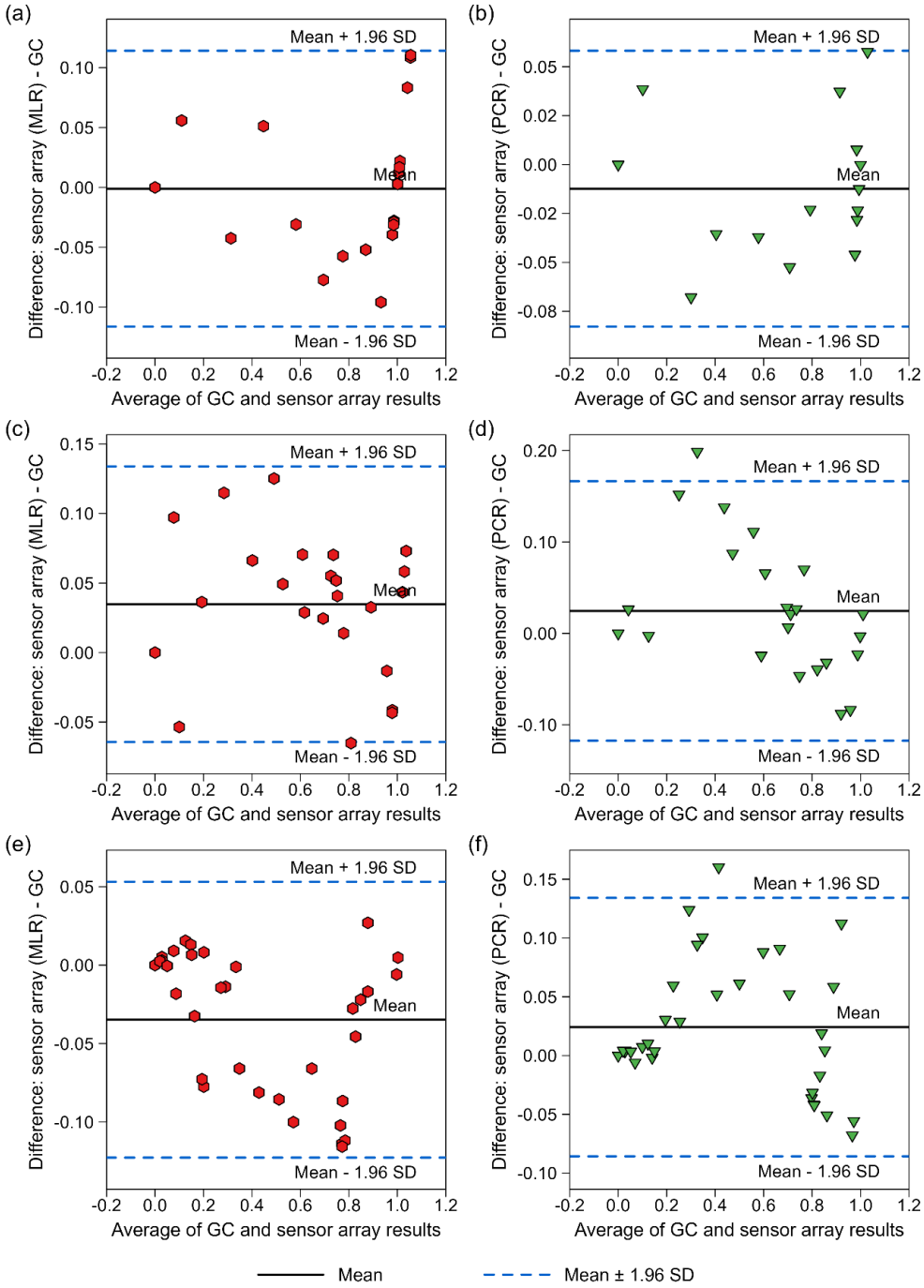


Figure 44. Bland-Altman comparison of GC and gas sensor array results obtained using MLR and PCR models for acetone (a, b), cyclohexane (c, d), and toluene (e, f) removal with OA:NA (1:1). Solid line - mean difference, dashed lines - mean ± 1.96 SD. Adopted from [271], © 2024 Elsevier Ltd.

A similar relationship was found for toluene (Figure 44e, f). For MLR, the bias was −0.035, SD 0.045, and the limits of agreement were −0.123 to 0.053. After applying PCR, the absolute value of the bias decreased to 0.024, but its sign changed from negative to positive. At the same time, the SD increased to 0.056, and the limits of agreement were −0.086 to 0.134. This means that PCR reduced the mean magnitude of the systematic shift but simultaneously increased the scatter of the differences. In contrast to the results obtained for toluene in Genosorb, the use of PCR did not result in a clear improvement of all compliance parameters.

The results for OA:NA (1:1) therefore demonstrate particularly clearly that agreement should not be assessed solely on the basis of bias values. A model characterized by a mean difference closer to zero may simultaneously exhibit larger SDs and wider limits of agreement, and thus larger differences between individual pairs of measurements. This phenomenon was observed primarily for cyclohexane and toluene after PCR. Comparison of the results for both absorbents indicates that the effect of the predictive model on GC-FID agreement was dependent on the process conditions. For Genosorb, PCR consistently reduced the absolute bias while leading to a slight or significant reduction in SD. For OA:NA (1:1), this relationship was not as clear. For cyclohexane and toluene, PCR reduced the absolute bias but simultaneously increased the SD and the width of the interval between the agreement limits. For acetone, MLR showed a bias of practically zero, while PCR was characterized by a narrower spread of differences in the analyzed set. These results indicate that improving one agreement parameter does not necessarily mean simultaneously improving all other parameters.

Table 18. Bland-Altman agreement parameters for the comparison of gas sensor array and GC-FID results during absorption experiments.

Compound	Absorbent	Model	Bias	SD	Lower LoA	Upper LoA
Acetone	Genosorb	MLR	-0.035	0.039	-0.112	0.041
		PCR	-0.028	0.038	-0.103	0.046
	OA:NA (1:1)	MLR	-0.001	0.059	-0.116	0.114
		PCR	-0.012	0.036	-0.083	0.058
Cyclohexane	Genosorb	MLR	-0.028	0.070	-0.165	0.109
		PCR	0.014	0.065	-0.114	0.142
	OA:NA (1:1)	MLR	0.035	0.051	-0.064	0.134
		PCR	0.024	0.072	-0.118	0.166
Toluene	Genosorb	MLR	-0.013	0.047	-0.104	0.078
		PCR	-0.002	0.033	-0.066	0.063
	OA:NA (1:1)	MLR	-0.035	0.045	-0.123	0.053
		PCR	0.024	0.056	-0.086	0.134

The graphs also show that some of the analyzed combinations contain individual observations located near or outside the limits of agreement. This does not change the overall nature of the observed relationships, but indicates that even with a small mean bias for individual

process steps, larger differences between the gas sensor array and GC-FID results can occur. Therefore, the interpretation of B-A plots should consider the location of the mean difference, the width of the limits of agreement, and the distribution of individual observations. A complete summary of bias values, standard deviations, and lower and upper limits of agreement for all analyzed compounds, absorbents, and prediction models is presented in Table 18.

8.4 Summary and conclusions

The conducted research have shown that a properly calibrated gas sensor array, working with MLR and PCR predictive models, can be used to quantitatively monitor the absorption removal of acetone, cyclohexane and toluene from a gas stream. The feasibility of such monitoring was confirmed for two different absorption liquids: Genosorb and OA:NA (1:1). The developed models enabled the mapping of changes in the concentration of analyzed VOCs, thus tracking the course and effectiveness of the process based on the response of the sensor array.

The obtained results are consistent with the current research direction of searching for new absorbing liquids for removing VOCs from gaseous streams. Deep eutectic solvents (DES) are of particular interest in this regard, being considered as an alternative to conventional absorbents. However, Makoś-Chełstowska [272] pointed out that, compared to the absorption of inorganic pollutants, the use of DES for VOC capture is still much less described in the literature. Research conducted in recent years has focused primarily on the absorption capacity of new DES, the influence of their physicochemical properties on the affinity for VOCs and the possibility of regeneration. For example, Moufawad et al. [273] investigated the static and dynamic adsorption of various VOCs in hydrophilic and hydrophobic DESs, while Gui et al. [274] demonstrated the potential of supramolecular DESs to capture VOCs and their reusability in subsequent absorption and desorption cycles.

Despite the growing research on VOCs absorption in DESs, the ongoing, quantitative monitoring of such processes using gas sensor arrays is a much less studied topic. The literature on electronic noses and sensor arrays largely focuses on the detection, discrimination, and classification of VOCs, while studies directly linking the sensor system to the assessment of absorption efficiency are scarce. Against the background of the available literature, the combination of VOCs absorption using alternative absorbents, including DES, with their quantitative monitoring using a gas sensor array can therefore be considered a relatively poorly explored research direction.

The results obtained in this chapter showed a high correlation between the sensor array readings and the reference GC-FID method. The coefficient of determination values for all analyzed combinations were in the range of 0.973 - 0.996. However, extending the evaluation with P-B regression, the CUSUM test, and B-A analysis allowed to demonstrate that the degree of quantitative agreement depended on the type of compound analyzed, the absorbent used, and the prediction model. The most favorable results were obtained for toluene absorbed in Genosorb using PCR. In this case, the P-B regression parameters were very close to a 1:1 relationship ($A = 0.002$, $B = 0.993$). The B-A analysis showed a bias of -0.002 and limits of agreement ranging

from −0.066 to 0.063. The CUSUM test results for the analyzed systems generally did not indicate any significant deviations from the linear nature of the relationship.

At the same time, no single prediction model was found to provide the best agreement with GC-FID, regardless of the type of system analyzed. For Genosorb, the PCR model generally led to a reduction in the absolute value of differences from GC-FID and their spread, whereas for OA:NA (1:1) this relationship was more complex. This result confirms the importance of tailoring the calibration method and mathematical model to the specific mixture and process conditions. This is consistent with current trends in sensor array development, where combining partially selective sensor responses with multidimensional data processing methods plays an increasingly important role. For this reason, the literature still points out such limitations of sensory systems as incomplete selectivity, the influence of environmental factors or signal drift, which justifies the need for their appropriate calibration and validation before quantitative application [28,275].

Based on the obtained results, it can be concluded that the first research hypothesis was confirmed in the absorption studies presented in chapter 8. Hypothesis assumes that properly designed and calibrated gas sensor arrays can be used to quantitatively monitor deodorization processes, enabling the determination of gas mixture component concentrations and the assessment of process efficiency with accuracy comparable to gas chromatography. The conducted studies demonstrated that after calibration against GC-FID and the use of appropriate prediction models, the sensor array enabled quantitative representation of changes in VOC concentration and monitoring of the absorption process. A high level of agreement between the results of both methods was achieved in many of the analyzed systems. At the same time, the observed dependence of prediction quality on the type of compound, absorbent, and model used confirms that the key condition for practical use of the array is its prior design, calibration, and validation for specific process conditions, which was one of the basic assumptions adopted in the verification of this hypothesis.

8.5 Publication basis of the chapter

This chapter is based in part on research previously published in:

Słupek E., Dobrzyniewski D., Makoś-Chełstowska P., Szulczyński B., Gębicki J. (2025). Monitoring of absorptive model biogas purification process using sensor matrices and gas chromatography. *Measurement,* 239, 11436. doi: 10.1016/j.measurement.2024.115436.

The original article was published by Elsevier Ltd. The material has been revised, adapted, and expanded for the purpose of this doctoral dissertation. The findings are discussed in the context of the main research objective of the thesis.

9. Identification and mapping of odor emission sources and modeling of odor plume dispersion using a gas sensor array

9.1 Purpose of the study

The aim this study was to estimate odor emissions and the odor dispersion plume from the active landfill cell of a municipal solid waste treatment plant (MSWTP) using measurements obtained with an unmanned aerial vehicle (UAV) equipped with a gas sensor array. The focus was on developing and validating an integrated approach that combines drone-based mobile gas sensor measurements, multivariate modeling, and dispersion analysis to quantify and map odor concentrations and emissions. Such a mobile platform monitoring odor air quality could be a modern alternative to traditional methods of determining odor emissions from surface sources, such as dynamic olfactometry. A unique aspect of the study was the transition from mapping gas concentrations or odor concentrations to developing spatial odor emission maps, which made it possible to identify local areas of increased emissions and estimate the total emissions from the active section of the landfill cell. A further development involved using emissions estimated based on UAV measurements as input data for odor dispersion modeling and comparing the results obtained with a variant based on emissions determined using the reference method. This made it possible to verify the developed approach both in terms of the source's characteristics and its predicted spatial odor impact.

9.2 Materials and methods

9.2.1 Test site description

The research was conducted at the Gdańsk Municipal Solid Waste Treatment Plant (Waste Utilization Facility Ltd. in Gdańsk), located in the southern part of the city. The plant is designed for comprehensive municipal waste management and includes a sorting plant, biological waste treatment facilities, a biogas capture and energy utilization system, a leachate pretreatment plant, and both active and closed waste storage facilities. The total area of the MSWPT is approximately 700,000 m^2, of which about 34,000 m^2 are landfill cells (closed, rehabilitated, and working). The study object was an active (working) landfill cell, shown in Figure 45, where waste was continuously deposited and formed into successive layers. The cell's surface is characterized by a heterogeneous structure resulting from the phased storage, compaction, and periodic covering of waste. Local variations in the intensity of landfill gas and odor emissions may occur within this cell due to factors such as the type and degree of decomposition of the deposited waste, humidity, temperature, and the tightness of the covering layers.

The active landfill cell is a large, surface source of fugitive emissions. Emissions can occur both at current waste storage sites and through temporarily covered surfaces, slopes, and sections of the cell with increased permeability. Meteorological conditions, particularly wind speed and direction, and atmospheric stability, also influence the spatial distribution of emitted

pollutants. The shape of the cell, the presence of technological infrastructure, and varying terrain elevations can further modify airflow and the spread of the odor plume.



Figure 45. Study site location: (a) boundary of the Waste Utilization Facility Ltd. in Gdańsk, (b) enlarged view of the active landfill cell selected for the UAV measurements.

9.2.2 Gas sensor array development

The crucial element of the mobile UAV-based measurement platform was a specially designed sensor system, whose task was to simultaneously monitor key components of landfill gas and substances with high odor causing potential. The array used combined various detection technologies, allowing for a multidimensional chemical image of the air above the landfill cell. The list of gas sensors used in the research is presented in Table 19.

Table 19. Technical specifications and detection profile of the gas sensors used in the array.

Sensor Type	Manufacturer	Model	Detected gases	Signal Processing
Photoionization detector	Alphasense Metek (Great Notley, Braintree, United Kingdom)	PID-A12	TVOCs	I-U transducer, ADC
Non-dispersive infrared (NDIR)	SGX Sensortech (Neuchatel, Switzerland)	INIR2-ME5	Methane	Optical signal, internal digital processing
Non-dispersive infrared (NDIR)	SGX Sensortech (Neuchatel, Switzerland)	INIR2-CD5	Carbon dioxide	Optical signal, internal digital processing
Electrochemical	Winsen Electronics Technology (Zhengzhou, China)	ME3-H2S	Hydrogen sulfide	I-U transducer, ADC
Electrochemical	Winsen Electronics Technology (Zhengzhou, China)	ME3-NH3	Ammonia	I-U transducer, ADC

The PID-A12 sensor, with its high sensitivity, low detection threshold, and fast response time, enables detection of low VOC concentrations associated with odor emissions from landfills. The SGX INIR2-ME5 and SGX INIR2-CD5 sensors utilize infrared absorption to ensure selectivity and measurement stability. Their ruggedness and durability make them suitable for field applications, including UAV measurements. The Winsen ME3-H2S and ME3-NH3 sensors, on the other hand, enable monitoring of hydrogen sulfide and ammonia, which are important components of odor emissions from waste decomposition.

9.2.3 UAV platform, sensing module, and measurement campaigns

The measurement system was installed on a DJI Phantom 4 Pro multi-rotor platform (SZ DJI Technology, Shenzhen, Guangdong, China), used for low-altitude environmental measurements. Its flight stability and precise positioning enabled repeatable routes over the landfill surface. Navigational information recorded during the measurement flights allowed for the assignment of appropriate geographic coordinates to each measurement. A compact module containing a set of gas sensors operating on various detection principles (Table 19) was placed beneath the UAV frame.



Figure 46. The DJI Phantom 4 Pro mobile UAV measurement platform in operational conditions: (a) the device on the launch platform prepared for data collection, (b) the drone during a measurement flight over the landfill site, (c) monitoring in the immediate vicinity of the degassing well.

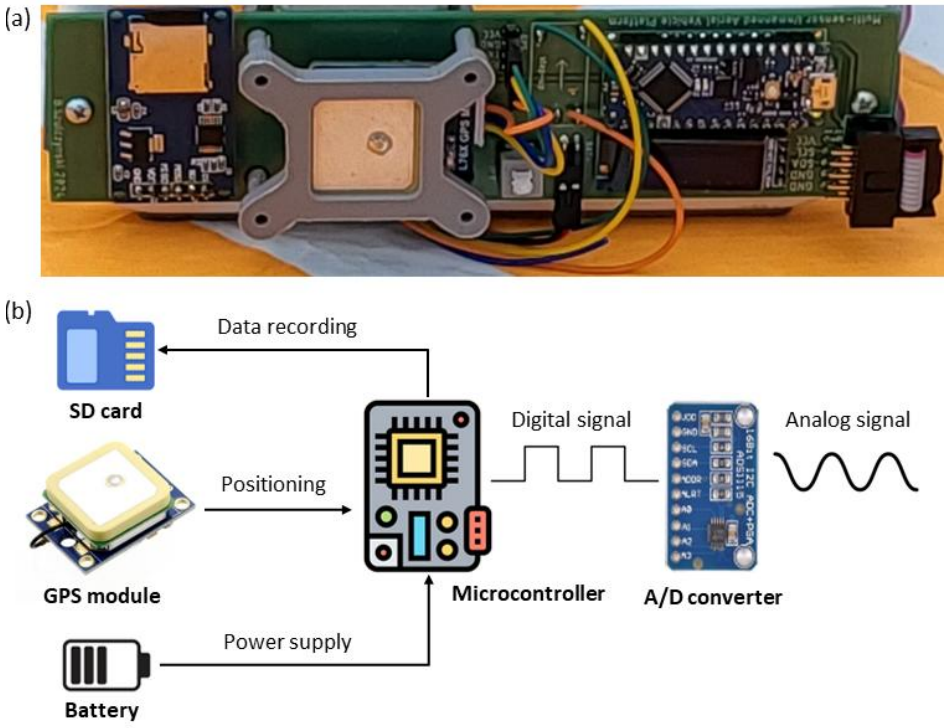


Figure 47. Architecture and technical implementation of the measurement module: (a) view of the actual electronic system integrated with the sensor array, (b) block diagram showing the internal architecture and signal flow from the sensors to the data recording system.

The system enabled simultaneous recording of landfill gas components and selected substances relevant to odor emissions. A view of the UAV with the measurement module installed is shown in Figure 46.The sensors were housed in a ventilated enclosure, ensuring constant

airflow during flight. Their signals were transmitted to the onboard acquisition system and recorded at a constant frequency. Each record included measurement signal values, position coordinates, and a timestamp. This provided a spatially dense dataset along the flight trajectory for processing and interpolation. Detection module was a standalone unit built around a microcontroller. It included an A-D converter (ADS1115, Texas Instruments, USA), a data logger with an SD card, an independent power supply, and a GPS receiver. Diagram of the system's internal architecture is shown in Figure 47. This configuration ensured synchronized recording of sensor signals, location data, time, and autonomous operation of the device during flights.

To complement the research goals, comprehensive measurement campaigns were conducted in April 2025. The measurement strategy was divided into three independent cycles, each comprising five full research flights over the active landfill cell. A total of 15 flights were conducted, enabling the collection of statistically significant data under stable and repeatable meteorological conditions. To ensure high spatial resolution and maximum gas detection sensitivity, DJI Phantom 4 Pro flights were conducted under a strictly defined technical regime. The measurements were taken at a constant height of approximately 1.5 meters above the ground and with a constant cruising speed. This flight height and speed were chosen to capture odor markers directly in their release zone (the ground-level atmosphere), while maintaining the drone's safety and stability. The drone moved according to a predefined grid of parallel lines (Figure 48), programmed into the flight control application (DJI GO 4). This flight pattern ensured homogeneous coverage of the entire survey area and enabled subsequent precise interpolation of the results. Gas sampling points for dynamic olfactometry analyses were located along the drone's flight path. Figure 48 also shows the area of the active landfill cell, which was estimated at approximately 10,216.53 m^2 using QGIS Solothurn version 3.44.6.

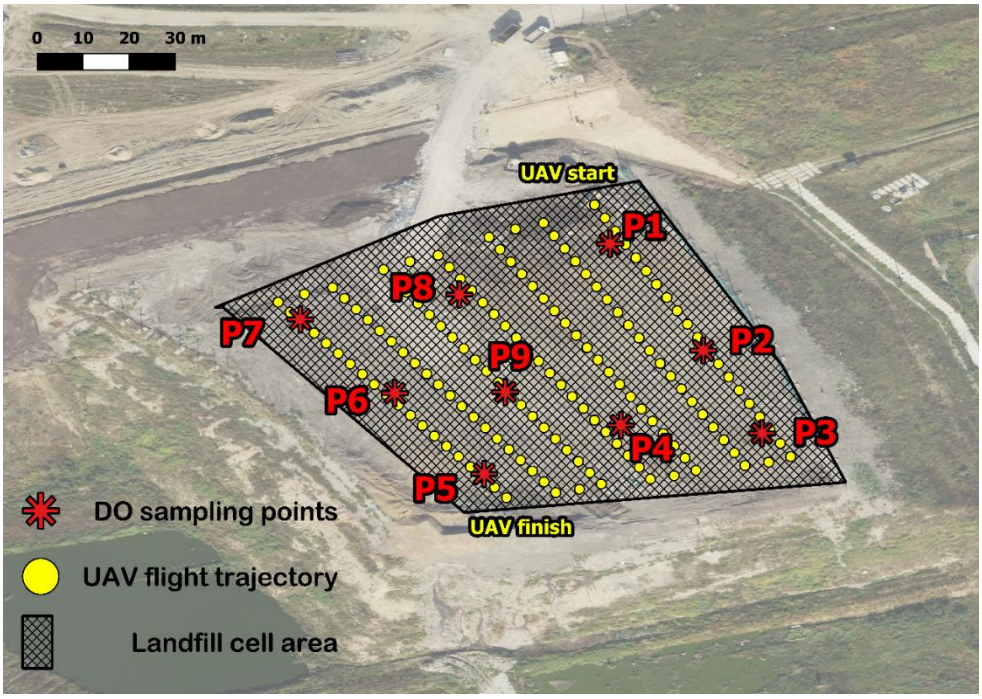


Figure 48. Situation plan of the research area over the active landfill cell: visualization of the UAV measurement flight trajectory with the marked operational area and the location of the points (P1–P9) where gas samples were collected for analysis using the dynamic olfactometry method.

9.2.4 Processing and spatial interpolation of UAV data

A key step in the analysis was to transform the raw measurement records into continuous models of concentration distribution across the study area. This process, which included advanced georeferenced data processing, was implemented in the QGIS environment (Solothurn version 3.44.6). Before spatial analysis, the raw dataset was screened to eliminate any incomplete records or georeferencing errors. Then the original geographic coordinates recorded by the drone's navigation system were reprojected to the metric system. This allowed for maintaining physical consistency in the calculations and eliminating distance errors during spatial operations. Separate sets of measurement points were generated for each measured substance.

Due to the specific linear structure of drone flights and the high sampling density, the triangulation method (triangulated irregular network - TIN) was chosen as the extrapolation algorithm. TIN precisely responds to sudden concentration peaks near emission sources without causing excessive smoothing. Thanks to the triangle-based structure, this method better handles the linear structure of drone measurements, enabling the creation of reliable, continuous maps of gas distribution (H_2S, NH_3, CO_2, CH_4, VOCs) across the entire surface of the landfill cell. In other words, it minimizes visual and mathematical errors resulting from the drone's movement along precisely defined flight axes. The resulting raster (extrapolated) surfaces were precisely trimmed to the landfill boundaries using a polygon mask.

The use of the TIN method in drone data processing allows, first of all, the elimination of artifacts that often appear when using distance-based interpolation methods (e.g., Inverse Distance Weighting - IDW). Data was collected very densely, but only along specific flight paths. Traditional interpolation methods can create unnatural "bands" or patterns in such conditions that reflect the aircraft's path rather than the actual gas distribution. The TIN method minimizes this phenomenon, creating a more realistic model. To integrate the data with regression algorithms, a raster-to-point transformation process was performed. The final dataset architecture was based on the following assumptions:

- A regular grid of points was generated, each representing an area unit of 0.5 m^2.
- This resolution was closely synchronized with the dimensions of the flux chamber (0.5 x 1.0 m), which ensured full compatibility of sensor data with the results of dynamic olfactometry (see chapter 9.2.5).
- The process resulted in the creation of a database of 20,415 measurement points (for each sensor), each of which had a unique set of coordinates and assigned interpolated gas concentrations.

The prepared matrix, exported in tabular format, constituted a complete input for the predictive PLS models (see chapter 9.2.6), enabling the final mapping of odor concentration and emission at the landfill cell. Figure 49 shows the effect of this transformation (raster-to-point transformation), which allowed the generation of a regular grid of 20,415 fully georeferenced points within the studied landfill cell.

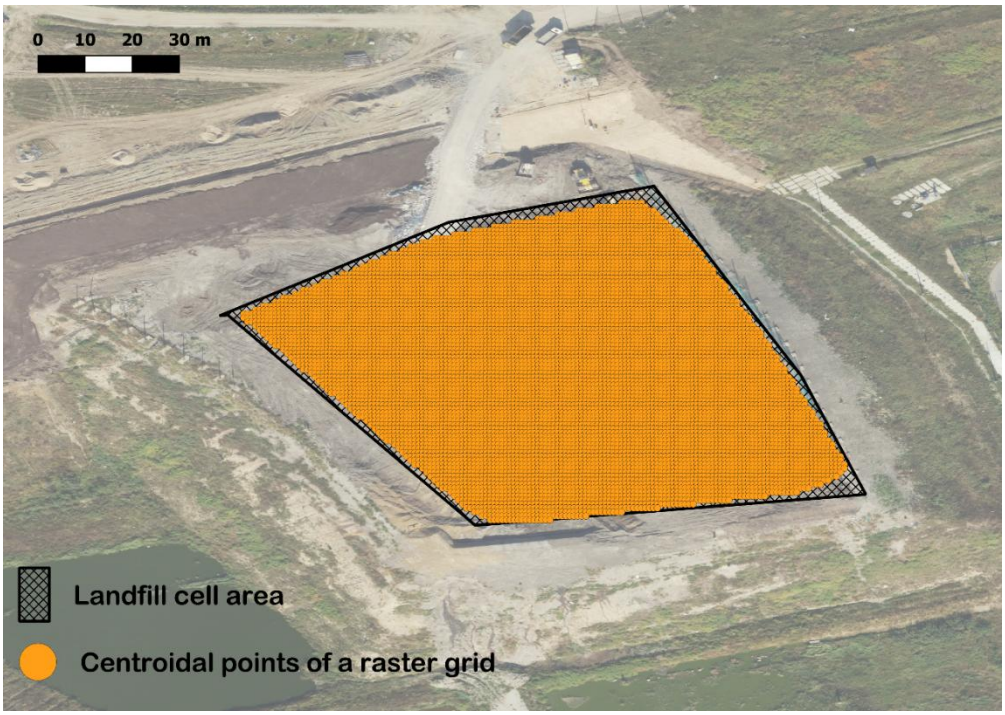


Figure 49. Generating a regular grid of spatial data in QGIS: visualization of the conversion of a concentration raster into a set of points with a resolution of 0.5 m², constituting the input for estimating odor concentration and odor emissions.

9.2.5 Reference equipment (Dynamic olfactometry)

Measurements and sampling methods should be representative of the emission magnitude under defined conditions, taking into account the purpose of the measurement. The objective of the measurements should focus on odor emissions during specific operating periods of the facility, peak emission events, or emissions from selected processes within the investigated site. Furthermore, the study's motivation may include assessing the performance of an odor deodorization unit. For the purposes of this study, 27 gas samples were collected (9 samples for each measurement campaign), with all sampling points located within the active landfill area. The exact locations of the sampling points along the drone flight path are shown in Figure 48. The sampling locations were not selected randomly. All gas samples were collected in the vicinity of degassing wells installed within the landfill cell, which represent primary sources of landfill gas release. This targeted sampling strategy ensured that the collected samples were representative of zones with elevated potential for odor emissions.

Gas sampling was performed from a passive surface source. In the case of diffuse or passive emissions, where no defined exhaust stream exists, it is recommended to use a surface sampling device that isolates a representative portion of the emitting surface and imposes a controlled airflow over it. Such an approach enables the generation of a defined and reproducible gas stream that can be sampled under well-defined hydrodynamic conditions. The sampling procedure involves forcing a sample of odorous gas into a NALOPHAN gas sampling bag, and the process directly affects the quality of the measurement results. To obtain a sample representative of the odor emission being tested, it is sometimes necessary to measure relevant parameters such as gas flow velocity or emitter diameter. This mainly applies to point emitters,

while for surface emitters, samples are forced into NALOPHAN bags using a special sampler, inside which a vacuum is created.

In this study, a surface flux chamber with an effective footprint of 0.5 x 1.0 m, equipped with a fan mounted on its top to induce a controlled gas flow over the surface enclosed by the chamber, was applied (Figure 50). The chamber enclosed a fragment of the landfill surface, creating a quasi-steady-state headspace above the emitting material. The fan mounted on the chamber roof induced a uniform airflow over the enclosed surface, ensuring sufficient mixing and transport of the emitted compound while minimizing disturbance to the surface. The chamber was additionally fitted with a vacuum sampler, through which air was drawn into specially prepared NALOPHAN bags at a flow rate of 1 L min^{-1}. The volume of each sample was 10 L (each NALOPHAN bag was filled over 10 min), which is sufficient for subsequent determination of odor concentration using dynamic olfactometry. This configuration follows the EN 13725 concept for sampling from passive sources, whereby odorous compounds released from the surface are entrained into an artificial carrier flow and conveyed to the sampling system. The generated gas stream is subsequently collected in sampling bags and analyzed by dynamic olfactometry. The use of a surface chamber provides a reproducible and representative means of converting diffuse surface emissions into a measurable sample, enabling quantitative determination of odor concentration and emission characteristics from area sources.



Figure 50. Gas sampling from the landfill cell surface: application of a flux chamber (0.5 m^2 area) to obtain landfill gas samples for reference olfactometric analyses.

Dynamic olfactometric measurements were performed using the Olfasense TO8 Evolution olfactometer (Olfasense GmbH, Kiel, Germany), in accordance with the requirements of EN 13725. Odor concentration was determined by presenting the samples to a panel of selected and trained assessors, while varying the concentration of odorants through dilution with neutral air. Samples were presented to the panel members in order of increasing concentration (from the most diluted), i.e. samples with lower concentrations were evaluated prior to those with higher concentrations. This procedure was applied to prevent undesirable effects such as adsorption/desorption phenomena and cross-contamination between samples. The sensory panel consisted of four specially selected and trained assessors. The selection of panel members was preceded by qualification procedures described in EN 13725 and involved a series of

measurements performed on gas samples of a reference odorant (n-butanol) with known concentrations. The qualification process comprised several measurement series to verify the individual sensitivity and repeatability of responses.

During the measurements, a standardized sensory evaluation technique - the YES/NO method - was applied. In this approach, the assessor was presented either with a diluted gas sample or with clean air and was asked to indicate whether an odor was perceived. Using this procedure, measurements were continued until the assessor positively detected the presence of odorants in the diluted sample. The individual odor detection threshold (Z_{ITE}) for a given gas mixture was then calculated as the geometric mean of the last negative and the first positive response. This step is performed for each panel member. Subsequently, a second geometric mean is calculated from the individual results obtained for all assessors ($\bar{Z}_{ITE}$), yielding the odor concentration for a single measurement series of the entire panel (C_{od}).

$$Z_{ITE} = \sqrt{Z_{YES} * Z_{NO}} \tag{51}$$

$$\bar{Z}_{ITE} = \prod_{i=1}^{n} Z_{ITE_n} \tag{52}$$

$$C_{od} = \sqrt[n]{\bar{Z}_{ITE}} = \sqrt[n]{\prod_{i=1}^{n} Z_{ITE_n}} \tag{53}$$

Where: Z_{YES} – the dilution level at which the odour was detectable, Z_{NO} – the dilution level at which the odour was undetectable, n – number of panel members participating in olfactometric measurements. To exclude panelists who showed deviant responses for the odorants in the samples, the retrospective panel screening was applied. It was carried out on the basis of the parameter ΔZ, which is the ratio between the individual threshold estimate and the geometric mean of all individual threshold estimates in a measurement.

$$If\ Z_{ITE} \geq \bar{Z}_{ITE}\ \ then\ \ \Delta Z = \frac{Z_{ITE}}{\bar{Z}_{ITE}} \tag{54}$$

$$If\ Z_{ITE} \leq \bar{Z}_{ITE}\ \ then\ \ \Delta Z = -\frac{Z_{ITE}}{\bar{Z}_{ITE}} \tag{55}$$

$$-5 \leq \Delta Z \leq 5 \tag{56}$$

If one or more individual threshold estimates of one or more panelists did not comply, all individual threshold estimates of the panelist with the largest ΔZ were excluded from the data set used to calculate the panel threshold for that measurement. The screening procedure was repeated until all panelists in the dataset complied. The last value of $\bar{Z}_{ITE}$ that was obtained was the dilution factor at the panel threshold $\bar{Z}_{ITE,pan}$.

9.2.6 Data analysis and mathematical modeling

Calculations, including model construction, validation, parameter estimation, and statistical analysis, were performed in RStudio software version 4.5.2 (RStudio Team, Boston,

MA, USA). Individual sensors were calibrated in the laboratory using standard mixtures covering the concentration range expected during field measurements. Instead of using the maximum signal level directly, the ΔS parameter, the difference between the mean baseline value and the largest response observed for a given gas concentration, was determined for each exposure. This parameter was adopted as the primary calibration variable. This method of describing the response limited the influence of zero-point drift and differences between sensor units. The obtained relationships were then used to convert the raw signals recorded during UAV flights into concentration values. Before estimation, all input variables were standardized, i.e., the mean value for the training set was subtracted from each value and the result was divided by the standard deviation. This prevented the excessive influence of variables with larger numerical values and ensured a comparable contribution of all sensors to the model. The same scaling parameters were later applied during forecasting to maintain consistency between the training stage and the spatial application.

$$x_j^* = \frac{x_j - \mu_j}{\sigma_j} \tag{57}$$

Where: μ_j – the mean of variable x_j in the training dataset, σ_j – standard deviation of variable x_j in the training dataset. Partial least squares (PLS) regression was used to relate the results obtained from the sensor array to the parameters determined by dynamic olfactometry. The model was developed separately for the natural logarithm of odor concentration and for the measured odor emission. The choice of PLS was based on the strong interdependencies between the signals from individual detectors and the limited number of reference measurements. In such conditions, classical multiple regression can be unstable, whereas PLS replaces the set of correlated variables with a smaller number of latent components, selected for their relationship to the dependent variable:

$$y_{OC} = f(\boldsymbol{X}) \tag{58}$$

$$y_E = f(\boldsymbol{X}) \tag{59}$$

Where: y_{OC} – natural logarithm of odour concentration, y_E – measured odour emission, $\boldsymbol{X} = [x_1, x_2, \cdots, x_p]$ is the vector of explanatory variables (gas concentrations), $f(\cdot)$ - regression function determined using the PLS method. PLS regression represents both the predictor matrix $\boldsymbol{X}$ and the response vector *y* through a reduced set of latent variables:

$$\boldsymbol{X} = \boldsymbol{T}\boldsymbol{P}^T + \boldsymbol{E}, \qquad y = \boldsymbol{T}\boldsymbol{q} + \boldsymbol{f} \tag{60}$$

Where: $\boldsymbol{T} = [t_1, t_2, \cdots, t_a]$ donates the latent score matrix, $\boldsymbol{P}$ is the loading matrix, $\boldsymbol{q}$ is the vector of regression coefficients in the latent space, $\boldsymbol{E}\ and\ \boldsymbol{f}$ are the corresponding residual terms, and a indicates the number of latent components retained in the model. These components were derived to maximise the shared covariance between the predictor variables and the response. This supervised construction differentiates PLS from principal component analysis, which is based only on the variance structure of the predictors. As a result, PLS is well suited to gas sensor array data, where substantial correlation among individual sensor signals is typically observed. After transformation back to the original predictor space, the model can be written as:

$$y_i = \beta_0 + \sum_{j=1}^{p} \beta_j x_j^* \quad (61)$$

Where: $\beta_0$is the intercept, x_j^* denotes the standardised value of the j-th predictor, and β_j is the corresponding regression coefficient estimated using the selected number of PLS components. The number of PLS components was determined using the leave-one-out cross-validation. The variant with the lowest RMSE calculated during validation was considered the final solution. Prediction quality was assessed based on the coefficient of determination (R^2) and the RMSE.

9.2.7 Odor emission modeling

The next stage of the research was to quantify the odor emission rate (OER) from the surface of the active landfill cell, develop a prediction model allowing for its spatial analysis and spatial validation using odor dispersion modeling. Odor emissions from landfill surface were determined using a dynamic flux chamber. The process was based on the following calculation steps:

- Flow rate measurement – the outlet air velocity was measured directly at the flux chamber outlet using an anemometer, which allowed the volume flow $(\dot{Q})$ to be calculated based on the outlet cross-sectional area.
- Point emission calculation – for each sampling point, the specific odor emission rate was determined as the product of the volumetric flow rate $(\dot{Q})$ and the odor concentration $(C_{od,i})$ determined by dynamic olfactometry:

$$OER_i = \dot{Q} \cdot C_{od,i} \quad [ou_E \cdot s^{-1}] \quad (62)$$

- Surface normalization – emission values were related to the flux chamber area $(A_{hood} = 0.5\ m^2)$, calculating the specific surface odor emission rate $SOER_i$:

$$SOER_i = E_{A,i} = \frac{OER_i}{A_{hood}} \quad [ou_e \cdot m^{-2} \cdot s^{-1}] \quad (63)$$

- Total emission estimation: the total odor emission for the active landfill cell was calculated as the product of the average surface odor emission rate $\bar{E}_A$ and the total source area $A_{landfill} = 10{,}216{,}53\ m^2$:

$$OER_{total} = \bar{E}_A \cdot A_{landfill} \quad [ou_E \cdot s^{-1}] \quad (64)$$

An additional approach to determining odor emissions across the entire landfill cell involved the use of a PLS regression model. The explanatory variables (X) were gas concentrations measured by the sensor array, and the dependent variable (y) was odor emissions determined using the reference method. The completed predictive model was superimposed on a grid of 20,415 measurement points generated in a QGIS environment, allowing for the assignment of emission values to each 0.5 m^2 point within the landfill cell. Next, a comparative analysis was conducted using odor dispersion modeling in OperatFB (v. 9.1.0.3), which implements a Gaussian model. The use of Gaussian plume model was justified by the fact that it is the only legally approved method for assessing atmospheric dispersion in Poland, in

accordance with the Regulation of the Minister of the Environment of 26 January 2010. The analysis proceeded according to the following scheme:

- Definition of emission scenarios – two independent scenarios were compared: (a) based on the total emission from dynamic olfactometry and (b) based on the emission predicted by the UAV-PLS model.
- Parametrization of the dispersion model – calculations were carried out for the receptor height $z = 1.5\,m$, (average human breathing zone) and the terrain roughness coefficient $z_0 = 0.87$, taking into account actual wind rose recorded during the measurement campaign (Figure 51).
- Analysis at receptor points – the results of both scenarios were compared at ten receptor points located around the periphery of the MSWTP.
- Evaluation criterion – the analysis aimed to check how differences in the total emission estimate propagate through the dispersion model and influence the predicted odor nuisance in the landfill's surroundings.

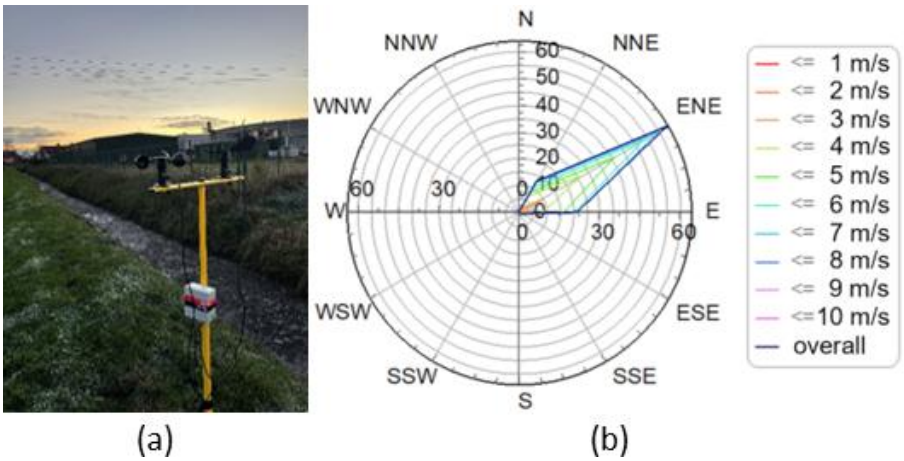


Figure 51. Characteristics of the metrological conditions of the measurement campaigns: (a) metrological station used to record atmospheric parameters, (b) wind rose showing the distribution of wind directions and speeds, consulting a metrological input for modeling odor dispersion.

9.3 Results and discussion

9.3.1 Olfactometric characteristics of landfill cell

The first stage of verifying the second research hypothesis involved carrying out tasks aimed at determining the spatial distribution of concentrations of selected gaseous odorants above the surface of the active section of the landfill cell and examining the extent to which they correlate with the odor concentration determined using the reference method. To provide a frame of reference, Table 20 summarizes the odor concentration values (C_{od}) and specific emission rates (OER) determined using the dynamic olfactometry method at nine designated measurement points (P1 - P9). These values represent means from three measurement campaigns. SD denotes standard deviation and CV the coefficient of variation between campaigns. Odor concentration obtained during each campaign was calculated as the geometric mean of measurements performed by four panelists.

Table 20. Olfactometric parameters (C_{od} and OER) determined using the dynamic olfactometry method (EN 13725) at reference points on the active surface of the landfill cell.

	Odor concentration		Odor emission		
Sampling point	**Mean [ou_e/m^3]**	**SD [ou_e/m^3]**	**Mean [ou_e/s]**	**SD [ou_e/s]**	**CV [%]**
P1	109.6	8.0	0.53	0.04	7.3
P2	846.0	61.3	4.06	0.29	7.3
P3	846.8	62.4	4.06	0.30	7.4
P4	230.4	18.3	1.11	0.09	7.9
P5	609.9	26.9	2.93	0.13	4.4
P6	328.6	14.6	1.58	0.07	.4.4
P7	421.4	19.0	2.02	0.09	4.5
P8	666.9	28.4	3.20	0.14	4.3
P9	1136.4	48.2	5.45	0.23	.4.2

The data in the table above clearly indicate the highly heterogeneous nature of odor emissions from a complex area source. Odor concentrations (C_{od}) ranged widely from 109.6 $\pm$ 8.0 ou/m^3 to 1136.4 $\pm$ 48.2 ou/m^3. In contrast, the determined emission rates (OER) ranged from 0.53 $\pm$ 0.04 ou/s to 5.45 $\pm$ 0.23 ou/s. Local peaks in odor nuisance (C_{od} > 845 ou/m^3) were concentrated in the vicinity of points P2, P3, P8, and P9. These points are located in the vicinity of degassing wells and active municipal waste disposal sites, which confirms their role as the dominant sources of odor nuisance.

9.3.2 Spatial distribution of gaseous components over landfill cell

Assessing the feasibility of replacing stationary, dynamic olfactometry measurements with continuous mobile detection required an analysis of continuous gas concentration fields (H_2S, NH_3, CH_4, CO_2, and VOCs), reconstructed from UAV flights using TIN spatial interpolation and superimposed on olfactometry reference points (Figure 52). An analysis of the relationship between the UAV profiles of individual compound concentrations and olfactometric values, as shown in the figure below, leads to significant observations of a physicochemical nature. First, the concentration fields for hydrogen sulfide (in the range of 0 - 20 ppm) and ammonia (in the range of 0 - 2 ppm) showed almost complete spatial correspondence with the areas of highest odor concentration. The highest concentrations of these gases occur in the areas of the landfill cell coinciding with the locations of points P2, P3, P8, and P9. This proves that it is the reduced inorganic molecules that determine the perceptible odor nuisance of landfill gas (vicinity of degassing wells).

Second, there is a clear spatial dissociation between the main components of biogas (CH_4 and CO_2) and odor nuisance. The concentration fields of methane (90 - 4,350 ppm) and carbon dioxide (720 - 900 ppm) exhibit different spatial patterns. Their maxima are located in the central part of the landfill cell. This phenomenon has an important technological rationale: methane and carbon dioxide are odorless (or barely odorous) products of deep anaerobic fermentation of biomass. Although they indicate general biological activity in the deposit, their high concentrations do not directly translate into the perception of an odor. The VOC

distribution (3 - 5 ppm) reveals moderate, diffuse spatial variation with several local peaks in the unloading zones. This indicates that synthetic organic compounds (derived from freshly deposited waste) contribute to the modification of the hedonic tone of the background odor. From the perspective of addressing the second research hypothesis, establishing spatial consistency between the signals from sensors installed on the UAV and odor nuisance provides empirical evidence that the mobile measurement system records the actual structure of the emission field above a passive surface source. This served as the foundation for the next step, namely the mathematical construction of multidimensional PLS regression models.

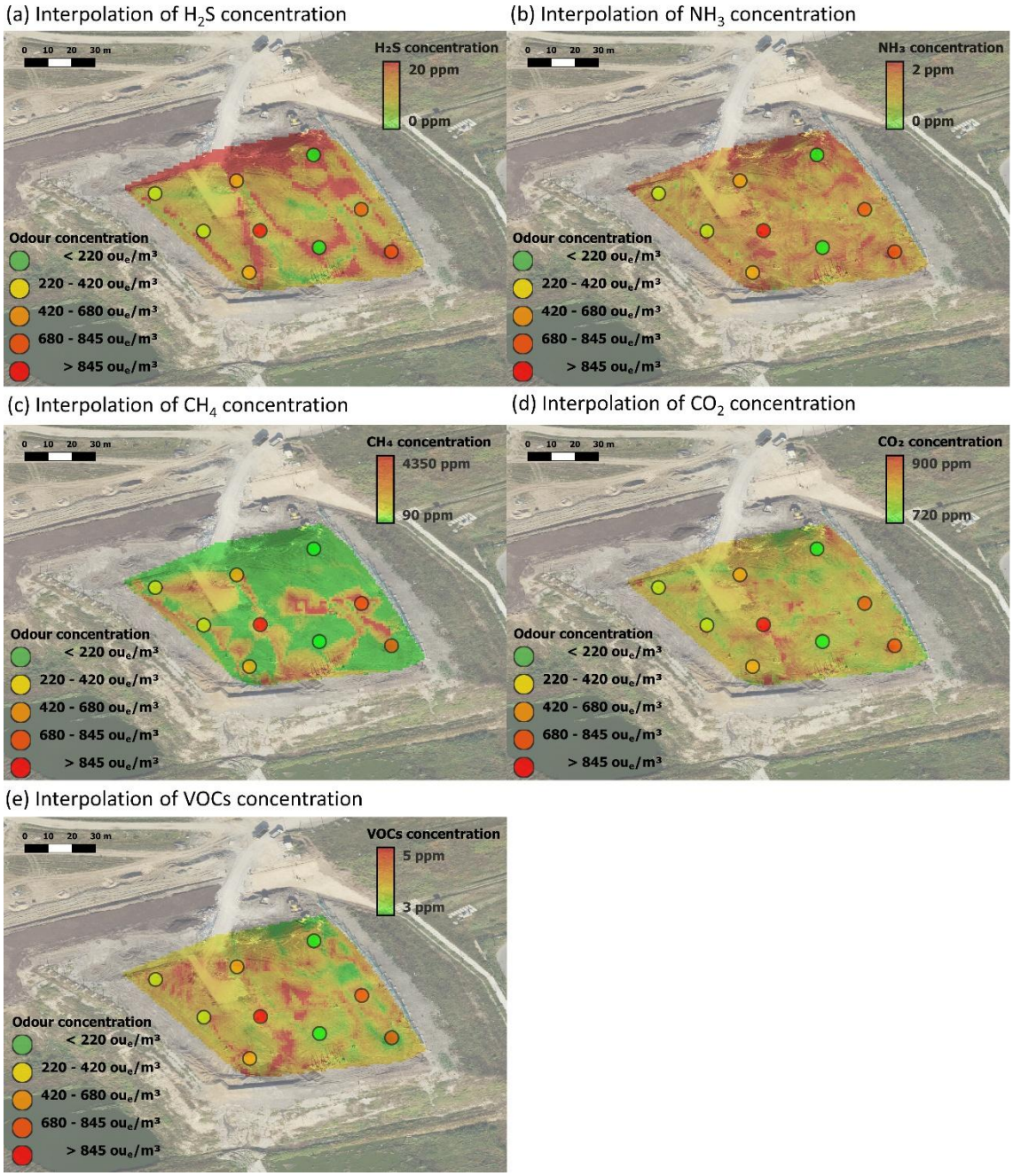


Figure 52. Reconstructed gas concentration fields (TIN interpolation from UAV flights) overlaid on point based dynamic olfactometry measurement results: (a) H_2S, (b) NH_3, (c) CH_4, (d) CO_2, (e) VOCs.

9.3.3 Calibration and parameterization of PLS regression models

To assess the agreement between the results obtained using the developed PLS models and the reference values, an analysis was conducted for odor concentration and odor emissions. The results for odor concentration were analyzed both on a logarithmic scale log(C_{od}), and for C_{od} expressed in original units ou_e/m^3. Both values refer, therefore, to the same predicted odor concentration result, presented on two different scales. Odor emission *E* was analyzed separately in units of ou_e/s. For each variant, 27 pairs of measured and predicted values were used. To quantitatively characterize the agreement, the coefficient of determination R^2, the slope and intercept of the regression of predicted values against measured values, as well as RMSE, MAE, and the mean systematic error (bias) were used (Table 21). These parameters allowed to assess both the degree of agreement between predicted and reference values and the direction and magnitude of the deviations.

Table 21. Statistical parameters describing the agreement between measured and PLS predicted values for the developed calibration models.

Model	**Slope**	**Intercept**	**R^2**	**RMSE**	**MAE**	**Bias**
log(C_{od}) – (a)	0.993	-0.113	0.971	0.199	0.166	-0.158
C_{od} – (b)	0.921	-31.854	0.976	93.163	79.251	-77.327
E – (c)	0.876	-0.002	0.980	0.438	0.348	-0.347

*Slope is dimensionless, whereas intercept, RMSE, MAE, and Bias are expresses in the units of the corresponding model output.

For all the relationships analyzed, high values of the coefficient of determination were obtained, ranging from 0.971 to 0.980. In the case of odor concentration analyzed on a logarithmic scale, the regression slope was 0.993, which is very close to 1 (the value corresponding to perfect agreement between predicted and measured values). When the results of the same model were presented in original units (ou_e/m^3), the regression slope was 0.921. However, this difference should not be interpreted as a comparison of the quality of two independent models, since both forms describe the same result of odor concentration prediction on different scales. For odor emissions, $R^2 = 0.980$ and a regression slope of 0.876 were obtained. A slope value less than one indicates that, as emissions increased, the predicted values increased more slowly than the corresponding measured values. For all analyzed variable forms, negative bias values were obtained, indicating a general tendency to underestimate the reference values. The bias was -0.158 on the log(C_{od}) scale, -77.327 ou_e/m^3 for odor concentration in primary units, and -0.347 ou_e/s for odor emission. The absolute values of RMSE, MAE, and bias should not be directly compared across these forms of results due to differences in scale and units.

To enable a comparison of the relative magnitudes of the errors in odor concentration and odor emission, the errors were normalized relative to the measured mean value. For odor concentration, the NRMSE was 16.14%, the NMAE was 13.73%, and the relative bias was -13.39%. For odor emissions, these values were 15.82%, 12.57%, and -12.51%, respectively. The relative magnitude of the errors was therefore similar for both quantities analyzed, with slightly lower error coefficients for odor emissions. Normalization was not applied when comparing the log(C_{od}) scale with the original scale, because such a comparison would involve

comparing errors expressed on different scales. To supplement the quantitative characterization of the models, the predicted values were plotted against their corresponding measured values (Figure 53). For odor concentration, both a logarithmic scale and the results in original units are shown, while for odor emission, the relationship is presented in ou_e/s. The graphs show a line of ideal 1:1 agreement and a regression line for the predicted values relative to the measured values.

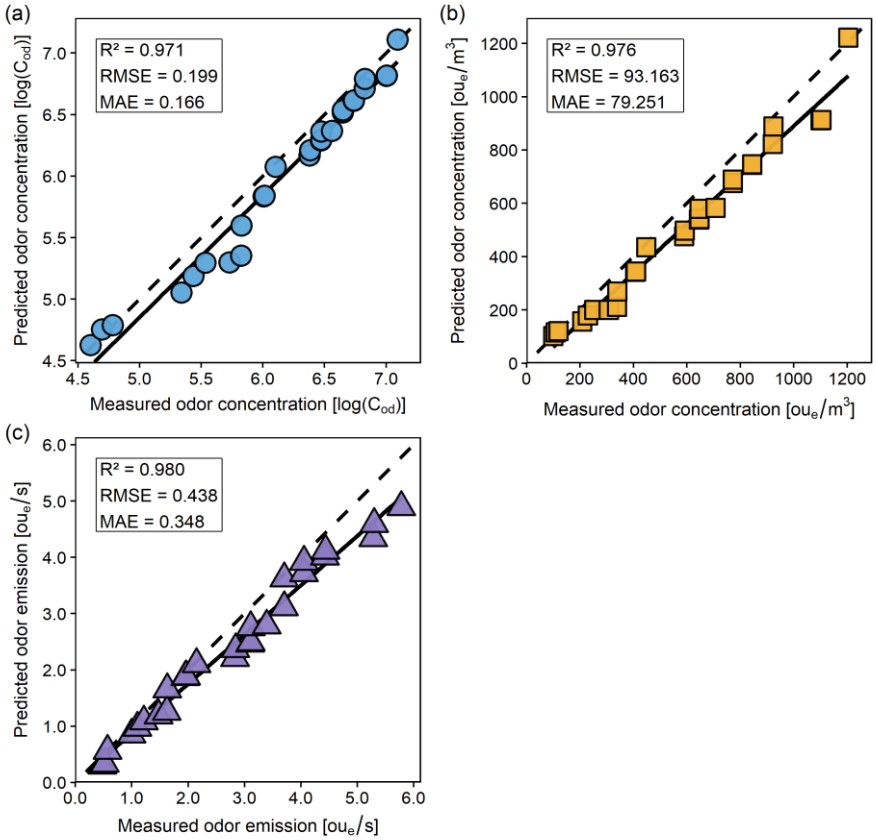


Figure 53. Comparison of measured and predicted values obtained using the developed calibration models: (a) logarithmically transformed odor concentration $\log(C_{od})$, (b) odor concentration expressed in ou_e/m^3, (c) odor emission expressed in ou_e/s. The dashed line represents the 1:1 relationship, whereas the solid line indicates the linear regression between measured and predicted values.

On a logarithmic scale, the points corresponding to odor concentration lie close to the 1:1 line, and the regression line closely follows it across most of the analyzed range. This is consistent with a regression slope of 0.993. The scatter of the points indicates that deviations of the predicted values from the measured values occurred in both directions. However, at the highest values, an overprediction is noticeable. When the results are presented in units of ou_e/m^3, the differences between the regression line and the 1:1 line become more apparent, especially in the upper part of the concentration range. This does not indicate a deterioration in the performance of the model, but is a consequence of presenting the same prediction result on a scale where the absolute magnitude of deviations increases with concentration. A regression slope of 0.921 and a negative bias confirm a tendency to underestimate higher concentration values. For odor emissions as well, a high linear correlation was observed between the measured and predicted values. The regression slope of 0.876 indicates an increasing deviation from a 1:1 relationship as emissions rise. The highest emission values were generally predicted to be below their corresponding

reference values. It is therefore important to note that high R^2 values confirm a strong relationship between measured and predicted values, but do not in themselves rule out the presence of systematic error. For this reason, the assessment was supplemented with a residual analysis.

To determine the nature of the errors more precisely, the residuals, defined as the difference between the predicted value and the measured value, were analyzed (Figure 54). This method of presentation allows for an assessment not only of the magnitude of the errors but also of whether their direction changes systematically as the analyzed quantity increases. The analysis of the residuals allowed to supplement the model evaluation with information regarding the structure of prediction errors. For the odor concentration presented on a logarithmic scale, the residuals formed a relatively compact cluster, and the trend line remained nearly horizontal. This indicates a weak dependence of the error magnitude on the concentration level on this scale and the absence of a clear increase in dispersion as the measured values increase.

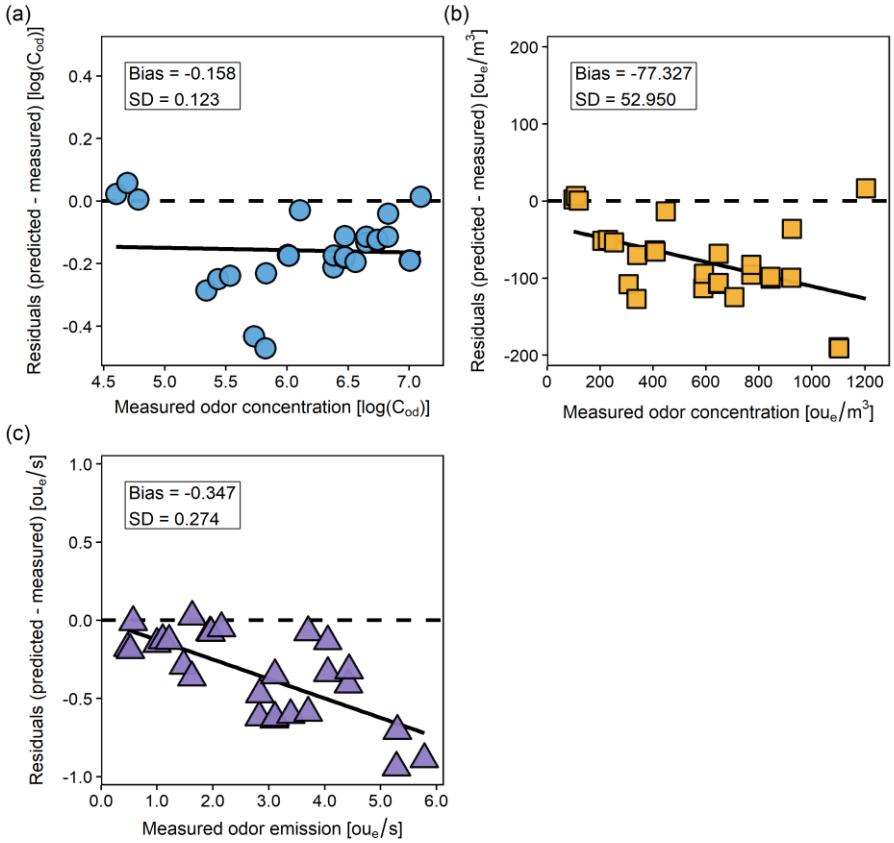


Figure 54. Residual analysis for the developed calibration models: (a) logarithmically transformed odor concentration $\log(C_{od})$, (b) odor concentration expressed in ou_e/m^3, (c) odor emission expressed in ou_e/s. Residuals were calculated as predicted minus measured values. The dashed horizontal line indicates zero residual, whereas the solid line represents the linear trend of residuals.

After presenting the odor concentration results in primary units, the distribution of the residuals was more orderly with respect to the measured values. Negative deviations dominated in the middle of the range, while the largest differences between predicted and measured values occurred at higher concentrations. This shows that retransforming the results to the original scale reveals the non-uniformity of the absolute error across the entire measurement range. For odor emissions, the relationship between residuals and measured values was most pronounced. As

emissions increased, the data points gradually shifted toward more negative residual values, and the largest deviations occurred in the upper part of the range. This means that the prediction error was not entirely random (its direction and magnitude were partially related to the emission level).

A comprehensive analysis of statistical parameters, the relationships between measured and predicted values, and the distribution of residuals indicates a high degree of agreement between the results obtained using the developed PLS models and the reference values in the analyzed dataset. At the same time, an analysis of the regression slope, bias, and residuals revealed a systematic tendency to underestimate values in the upper part of the measurement range. For odor concentration, this phenomenon is less apparent on a logarithmic scale but becomes more pronounced when the results are presented in original units. Normalized error measures, however, indicate a similar relative level of error for odor concentration and odor emissions, with NRMSE values of 16.14% and 15.82%, respectively.

9.3.4 Spatial mapping of odor concentrations and odor emissions

PLS regression models were implemented in the QGIS environment to convert continuous fields of gas component concentrations into spatial distributions of odor parameters over the surface of the active landfill cell, which has an area of 10,216.53 m^2. In accordance with the adopted methodology, the concentration fields of individual gases were subjected to spatial discretization (raster-to-point transformation). Regular measurement grid consisting of 20,415 calculation points was obtained. Each grid point represented a unit area of 0.5 m^2, which corresponded to the surface area of the flux chamber used to collect reference samples. For each of the 20,415 points, the predicted odor concentration and the odor emission rate were calculated, generating high-resolution odor nuisance maps. The results of this work are shown in Figure 55.

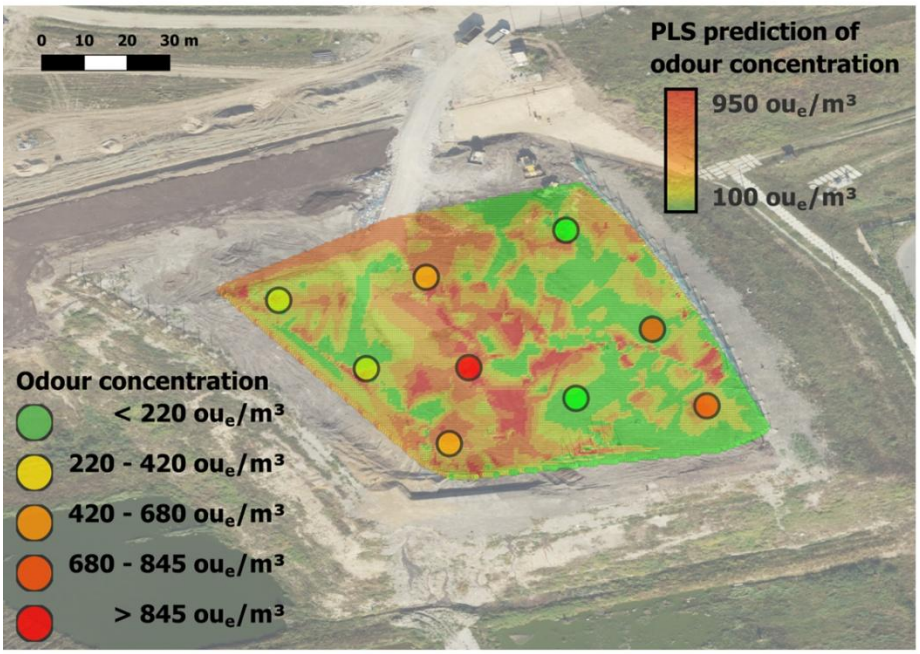
An analysis of the odor concentration map (Figure 55a) indicates a very wide variation in odor concentration in the surface layer above the landfill cell. The predicted values ranged from 100 ou_e/m^3 to 950 ou_e/m^3. Overlaying the dynamic olfactometry point results (P1 - P9, represented by colored circles with defined concentration ranges from < 220 ou_e/m^3 to > 845 ou_e/m^3) onto the generated map demonstrates a high degree of spatial agreement between the two methods. The olfactometric points with the highest recorded odor concentrations (P2, P3, P8, P9, marked in orange and red, $C_{od} > 845$ ou_e/m^3) lie within the zones for which the PLS model estimated concentrations in the range of 680 – 950 ou_e/m^3. In the peripheral parts of the landfill cell (e.g., point P1, $C_{od} = 109.6$ ou_e/m^3), the prediction shows low values, in the range of 100 - 220 ou_e/m^3.

Minor, localized discrepancies between point measurements and continuous field measurements stem from the specific characteristics of both techniques. Dynamic olfactometry involves a measurement at a specific point in time, whereas the PLS model is based on an averaged profile of signals from drone flights. Furthermore, human sensory perception takes into account the phenomena of synergy and masking of odorants, which are represented in a simplified manner by the system of five gas sensors.

The distribution of the odor emission (Figure 55b) provides key information for managing MSWTP operations. The values for the landfill cell ranged from 0.0 ou_e/s to 4.5 ou_e/s. This

visualization made it possible to carry out one of the research tasks, namely, to locate the so called emission hotspots. The areas with the highest odor emission (> 4.0 ou_e/s) are concentrated in the central and lower right parts of the landfill cell. These areas coincide directly with the locations of active degassing wells (corresponding to points P2, P3, P8, and P9) and with zones of fresh municipal waste unloading and compaction. Leaks around wellheads and the absence of a continuous sealing layer allow for the uncontrolled escape of landfill gas rich in hydrogen sulfide, ammonia, and VOCs. The peripheral areas of the landfill cell and the sectors covered by a compacted layer of insulating material exhibit low emission rates (< 1.0 ou_e/s).

(a) Odor concentration spatial map



(b) Odor emission spatial map

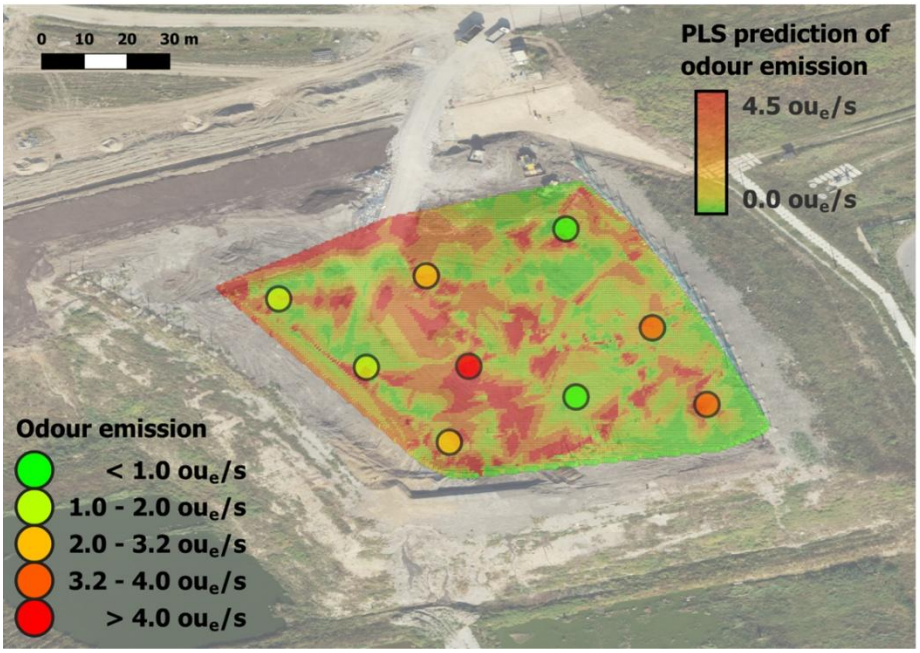


Figure 55. Spatial maps of the distribution of odor parameters across the active area of the landfill cell, determined using the PLS model: (a) odor concentration (ou_e/m^3), (b) odor emission (ou_e/s).

The results obtained show that the integration of UAV, gas sensor array, PLS regression, and GIS tools makes it possible to generate a continuous emissions map and precisely locate critical points, which offers unique value compared to manual point measurements.

9.3.5 Comparative modeling of odor plume dispersion

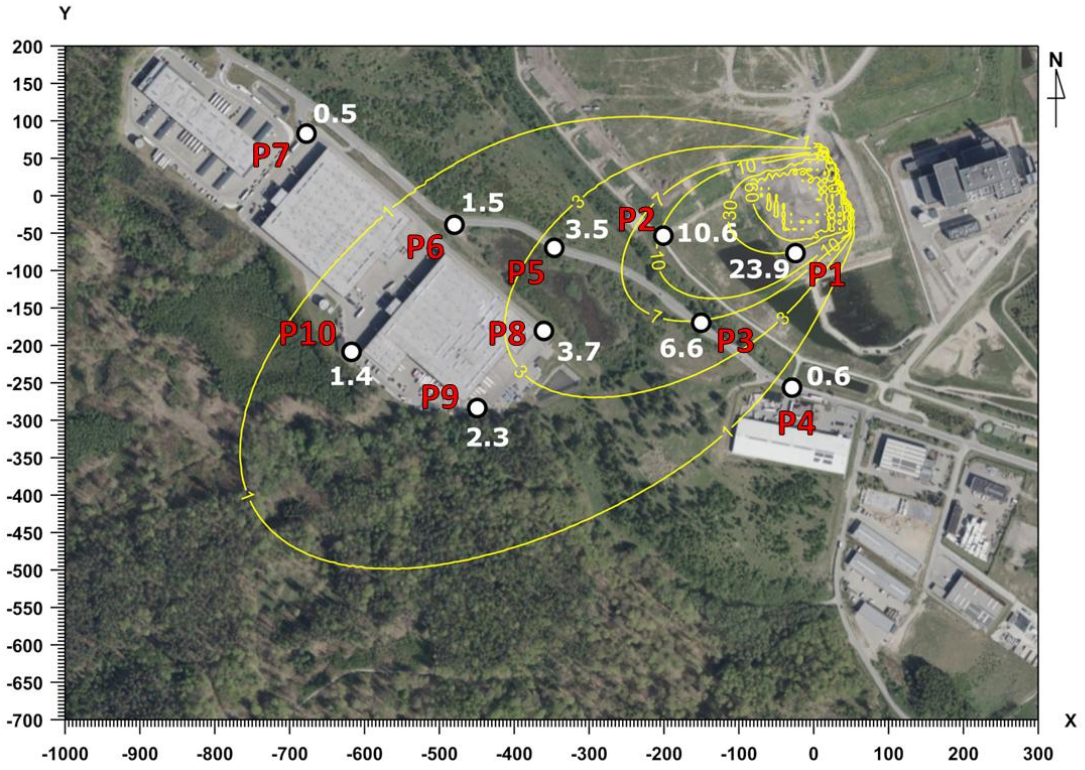
By discretizing the area into 20,415 central points, it was possible to perform a full surface integration of the OERs and compare the results with the reference method. The UAV-PLS estimation predicted total odor emissions from the landfill cell at 47,150 ou_e/s. Calculating total odor emissions using the traditional method (dynamic olfactometry estimation), by multiplying the average OER by the total area of the landfill cell, yielded a result of 56,633 ou_e/s. This means that the relative difference between the two methods was 16.7%. The final test of the UAV-PLS method's usefulness in environmental management was to verify its effect on the delineation of odor impact zones in the vicinity of the MSWTP. To verify whether this 16.7 percent balance deviation leads to significantly different conclusions regarding the spread of odor nuisance in the vicinity of the landfill, two independent simulations of odorant dispersion in the atmosphere were conducted. A visual comparison of the generated isolines of average odor concentration in the surface layer for both emission scenarios is shown in Figure 56.

A comparison of the dispersion images in the figure below shows a high degree of agreement between the two odor plume spreads. The odor concentration isolines in both scenarios take on an almost identical geometric shape and spatial pattern, consistent with the prevailing wind direction. The difference between the variants boils down solely to a slight shift in values within the plume, while maintaining full compliance with the spatial coverage of the basic odor nuisance thresholds. To ensure precise quantitative verification, odor concentration values in the surface layer were assessed at ten representative receptor points (P1 - P10), located on the periphery of the landfill cell and at various distances from the geometric center of the source. The aggregate results of the odor emission predictions for both scenarios and the absolute concentration differences (ΔC_{od})are summarized in Table 22.

Table 22. A comparison of the predicted odor concentrations Cod (ou_e/m^3) at receptor points P1 - P10 for the olfactometric scenario (DO) and the UAV-PLS model, along with the absolute difference in concentrations as a function of distance from the geometric center of the source.

Receptor point	Distance from the source - *x*	Odor concentration (DO) - C_{od}	Odor concentration (UAV-PLS) - C_{od}	Results difference - ΔC_{od}
	[m]	[ou_e/m^3]	[ou_e/m^3]	[ou_e/m^3]
P1	80.4	23.9	19.9	4.0
P2	207.0	10.6	8.8	1.8
P3	230.2	6.6	5.5	1.1
P4	257.5	0.6	0.5	0.1
P5	352.6	3.5	2.9	0.6
P6	480.5	1.5	1.3	0.2
P7	684.2	0.5	0.4	0.1
P8	403.4	3.7	3.1	0.6
P9	530.4	2.3	1.9	0.4
P10	652.1	1.4	1.2	0.2

(a) Emission scenario based on dynamic olfactometry



(b) Emission scenario based on UAV-PLS method

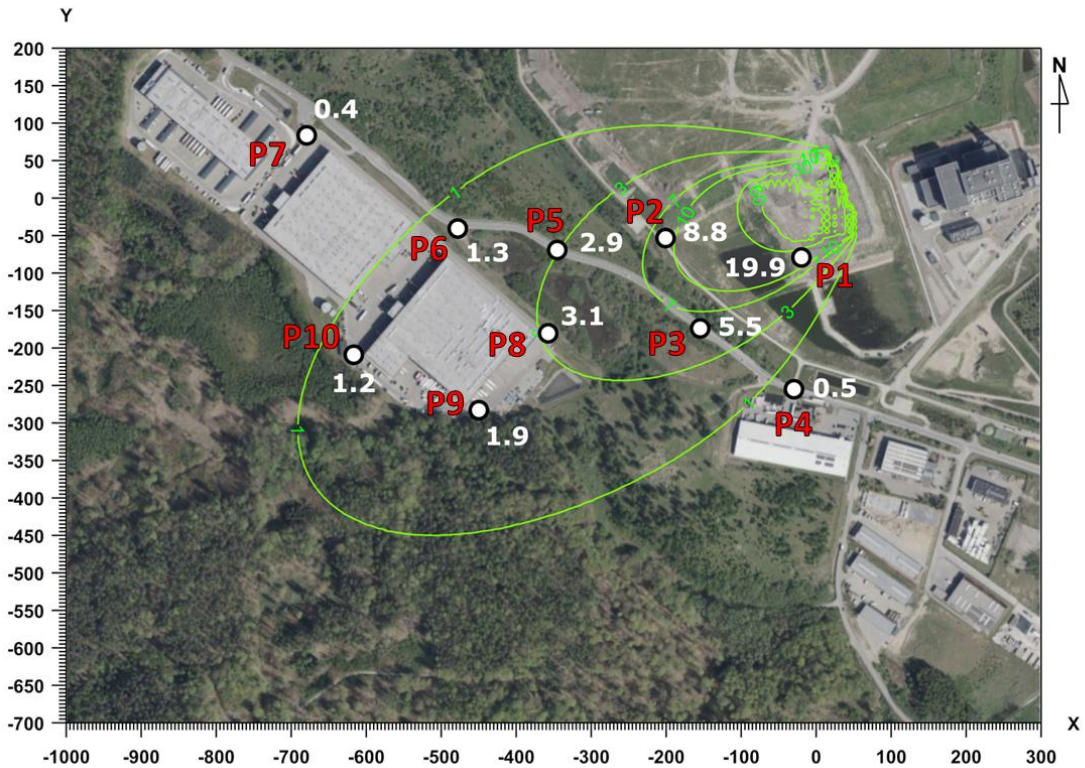


Figure 56. Isolines of average odor concentration in the surface layer (z = 1.5 m) obtained from the dispersion modeling of Gaussian plumes (OperatFB): (a) emission scenario based on reference dynamic olfactometry, (b) emission scenario based on UAV-PLS prediction model.

An analysis of the data from the Table 22 reveals a certain pattern. The variant based on dynamic olfactometry (DO) generates slightly higher odor concentration values at all receptor points, which is a direct consequence of the higher initial odor emission. However, the key factor in assessing the suitability of the UAV-PLS method is the disappearance of the concentration difference as the distance from the geometric center of the landfill cell increases. The relationship between the absolute difference in odor concentrations ((ΔC_{od}) among the simulations and the distance from the source is shown graphically in Figure 57.

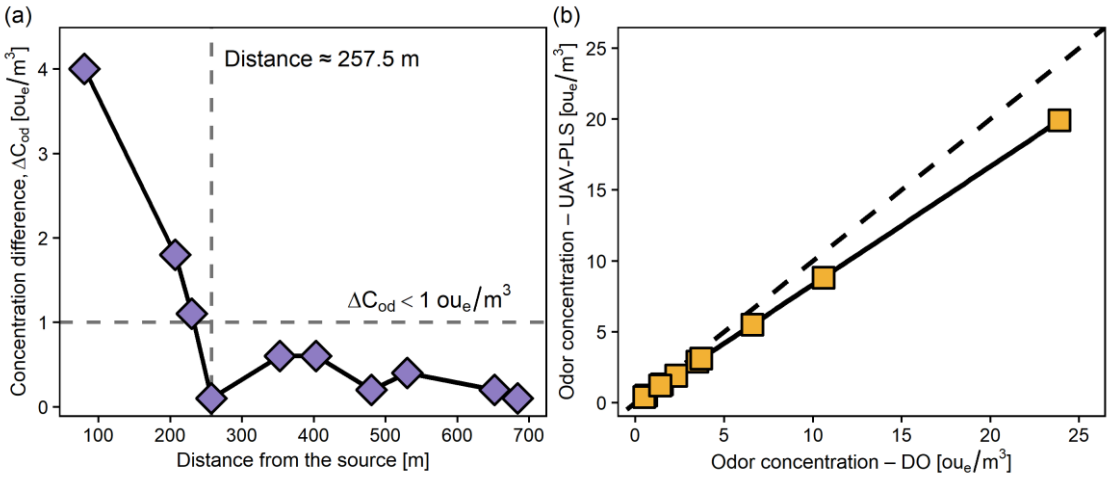


Figure 57. Comparison of results from the dynamic olfactometric scenario (DO) and the UAV-PLS model: (a) absolute difference in odor concentration as a function of distance from the geometric center of the source, (b) relationship between concentrations determined by both methods.

The highest discrepancies occur in the immediate vicinity of the landfill cell. For point P1 (distance 80.4 m), the difference is 4.0 ou_e/m^3 . This is likely due to the fact that, in this area, the odors emitted have not yet been diluted in the air. At a distance of approximately 230 m from the source (point P3, distance 230.2 m), the absolute concentration difference drops to 1.1 ou_e/m^3. According to the definition of an odor unit (where 1 ou_e/m^3 corresponds to the detection threshold for 50% of the population), a difference of $\leq$ 1.0 ou_e/m^3 represents the threshold below which a statistical observer is unable to distinguish the differences between the two scenarios. Above approximately 250 m, more precisely, from 257.5 m onward, this difference was less than 1 ou_e/m^3. This means that at greater distances, the discrepancy between the DO and UAV-PLS results was less than the value corresponding to one European odor unit.

The results indicate that the UAV-PLS model accurately captures changes in odor concentration determined based on an olfactometric scenario, while maintaining a consistent trend in changes as a function of distance from the source. At the same time, the observed tendency to slightly underestimate values suggests that the model can be used to assess the spatial variation in odor concentration, while remaining aware of the systematic error present.

Shifting the burden of measurement from traditional sampling to continuous UAV flights frees the environmental assessment process from cost and time constraints, while providing the dense data grid necessary for precise source mapping. In addition, the UAV-PLS method

provides data of a quality that is fully sufficient for conducting simulations of odor dispersion, planning buffer zones around landfills, and objectively resolving social conflicts.

9.4 Summary and conclusions

The overall results of the research conducted using an unmanned aerial vehicle (UAV) and multidimensional spatial modeling fully confirmed the validity of the second research hypothesis. It was demonstrated that integrating a gas sensor array with a drone enables precise spatial identification, quantitative assessment of odor emissions, and the localization of zones of elevated emissions (hotspots) at a passive area source. The acquired data constitute fully reliable input for modeling the dispersion of odor nuisance in the vicinity of the MSWTP.

As part of the verification of the second hypothesis, all specific research tasks were completed. Low altitude drone flights (1.5 m) with continuous measurement of sulfur compounds (H_2S), nitrogen (NH_3), volatile organic compounds, and the main components of biogas (CH_4, CO_2) have demonstrated that the mobile UAV platform enables the safe and rapid acquisition of a dense data grid in conditions inaccessible to traditional stationary equipment. The use of partial least squares (PLS) regression made it possible to eliminate the problem of signal multicollinearity and achieve high predictive accuracy for odor concentration and odor emission.

Processing continuous concentration fields using the TIN spatial interpolation method in QGIS and discretizing them into a regular grid of 20,415 calculation points (with a unit resolution of 0.5 m^2) made it possible to reconstruct the actual, heterogeneous structure of the emission field over the entire landfill cell. The UAV-PLS method precisely located emission peaks associated with leaks around degassing wellheads and the waste discharge front. The estimated total odor emissions from the landfill cell, determined using the UAV-PLS method, were at a level similar to that of the reference dynamic olfactometry method, showing a slight balance difference of 16.7%.

Comparative odor dispersion simulations using the OperatFB program (Gaussian plume model) showed that the determined spatial extent of odor concentration isolines in the surface layer is nearly identical for both emission scenarios. At a distance of more than 230 m from the source, the absolute difference in concentrations falls below 1.0 ou_e/m^3 (the threshold of human perception), and in the zone beyond 600 m, it reaches negligible values.

The use of unmanned aerial vehicles (UAVs) to monitor air quality at industrial facilities is one of the most rapidly developing areas in modern environmental engineering. A review of the current state of knowledge indicates, however, that the vast majority of studies to date have focused on narrowly defined measurement tasks. Many research teams have limited the use of drones to quantitative estimates of methane emissions using mass balance or individual laser/or NDIR sensors [250,251,255,256]. Other implementations involved the assessment of concentrations of air pollutants (CO, NO_2, SO_2, O_3) and particulate matter in urban and industrial areas [249,252,253,260].

With regard to measuring odor nuisance using drones, the literature indicates that only a few studies have been conducted, primarily at wastewater treatment plants. Studies by Burgués

et al. [244,245] demonstrated the possibility of mapping odors around wastewater treatment facilities using sensor arrays and e-noses mounted on drones.

Against this backdrop, the UAV-PLS-GIS methodology developed in this dissertation represents a new level of scientific and practical value:

- Comprehensive studies were conducted on a complex, highly heterogeneous areal source (active section of a MSWTP landfill cell).
- A multi-sensor gas sensor array (PID, NDIR, electrochemical sensors) was combined with PLS regression, and the results were compared to a reference method (dynamic olfactometry).
- The use of the UAV-PLS-GIS processing workflow and TIN interpolation on a grid of 20,415 center points made it possible to overcome the limitations of traditional olfactometry, which is characterized by low sampling density over large areas. As a result, full spatial representativeness of emission variability across the entire sector was achieved.
- The method's validity was demonstrated not only during the characterization of the source itself, but also in the receptor zone. Simulations using the OperatFB software demonstrated that a 16.7 percent difference in total odor emission does not affect the legal and social assessment of odor nuisance in the vicinity of the MSWTP, as the differences in odor concentrations are negligible.

9.5 Publication basis of the chapter

This chapter presents the research results from a manuscript currently under review:

Dobrzyniewski D., Szulczyński B., Czaplicka N., Gębicki J. (2026). Estimation of odour emission from a Municipal Landfill using UAV-based measurements. *Sensors and Actuators B: Chemical.*

The content has been revised and expanded for the purpose of this doctoral dissertation. In the thesis, the findings are discussed in the context of the main research objective.

10. Implementation of a gas sensor array for instrumental assessment of odor nuisance in field conditions

10.1 Purpose of the study

This work tested the capabilities of sensor arrays for assessing odor nuisance and odorous air quality. The research was conducted in the field at a municipal treatment plant located in central Poland (MZO Pruszków). The main goal was to create an instrumental odor air quality index ($OAQI_I$) that would allow the determination of all basic odor features (odor concentration - OC, hedonic tone - HT, and odor intensity - OI) using only one device – the sensor array. Another important element of the methodological innovation was the development of hybrid predictive models combining the analysis of multidimensional sensor signals with a psychophysical description of odor perception. A logarithmic representation of sensor responses based on Weber–Fechner's law was used, as well as models based on Stevens' law, including an approach combined with principal component analysis. This approach was complemented by the development of a custom sensor array configuration, as well as its field calibration and validation against field olfactometry. As a result the transition from the instrumental determination of the concentrations of individual substances to the instrumental assessment of odor air quality as perceived by humans was possible.

10.2 Materials and methods

10.2.1 Test site description

Field studies and data collection were conducted at the Municipal Treatment Plant (MZO Pruszków) located in the interior of Poland. This location was chosen because of the need to perform analyses under real-world conditions, characterized by high variability in odorous substance emissions. The gas sensor array was installed at the compost screening yard. This location was identified as a crucial source of odor emissions throughout the MTP. Additionally, it provided a wide range of odor concentrations, from episodic, high values directly related to mechanical screening processes to relatively low background concentrations during periods of operational downtime. Such a high rate of change was essential for the correct calibration and subsequent validation of the mathematical models.

Selecting a composting site as a testing ground allowed the gas sensor array to be tested in an environment with a complex chemical profile, including ammonia, hydrogen sulfide, and a wide spectrum of VOCs typical of waste treatment processes. The idea of the work was to train a sensor matrix to predict odor concentration and, on the scale of the proposed index, convert these concentrations into the other odor parameters. This approach would enable a comprehensive, complementary analysis of the air around the plant for odors using a single device. Additionally, the measurement could be continuous and made available online for residents unfamiliar with the concept of odor nuisance, providing them with uncomplicated

information, for example, in graphical form. The location of the MTP and the view of the compost screening site, which was the main measurement point, are shown in Figure 58.

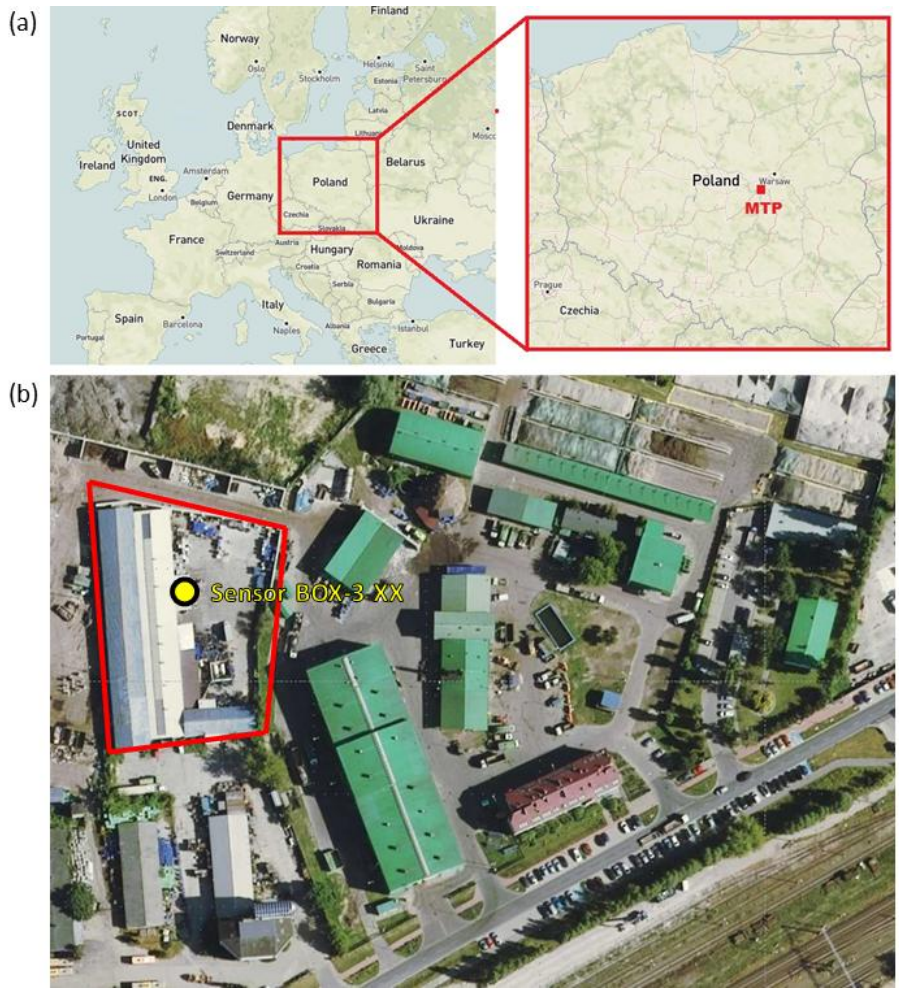


Figure 58. Location and place of research: (a) a map showing the location of the MTP, (b) the compost screening site where a gas sensor array (sensor BOX-3 XXXX) was installed. Adapted from [276], licensed by CC BY 4.0.

10.2.2 Reference equipment (Field olfactometry)

Field olfactometry (FO) was used as the reference technique to determine the actual odor concentration, which was necessary for the calibration and validation of the sensor array. These measurements enabled correlating instrumental signals with the panelists' objective organoleptic sensations. Portable Nasar Ranger field olfactometers (St. Croix Sensory, USA) were used. This device allows direct determination of odorant concentrations near the emission source, without the need for sampling. Each analysis was conducted by a team of at least 2 panelists, following rigorous measurement procedures. The final odor concentration value, expressed in ou/m^3 was determined as the geometric mean of the individual estimates collected by the measurement team, according to the mathematical relationships presented in chapter 4.2.1 (Eq. 7-10). The use of the Nasal Ranger olfactometer directly adjacent to the sensor array allowed the creation of a training database, which became the foundation for the development of mathematical models (MLR, PCR and hybrid) capable of predicting odor nuisance in a continuous mode.

10.2.3 Gas sensor array development

The constructed device, containing an array of five commercially available sensors, was placed in a compost screening yard. Three MOS sensors from the TGS series, manufactured by Figaro Engineering Inc. (Osaka, Japan), and two EC sensors selective for ammonia and hydrogen sulfide, manufactured by Alphasense (Braintree, UK), were selected. The characteristics of the individual sensors used in the device (sensor BOX-3 XXXX) are presented in Table 23.

Table 23. Basic parameters of the gas sensors used in the sensor BOX-3 XXXX.

Model	Producer	Sensing principle	Target gases	Signal conditioning
TGS2602	Figaro Engineering Inc. (Mino, Osaka, Japan)	MOS type	Air contaminants (hydrogen, ethanol)	Voltage divider
TGS2603	Figaro Engineering Inc. (Mino, Osaka, Japan)	MOS type	Air contaminants (trimethylamine)	Voltage divider
TGS2612	Figaro Engineering Inc. (Mino, Osaka, Japan)	MOS type	Air contaminants (VOCs, ammonia, H_2S)	Voltage divider
H2S-A4	Alphasense (Braintree, UK)	EC type	Hydrogen sulfide (0-50 ppm)	I-U converter
NH3-B1	Alphasense (Braintree, UK)	EC type	Ammonia (0-100 ppm)	I-U converter

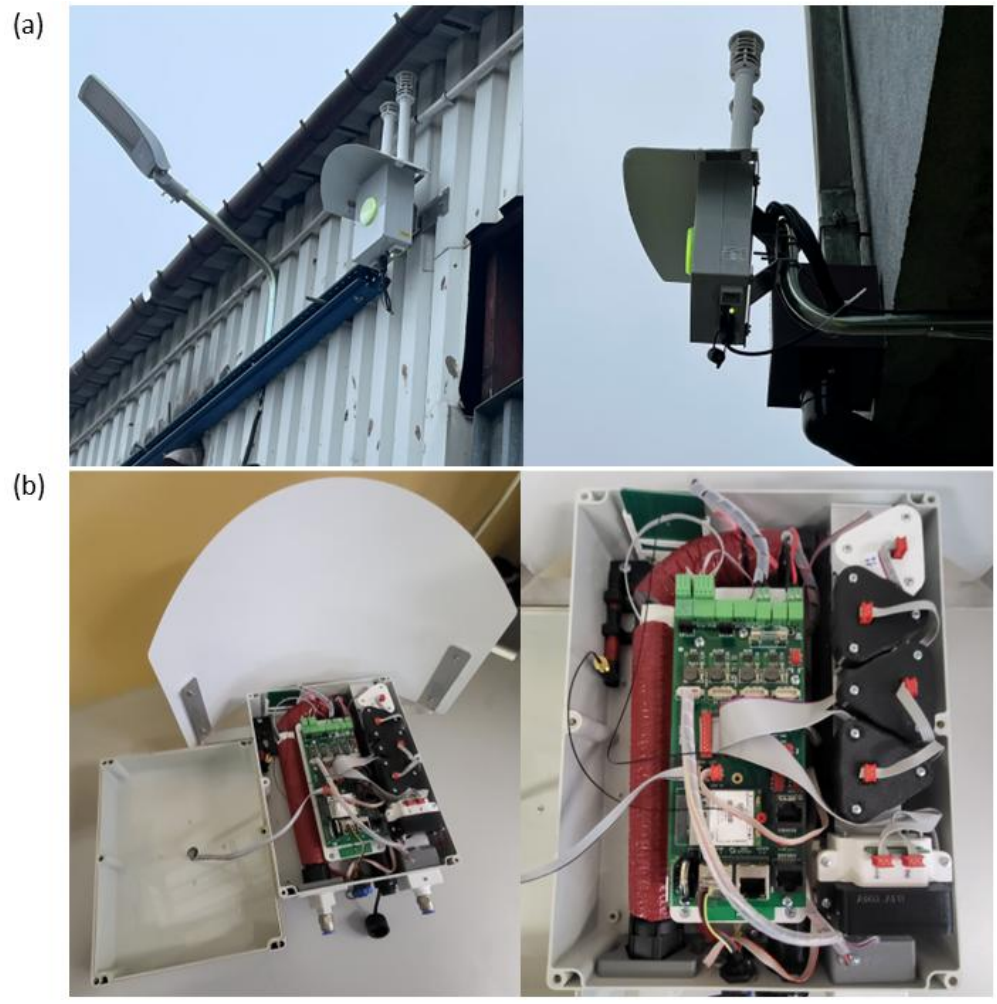


Figure 59. Design characteristics and location of the sensor BOX-3 XXXX: (a) view of the device installed at the compost screening site at the WTP, (b) interior of the device with the visible set of gas sensors.

Technical concept of the device, including the design of internal circuits, data acquisition system, wireless transmission, and archiving, was developed in cooperation with an external technology company, Dacsystem LLC. This enabled the creation of a fully automated device capable of operating continuously directly at the point of odor emission. One of the main elements of the system was a precise 16-bit A-D converter, the ADS1115 (Texas Instruments, Dallas, TX, USA), which digitized sensor signals and recorded them on the control unit.

The structure of the measuring device is presented in Figure 59. Part (a) shows the final product in operational conditions, while part (b) shows its internal architecture. The central element of the device was an array of gas sensors. These sensors are operated by a complete electronic system that includes dedicated control boards and connection systems, ensuring stable sensor operation. In accordance with the adopted design concept, the electronic layer of the entire control system and data recording protocols have been optimized for the acquisition and safe transmission of measurement data to the central unit for further statistical processing.

10.2.4 Measurement procedure

The measurement campaign was divided into stages conducted in different seasons (autumn, winter, spring), which allowed for accounting for the impact of changing weather conditions on sensor stability and odorant dispersion. A station for the olfactometry panelist team was designated in the immediate vicinity of the device (sensor BOX-3 XXXX). Field measurements using the Nasal Ranger olfactometer were conducted regularly at the gas sensor array installation site, enabling direct correlation of instrumental signals with the actual odor concentration (ou/m³) present at the compost screening site. A total of 60 olfactometric measurement series were performed, which were carried out in three main measurement campaigns, taking into account variable atmospheric conditions:

- Campaign I (September 2021): Fall campaign – 20 measurement series.
- Campaign II (December 2021): Winter campaign – 20 measurement series.
- Campaign III (March 2022): Spring campaign – 20 measurement series.

Each of the above stages was carried out over two measurement days, during which 10 olfactometric measurement series were taken daily directly at the sensor array location. Measurements from the first two stages (40 series in total) served as a training dataset for device calibration and predictive modeling. The third stage (20 series) was used for their validation. Additionally, a week-long continuous monitoring period was conducted in April 2022 to verify the system's effectiveness. After implementing the mathematical models into the device, plant employees performed daily olfactometric measurements in the surrounding area. The process of collecting reference data at the MTP is shown in Figure 60. The panelist visible in the photo determined the odor concentration in real time, working in parallel with a continuously operating gas sensor array. Traditional field olfactometry, despite its precision, provides only a limited number of measurements and is difficult for residents to interpret directly. For this reason, the aim of this work was to train a sensor array to predict odor concentration and, on the scale of the proposed index, convert these concentrations into the other odor parameters. This approach

would enable a comprehensive, complementary analysis of the air around the plant for odors using a single device. Additionally, the measurement could be continuous and made available online for residents unfamiliar with the concept of odor nuisance, providing them with uncomplicated information, for example, in graphical form.



Figure 60. Reference measurements in the field conditions: the panelist team during the determination of odor concentration using Nasal Ranger field olfactometers in the immediate vicinity of the device.

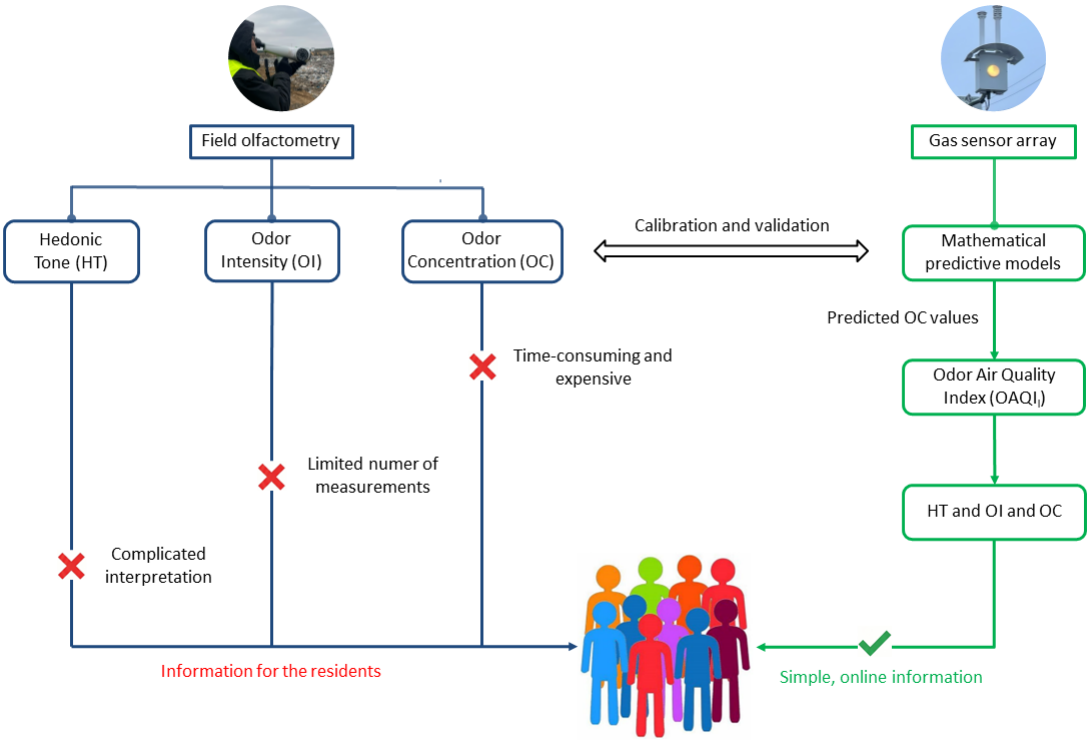


Figure 61. The $OAQI_I$ operational model: integrating chemical signals with human perception to objectify odor nuisance assessment. Adapted from [276], licensed by CC BY 4.0.

Figure 61 shows the main idea of the study and the concept of the Instrumental Odor Air Quality Index ($OAQI_I$). The scale of the proposed $OAQI_I$ is based on the dependence of HT and OI on odor concentration. To assign specific odor-concentration values to the corresponding values of the other two parameters, parametric measurements (numerical scales) were conducted. OI and HT measurements were performed during the same measurement campaigns as the olfactometric ones. The panelist team consisted of four people, allowing the creation of a dataset of 240 measurements that directly linked odor concentration values to OI and Ht values. According to Weber-Fechner's law (Eq. 5), the relationship between the logarithm of odor concentration and the OI and HT should be linear. On this basis, mathematical relations were derived to describe the dependencies among these parameters.

The Odor Air Quality Index developed on the basis of the above considerations is a four-point scale that allows for an objective assessment of odor nuisance. The proposed $OAQI_I$ scale ranges are presented in Table 24. The main goal of introducing the $OAQI_I$ is to address the complex interpretation of sensory data and provide the public with a comprehensive, online overview of current odor air quality. Individual classes of odor nuisance, according to the proposed index, were visualized in infographics, which are also presented in the table below.

Table 24. The four-level $OAQI_I$ scale: a classification of odor nuisance based on OI, HT and odor concentration ranges.

$OAQI_I$ scale	**OI**	**HT**	**OC [ou/m^3]**	**Infographic**
0 - very good	Non-perceptible and very weak	Extremely pleasant Very pleasant Moderately pleasant Slightly pleasant Natural Slightly unpleasant	$0 < C_{OD} \leq 3$	
1 - moderate	Weak	Moderately unpleasant	$3 < C_{OD} \leq 10$	
2 - bad	Distinct and strong	Very unpleasant	$10 < C_{OD} \leq 60$	
3 - very bad	Very strong and Extremely strong	Extremely unpleasant	$C_{OD} \geq 60$	

VDI 3882 qualitative scale for assessment of odor intensity (OI)		Hedonic tone (quality) scale (HT)	
0	Non-perceptible	4	Extremely pleasant
1	Very weak	3	Very pleasant
2	Weak	2	Moderately pleasant
3	Distinct	1	Slightly pleasant
4	Strong	0	Natural
5	Very strong	-1	Slightly unpleasant
6	Extremely strong	-2	Moderately unpleasant
		-3	Very unpleasant
		-4	Extremely unpleasant

10.2.5 Data analysis and mathematical modeling

Since the sensor array was to be trained for the quantification of odor nuisance, a lot of attention was paid to the process of data analysis, selection of the optimal mathematical model,

and statistical analysis of the accuracy of its predicted values with olfactometric measurements, as well as the accordance and correspondence of actual and predicted readings of HT and OI with respect to the scale of the proposed index. Two methods of extracting sensor signals from the matrix were used. The first was to use the maximum value of the signal from a given sensor (S_{max}) as an independent variable, while the second was to reflect the mechanism of human olfactory perception and was based on a logarithmic ratio of the maximum value of the signal to the baseline of the individual sensor (S_{dB}). The baseline (S_0) of each sensor used was determined using synthetic air.

The adoption of a logarithmic method for describing sensor signals was an attempt to model the response of living organisms to stimuli. The relationship between stimulus intensity and the evoked sensation is not linear (Weber–Fechner law). Therefore, a logarithmic scale is appropriate for analyzing psychophysical phenomena and signals spanning a wide range of values. The decibel (dB), a unit equal to one-tenth of a bel, was used as a measure. It allows the ratio of two values to be expressed as a logarithmic relationship, facilitating the comparison of signals with significantly different levels. The signal value obtained from each sensor in the array was then converted to the decibel scale using the following equation:

$$S_{dB} = 10log_{10}\left(\frac{S_{max}}{S_0}\right) \tag{65}$$

Moreover, the calibration process tested five different mathematical models designed to predict the odor concentration. From the standard MLR and PCR models used for this purpose, through three models based on the modified Steven's power law, in which as the exponent of the power following was used: the signal from the individual sensor (in the form depending on the method of its obtaining from the matrix, eq. 68), the geometric mean of all signals from the sensors installed in the gas sensor array (eq. 69), and the first principal component of the data set determined with the use of Principal Component Analysis – PCA (eq. 70):

- Model 1: Multiple Linear Regression (MLR)

$$C_{OD} = a_0 + \sum_{i=1}^{n}(a_i \cdot S_i) \tag{66}$$

where: a_0 is the intercept, a_i regression coefficients, S_i sensor signal (depending on the signal feature extraction method), n number of explanatory variables.

- Model 2: Principal Component Regression (PCR)

$$C_{OD} = a_0 + \sum_{i=1}^{n}(a_i \cdot PC_i) \tag{67}$$

where: a_0 is the intercept, a_i regression coefficients, PC_i principal components, n number of principal component.

- Model 3: Steven's power law with the signal from a single sensor used as the exponent

$$C_{od} = ab^S \tag{68}$$

where: a is the first model coefficient, b second model coefficient, S sensor signal, (depending on the signal feature extraction method).

- Model 4: Steven's power law with the geometric mean of the sensor signals used as the exponent

$$C_{od} = ab^{\sqrt[n]{\prod_{i=1}^{n} S_{dB,i}}} \tag{69}$$

where: a is the first model coefficient, b second model coefficient, $S_{dB,i}$ sensor signal value in dB scale, n number of sensors in the array.

- Model 5: Steven's power law integrated with Principal Component Analysis (PCA)

$$C_{od} = ab^{PC_1} \tag{70}$$

where: a is the first model coefficient, b second model coefficient, PC_1 first principal component.

The optimal model for each signal extraction method was selected based on two parameters. The first was the RMSE, a measure of the match between the models' predicted values and the actual measurements, and the second was the so-called accordance. It was defined as the ratio of the number of measurements classified by the model and olfactometric measurements to the same index scale, and the total number of measurements performed:

$$Accordance = \frac{n_{correct}}{N} \tag{71}$$

where: N is the total number of observations included in the analysis, $n_{correct}$ number of observations classified into the same index class.

10.3 Results and discussion

10.3.1 Development of predictive models of odor concentration

Based on the results obtained during the calibration campaign, mathematical models were developed to predict odor concentration using the response of a gas sensor array. A training set of 40 measurements was used for calibration, and the two sensor response representations considered, S_{max} and S_{dB}, were analyzed independently. For models using S_{max}, the relationships between the odor concentration determined olfactometrically and the predicted values are presented in Figure 62. In this case, four variants were analyzed: Models 1, 2, 3, and 5. Model 4 was not considered in this group because in the adopted construction it was defined only for S_{dB} signals, using their geometric mean as the exponent in the relationship based on Stevens' law. Therefore, the absence of Model 4 in the S_{max} group resulted from the adopted form of this model, and not from its rejection based on the quality of fit.

The highest coefficients of determination were obtained for Model 1 and Model 2, R^2 = 0.993 and R^2 = 0.990, respectively. In both cases, the measurement points were located close to the line corresponding to perfect agreement y = x, indicating good representation of changes in odor concentration within the calibration range. At the same time, no clear, unidirectional shift of the entire series of results relative to the reference line was observed. Significantly larger differences occurred in Model 3 and Model 5, for which R^2 was 0.922 and 0.932, respectively. While in the low and medium concentration range the predicted values remained relatively close to the reference results, at higher concentrations the scatter of points

increased. This was particularly evident for Model 5, where some of the values corresponding to the highest concentration level were clearly above the y = x line. This means that a high coefficient of determination does not necessarily mean the same accuracy of the model across the entire measurement range, and errors may be concentrated primarily in its upper part.

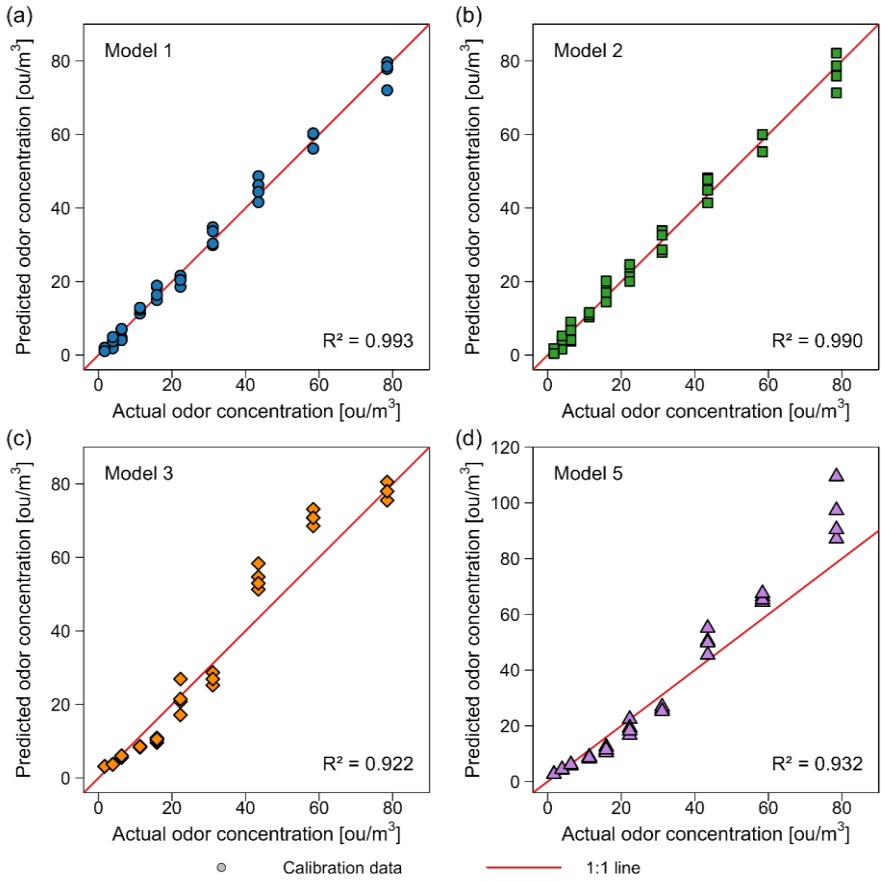


Figure 62. Calibration relationships between odor concentrations determined by field olfactometry and values predicted by the gas sensor array using models based on S_{max} signal features: (a) Model 1, (b) Model 2, (c) Model 3, and (d) Model 5. Adapted from [276], licensed by CC BY 4.0.

For signals presented in the form S_{dB}, it was possible to compare five models (Figure 63). In this group, all relationships were characterized by high coefficients of determination, ranging from 0.938 to 0.989. The highest values were obtained for Model 4 (R^2 = 0.989) and Model 5 (R^2 = 0.988). Very good fit was also observed for Model 1 and Model 2, for which R^2 was 0.976 and 0.974, respectively. The lowest value was again obtained for Model 3 (R^2 = 0.938). However, it is not only the comparison of R^2 values that is important. In the graphs for S_{dB}, Models 4 and 5 demonstrate very good agreement with the reference line across a significant portion of the analyzed range, while for Model 3, at the highest concentrations, a clear overestimation of some results is visible. In Model 5 the opposite tendency appears at the upper end of the range, i.e., an underestimation of the concentration. This indicates that models with similar global values of R^2 may differ in the direction and magnitude of the error in individual concentration ranges.

To further illustrate these differences, an additional residual analysis was performed, the results of which are presented in Figure 64. The residual was defined as the difference between the model-predicted concentration and the reference concentration. Positive values indicate an

overestimation, while negative values indicate an underestimation of the odor concentration. The graph presents the mean residual for each concentration level along with the standard deviation, allowing for a simultaneous assessment of the direction of error and its variability.

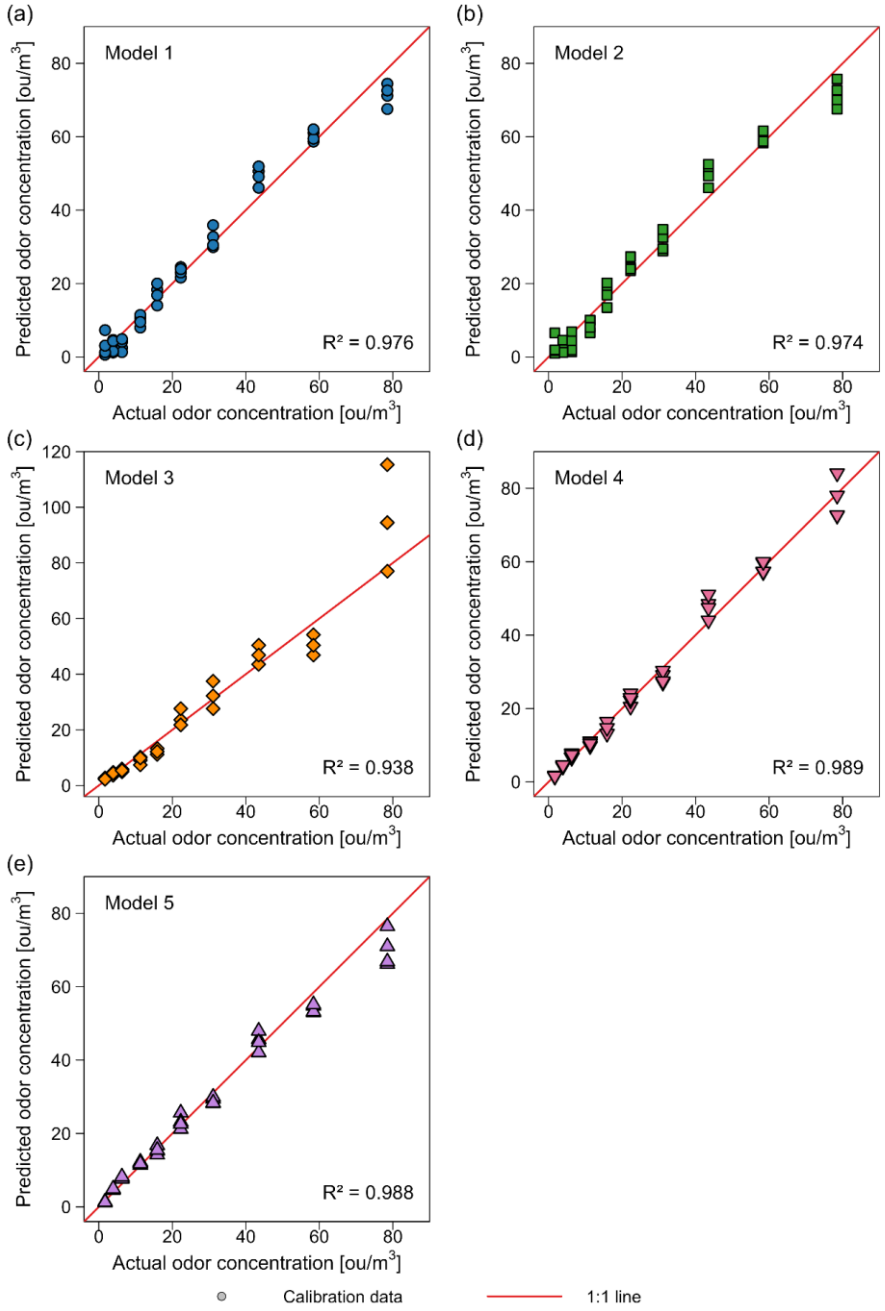


Figure 63. Calibration relationships between odor concentrations determined by field olfactometry and values predicted by the gas sensor array using models based on S_{dB} signal features: (a) Model 1, (b) Model 2, (c) Model 3, and (d) Model 4, (e) Model 5. Adapted from [276], licensed by CC BY 4.0.

The analysis of the residuals confirmed that the greatest differences between the models were revealed primarily in the upper concentration range. For S_{max}, the mean values of the residuals of Model 1 and Model 2 remained relatively close to zero in most of the range, while for Model 5 at the highest concentration a clear shift towards positive values was observed, indicating a tendency to overestimate. In the case of S_{dB}, a particularly large positive residual occurred for Model 3 at the highest concentration level, while Model 5 tended to underestimate in the same

range. Model 4, on the other hand, maintained relatively small mean deviations from zero over much of the calibration range. At the same time, the standard deviation bars indicate that for some models the error variability increased with increasing concentration.

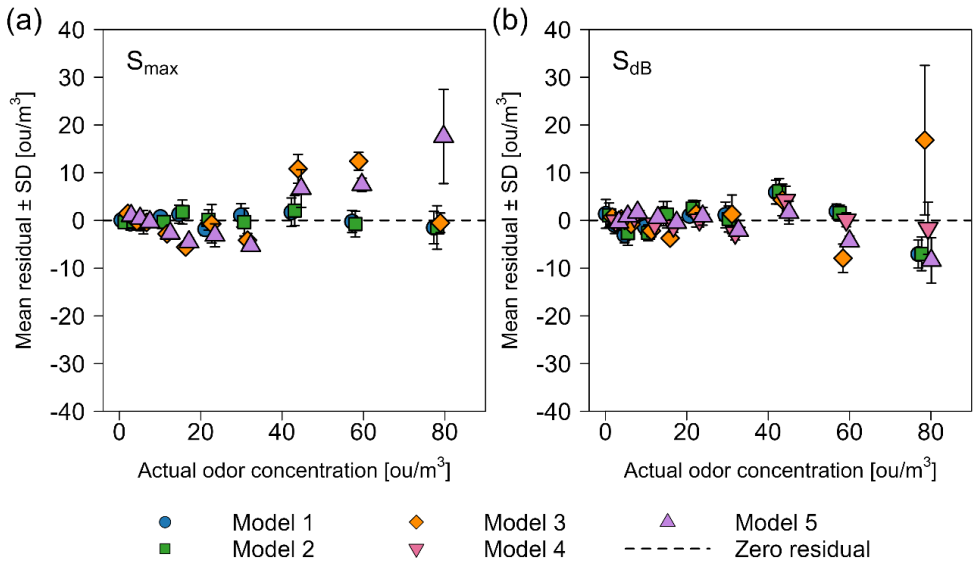


Figure 64. Mean prediction residuals with standard deviations for odor concentration models based on S_{max} (a) and S_{dB}(b). Points represent mean residuals at individual odor concentration levels, and error bars indicate ±SD. The dashed horizontal line denotes zero residual.

The obtained results indicate that all analyzed approaches were able to reproduce changes in odor concentration in the calibration set, but the quality of this reproduction was not uniform across the entire measurement range. Supplementing the R^2 assessment with residual analysis proved particularly important, as it revealed local tendencies towards overestimation or underestimation that are not directly visible based on a single parameter describing the global model fit. During the calibration stage favorable results were obtained for Models 1 and 2 using S_{max} and Models 4 and 5 using S_{dB}. This does not constitute a basis for the final model selection, as assessing its predictive ability requires the use of data independent of the calibration set. Therefore, the next step was to validate the models on a separate measurement set.

10.3.2 Evaluation and validation of odor concentration prediction models

After developing predictive models based on the training data set, they were evaluated using an independent validation data set. This set included 20 observations representing different odor concentration levels. Using data not previously used in model parameter estimation allowed for an assessment of their ability to predict new odor concentration values, thereby limiting the impact of the quality of the training set fit on the final model evaluation. The models were assessed in parallel from two perspectives. The first concerned the accuracy of quantitative odor concentration determination, while the second concerned the consistency of the classification results with the $OAQI_I$ classes. This approach is particularly important from the perspective of the target application of the gas sensor array. The model can generate a relatively small error in the numerical value, and at the same time, crossing the boundary between adjacent classes can lead to the assignment of a different odor air quality category.

The basic parameter for assessing quantitative error was the RMSE. However, the analysis was extended to include two additional indices calculated for the validation data: the mean absolute error (MAE) and the mean systematic error (Bias). MAE measures the average error size, regardless of its direction, while Bias identifies the systematic tendency of the model to overestimate or underestimate results. A positive Bias value indicates a predominance of overestimation, while a negative value indicates a predominance of underestimation. The second evaluation criterion was the *Accordance* parameter, expressing the percentage of observations for which the predicted and reference concentrations were assigned to the same $OAQI_I$ class. Graphical evaluation was performed by comparing the reference and predicted odor concentrations. In addition to the 1:1 agreement lines, the graphs also marked the boundaries of the $OAQI_I$ classes and their corresponding areas. Red points represent cases in which the predicted value fell into a different $OAQI_I$ class than the corresponding reference value. This allows for the simultaneous assessment of both the magnitude of the quantitative error and its significance for odor air quality classification.

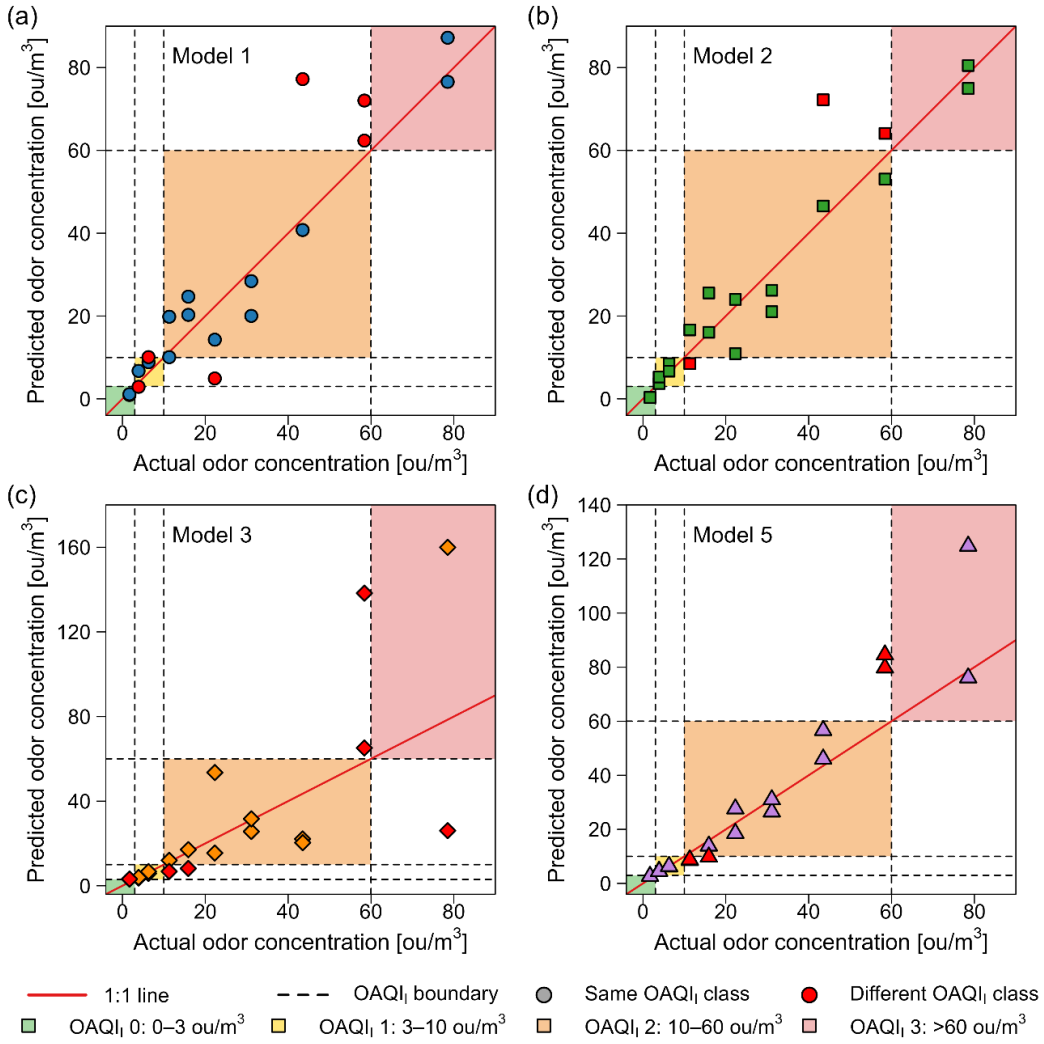


Figure 65. Validation of odor concentration prediction models based on S_{max} signal features: (a) Model 1, (b) Model 2, (c) Model 3, and (d) Model 5. Colored areas correspond to the $OAQI_I$ class ranges, dashed lines indicate the boundaries between classes, and the solid line represents the 1:1 relationship. Red symbols indicate cases in which the predicted odor concentration was assigned to a different $OAQI_I$ class than the reference value. Adapted from [276], licensed by CC BY 4.0.

First, the models using the maximum values of signals from individual sensors, S_{max} feature, were analyzed. A comparison of the reference and predicted values is presented in Figure 65. The results indicate clear differences in the way odor concentrations were represented by the individual model variants. Model 1 maintained the general relationship between the increase in the reference and predicted values, but in several cases the predicted value exceeded the boundary of its corresponding $OAQI_I$ class. 14 of 20 observations were correctly classified (*Accordance* of 0.70). Better properties were obtained for Model 2. Most of the points remained in the areas corresponding to the correct index class, and the classification agreement was 0.85 (17 correct cases out of 20). MAE of 5.059 ou/m^3 and the Bias of 0.972 ou/m^3 indicate that the average deviation of the prediction from the reference values was relatively small, and the tendency to systematically overestimate the results was limited.

The greatest dispersion of results occurred in the case of Model 3. Especially for higher concentrations, significant deviations of points from the 1:1 line were observed. This is reflected in both the high RMSE value and the MAE of 16.369 ou/m^3. This model was also characterized by the lowest classification agreement in the S_{max} group. Only 13 out of 20 observations were assigned to the correct class, which corresponds to an *Accordance* of 0.65. This result indicates that good representation of part of the measurement range was not sufficient to ensure stable prediction across the entire analyzed range. Model 5 showed less dispersion than Model 3, but still contained errors leading to a change in the $OAQI_I$ class. 15 of 20 observations were correctly classified, yielding an *Accordance* of 0.75. Despite the low reported RMSE, additional analysis indicated MAE of 7.123 ou/m^3 and bias of 4.668 ou/m^3. This indicates that, compared to Model 2, there was a stronger tendency to overestimate the predicted concentration.

The obtained results show that in the group of S_{max} models, an assessment based solely on a single error indicator does not allow for a full determination of the model's suitability for determining the $OAQI_I$. From the point of view of classification application, it is more advantageous to simultaneously take into account the error size, its direction, and the number of cases in which the error causes the boundary between classes to be crossed.

A similar analysis was performed for models using the logarithmic representation of signals S_{dB}. The results are presented in Figure 66. For Model 1, an *Accordance* of 0.75 was obtained, corresponding to 15 correct classifications. The MAE was 3.922 ou/m^3, while a positive Bias of 2.175 ou/m^3 indicated a moderate tendency to overpredict concentrations. Model 2 improved both classification agreement and quantitative accuracy. *Accordance* was 0.85, corresponding to 17 correct classifications, with an MAE of 3.881 ou/m^3 and Bias of 1.212 ou/m^3. These results indicate a reduction in bias relative to Model 1. Model 3 again revealed problems with correctly representing part of the concentration range. The graph shows cases where incorrect predictions resulted in exceeding the class boundaries $OAQI_I$. The model achieved the *Accordance* of 0.70, corresponding to 14 correct classifications. The MAE of 5.004 ou/m^3 was the highest among the analyzed S_{dB} models. At the same time, the Bias of -0.254 ou/m^3 remained close to zero. This means that the lack of a significant systematic error did not equate to a small error in individual predictions (positive and negative biases partially compensated each other).

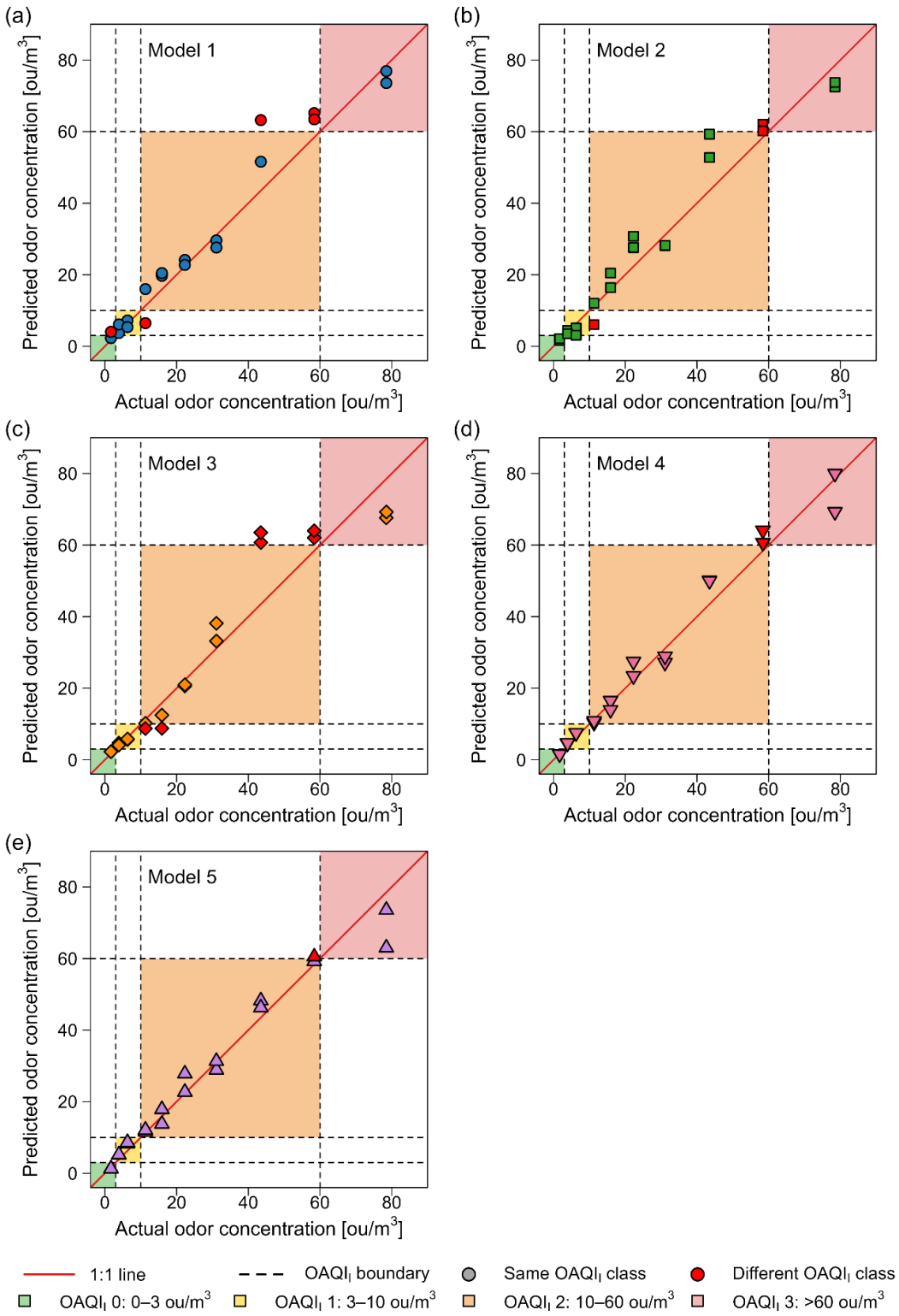


Figure 66. Validation of odor concentration prediction models based on S_{dB} signal features: (a) Model 1, (b) Model 2, (c) Model 3, and (d) Model 4, (e) Model 5. Colored areas correspond to the $OAQI_I$ class ranges, dashed lines indicate the boundaries between classes, and the solid line represents the 1:1 relationship. Red symbols indicate cases in which the predicted odor concentration was assigned to a different $OAQI_I$ class than the reference value. Adapted from [276], licensed by CC BY 4.0.

The lowest reported RMSE value in the S_{dB} group, equal to 3.667 ou/m^3, was obtained for Model 4. This model was also characterized by a low MAE of 2.614 ou/m^3 and a small positive Bias of 0.730 ou/m^3. It correctly classified 18 out of 20 observations, which corresponds to the

Accordance of 0.90. The results therefore indicate a very good ability to quantitatively represent odor concentration. A slightly different result profile was obtained for Model 5. Its RMSE was 4.220 ou/m^3, which was slightly higher than for Model 4, while MAE reached the lowest value in the entire S_{dB} group, equal to 2.596 ou/m^3. Bias was only −0.152 ou/m^3, which indicates a practical lack of a clear tendency to systematically over- or underestimate the results. Out of 20 observations, only one was assigned to the incorrect $OAQI_I$ class, which gives the *Accordance* of 0.95. A summary of all validation parameters is presented in Table 25.

Table 25. Validation performance of odor concentration prediction models developed using S_{max} and S_{dB} signal features. Adapted from [276], licensed by CC BY 4.0.

Signal feature	Model	RMSE [ou/m^3]	MAE [ou/m^3]	Bias [ou/m^3]	$OAQI_I$ Accordance
S_{max}	Model 1	10.302	6.914	2.177	0.70
	Model 2	8.092	5.059	0.972	0.85
	Model 3	67.973	16.369	4.145	0.65
	Model 5	7.399	7.123	4.668	0.75
S_{dB}	Model 1	5.754	3.922	2.175	0.75
	Model 2	5.420	3.881	1.212	0.85
	Model 3	7.120	5.004	-0.254	0.70
	Model 4	3.667	2.614	0.730	0.90
	Model 5	4.220	2.596	-0.152	0.95

The combined analysis of the results indicates the advantage of the models using the S_{dB} feature in terms of quantitative accuracy. The MAE values for the best models in this group were significantly lower than for the models based on S_{max}. Model 4 and Model 5 achieved the highest *Accordance* values among all analyzed variants. Of particular importance is the low absolute Bias value for Model 5, indicating an even distribution of deviations on both sides of the reference values. Comparison of RMSE, MAE, and Bias also shows that these parameters provide complementary information. RMSE more strongly accounts for single large deviations, MAE describes the average error size, and Bias allows for assessing its direction. Consequently, a model with a small Bias does not necessarily have to have a small prediction error, as exemplified by Model 3 for S_{dB}. In turn, the very small difference between the quantitative results of Model 4 and Model 5 becomes more significant only after accounting for classification agreement. The validation performed indicates that, in the case of models intended for instrumental determination of the odor air quality index, the use of a single statistical criterion is insufficient. In addition to the accuracy of the concentration representation, it is important whether the resulting error changes the interpretation of the result by assigning it to a different $OAQI_I$ class.

Based on the analysis, Model 2 was selected for further testing among the models using the S_{max} feature. Compared to the other S_{max} models, it provided the most balanced combination of quantitative accuracy, small systematic error, and the ability to maintain the correct $OAQI_I$ class. In the group of models using S_{dB} feature, the choice required considering the difference between Model 4 and Model 5. Model 4 achieved the lowest RMSE value, but Model 5 was characterized by a slightly lower MAE, a significantly lower absolute Bias value, and the highest classification agreement. From the point of view of the target application, in which the quantitative result is to

be the basis for assigning air quality to a specific class, this advantage justified the selection of Model 5. Ultimately, Model 2, using S_{max}, and Model 5, using S_{dB}, were qualified for the next stage of the study. In the next stage, these models were evaluated under continuous monitoring conditions, with particular emphasis on their ability to reproduce changes in odor concentration and their consistency with the results of reference olfactometric measurements.

10.3.3 Application of selected models for continuous odor monitoring

After selecting Model 2 using the S_{max} feature and Model 5 using the S_{dB} feature, the models were used to continuously determine odor concentration during field monitoring. The analyzed set included 179 consecutive hourly values recorded from April 12, 2022, to April 19, 2022. Time courses, along with the results of seven field olfactometry measurements, are presented in Figure 67. To facilitate the interpretation of the results, the ranges of individual $OAQI_I$ classes are also marked on the graph. Both models reproduced the variability of odor concentration over time, but the nature of the obtained curves was clearly different. Model 2, based on S_{max}, generated values ranging from 16.2 to 63.5 ou/m^3 and was characterized by a relatively smaller amplitude of changes. For most of the period, the predicted values remained within the range corresponding to class $OAQI_I = 2$. Of the 179 hourly values, 177 were assigned to this class, while only two exceeded the limit of 60 ou/m^3 and fell into class $OAQI_I = 3$. This indicates relatively small variability in the air quality classification obtained using this model.

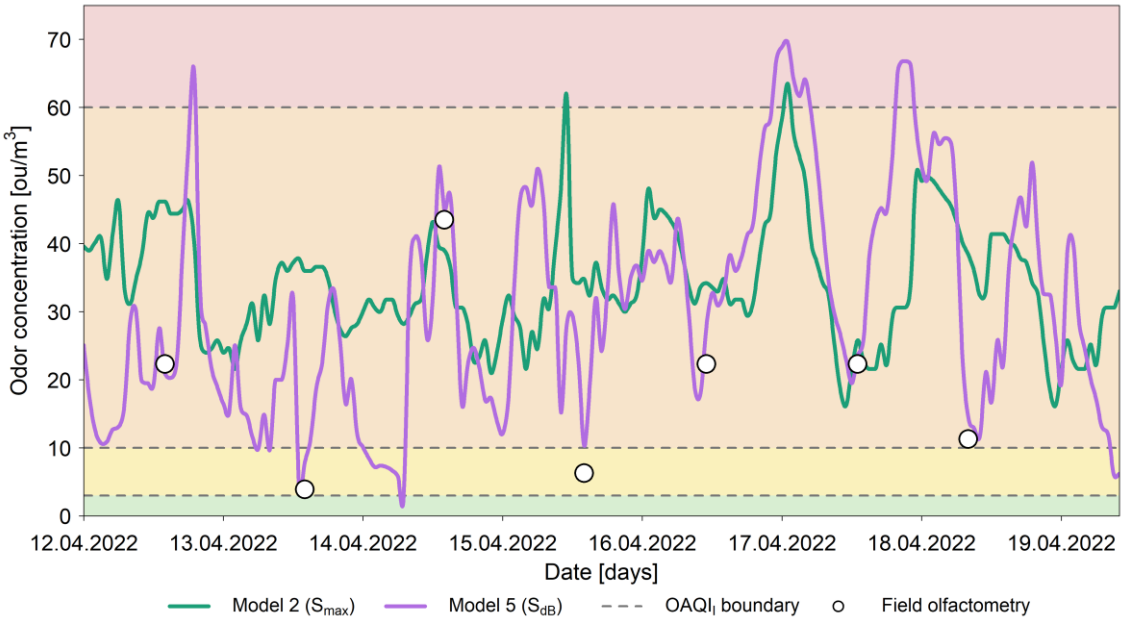


Figure 67. Temporal variation in odor concentration predicted by Model 2 based on S_{max} and Model 5 based on S_{dB} during field monitoring. Reference values obtained by field olfactometry are shown as individual points. Colored background areas represent the $OAQI_I$ class ranges, while dashed horizontal lines indicate the boundaries between classes. Adapted from [276], licensed by CC BY 4.0.

A significantly greater dynamics of change was observed for Model 5 using S_{dB}. Predicted concentrations fell within a wider range from 3.1 to 69.5 ou/m^3. This model recorded both periods of significant concentration decreases and short-term increases exceeding 60 ou/m^3. Consequently, the predicted values included three index classes: $OAQI_I = 1$, $OAQI_I = 2$, and

$OAQI_I$ = 3. Class 1 was assigned 13 hourly values, class 2 - 156, and class 3 - 10 values. Compared to Model 2, the course obtained for Model 5 indicates a greater ability to represent short-term changes in odor concentration levels. A particularly marked increase in concentration occurred during the period of April 16-17. For Model 5, the values reached a maximum of 69.5 ou/m^3 during this time, while Model 2 reached a maximum of 63.5 ou/m^3. In both cases, the maximum occurred on April 17 around 1:00 a.m., which indicates that both models recorded the same episode of elevated concentration. However, the differences concerned its course and the duration of the high level. The model based on S_{dB} showed a greater amplitude of changes and more frequent exceedances of the $OAQI_I$ = 3 class limit, while the course of Model 2 remained more stable.

The different behavior of the models was particularly evident during periods of low concentrations. The minimum value obtained for Model 5 was 3.1 ou/m^3, while the lowest value for Model 2 was 16.2 ou/m^3. This means that Model 2 did not indicate a concentration corresponding to the $OAQI_I$ = 1 class throughout the monitoring period. This may indicate a lower ability of this model to represent concentration decreases in the lower measurement range. In turn, the greater variability of Model 5 allowed for the identification of both low-odor episodes and short-term increases to the highest analyzed index class. The figure also shows points corresponding to the results of measurements taken using field olfactometry. Their position relative to the two curves suggests differences in the degree of agreement between the models and the reference values. However, visual assessment is not sufficient to clearly determine the quality of the reference method's representation, especially with a small number of olfactometry measurements. Therefore, in the next step, a quantitative comparison of the values obtained using both models with the corresponding field olfactometry results was conducted.

The comparison was carried out for seven measurement dates for which the odor concentration values determined by the olfactometric method and the corresponding values predicted by Model 2 using the S_{max} feature and Model 5 using the S_{dB} feature were simultaneously available. The RMSE, MAE, Bias, and Lin's coefficient of concordance (CCC) were used for the assessment. The Bias value was calculated as the difference between the odor concentration predicted by the model and the value obtained by the olfactometric method. Therefore, a positive value of this parameter indicates a tendency for the model to overestimate the odor concentration. The CCC coefficient was used to assess the degree of concordance between the results of both methods. Unlike the classical correlation coefficient, it considers not only the strength of the relationship between values but also their concordance with the identity line (y = x). A CCC value close to 1 indicates high agreement between the sensor method and field olfactometry, 0 indicates no agreement, and negative values indicate strong disagreement. The results obtained for these parameters are presented in Table 26.

In the case of Model 2, relatively high values of both error measures were obtained: RMSE was 26.586 ou/m^3, while MAE was 18.786 ou/m^3. The positive Bias value of 17.500 ou/m^3 indicates a clear tendency to overestimate the odor concentration compared to the field olfactometry results. The very low CCC coefficient value of 0.041 also indicates poor agreement

between the values predicted by Model 2 and the results of the reference method. Significantly better results were obtained for Model 5. The RMSE value in this case was 3.041 ou/m^3, and the MAE was 2.971 ou/m^3, which indicates smaller deviations of the predictions from the reference values. The bias of 2.571 ou/m^3 indicates a slight tendency to overestimate the odor concentration, but the scale of this shift was smaller than in the case of Model 2. The CCC value of 0.966 indicates a very high agreement of the Model 5 results with the olfactometric measurements.

Table 26. Quantitative comparison of odor concentrations predicted by the selected sensor-based models with field olfactometry.

Model	RMSE [ou/m^3]	MAE [ou/m^3]	Bias [ou/m^3]	CCC [-]
Model 2 (S_{max})	26.586	18.786	17.500	0.041
Model 5 (S_{dB})	3.041	2.971	2.571	0.966

The comparison of all the used indicators leads to a consistent conclusion that in the analyzed field conditions Model 5 reproduced the results of the reference method much better than Model 2. The advantage of Model 5 concerned both the magnitude of prediction errors and the reduction of systematic error as well as the agreement between the predicted and reference values. However, classical error measures and the CCC coefficient primarily provide aggregate information about the quality of the prediction. Therefore, the assessment was supplemented with a Bland-Altman analysis (Figure 68), which allowed to determine the average offset between the gas sensor array method and field olfactometry, as well as the range of variability of the differences between the corresponding results. The difference was defined as the value predicted by the model minus the value obtained by the olfactometry method.

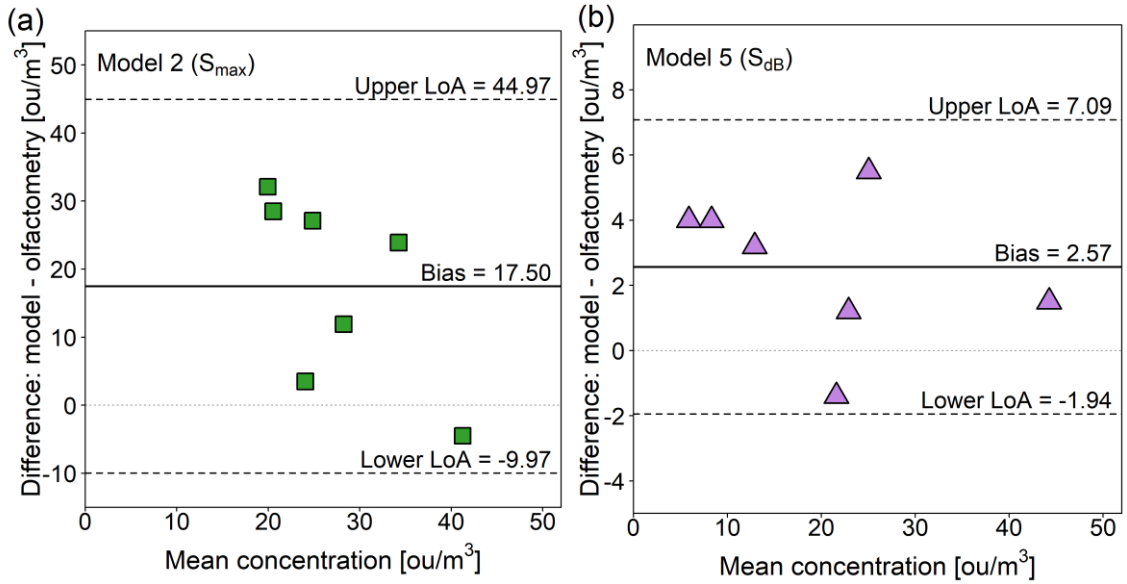


Figure 68. Bland-Altman analysis of agreement between odor concentrations predicted by the mathematical models and field olfactometry: (a) Model 2 based on S_{max} and (b) Model 5 based on S_{dB}. The solid line represents the mean difference (Bias), dashed lines indicate the 95% limits of agreement (Bias$\pm$1.96 SD), and the dotted line denotes zero difference.

Bland–Altman analysis revealed clear differences in the nature of the two models' agreement with field olfactometry. For Model 2 the lower limit of agreement was

−9.97 ou/m^3, while the upper limit was 44.97 ou/m^3. The positive Bias value thus confirms the previously observed tendency of Model 2 to overestimate odor concentration. The large distance between the lower and upper limits of agreement indicates significant variability in the differences between the model and field olfactometry results. For Model 5 the limits of agreement ranged from −1.94 to 7.09 ou/m^3. This indicates both a much smaller systematic shift relative to the reference method and significantly less variability in the differences between methods. Compared to Model 2, the results of Model 5 remained much closer to the values obtained with the olfactometric method. It is worth emphasizing that the mere occurrence of all observations within the limits of agreement is not a sufficient criterion for assessing the quality of method agreement. The width of these limits and the magnitude of the bias are also important. In this respect, Model 5 demonstrated significantly better characteristics, as both the bias and the range of the limits of agreement were significantly smaller than for Model 2.

The results of the Bland-Altman analysis are therefore consistent with those obtained from RMSE, MAE, Bias, and CCC. Both evaluation methods indicate that Model 5 performed significantly better in terms of the field reference olfactometry, while Model 2 was characterized by a significant positive bias and significantly greater error variability. However, when interpreting the results of this part of the analysis, it is important to consider the limited number of available reference measurements. The comparison was performed for seven pairs of observations, so the determined Bias values and Bland-Altman limits of agreement should be considered primarily as characteristics of the field experiment under study. Overall, the results of the quantitative comparison of the gas sensor array results with field olfactometry indicate a clear advantage of Model 5 based on S_{dB}. This model was characterized by lower error values, a small positive bias, high agreement as determined by the CCC coefficient, and significantly narrower limits of agreement in the Bland-Altman analysis. This indicates that under the conditions of the conducted monitoring, the way the sensor array response was represented had a significant impact on the model's ability to maintain agreement with the reference method.

10.4 Summary and conclusions

The conducted research demonstrated the feasibility of using a properly calibrated gas sensor array for instrumental determination of odor concentration and continuous monitoring of changes in odor air quality. The procedure involved developing calibration models, validating them on an independent set of test data, and then using selected models in real-world field monitoring conditions. The results of the individual stages indicated that the prediction effectiveness depended not only on the model design but also on the way the gas sensor array response was represented. This was particularly evident during field monitoring, for which an RMSE of 26.5 ou/m^3 was obtained for Model 2 based on S_{max} and 3.0 ou/m^3 for Model 5 using S_{dB}. Additional analysis conducted as part of this thesis, including MAE, Bias, CCC, and B-A analysis, confirmed significantly better agreement of Model 5 with the field olfactometry results.

The obtained results are consistent with the current direction of development of instrumental odor monitoring systems. Ratti et al.[225] demonstrated that appropriate signal

processing, including compensation for humidity effects, significantly improves the performance of IOMS. After applying compensation, the two electronic noses analyzed correctly classified samples into their respective odor classes with an accuracy of 97% and 100%, respectively, on an independent test set. The authors also demonstrated the ability to quantitatively estimate odor concentration and compare it with dynamic olfactometry results.

Similar results were presented by Lotesoriere et al. [224], who used an electronic nose to continuously monitor odors at the edge of a landfill. In field tests, the system correctly detected the presence of landfill odors in 94% of cases, and the correct assignment of detected odors to the appropriate class was achieved in 93% of cases. For the tested odor classes, the lower limit of effective detection and classification was approximately 50-60 ou_E/m^3. The authors also demonstrated that the accuracy of quantitative odor concentration prediction can be improved by using a two-step approach, in which, after identifying the odor type, a regression model developed specifically for a given class is used. The obtained values were compared with the results of dynamic olfactometry as a reference method. More recent studies by Szyłak-Szydłowski et al. [277], conducted directly during composting, confirmed the consistency of changes recorded by different methods. For several PEN3 sensor arrays, the obtained values of the absolute correlation coefficient with the logarithm of VOC concentration exceeded 0.7, while the correlations between VOC and odor concentration in subsequent measurement series ranged from $R^2 = 0.981$ to $R^2 = 0.993$.

Compared to these studies, the approach used in this dissertation was distinguished not only by predicting odor concentration values. The results of the gas sensor array were linked to the developed $OAQI_I$ scale, which uses the relationships between odor concentration, intensity, and hedonic tone to classify odor air quality. This allowed to expand functionality of the gas sensor array from a tool solely for quantitative prediction of odor concentration to a system enabling the instrumental assessment of odor air quality classes. In the cited literature, the primary tasks of the sensor systems were primarily identifying the source or class of odor and estimating its concentration.

The second important element of the conducted research was the comparison of two methods of representing the gas sensor array response - S_{max} and S_{dB} - at subsequent stages including calibration, independent validation and field monitoring. This demonstrated that a positive model evaluation at the validation stage does not necessarily guarantee equally good prediction quality during long-term operation in real-world conditions. In the analyzed case, the S_{dB} signal feature provided significantly greater model robustness in field conditions. An additional value was the analysis of agreement with the reference method carried out in this thesis using MAE, Bias, CCC and the Bland-Altman method, which allowed for the assessment not only of the error magnitude but also of its direction and variability.

Based on the obtained results, the first part of third hypothesis, concerning the possibility of using an appropriately calibrated gas sensor array for continuous instrumental assessment of odorous air quality, can be considered confirmed. The developed and validated models enabled the determination of odor concentration based on multidimensional signals from the sensor array,

and linking the predicted values to the developed $OAQI_I$ scale, which takes into account odor intensity and hedonic tone, allowed for the classification of air odor quality. The field monitoring results also confirmed the possibility of continuous tracking of changes in odor concentration under actual operating conditions. This demonstrated the usefulness of a single sensor system as a complementary tool to olfactometric measurements. The second part of third hypothesis, concerning the integration of multiple devices into a network enabling spatial and temporal assessment of odor nuisance, is presented in chapter 11.

10.5 Publication basis of the chapter

This chapter is based in part on research previously published in:

Dobrzyniewski D., Szulczyński B., Gębicki J. (2022). Determination of Odor Air Quality Index ($OAQI_I$) Using Gas Sensor Matrix. *Molecules,* 27(13), 40180. doi: 10.3390/molecules27134180.

The article is distributed under the Creative Commons Attribution 4.0 International License (CC BY 4.0). The material has been revised, adapted, and expanded for the purpose of this doctoral dissertation. The findings are discussed in the context of the thesis's main research objective.

11. Development of Instrumental Odor Monitoring System Network (IOMSN) for continuous assessment of odor air quality at a MSWTP

11.1 Purpose of the study

The main aim of this work was to comprehensively assess the effectiveness, stability, and measurement uncertainty of the Instrumental Odor Monitoring System Network (IOMSN) under the operational conditions of the MSWTP. This research was a key extension and industrial application of the methodologies developed in earlier stages of the thesis. The system consisted of seven identical gas sensor arrays deployed in various process areas of the plant. A key methodological element was a multi-season calibration strategy conducted using field olfactometry as a reference technique, followed by independent validation of the models under operating conditions. This made it possible to assess the stability of the devices' performance under varying temperatures, humidity, local chemical background, and long-term changes in sensor response characteristics.

11.2 Materials and methods

11.2.1 Test site description

Detailed technical characteristics and basic operational statistics of the MSWTP (Waste Utilization Facility Ltd. in Gdańsk), including its area and annual waste-processing efficiency, were presented earlier in the thesis (chapter 9.2.1). In this stage of the research, focusing on long-term stationary monitoring, the facility was treated as a complex system of strategic emission points with diversified and time-varying odor profiles. In order to ensure full control over the main sources of odors, a network of seven identical gas sensor arrays was installed at the plant, located in the following operational zones:

- Landfill cells sector – monitoring covered the area of the reclaimed landfill cell (sensor BOX-3 4095) and the vicinity of the currently used landfill cell (sensor BOX-3 2715).
- Biological processing complex – monitoring devices were located at the key points for aerobic processes: at the biofilter of the tunnel composting plant (sensor BOX-3 3965), at the compost maturing area (sensor BOX-3 2176), and in the compost screening zone (sensor BOX-3 3968).
- Logistics and technical infrastructure – the sensor BOX-3 4088 monitored emissions along the main transport road, while the sensor BOX-3 4077 was installed in the area of the waste thermal treatment installation.

The IOMSN network configuration, defined in this way, allowed simultaneous tracking of odor air quality from various technological units, enabling verification of the system's effectiveness under extreme variability in the chemical background and the plant's specific meteorological conditions. The detailed arrangement of the seven measurement units of the IOMSN is shown in Figure 69. This figure also present a satellite view of the MSWTP with the installations with the highest emission potential marked: (1) – truck scale, (2) – selective municipal waste collection

point, (3) – compost maturation area, (4) – waste sorting facility, (5) – material storage bays, (6) – tunnel composting plant, (7) – enclosed composting plant, (8) – bulky waste, (9) – old reclaimed landfill cell, (10) – new reclaimed landfill cell, (11) – active landfill cell, (12) – leachate pre-treatment installation, (13) – biogas plant, (14) – compost screening area, (15) – biofilter.

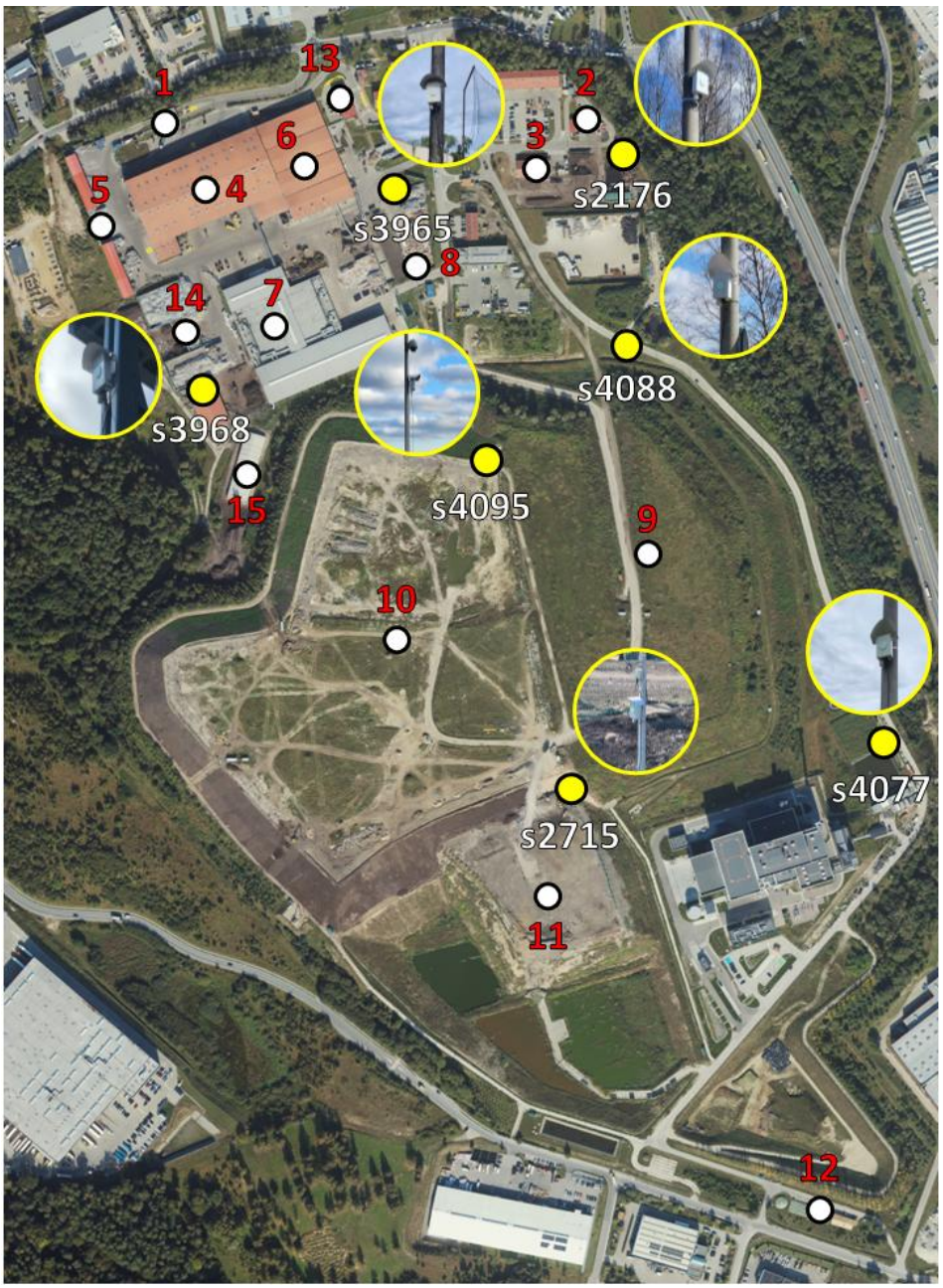


Figure 69. Arrangement of elements of the IOMSN: strategic location of measuring devices (sensor BOX-3 XXXX) in the operational zones of the MSWTP, against the background of the main emission sources, including landfill cells, composting areas and logistic infrastructure.

11.2.2 Characteristics and structure of IOMSN

The research used a network of seven identical measuring devices (sensor BOX-3 XXXX), that design and selection of gas sensors are fully consistent with the configuration developed and characterized in the earlier part of the thesis (chapter 10.2.3, Table 23). Each of the seven IOMSN network units was equipped with a set of sensors (MOS and electrochemical)

dedicated to the detection of odor markers typical for waste management, such as hydrogen sulphide, ammonia and volatile organic compounds.

The crucial element of this stage was scaling a single prototype solution into a distributed monitoring network. The use of identical gas sensor arrays in each of the seven devices was intended to ensure full comparability of data collected in different operational zones of the plant. The IOMSN system was fully integrated with an advanced IoT cloud infrastructure and a dedicated software application, developed in collaboration with Dacsystem LLC in Gdańsk. This solution enabled real-time data processing and visualization in the form of an interactive Decision Support System (DSS). Thanks to DACSYSTEM's technological support, the IOMSN system not only enabled real-time tracking of odorant concentrations but also immediate identification of dynamic odor peaks and optimization of deodorization processes throughout the facility.

11.2.3 IOMSN calibration using field olfactometry

The calibration and validation process for the seven devices included in the IOMSN was based on results obtained using field olfactometry, which was the reference technique in this study. Nasal Ranger field olfactometers (St. Croix Sensory, Inc., USA) were used to determine odor concentration under operational conditions, allowing for direct determination of the D/T ratio. Measurements were performed by a team of panelists meeting the requirements for detection threshold and response repeatability specified in the PN-EN 13725:2022 standard. A detailed calculation procedure for transforming olfactometric readings (D/T) into odor concentration values was presented earlier in this thesis (chapter 4.2.1). Calibration campaigns were planned to take into account the facility's seasonal and technological variability as much as possible. The process was implemented in three main stages in 2024–2025:

- Calibration stage I (three days) – June and July 2024.
- Calibration stage II (three days) – March and April 2025.
- Calibration stage III (three days) – August and September 2025.



Figure 70. Selected odor monitoring devices (sensor BOX-3 XXXX) during a field calibration campaign: photos document how devices were installed in operational conditions.

The studies were conducted at all seven strategic locations within the IOMSN, allowing for the collection of calibration data across a broad spectrum of chemical backgrounds (landfill

sites, composting complex, and transport routes). The observed odor concentration ranged from 0 to approximately 80 ou/m^3. A key element of the procedure was the synchronization of each reading from the Nasal Ranger olfactometer with the recording of electrical signals from the arrays installed in each sensor BOX-3 XXXX. This formed the foundation for the IOMSN predictive algorithms. Photographic documentation showing selected devices installed in target locations on the MSWTP premises during the calibration campaigns is presented in Figure 70.

11.2.4 Statistical and exploratory data analysis

To provide an initial overview of the dataset, an exploratory data analysis (EDA) was conducted. The purpose of this analysis was to assess the distribution of the variables, identify relationships between sensor signals, and detect potential outliers. The correlation matrix between sensor signals was calculated using Pearson's correlation coefficient. The relationships between the variables were visualized as a correlation map, which allowed assessment of the strength and direction of linear relationships. In addition, pairwise plots were used, which allow for the simultaneous display of variable distributions, scatter plots for each pair of variables, and correlation coefficients. This approach enables a comprehensive assessment of the data structure and the identification of potential nonlinear relationships. The distributions of signal values for individual sensors were also presented using box plots, which allow for an assessment of the median, the spread of the data, and the presence of outliers. All analyses and visualizations were performed in the *R statistical environment* (version 4.5.2) using RStudio (RStudio Team, Boston, MA, USA) and the *ggplot2, GGally,* and *corrplot* packages.

In the next stage of the analysis, Principal Component Analysis (PCA) was used to reduce data dimensionality and identify the principal directions of variation. The PCA method transforms the original variables into a new set of orthogonal components that maximize the explained variance of the data. Prior to analysis, the data were centered and rescaled to ensure that all variables had a comparable impact on the analysis results. PCA was performed using the *princomp* function available in the *R environment.* To assess the number of significant components, a scree plot was used to show the proportion of variance explained by successive principal components. The structure of the data in the reduced-dimensional space was analyzed using score plots, which illustrate the distribution of observations in the first two components. The loadings, which indicate the contribution of individual variables to the construction of the principal components, were also analyzed.

11.2.5 Hybrid predictive mathematical model of odor concentration

The implementation of IOMSN required the use of standardized and stable predictive algorithm for all seven measurements units. Instead of conducting another comparative analysis of various statistical techniques (mathematical models), this study implemented the predictive model that had been identified as the most optimal during earlier stages of development (chapter 10). For this reason, in order to convert multidimensional signals from sensor arrays into odor

concentration values, a unified mathematical model described by the following equation has been implemented in IOMSN devices:

$$C_{od} = ab^{PC_1} \tag{72}$$

Where: a is the first model coefficient, b second model coefficient, PC_1 first principal component. The selection of this model is based directly on the results of extensive modeling studies presented in chapter 10 of this dissertation. After testing five different mathematical models, it was this hybrid solution that demonstrated the highest statistical accuracy in predicting odor concentrations compared to reference techniques. The model used integrates three key analytical and psychophysical aspects:

- Stevens' power law - the structure of the equation mimics natural models of stimulus perception, in which the signal from the sensor array replaces an empirical constant in the power exponent.
- Principal Component Analysis (PCA) - the first principal component (PC1) was used as the input variable, which aggregates information from the entire sensor array, eliminating information noise and resolving the problem of signal interdependence.
- Decibel (dB) scale - the use of logarithmic signals allows for the linearization of sensor responses and reflects the nonlinear response of the human sense of smell to stimulus intensity (in accordance with Weber–Fechner's law).

11.2.6 Predictive model validation under operational conditions

The final stage of the methodological work was the validation of the developed models under the MSWTP actual operating conditions, which was conducted over a long time horizon - from August 2024 to March 2026. The purpose of this process was to independently assess the predictive capability of the IOMSN outside of the controlled phases of the calibration campaigns. The validation procedure consisted of the following steps:

- Reference measurements - MSWTP staff conducted regular odor concentration measurements using field olfactometers in the immediate vicinity of the seven measurement units (sensor BOX-3 XXXX).
- Data synchronization - from the continuous time series generated by the IOMSN system, model-predicted values were extracted that corresponded exactly to the times when the olfactometric measurements were taken.
- Data set independence - only data that had not been used in the algorithm training (calibration) process were used for validation, which allowed for an objective determination of the system's measurement uncertainty.

The effectiveness of the models was evaluated using two main statistical indicators. The root mean square error (RMSE), which was used to quantitatively assess the differences between measured and predicted values, and the *Accordance* index, developed in earlier studies. This parameter specifies the percentage of measurements that were classified by the model into the same odor nuisance class as the olfactometric measurement. This classification was based on

four concentration thresholds defined in the $OAQI_I$ index, which was also developed in an earlier phase of the research. The validation process designed in this way made it possible to confirm the system's operational stability over a full seasonal cycle and to demonstrate its resistance to sensor drift and the MSWTP variable chemical background.

11.3 Results and discussion

11.3.1 Exploratory data analysis and sensor signal correlation

The implementation of research tasks related to the calibration of the IOMSN in variable environmental conditions required an in-depth assessment of the structure of multidimensional signals generated by gas sensor arrays. For the preliminary exploratory data analysis (EDA), a combined measurement data set from all three seasonal calibration campaigns was used, including recordings from seven measurement devices (s2176, s2715, s3965, s3968, s4077, s4088, s4095) located in the key emission zones of the MSWTP. To reflect the non-linear perception of the human sense of smell and to ensure linearization of the sensory response, the measurement signals were transformed to the decibel scale (S_{dB} – Eq. 65). Distributions of signal values for individual sensors in all locations are presented in the form of box plots (Figure 71).

Analysis of box plots reveals significant differences in the dynamics of sensor responses depending on the location of devices within the MSWTP. The TGS series of MOS sensors demonstrated a wide and consistent response range to a mixture of VOCs. Among this group, the TGS2612 sensor had the highest median and widest signal spread at points located in the waste disposal area. Especially for the s2715 device at the new landfill cell (where the signal median exceeded 20) and the s4095 at the reclaimed landfill cell (median around 12). Comparison of the EC sensors showed a clear dominance of the NH3-B1 sensor in terms of signal variability. While the H2S-A4 sensor was characterized by a concentrated distribution around low background values, the NH3-B1 sensor exhibited a very wide interquartile range. Particularly high ammonia fluctuations were recorded in the compost screening zone (s3968, range 0 to 12) and near the reclaimed landfill cell (s4095).

The graphs also show numerous outlier values, including those for the TGS2612 sensor in the compost maturation area (s2176) and the NH3-B1 sensor in the old landfill cell (s4095). In the context of odor nuisance monitoring, these incidents may provide evidence of the IOMSN's ability to continuously record short-term episodes of high emissions (odor peaks), which, due to their fleeting nature, are impossible to capture during routine periodic measurements. Detailed information on the chemical-spatial structure and signal interdependencies is provided by the analysis of the Pearson correlation matrix with density distributions (Figure 72). In all analyzed measurement points, strong, positive linear correlations were observed between TGS sensors ($r > 0.70$, $p < 0.001$), which confirms the consistency of their response to the incoming odor plume. However, the analysis revealed key differences in the IOMSN behavior in individual operational zones. In the case of the device located in the old landfill cell (s4095), the most orderly, strictly linear relationship was observed. The correlation coefficient between the H2S-A4 sensor and the TGS2612 reached $r = 0.964$ ($p < 0.001$), while the correlation between the

TGS2603 and NH3-B1 was r = 0.958. This indicates a constant, repeatable chemical profile of the landfill gas in this part of the MSWTP.

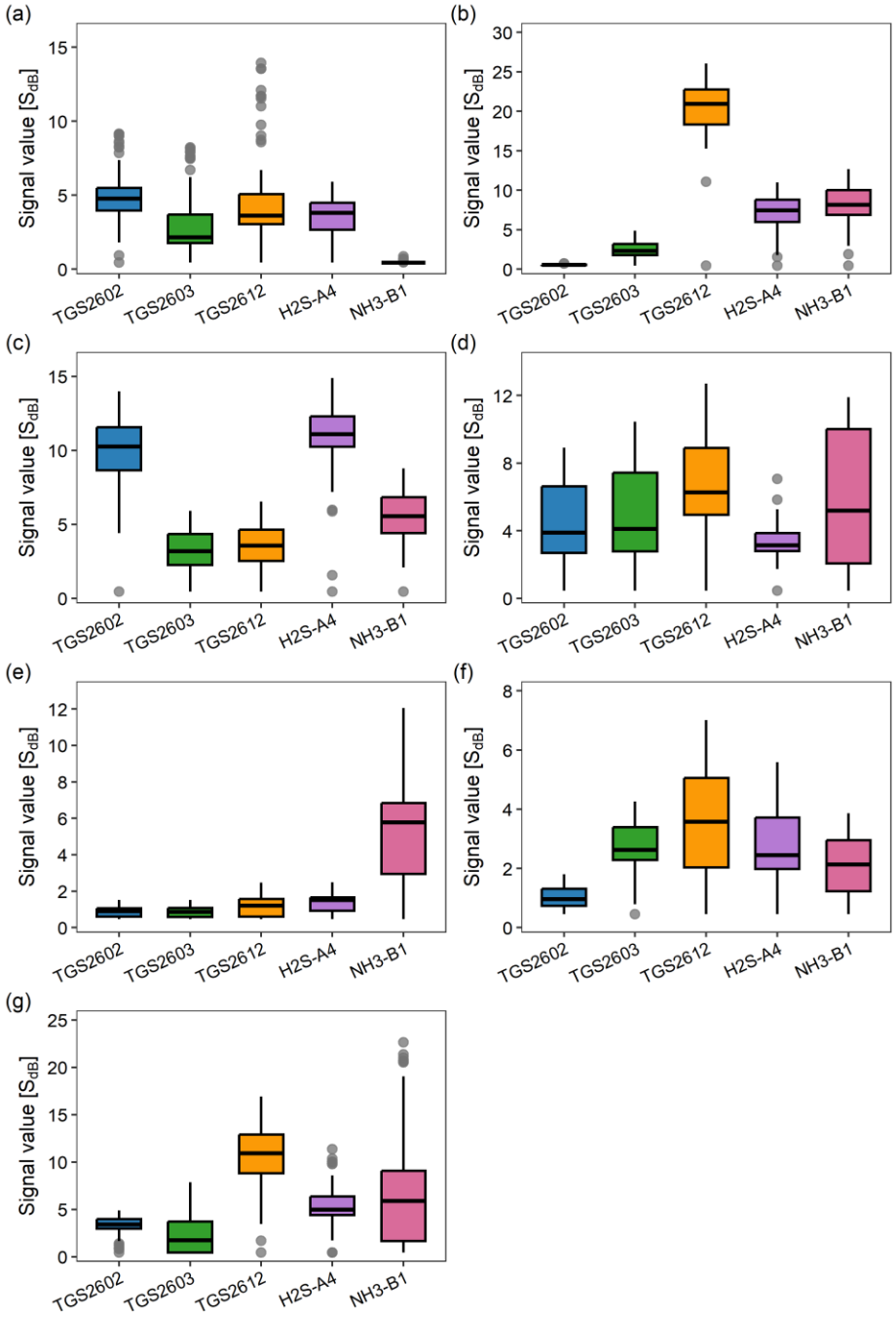


Figure 71. Distribution of S_{dB} signal values recorded by individual gas sensors in seven sensorboxes: (a) s2176, (b) s2715, (c) s3965, (d) s3968, (e) s4077, (f) s4088, and (g) s4095. Boxes represent the interquartile range, the horizontal line denotes the median, whiskers indicate the data range excluding outliers, and individual points represent outlying observations.

In the vicinity of the waste thermal treatment installation, the diagonal density plots and scatterplots for the s4077 device clearly revealed a bimodal distribution (a division of the data into two distinct clusters of points). This phenomenon demonstrates the presence of two dominant, distinct aerodynamic and emission states in this zone, related to wind direction and the variable activity of neighboring industrial facilities.

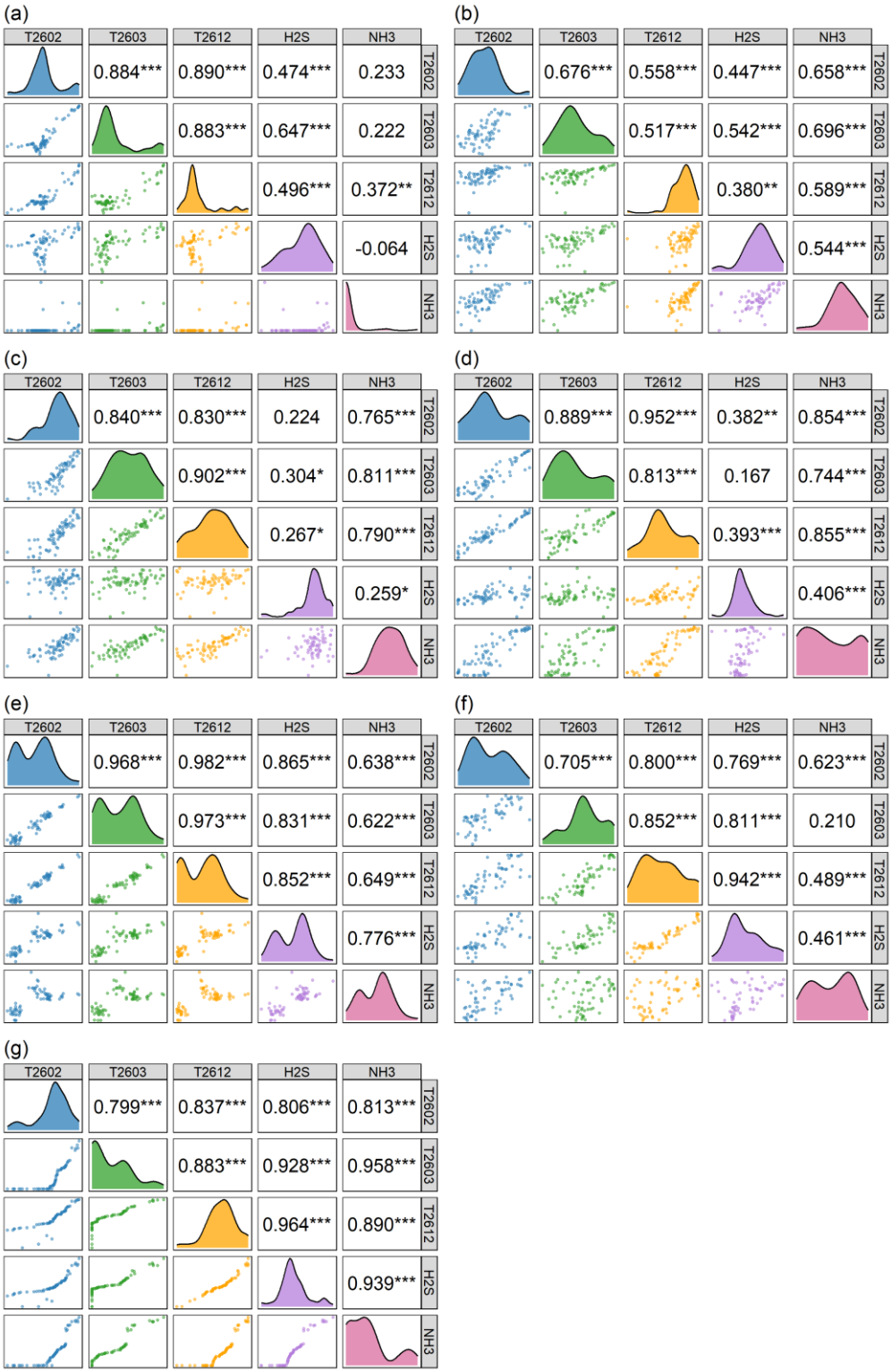


Figure 72. Scatterplot matrices and Pearson correlation coefficients between the signals of five gas sensors in seven sensorboxes: (a) s2176, (b) s2715, (c) s3965, (d) s3968, (e) s4077, (f) s4088, and (g) s4095.

The degree of correlation of the NH3-B1 sensor signal with other sensors is a sensitive indicator of the type of technological process. In the zones of intense aerobic processes, at the biofilter of the tunnel composting plant (s3965) and at the compost screening site (s3968), the NH3-B1 sensor showed a very high correlation with the TGS sensor group ($r = 0.744$ - 0.855, $p < 0.001$). A completely different relationship was observed in the compost maturation area

(s2176), where the correlation of ammonia with TGS sensors dropped drastically to low and statistically insignificant values (r = 0.222 - 0.233), and the correlation with H2S-A4 became negative (r = -0.064). The phenomenon of signal decorrelation in the compost maturing area (s2176) is of fundamental scientific importance. It demonstrates that ammonia release during the maturing phase occurs independently of VOCs or sulfur compound emissions. This signal separation allows the distributed IOMSN network to selectively distinguish the source's nature and prevents misinterpretation of a multicomponent plume as a single contaminant.

Initial data exploration confirmed the high sensitivity and repeatability of the sensor arrays. Very strong interdependencies between individual input variables revealed their collinearity. Directly introducing such strongly correlated signals into multivariate regression models would have led to their instability and overfitting. This observation provided a direct methodological rationale for implementing a dimensionality reduction technique in the form of PCA, enabling the aggregation of information into the PC1 prior to odor concentration prediction.

11.3.2 Calibration and parameterization of predictive models.

Due to the problem of collinearity of signals from individual sensors confirmed in the previous point, the process of calibration of predictive models was based on a dedicated, hybrid mathematical model described by the eq. 72. The first stage of parameterization was to assess the ability of the PC1 component to represent the total variance of the data set. These results, along with the estimated values of the structural parameters *a* and *b* for the individual stages of the calibration database expansion (Calibration I, I+II and I+II+III), are summarized in Table 27.

Table 27. Evolution of the structural parameters (a, b) of the hybrid model and the degree of representativeness of the PC1 in subsequent stages of the multi-season calibration of the IOMSN.

	Configuration of training dataset								
	CALIBRATION I			**CALIBRATION I + II**			**CALIBRATION I + II + III**		
	a	**b**	**PC1 variance**	**a**	**b**	**PC1 variance**	**a**	**b**	**PC1 variance**
	-	**-**	**%**	**-**	**-**	**%**	**-**	**-**	**%**
s2176	9.665	1.431	72.29	6.026	1.480	75.31	5.031	1.439	76.49
s2715	6.038	1.182	64.16	10.309	1.457	70.19	9.360	1.452	75.21
s3965	7.331	1.317	71.58	8.356	1.279	73.26	7.754	1.251	73.51
s3968	36.138	1.492	74.51	26.421	1.459	76.47	21.656	1.433	76.97
s4077	6.050	1.174	66.41	4.285	1.299	82.69	3.544	1.323	85.70
s4088	3.529	1.376	69.81	6.580	1.480	70.64	5.703	1.372	74.74
s4095	6.316	1.345	90.04	6.807	1.416	90.64	7.126	1.469	91.17

Analysis of the data contained in the table above allowed to draw key conclusions regarding the mathematical nature of predictive models. The value of the variance explained by the PC1 ranged from 64.16% (for s2715 in phase I) to as much as 91.17% (for s4095 in phase III). This high share confirms that reducing the five variables to the PC1 component preserves most of the measurement information, effectively eliminating information noise. The *b* parameter showed very low variability between different devices and calibration phases, assuming values in a narrow range of 1.17-1.49. It acted as a universal standardizing constant, defining the

sensitivity of the gas sensor array to the increase in chemical stimulus. In contrast to *b* parameter, coefficient *a* was characterized by a very wide range of variability: from 3.54 for s4077 (the vicinity of the waste thermal treatment installation) to 36.14 for s3968 (the compost screening zone). Parameter *a* therefore acted as a local scaling factor, adapting the model to the constant emission background in a given operational zone.

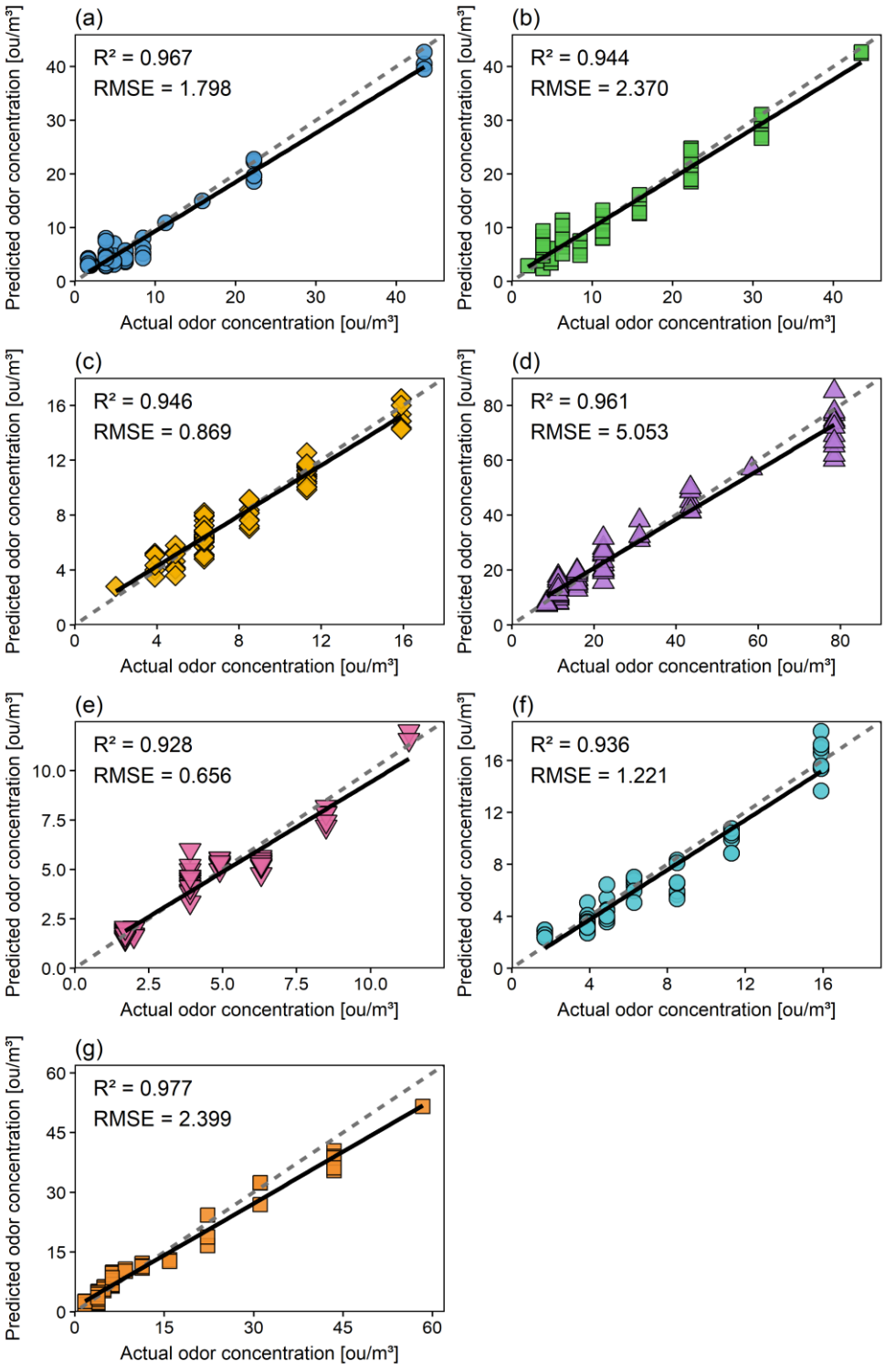


Figure 73. Calibration plots comparing actual and predicted odor concentrations for seven sensorboxes: (a) s2176, (b) s2715, (c) s3965, (d) s3968, (e) s4077, (f) s4088, and (g) s4095. Dashed lines indicate the 1:1 relationship and solid lines the linear regression.

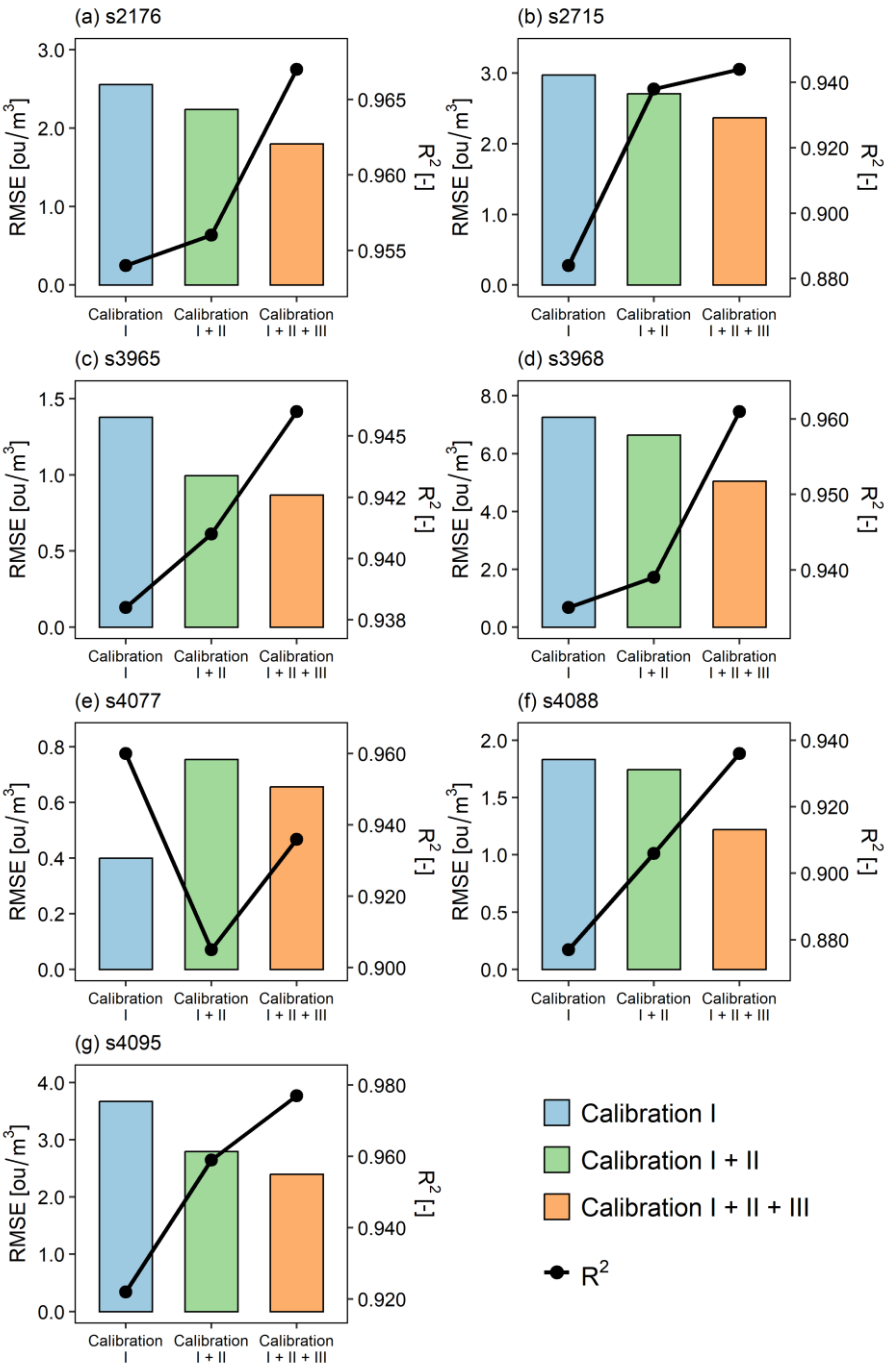


Figure 74. Evolution of model performance during successive calibration stages for seven measuring devices, assessed using RMSE and the coefficient of determination (R^2).

The assessment of the degree of agreement between the data from the gas sensor arrays, after accounting for the full cycle of three calibration campaigns, was verified by comparing the odor concentration values measured using field olfactometry with the values predicted by the model. These relationships for all seven measurement devices are shown in Figure 73. As can be seen from the analysis of this figure, the measurement points for all analyzed devices are tightly clustered around the line of best fit, y = x. The graphs clearly demonstrate that the model maintains a high degree of fit and linearity across the entire concentration range. From low odor

concentration values (0-3 ou/m^3 for s4077) to very high concentrations reaching 80 ou/m^3 at the compost screening site (s3968) and 60 ou/m^3 at the reclaimed landfill cell (s4095).

To quantitatively assess the impact of gradually expanding the database with subsequent seasonal calibration campaigns on prediction accuracy, changes in the R^2 and RMSE were analyzed. These values are summarized in Table 28, and their trends over time are illustrated in Figure 74. The presented data reveal a clear downward trend in the RMSE, accompanied by an increase in the R^2, as the calibration progresses from phase I to phase III. After completing the third calibration campaign, the R^2 values for all devices reached high levels ranging from 0.928 to 0.977. A particularly noticeable decrease in RMSE was observed in areas with the highest odor nuisance levels. For device s3968, the RMSE decreased from 7.262 ou/m^3 (after summer calibration) to 5.053 ou/m^3 after accounting for the full seasonal cycle. The aforementioned flattening and stabilization of the fit indices in phase III may indicate that the model has reached a state of information saturation. This means that incorporating temperature and humidity variations across the three seasons has made the algorithm completely immune to meteorological fluctuations, creating a stable foundation for long-term online operational validation.

Table 28. The effect of seasonal variations in training data on model fit statistics (R^2 and RMSE) for seven measurement devices.

	RMSE $[ou/m^3]$			**R^2** $[-]$		
	CALIBRATION I	**CALIBRATION I + II**	**CALIBRATION I + II + III**	**CALIBRATION I**	**CALIBRATION I + II**	**CALIBRATION I + II + III**
s2176	2.557	2.241	1.799	0.954	0.956	0.967
s2715	2.974	2.710	2.370	0.884	0.938	0.944
s3965	1.379	0.995	0.869	0.938	0.941	0.946
s3968	7.262	6.645	5.053	0.935	0.939	0.961
s4077	0.400	0.755	0.656	0.960	0.905	0.928
s4088	1.835	1.744	1.221	0.877	0.906	0.936
s4095	3.672	2.798	2.399	0.922	0.959	0.977

11.3.3 Long-term operational validation of the IOMSN under field conditions

The final and crucial stage in verifying the third research hypothesis was the long-term operational validation of the IOMSN, conducted under real-world operating conditions at the MSWTP from August 2024 to March 2026. Validation was based on an independent dataset obtained from routine olfactometric measurements performed by plant employees in the immediate vicinity of the seven measuring devices. These measurements were not used during the model training phase, which ensured the objective assessment of the network's predictive capabilities. Validation process was divided into three successive phases, corresponding to the implementation of successive versions of the predictive models (Calibration I, II, and III):

- Phase I (August 2024 - April 2025) - model trained exclusively on data from the summer calibration campaign.
- Phase II (April 2025 - October 2025) - model incorporating data from both the summer and spring seasons.
- Phase III (October 2025 - March 2026) – model covering a full seasonal cycle (summer, spring, fall).

The distribution of odor concentration predicted values over time, compared to point reference measurements from field olfactometry, was first analyzed for the s3968 device, located at the compost screening area (the zone with the highest level of odor nuisance). These relationships are shown in Figure 75a. As illustrated in this figure, the solid line representing the model's continuous prediction records several dynamic emission events (odor peaks), ranging from 40 to 60 ou/m^3, which due to the discrete nature of the reference measurements (red dots), were completely overlooked by traditional monitoring procedure.

To accurately assess the model's classification accuracy for device s3968, Figure 75b compares measured and predicted odor concentrations, broken down into the four odor nuisance ranges defined by the OAQI$_I$. The degree of agreement was assessed using the *Accordance* parameter, which indicates the percentage of measurement points classified by the model into the same odor air quality category as the olfactometric measurement.

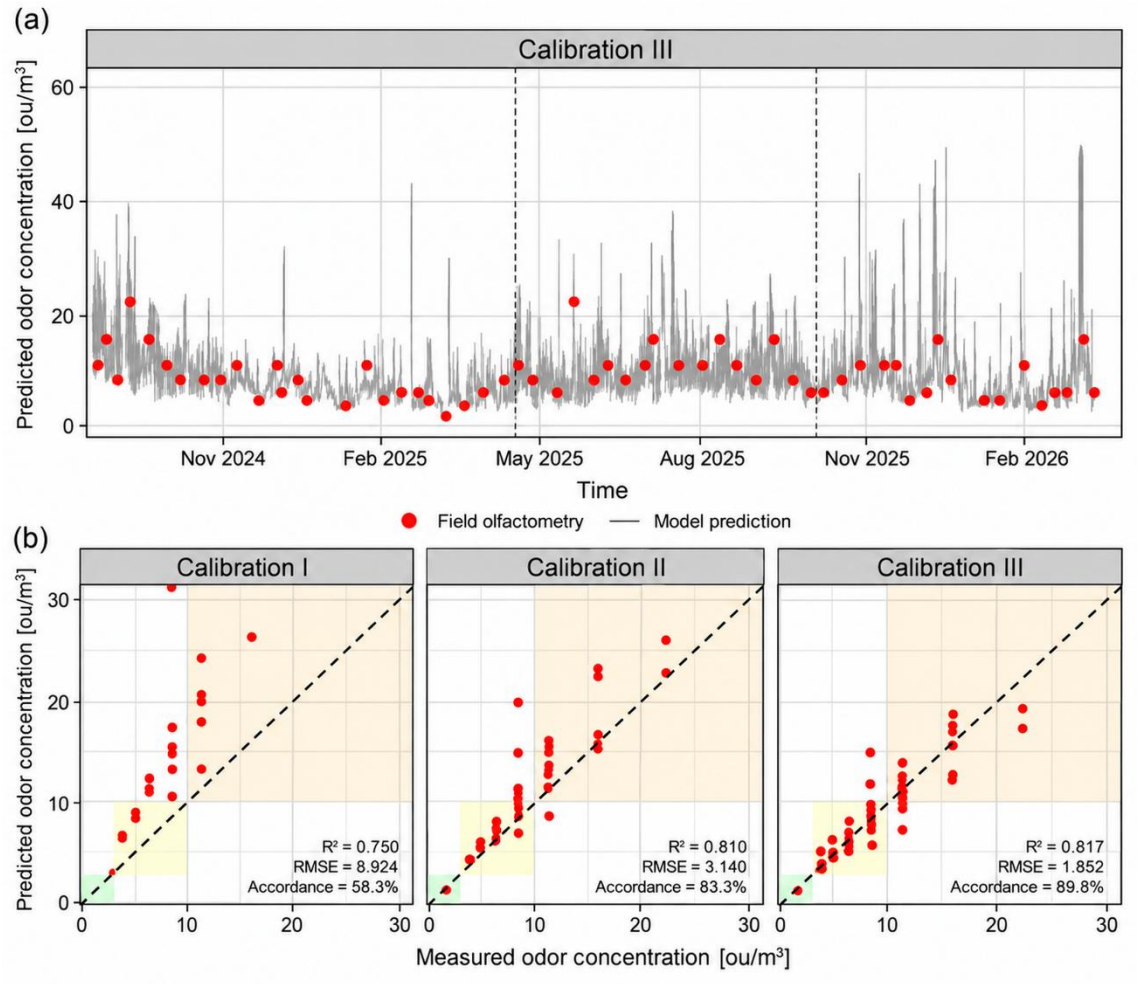


Figure 75. SENSORBOX s3968 model performance and validation: (a) Timeline of predicted odor concentrations for Calibration III and corresponding field olfactometric measurements (validation campaigns). The solid line represents model predictions, red dots indicate field measurements, and vertical dashed lines mark changes in model calibration. (b) Comparison of measured and predicted odor concentrations for successive model validations (Calibrations I–III). The dashed $y = x$ line indicates perfect agreement between measured and predicted values. Background shading represents odor concentration classes used to assess classification performance. R^2, RMSE, and Accordance values demonstrate the improvement in model performance across successive calibrations.

An analysis of the graphs in Figure 75b clearly reveals the qualitative evolution of the algorithm. In Phase I (Calibration I), a significant overestimation of odor concentrations is evident, which resulted in a low *Accordance* of only 58.3% and a high RMSE of 8.924 ou/m^3. In Phase III (Calibration III), the measurement points are tightly clustered along the diagonal line of the ideal fit, y = x. The *Accordance* rose to 89.8%, the RMSE fell to 1.852 ou/m^3, and the coefficient of determination R^2 reached 0.817. Similar analyses of time series and classification plots were conducted for the remaining six measuring devices. All of them showed the same consistent trend. A summary of statistical indicators (R^2, RMSE, *Accordance*) for the entire IOMSN, presented in a comparative format, is shown in Table 29.

Table 29. A summary of predictive performance metrics (R^2, RMSE, Accordance) for seven IOMSN network measuring devices at various stages of long-term validation.

		s2176	s2715	s3965	s3968	s4077	s4088	s4095
R^2 [-]	Validation I	0.762	0.876	0.903	0.750	0.718	0.936	0.877
	Validation II	0.853	0.951	0.907	0.810	0.828	0.944	0.906
	Validation III	0.895	0.972	0.957	0.817	0.846	0.958	0.919
RMSE [ou/m^3]	Validation I	6.586	7.824	2.213	8.924	2.858	2.522	1.928
	Validation II	3.372	3.803	1.517	3.140	0.978	1.826	1.536
	Validation III	2.409	1.537	1.491	1.852	0.568	0.875	0.938
Accordance [%]	Validation I	54.2	40.0	100.0	58,3	59.3	81.5	87.5
	Validation II	80.5	85.4	92.7	83,3	88.1	88.1	87.8
	Validation III	81.4	86.4	89.7	89,8	93.2	91.5	96.6

The values presented in Table 29 confirm the universal applicability of the developed calibration methodology throughout the entire plant. After the third calibration, the class compliance rate hovered around 90% for most measuring devices. The highest level (96.6%), was recorded for the s4095 device located on the reclaimed landfill cell, which demonstrates the hybrid model's exceptional resistance to interference caused by landfill degassing. The greatest RMSE reduction was achieved in the new landfill cell (device s2715), where the RMSE was reduced from 7.824 ou/m^3 (phase I) to 1.537 ou/m^3 (phase III), and in the vicinity of the waste thermal treatment plant (device s4077), where the final RMSE was only 0.568 ou/m^3. The R^2 values in phase III for all measuring devices ranged from 0.817 to 0.972, which means that the model explains more than 80-97% of the total variability in odor nuisance at the MSWTP.

To facilitate comparison of the results obtained for individual devices at successive stages of validation, the data summarized in Table 29 are also presented graphically (Figure 76). The graph shows the RMSE and R^2 values as well as the *Accordance* parameter, allowing to track changes in the parameters characterizing the performance of the models for the seven sensorboxes between successive validation stages. The bar colors reflect the *Accordance* level (ranging from light gray for the lowest values to green for the highest values, individually for each device). In summarizing the results of the long-term operational validation, several key conclusions can be drawn. First, the elimination of seasonal error was achieved by incorporating a full cycle of meteorological variability into the training dataset. This eliminated the problem of thermal and humidity drift in the TGS series of semiconductor sensors. Second, the precise differentiation of emission zones. IOMSN maintains high measurement accuracy both in zones

with low emission backgrounds (s4077, s4088, where concentrations rarely exceed 10 ou/m^3) and in areas with extremely high odor levels (s3968, s2176, s4095), showing no signs of sensor saturation at concentrations exceeding 60-80 ou/m^3. The long-term results obtained provide direct evidence that a multipoint network of odor monitoring devices, calibrated based on a hybrid model and field olfactometry, ensures a stable, continuous, and reliable assessment of odor air quality under real-world MSWTP operating conditions.

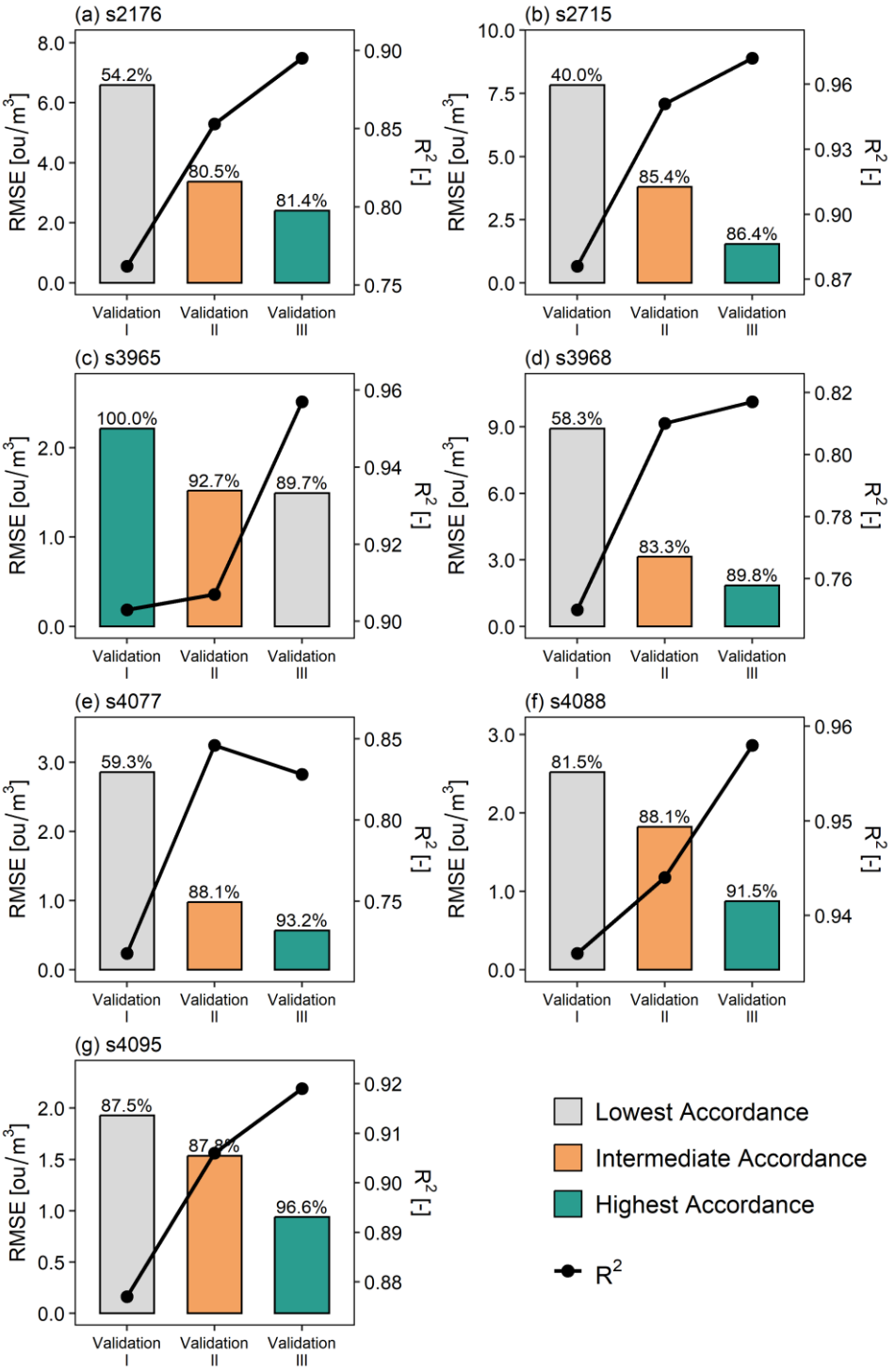


Figure 76. Model performance across three validation stages for seven sensorboxes. Bars represent RMSE, the black line represents R^2, and percentages above the bars indicate Accordance (bar colors denote the relative Accordance level within each sensorbox).

11.3.4 Integration of IOMSN with the IoT cloud and the DSS

The culmination of the work on implementing the IOMSN was its full integration with an advanced Internet of Things (IoT) cloud infrastructure and the development of a dedicated decision support system (DSS). The completion of this stage directly addressed research task of the third hypothesis, which aimed to transform raw, multidimensional measurement signals into a clear and operational tool for plant personnel. The main engineering challenge at this sprawling industrial facility was the need to continuously collect, transmit, and process, in real time, data streams from seven measurement devices operating continuously. The implemented cloud architecture (*EnviroCas*, developed in collaboration with Dacsystem LLC in Gdańsk) enables the automatic processing of signals from sensor arrays using a calibrated hybrid predictive model, followed by their immediate presentation to users via a web and mobile application. A key module of the operational interface is the spatial visualization of the odor air quality status on an interactive map of the MSWTP (Figure 77).

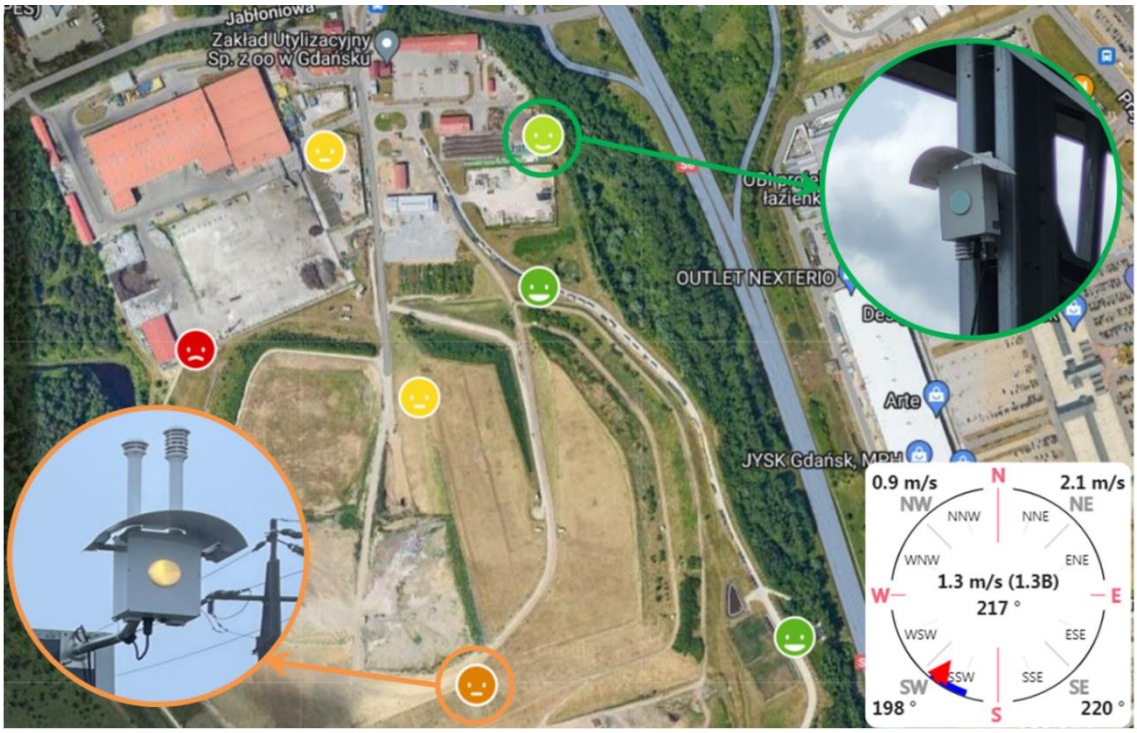


Figure 77. The IOMSN system's user interface in the mobile app: a spatial representation of the locations of seven monitoring devices on a map of the MSWTP, with automatic classification of odor nuisance based on the $OAQI_I$ index.

The current odor situation in the vicinity of each of the seven monitoring devices (sensorboxes) is represented using an intuitive color-coding system. The thresholds for the individual icons are closely linked to the four odor nuisance classes defined as part of the $OAQI_I$ index (see Table 24). This approach to data presentation allows a dispatcher or facility operator (even without specialized knowledge of olfactometry) to immediately identify the area where an odor emission problem is occurring. The appearance of a red or orange icon in a specific subsector (e.g., during compost screening - s3968) automatically signals the need to take immediate corrective action (e.g., adjusting aeration, sealing the compost pile, or intensifying

biofiltration). In addition to the spatial overview, the application provides an advanced temporal analysis module. Figure 78 shows a summary graph of the temporal trends in odor concentrations for all seven monitoring devices over a sample operating period. An analysis of the data in Figure 78 reveals a number of unique characteristics of the IOMSN that cannot be achieved using traditional (reference) methods.

First, the high sampling frequency allows for precise recording of occasional, short-lived increases in odor concentration (odor peaks), reaching values of 35-40 ou/m^3 for device s3968. These peaks are most often associated with specific operational activities, such as turning or screening compost piles or forming a working front in a composting area or landfill cells.

Second, the parallel display of signals from all sensor boxes on a single timeline makes it possible to track the movement of odorants. An increase in odor concentration at a station located directly at the source (e.g., s3968) correlates with correspondingly smaller, time-delayed responses at neighboring stations (e.g., s3965 or s4088), which, when combined with data from the meteorological station, allows for a precise determination of the direction in which the odor plume is spreading.

Third, constant access to the full archive of measurement data in the IoT cloud is a key tool in managing social conflicts. If a complaint is received from residents of nearby neighborhoods, plant personnel can identify the exact time the complaint was filed and verify whether the monitoring stations at the plant's perimeter recorded an emission event at that time and whether the wind direction was conducive to carrying odors toward the complainant.

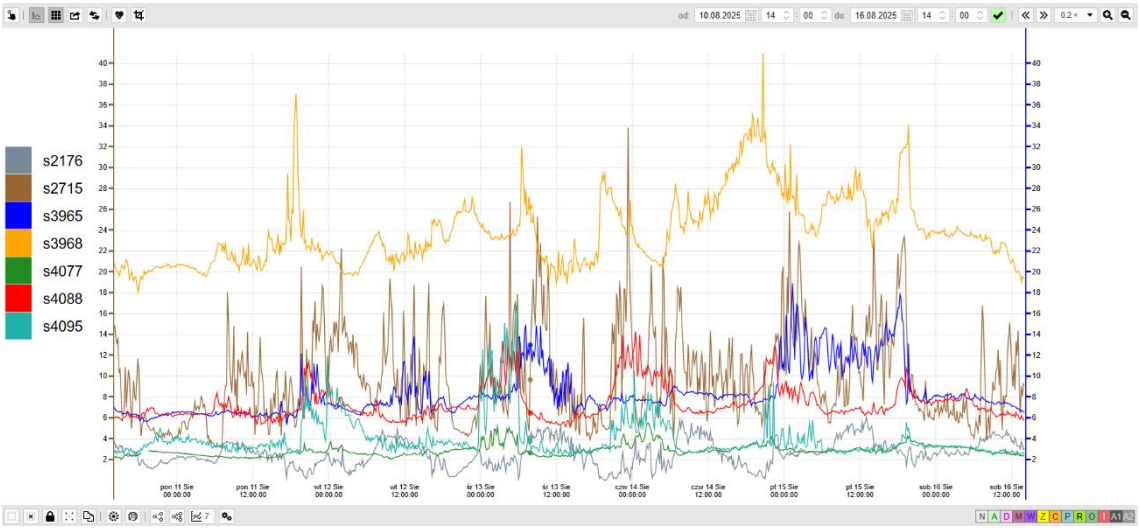


Figure 78. A consolidated summary of the weekly time-series data for predicted odor concentrations (ou/m^3) continuously recorded by all monitoring devices in the IOMSN.

In summary, the integration of the IOMSN with the IoT cloud and the DSS has enabled the full automation of the odor air quality control process. The system is no longer merely a measurement tool but has become an active component of Waste Utilization Facility Ltd. in Gdańsk technological and environmental management, thereby confirming the validity of the third research hypothesis.

11.4 Summary and conclusions

Long-term studies conducted at the Waste Utilization Facility Ltd. in Gdańsk fully confirmed the validity of the third research hypothesis, which posits that properly calibrated gas sensor arrays connected in a multipoint measurement network enable continuous, objective assessment of odor nuisance, both spatially and temporally, under real-world conditions at a MSWTP. The completion of the individual research tasks assigned to the third hypothesis led to the formulation of the following scientific and implementation findings:

- A proprietary hybrid predictive model was developed and validated, using field olfactometry (with the Nasal Ranger olfactometer) as the reference technique. The application of a logarithmic transformation of the signals to the decibel scale and the first principal component eliminated the problem of collinearity among the input variables and ensured a high model fit.
- The measured odor concentrations were correlated with human sensory perception and incorporated into the 4 class Odor Air Quality Index ($OAQI_I$) scale. The defined odor concentration thresholds enabled non-operational and automatic classification of odor air quality ranging from background levels to extreme nuisance.
- It has been demonstrated that continuous odor nuisance measurements are fully feasible under field conditions using a single sensor array. The measuring device has proven its ability to respond immediately to fluctuations in concentrations around local emission sources, such as a compost screening area or a landfill cell.
- The solution was scaled to the IOMSN consisting of seven identical measurement stations located at key technological nodes of the facility. The two year research program included a three stage calibration of the network over a full seasonal cycle (summer 2024, spring 2025, fall 2025), which effectively made the algorithms resistant to fluctuations in temperature and relative humidity.
- Long-term validation conducted from 2024 to 2026 under routine MSWPT operating conditions confirmed the high stability of the IOMSN. After accounting for the full calibration cycle, the class agreement index (Accordance) exceeded 90% for most devices (reaching 96.6% for device s4095 in the reclaimed landfill cell), with an RMSE ranging from 0.568 ou/m^3 to 2.409 ou/m^3. The IOMSN demonstrated a unique ability to continuously record short-term discharge and process-related episodes (odor “peaks” reaching 40-60 ou/m^3, which are completely overlooked in traditional manual measurements).
- A complete IoT cloud infrastructure was built, integrated with a dedicated web and mobile app for plant employees. The implemented interactive map, featuring the $OAQI_I$ color scheme, and a time-series module enable the immediate localization of emission sources, objective verification of residents’ complaints based on the data archive, and real-time optimization of deodorization systems.

An analysis of the current state of knowledge points to the dynamic development of instrumental odor monitoring systems (IOMS). However, the vast majority of studies to date have been limited to the use of a single sensor array on a laboratory or pilot scale. In field studies, systems consisting of no more than two devices operating in a source - receiver configuration predominate (e.g., one station at the plant boundary and another in a residential area or near a school). Multipoint monitoring networks consisting of more than two measuring devices are rare in the international literature. A review of the literature identified only a few exceptions with this type of architecture [261,262].

The small number of multipoint deployments is due to technological and economic barriers: the lack of full standardization of field procedures, the high costs of individually calibrating each device in the network, and the need to process complex data streams in real time. Against this backdrop, the Instrumental Odor Monitoring System Network (IOMSN), implemented as part of this dissertation, consisting of 7 identical monitoring devices distributed across an area of approximately 700,000 m^2 at the Waste Utilization Facility Ltd. in Gdańsk, is the first in Poland and one of the first in the world to be such an extensive, operational network of gas sensor arrays implemented on an industrial scale at a waste management facility.

11.5 Publication basis of the chapter

This chapter presents the research results from a manuscript currently under review:

Dobrzyniewski D., Szulczyński B., Czaplicka N., Kiszkurno S., Kosiak T., Gębicki J. (2026). Instrumental Odor Monitoring System Network (IOMSN) for real-time odor nuisance control at the Municipal Solid Waste Treatment Plant – Long Term Study. *Measurement.*

The content has been revised and expanded for the purpose of this doctoral dissertation. In the thesis, the findings are discussed in the context of the main research objective.

12. General conclusions and future research directions

12.1 Summary of the results and general conclusions

The primary objective of the doctoral dissertation was to demonstrate the potential of using appropriately designed, calibrated, and validated gas sensor arrays as rapid, objective, and cost-effective tools for the continuous monitoring of deodorization processes and odor nuisance at both laboratory and industrial scales. The fulfilment of the established indirect tasks and objectives led to the full verification and experimental confirmation of the three formulated research hypotheses.

Verification of the first research hypothesis demonstrated that gas sensor arrays integrated with appropriate mathematical models constitute a reliable alternative to reference chromatographic techniques for the quantitative monitoring of gas purification processes involving volatile organic compounds (VOCs). Statistical equivalence was demonstrated between the gas sensor arrays results and the reference gas chromatography (GC-FID) method, along with a high level of agreement in the presence of interfering substances during absorption processes (using commercial absorbents and green deep eutectic solvents - DES) and trickling biofiltration.

Verification of the second research hypothesis demonstrated that integrating a gas sensor array with an unmanned aerial vehicle (UAV) enables the spatial identification and mapping of gas concentration fields and odor emissions from complex, passive area sources (landfill cell). The application of multidimensional PLS models within the QGIS environment enabled the precise identification of zones of elevated emissions around leaks in degassing wells and the estimation of the total odor emission. Furthermore, it was demonstrated that emission data obtained from UAVs yield an odor nuisance range in dispersion modeling equivalent to the results of traditional dynamic olfactometry.

Verification of the third research hypothesis confirmed that a multipoint gas sensor array network enables continuous spatial and temporal assessment of odor nuisance under real-world industrial conditions. It has been confirmed that a distributed network of stationary e-noses (IOMSN), integrated with a proprietary Odor Air Quality Index ($OAQI_I$), an IoT cloud, and a decision support system (DSS), enables continuous assessment of odor nuisance across the entire MSWTP. The application of a hybrid predictive model (decibel scale, Stevens's law, PCA) ensured high accuracy in classifying odor nuisance. Long-term operational validation demonstrated the system's ability to identify short-term emission episodes (odor peaks) and to objectively verify community complaints.

12.2 Limitations of the applied methods and solutions

Despite the demonstrated high effectiveness and agreement of the implemented measurement systems (gas sensor arrays) compared to reference methods, significant methodological, technical, and application related limitations identified at various stages of the research must be noted.

First, MOS sensors exhibit a natural drift phenomenon, a gradual shift in the electrical output signal corresponding to clean air (the so-called baseline), caused by the aging of sensing elements and changes in ambient temperature and humidity. In this dissertation, this limitation was minimized by applying a logarithmic signal transformation, incorporating environmental parameters into the predictive model equations, and conducting a three-stage, multi-seasonal calibration (covering summer, spring, and autumn), which enriched the models with information regarding background variability.

Second, regression models developed at the laboratory scale for absorption and biofiltration processes demonstrate very high precision under controlled conditions (for two- and three-component mixtures). However, actual waste gas streams from waste management facilities contain hundreds of variable organic and inorganic compounds. The appearance of unforeseen interfering substances in the process stream, or sudden bed or absorbent breakthrough, can lead to a transient increase in the concentration prediction error.

Third, emission measurements using UAVs are constrained by battery life and meteorological conditions (wind speed, precipitation), resulting in data that is temporally discrete. Furthermore, the application of spatial interpolation methods (such as TIN) on a computational grid within the QGIS environment entails a natural mathematical smoothing effect on extreme values. This can lead to a slight underestimation of localized, extremely high emission hotspots when calculating the total emission balance.

Last but not least, a key barrier to the large scale commercial deployment of multipoint IOMSN networks remains the absence of universally applicable legal standards recognizing electronic noses as an official data source in integrated permitting procedures and environmental decision making. Furthermore, due to the unique chemical profile of each facility, every monitoring station in the network requires costly and labor intensive calibration campaigns involving reference field or dynamic olfactometry.

12.3 Directions for future research and development prospects

Based on the conclusions drawn in the dissertation, the following promising directions for future research and implementation work have been identified:

- Network scaling and swarm intelligence – A promising direction in the development of mobile measurements is the use of autonomous drone swarms (UAV swarms) collaborating in real time, enabling three-dimensional (3D) mapping of the dynamic dispersion of odor plumes over complex industrial facilities.
- Integration with Citizen Science and dynamic modeling - Future versions of DSS systems should integrate data from the IOMSN network with geolocation-based applications for residents (Citizen Science). Automatically cross-referencing a spatial and temporal odor report with current station readings and wind trajectory data will enable the immediate verification of community complaints.
- Deep learning algorithms and auto-calibration - The development of predictive models within the IoT cloud should aim to implement deep neural networks (ANN) and

auto-calibration algorithms. This will enable automatic compensation for chemical sensor aging and allow the models to continuously adapt to the changing technological environment of the plant.

- Standardization and legislation of IOMSN procedures - A key challenge for the widespread commercial use of multipoint gas sensor arrays odor monitoring network remains the development of consistent legal standards and accreditation procedures (modeled on the Italian standard UNI 11761:2023), which would enable IOMSN results to be accepted as evidence in integrated permits and environmental decisions.

References

1. Arman, F.; Mohseni Bandpey, A.; Shahsavani, A.; Saadani, M.; Saeedi, R.; Abtahi, M. Characterization, Source Identification, and Health Risk Assessment of Odorous Compounds in Solid Waste Management Facility of Tehran. *Air Qual. Atmos. Health* **2022**, *15*, 1609–1621, doi:10.1007/s11869-022-01205-z.
2. Fang, W.; Huang, Y.; Ding, Y.; Qi, G.; Liu, Y.; Bi, J. Health Risks of Odorous Compounds during the Whole Process of Municipal Solid Waste Collection and Treatment in China. *Environ. Int.* **2022**, *158*, 106951, doi:10.1016/j.envint.2021.106951.
3. Piccardo, M.T.; Geretto, M.; Pulliero, A.; Izzotti, A. Odor Emissions: A Public Health Concern for Health Risk Perception. *Environ. Res.* **2022**, *204*, 112121, doi:10.1016/j.envres.2021.112121.
4. Zhang, Y.; Ning, X.; Li, Y.; Wang, J.; Cui, H.; Meng, J.; Teng, C.; Wang, G.; Shang, X. Impact Assessment of Odor Nuisance, Health Risk and Variation Originating from the Landfill Surface. *Waste Manag.* **2021**, *126*, 771–780, doi:10.1016/j.wasman.2021.03.055.
5. Biegańska, J.; Tora, B. Odours in Waste Management – Problems at Landfills. *Rocz. Ochr. Śr.* **2025**, *27*, 667–676, doi:10.54740/ros.2025.053.
6. Cruz, L.P.S.; Alves, R.S.; Da Rocha, F.O.C.; Moreira, M.S.; Dos Santos Júnior, A. Atmospheric Levels, Multivariate Statistical Study, and Health Risk Assessment of Odorous Compounds (H2S and NH3) in Areas near Polluted Urban Rivers in the City of Salvador, in Northeastern Brazil. *Air Qual. Atmos. Health* **2022**, *15*, 159–176, doi:10.1007/s11869-021-01095-7.
7. Dong, Y.; Ma, L.; Peng, Y.; Hu, Z.; Xu, Z.; Jiang, X.; Cheng, R.; Chen, H.; Yang, Q. Nitrogen-Containing Malodorous Gas Pollutants Emission Characteristics and Health Risk Assessment from an A/O Wastewater Treatment Plant. *J. Water Process Eng.* **2023**, *54*, 103961, doi:10.1016/j.jwpe.2023.103961.
8. Szulczyński, B.; Gębicki, J. Determination of Odor Intensity of Binary Gas Mixtures Using Perceptual Models and an Electronic Nose Combined with Fuzzy Logic. *Sensors* **2019**, *19*, 3473, doi:10.3390/s19163473.
9. Szulczyński, B.; Armiński, K.; Namieśnik, J.; Gębicki, J. Determination of Odour Interactions in Gaseous Mixtures Using Electronic Nose Methods with Artificial Neural Networks. *Sensors* **2018**, *18*, 519, doi:10.3390/s18020519.
10. Hawko, C.; Verriele, M.; Hucher, N.; Crunaire, S.; Leger, C.; Locoge, N.; Savary, G. A Review of Environmental Odor Quantification and Qualification Methods: The Question of Objectivity in Sensory Analysis. *Sci. Total Environ.* **2021**, *795*, 148862, doi:10.1016/j.scitotenv.2021.148862.
11. Toledo, M.; Muñoz, R. Odour Prevention Strategies in Wastewater Treatment and Composting Plants: A Review. *J. Environ. Manage.* **2025**, *375*, 124402, doi:10.1016/j.jenvman.2025.124402.
12. Pawnuk, M.; Grzelka, A.; Miller, U.; Sówka, I. Prevention and Reduction of Odour Nuisance in Waste Management in the Context of the Current Legal and Technological Solutions. *J. Ecol. Eng.* **2020**, *21*, 34–41, doi:10.12911/22998993/125455.
13. Czarnota, J.; Masłoń, A.; Pajura, R. Wastewater Treatment Plants as a Source of Malodorous Substances Hazardous to Health, Including a Case Study from Poland. *Int. J. Environ. Res. Public. Health* **2023**, *20*, 5379, doi:10.3390/ijerph20075379.
14. Han, Y.; Wang, Y.; Chai, F.; Ma, J.; Li, L. Biofilters for the Co-Treatment of Volatile Organic Compounds and Odors in a Domestic Waste Landfill Site. *J. Clean. Prod.* **2020**, *277*, 124012, doi:10.1016/j.jclepro.2020.124012.
15. Rolewicz-Kalińska, A.; Lelicińska-Serafin, K.; Manczarski, P. Volatile Organic Compounds, Ammonia and Hydrogen Sulphide Removal Using a Two-Stage Membrane Biofiltration Process. *Chem. Eng. Res. Des.* **2021**, *165*, 69–80, doi:10.1016/j.cherd.2020.10.017.
16. Stanley, W.B.M.; Muller, C.O. CHOOSING AN ODOR CONTROL TECHNOLOGY – EFFECTIVENESS AND COST CONSIDERATIONS. *Proc. Water Environ. Fed.* **2002**, *2002*, 259–276, doi:10.2175/193864702785140023.
17. Zhang, B.; Ma, Z.; Zhang, Y.; Wang, L.; Yan, J.; Ling, S.; Fang, X. Odor Control Technologies for Municipal Solid Waste Mechanical Biological Treatment Plant: A Review. *Clean Technol. Environ. Policy* **2025**, *27*, 2741–2758, doi:10.1007/s10098-024-02952-6.
18. Wysocka, I.; Gębicki, J.; Namieśnik, J. Technologies for Deodorization of Malodorous Gases. *Environ. Sci. Pollut. Res.* **2019**, *26*, 9409–9434, doi:10.1007/s11356-019-04195-1.

19. Vitko, T.G.; Cowden, S.; Suffet, I.H. (Mel) Evaluation of Bioscrubber and Biofilter Technologies Treating Wastewater Foul Air by a New Approach of Using Odor Character, Odor Intensity, and Chemical Analyses. *Water Res.* **2022**, *220*, 118691, doi:10.1016/j.watres.2022.118691.
20. Estrada, J.M.; Kraakman, N.J.R.B.; Muñoz, R.; Lebrero, R. A Comparative Analysis of Odour Treatment Technologies in Wastewater Treatment Plants. *Environ. Sci. Technol.* **2011**, *45*, 1100–1106, doi:10.1021/es103478j.
21. Wang, Y.; Shao, L.; Kang, X.; Zhang, H.; Lü, F.; He, P. A Critical Review on Odor Measurement and Prediction. *J. Environ. Manage.* **2023**, *336*, 117651, doi:10.1016/j.jenvman.2023.117651.
22. Brattoli, M.; De Gennaro, G.; De Pinto, V.; Demarinis Loiotile, A.; Lovascio, S.; Penza, M. Odour Detection Methods: Olfactometry and Chemical Sensors. *Sensors* **2011**, *11*, 5290–5322, doi:10.3390/s110505290.
23. Van Ruth, S.M. Methods for Gas Chromatography-Olfactometry: A Review. *Biomol. Eng.* **2001**, *17*, 121–128, doi:10.1016/S1389-0344(01)00070-3.
24. Mahmoud, M.A.A.; Zhang, Y. Enhancing Odor Analysis with Gas Chromatography–Olfactometry (GC-O): Recent Breakthroughs and Challenges. *J. Agric. Food Chem.* **2024**, *72*, 9523–9554, doi:10.1021/acs.jafc.3c08129.
25. Jońca, J.; Pawnuk, M.; Arsen, A.; Sówka, I. Electronic Noses and Their Applications for Sensory and Analytical Measurements in the Waste Management Plants—A Review. *Sensors* **2022**, *22*, 1510, doi:10.3390/s22041510.
26. Ijaz, U.; Ali, M.; Ahmad, I.; Hamza, S.A.; Kim, H.-D. A Comprehensive Review of Electronic Nose Systems: Design, Sensors, and Future Directions. *Chem. Eng. J.* **2025**, *524*, 169482, doi:10.1016/j.cej.2025.169482.
27. Capelli, L.; Sironi, S.; Del Rosso, R. Electronic Noses for Environmental Monitoring Applications. *Sensors* **2014**, *14*, 19979–20007, doi:10.3390/s141119979.
28. Li, Y.; Wang, Z.; Zhao, T.; Li, H.; Jiang, J.; Ye, J. Electronic Nose for the Detection and Discrimination of Volatile Organic Compounds: Application, Challenges, and Perspectives. *TrAC Trends Anal. Chem.* **2024**, *180*, 117958, doi:10.1016/j.trac.2024.117958.
29. Ivanov, S.; Wilk-Jakubowski, J.Ł.; Ciopiński, L.; Pawlik, Ł.; Wilk-Jakubowski, G.; Mihalev, G. Modern Trends in the Application of Electronic Nose Systems: A Review. *Appl. Sci.* **2025**, *15*, 10776, doi:10.3390/app151910776.
30. Girmatsion, M.; Tang, X.; Zhang, Q.; Li, P. Progress in Machine Learning-Supported Electronic Nose and Hyperspectral Imaging Technologies for Food Safety Assessment: A Review. *Food Res. Int.* **2025**, *209*, 116285, doi:10.1016/j.foodres.2025.116285.
31. Sberveglieri Giorgio; Genzardi Dario; Greco Giuseppe; Nunez-Carmona Estefania; Pezzottini Simone; Sberveglieri Veronica The Electronic Nose: Review on Sensor Arrays and Future Perspectives. *Chem. Eng. Trans.* **2022**, *95*, 265–270, doi:10.3303/CET2295045.
32. *Metody identyfikacji odorotwórczych gazów emitowanych z obiektów przemysłowych*; Prace Naukowe Instytutu Inżynierii Ochrony Środowiska Politechniki Wrocławskiej; Oficyna Wydawnicza Politechniki Wrocławskiej: Wrocław, 2011;
33. Rappert, S.; Müller, R. Microbial Degradation of Selected Odorous Substances. *Waste Manag.* **2005**, *25*, 940–954, doi:10.1016/j.wasman.2005.07.015.
34. Kośmider, J.; Mazur-Chrzanowska, B.; Wyszyński, B. *Odory*; Wyd. 1-1 dodr.; Wydawnictwo Naukowe PWN: Warszawa, 2012; ISBN 978-83-01-13744-1.
35. Szynkowska, M.I.; Wojciechowska, E.; Węglińska, A.; Paryjczak, T. Odory. Aktualny problem w ochronie środowiska. *Przeymysł Chem.* **2009**, *88*, 712–720.
36. Revah, S.; Morgan-Sagastume, J.M. Methods of Odor and VOC Control. In *Biotechnology for Odor and Air Pollution Control*; Shareefdeen, Z., Singh, A., Eds.; Springer-Verlag: Berlin/Heidelberg, 2005; pp. 29–63 ISBN 978-3-540-23312-1.
37. Barczak, R.J.; Możaryn, J.; Fisher, R.M.; Stuetz, R.M. Odour Concentrations Prediction Based on Odorants Concentrations from Biosolid Emissions. *Environ. Res.* **2022**, *214*, 113871, doi:10.1016/j.envres.2022.113871.
38. Bax, C.; Sironi, S.; Capelli, L. How Can Odors Be Measured? An Overview of Methods and Their Applications. *Atmosphere* **2020**, *11*, 92, doi:10.3390/atmos11010092.
39. Brancher, M.; Griffiths, K.D.; Franco, D.; De Melo Lisboa, H. A Review of Odour Impact Criteria in Selected Countries around the World. *Chemosphere* **2017**, *168*, 1531–1570, doi:10.1016/j.chemosphere.2016.11.160.
40. Xu, X.; Gu, H.; Zhang, Z.; Liu, Y.; Zhang, L.; Wang, J.; Chen, M.; Huang, Y.; Cao, J.; Lee, S.; et al. Advancements in Understanding Emission Characteristics, Data-Driven Olfactory-

Chemical Measurements, and Health Impacts of the Emerging Odor Pollution. *Environ. Int.* **2025**, *201*, 109596, doi:10.1016/j.envint.2025.109596.
41. Rybarczyk, P.; Szulczyński, B.; Gębicki, J.; Hupka, J. Treatment of Malodorous Air in Biotrickling Filters: A Review. *Biochem. Eng. J.* **2019**, *141*, 146–162, doi:10.1016/j.bej.2018.10.014.
42. Szulczyński, B.; Wasilewski, T.; Wojnowski, W.; Majchrzak, T.; Dymerski, T.; Namieśnik, J.; Gębicki, J. Different Ways to Apply a Measurement Instrument of E-Nose Type to Evaluate Ambient Air Quality with Respect to Odour Nuisance in a Vicinity of Municipal Processing Plants. *Sensors* **2017**, *17*, 2671, doi:10.3390/s17112671.
43. Amoore, J.E.; Hautala, E. Odor as an Ald to Chemical Safety: Odor Thresholds Compared with Threshold Limit Values and Volatilities for 214 Industrial Chemicals in Air and Water Dilution. *J. Appl. Toxicol.* **1983**, *3*, 272–290, doi:10.1002/jat.2550030603.
44. Nagata, Y. Measurement of Odor Threshold by Triangle Odor Bag Method.
45. Mckittrick, J.; Hadgraft, N.; Fry, K.L.; Mikkonen, A.T.; Mavoa, S. Industrial Odour and Psychosocial Wellbeing: A Systematic Review. *Environments* **2025**, *12*, 364, doi:10.3390/environments12100364.
46. Cavalcante, F.R.; Machado, M.; Reisen, V.A.; Furieri, B.; Goulart, E.V.; Ponce De Leon, A.; Reis, N.C.; Frère, S.; Santos, J.M. Determinants of Odor-Related Perception: Analysis of Community Response. *Atmosphere* **2025**, *16*, 1176, doi:10.3390/atmos16101176.
47. Özkal, C.B.; Tecer, L.H. Interpretation of Odor Complaint Records with BTEX Pollutants and Meteorological Factors: Çorlu Case Study. *Environ. Res. Technol.* **2023**, *6*, 118–132, doi:10.35208/ert.1235618.
48. Wojnarowska, M.; Plichta, G.; Sagan, A.; Plichta, J.; Stobiecka, J.; Sołtysik, M. Odour Nuisance and Urban Residents' Quality of Life: A Case Study in Kraków's in Plaszow District. *Urban Clim.* **2020**, *34*, 100704, doi:10.1016/j.uclim.2020.100704.
49. Herrera, C.; Cabrera-Barona, P. Impact of Perceptions of Air Pollution and Noise on Subjective Well-Being and Health. *Earth* **2022**, *3*, 825–838, doi:10.3390/earth3030047.
50. Wysocka, I.; Dębowski, M. Advantages and Limitations of Measurement Methods for Assessing Odour Nuisance in Air—A Comparative Review. *Appl. Sci.* **2025**, *15*, 5622, doi:10.3390/app15105622.
51. Pawnuk, M.; Sówka, I.; Naddeo, V. Sensorial Techniques of Odour Measurements - a Relationship between Odour Concentration and Odour Intensity for a Selected Waste Management Facility. *Zesz. Nauk. SGSP* **2023**, *87*, 99–120, doi:10.5604/01.3001.0053.9113.
52. Liu, N.; Ning, Z.; Jia, Y.; Ren, Y.; Liu, W.; Zhang, Y.; Zhao, P.; Sun, P.; Zhang, J.; Liu, J. Indoor Odor Pollution: An Interdisciplinary Review from Sources to Control and an Intelligent Building Environment Management Framework. *Buildings* **2026**, *16*, 687, doi:10.3390/buildings16040687.
53. Both, R.; Sucker, K.; Winneke, G.; Koch, E. Odour Intensity and Hedonic Tone - Important Parameters to Describe Odour Annoyance to Residents? *Water Sci. Technol.* **2004**, *50*, 83–92, doi:10.2166/wst.2004.0227.
54. Gostelow, P.; Parsons, S.A.; Stuetz, R.M. Odour Measurements for Sewage Treatment Works. *Water Res.* **2001**, *35*, 579–597, doi:10.1016/S0043-1354(00)00313-4.
55. Li, J.; Zou, K.; Li, W.; Wang, G.; Yang, W. Olfactory Characterization of Typical Odorous Pollutants Part I: Relationship Between the Hedonic Tone and Odor Concentration. *Atmosphere* **2019**, *10*, 524, doi:10.3390/atmos10090524.
56. Makles, Z.; Galwas-Zakrzewska, M. Złowonne Gazy w Środowisku Pracy. *Bezp. Pr. Nauka Prakt.* **2005**, 12–16.
57. Makles, Z.; Domański, W. Odory w Środowisku Pracy Rolnika-Hodowcy. Źródła, Zagrożenia, Usuwanie. *Bezp. Pr. Nauka Prakt.* **2008**, 10–13.
58. Sówka, I.; Zwoździak, P.; Zwoździak, A.; Zwoździak, J. *Problem uciążliwości zapachowej wybranych obiektów gospodarki komunalnej*; Politechnika Wrocławska, Instytut Inżynierii Ochrony Środowiska; pp. 409–414;.
59. Mielcarek, P.; Rzeźnik, W. Odor Emission Factors from Livestock Production. *Pol. J. Environ. Stud.* **2015**, *24*, 27–35, doi:10.15244/pjoes/29944.
60. Autelitano, F.; Giuliani, F. Influence of Chemical Additives and Wax Modifiers on Odor Emissions of Road Asphalt. *Constr. Build. Mater.* **2018**, *183*, 485–492, doi:10.1016/j.conbuildmat.2018.06.168.
61. Amenduni, A.; Brattoli, M.; Gennaro, G.D.; Massari, F.; Palmisani, J.; Tutino, M. CHEMICAL CHARACTERIZATION OF ODOR ACTIVE VOLATILE ORGANIC COMPOUNDS EMITTED

FROM PERFUMES BY GC/MS-O. *Environ. Eng. Manag. J.* **2016**, *15*, 1963–1969, doi:10.30638/eemj.2016.211.
62. Li, C.; Jia, Y.; Qiu, Y.; Cordeiro, C.M.; Li, S.; Chen, Y.; Liu, J.; Siesler, H.W.; Wu, H.; Zhao, R. Analysis of Odor and VOCs Pollution in Industrial Parks of Central Inner Mongolia Autonomous Region Based on Mobile Monitoring. *Atmos. Environ.* **2026**, *366*, 121703, doi:10.1016/j.atmosenv.2025.121703.
63. Liu, C.; Yang, P.; Wang, H.; Song, H. Identification of Odor Compounds and Odor-Active Compounds of Yogurt Using DHS, SPME, SAFE, and SBSE/GC-O-MS. *LWT* **2022**, *154*, 112689, doi:10.1016/j.lwt.2021.112689.
64. Michalak, M.; Kogut, K.; Burmistrz, P. Analysis of Odor Nuisance Emitted by a Rendering Plant Processing Animal By-Products, Which Is Located in the Center of a Several-Thousand Population Village. *Rocz. Ochr. Śr.* **2024**, *26*, 305–312, doi:10.54740/ros.2024.030.
65. Pendashteh, A.R.; Fathi, H.; Ansari, A.R.; Niazmehr, F.; Rahmaninezhad, S.A. Odor Removal from a Fish Meal Plant by Oxidative Scrubber (a Pilot Study). *Nat. Resour.* **2015**.
66. LeBouf, R.F.; Blackley, B.H.; Fortner, A.R.; Stanton, M.; Martin, S.B.; Groth, C.P.; McClelland, T.L.; Duling, M.G.; Burns, D.A.; Ranpara, A.; et al. Exposures and Emissions in Coffee Roasting Facilities and Cafés: Diacetyl, 2,3-Pentanedione, and Other Volatile Organic Compounds. *Front. Public Health* **2020**, *8*, 561740, doi:10.3389/fpubh.2020.561740.
67. González, D.; Gabriel, D.; Sánchez, A. Odors Emitted from Biological Waste and Wastewater Treatment Plants: A Mini-Review. *Atmosphere* **2022**, *13*, 798, doi:10.3390/atmos13050798.
68. Zhang, S.; Cai, L.; Koziel, J.A.; Hoff, S.J.; Schmidt, D.R.; Clanton, C.J.; Jacobson, L.D.; Parker, D.B.; Heber, A.J. Field Air Sampling and Simultaneous Chemical and Sensory Analysis of Livestock Odorants with Sorbent Tubes and GC–MS/Olfactometry. *Sens. Actuators B Chem.* **2010**, *146*, 427–432, doi:10.1016/j.snb.2009.11.028.
69. De Vela, R.J.L. Control of Odour and Gaseous Emissions from Livestock Buildings: Recent Research and Developments. *Res. Agric. Eng.* **2024**, *70*, 181–197, doi:10.17221/55/2024-RAE.
70. Cheng, Z.; Sun, Z.; Zhu, S.; Lou, Z.; Zhu, N.; Feng, L. The Identification and Health Risk Assessment of Odor Emissions from Waste Landfilling and Composting. *Sci. Total Environ.* **2019**, *649*, 1038–1044, doi:10.1016/j.scitotenv.2018.08.230.
71. Schlegelmilch, M.; Streese, J.; Biedermann, W.; Herold, T.; Stegmann, R. Odour Control at Biowaste Composting Facilities. *Waste Manag.* **2005**, *25*, 917–927, doi:10.1016/j.wasman.2005.07.011.
72. Agus, E.; Zhang, L.; Sedlak, D.L. A Framework for Identifying Characteristic Odor Compounds in Municipal Wastewater Effluent. *Water Res.* **2012**, *46*, 5970–5980, doi:10.1016/j.watres.2012.08.018.
73. Han, Z.; Qi, F.; Wang, H.; Li, R.; Sun, D. Odor Assessment of NH3 and Volatile Sulfide Compounds in a Full-Scale Municipal Sludge Aerobic Composting Plant. *Bioresour. Technol.* **2019**, *282*, 447–455, doi:10.1016/j.biortech.2019.03.062.
74. Jachnik, E. Prawne aspekty ochrony zapachowej jakości powietrza. *Przegląd Prawa Rolnego* **2017**, *20*, 149–163.
75. Bokowa, A.; Diaz, C.; Koziel, J.A.; McGinley, M.; Barclay, J.; Schauberger, G.; Guillot, J.-M.; Sneath, R.; Capelli, L.; Zorich, V.; et al. Summary and Overview of the Odour Regulations Worldwide. *Atmosphere* **2021**, *12*, 206, doi:10.3390/atmos12020206.
76. Douša, J. Comparison Access to Odor Problems in Selected European Countries. *Inż. Miner.* **2019**, *1*, doi:10.29227/IM-2019-01-15.
77. Folgier, A. Regulacje Prawne Dotyczące Uciążliwości Zapachowej (Stan Obecny Oraz Projektowane Zmiany). *Acta Univ. Lodz. Folia Iurid.* **2023**, 81–90, doi:10.18778/0208-6069.S.2023.07.
78. Capelli, C.; Izquierdo, C.; Capelli, L.; Arias, R.; Seoane, N.S. *Analysis of Existing Regulations in Odour Pollution, Odour Impact Criteria 1*; H2020-SwafS-23-2017-789315; D-NOSES (Horizon 2020 Project), 2019;
79. Vehmaanperä, P.; Erle, A.; Pavlovs, D.; Zilenas, D.; Chliopanou, E.; Santos, E.; Kwiatkowski, K.; Baltrusaityte, L.; Kropsch, M.; Vinuesa, R.B.; et al. *Public Nuisance of Industrial Odors*; IMPEL - European Union Network for the Implementation and Enforcement of Environmental Law: Brussels, Belgium, 2024;
80. Marina, Z.; Selena, S. New Guidelines in Italy for the Regulation of Odour Emissions. *Chem. Eng. Trans.* **2024**, *112*, 13–18, doi:10.3303/CET24112003.
81. Nicell, J.A. Assessment and Regulation of Odour Impacts. *Atmos. Environ.* **2009**, *43*, 196–206, doi:10.1016/j.atmosenv.2008.09.033.

82. Hejbudzki, M. Publicznoprawne Formy Przeciwdziałania Zjawisku Tzw. Uciążliwości Odorowej Wynikającej z Działalności Rolniczej Opartej Na Produkcji Trzody Chlewnej w Fermach Wielkotowarowych. *Acta Sci. Pol. Adm. Locorum* **2018**, *17*, 347–362, doi:10.31648/aspal.2615.
83. Krystek, J.J. Uciążliwość Zapachowa Przedsięwzięć. *Stud. Prawnicze KUL* **2023**, doi:10.31743/sp.14192.
84. Schlegelmilch, M.; Streese, J.; Stegmann, R. Odour Management and Treatment Technologies: An Overview. *Waste Manag.* **2005**, *25*, 928–939, doi:10.1016/j.wasman.2005.07.006.
85. *Podstawy inżynierii chemicznej i procesowej: wybrane zagadnienia wraz z zadaniami do ćwiczeń rachunkowych, projektowych i laboratoryjnych*; Andrzejewski, T., Chachulski, B., Gębicki, J., Hołowacz, I., Kamiński, M., Konopacka-Łyskawa, D., Eds.; Wydawnictwo Politechniki Gdańskiej: Gdańsk, 2012; ISBN 978-83-7348-459-7.
86. *Inżynieria chemiczna i procesowa: wybrane zagadnienia*; Andrzejewski, T., Gębicki, J., Szulczyński, B., Hołowacz, I., Konopacka-Łyskawa, D., Makoś-Chełstowska, P., Rybarczyk, P., Eds.; Wydanie II.; Wydawnictwo Politechniki Gdańskiej: Gdańsk, 2024; ISBN 978-83-7348-917-2.
87. Watanabe Neto, M.; Góis, L.M.N.D.; Simonelli, G. Simulation and Modeling of Mass Transfer in Packed Absorption Columns for the Acetone-Water System: A Review. *Rev. Gest. E Secr.* **2025**, *16*, e5305, doi:10.7769/gesec.v16i10.5305.
88. Afkhamipour, M.; Mofarahi, M. Review on the Mass Transfer Performance of CO_2 Absorption by Amine-Based Solvents in Low- and High-Pressure Absorption Packed Columns. *RSC Adv.* **2017**, *7*, 17857–17872, doi:10.1039/C7RA01352C.
89. Ansarpour, M.; Mofarahi, M. Principles of Gas Absorption. In *Mass Transfer Operations in the Food Industry*; Elsevier, 2025; pp. 123–163 ISBN 978-0-12-819536-9.
90. Rinprasertmeechai, S.; Chavadej, S.; Rangsunvigit, P.; Kulprathipanja, S. Carbon Dioxide Removal From Flue Gas Using Amine-Based Hybrid Solvent Absorption. **2012**, doi:10.5281/ZENODO.1332828.
91. Üresin, E. Experimental and Simulation-Based Study of Acid Gas Removal in Packed Columns with Different Packing Materials. *Sustainability* **2025**, *17*, 10495, doi:10.3390/su172310495.
92. Sheoran, K.; Siwal, S.S.; Kapoor, D.; Singh, N.; Saini, A.K.; Alsanie, W.F.; Thakur, V.K. Air Pollutants Removal Using Biofiltration Technique: A Challenge at the Frontiers of Sustainable Environment. *ACS Eng. Au* **2022**, *2*, 378–396, doi:10.1021/acsengineeringau.2c00020.
93. Rybarczyk, P. Removal of Volatile Organic Compounds (VOCs) from Air: Focus on Biotrickling Filtration and Process Modeling. *Processes* **2022**, *10*, 2531, doi:10.3390/pr10122531.
94. Barbusiński, K.; Urbaniec, K.; Kasperczyk, D.; Thomas, M. Biofilters versus Bioscrubbers and Biotrickling Filters: State-of-the-Art Biological Air Treatment. In *From Biofiltration to Promising Options in Gaseous Fluxes Biotreatment*; Elsevier, 2020; pp. 29–51 ISBN 978-0-12-819064-7.
95. Hernandez-Shek, M.A.; Gracian, C.; Nastasi, V. Odor Removal via High-Speed Biofiltration in Headwork Operations of Wastewater Treatment Plants. *Water Sci. Technol.* **2025**, *92*, 220–234, doi:10.2166/wst.2025.100.
96. Ralebitso-Senior, T.K.; Senior, E.; Di Felice, R.; Jarvis, K. Waste Gas Biofiltration: Advances and Limitations of Current Approaches in Microbiology. *Environ. Sci. Technol.* **2012**, *46*, 8542–8573, doi:10.1021/es203906c.
97. Mudliar, S.; Giri, B.; Padoley, K.; Satpute, D.; Dixit, R.; Bhatt, P.; Pandey, R.; Juwarkar, A.; Vaidya, A. Bioreactors for Treatment of VOCs and Odours – A Review. *J. Environ. Manage.* **2010**, *91*, 1039–1054, doi:10.1016/j.jenvman.2010.01.006.
98. Pachaiappan, R.; Cornejo-Ponce, L.; Rajendran, R.; Manavalan, K.; Femilaa Rajan, V.; Awad, F. A Review on Biofiltration Techniques: Recent Advancements in the Removal of Volatile Organic Compounds and Heavy Metals in the Treatment of Polluted Water. *Bioengineered* **2022**, *13*, 8432–8477, doi:10.1080/21655979.2022.2050538.
99. Liu, S.; Gao, P.-F.; Li, S.; Fu, H.; Wang, L.; Dai, Y.; Fu, M. A Review of the Recent Progress in Biotrickling Filters: Packing Materials, Gases, Micro-Organisms, and CFD. *Environ. Sci. Pollut. Res.* **2023**, *30*, 125398–125416, doi:10.1007/s11356-023-31004-7.

100. Wang, L.; Gao, P.; Li, S.; Fu, H.; Yang, A.; Wu, Y.; Dai, Y.; Liu, S. Performance Evaluation of a Novel Bio-Trickling Filter for Styrene Waste Gas Treatment. *Sustainability* **2023**, *15*, 4226, doi:10.3390/su15054226.
101. Rouhollahi, A.A.; Giyahchi, M.; Dastgheib, S.M.M.; Moghimi, H. Assessing the Efficiency and Microbial Diversity of H2S-Removing Biotrickling Filters at Various pH Conditions. *Microb. Cell Factories* **2024**, *23*, 157, doi:10.1186/s12934-024-02427-9.
102. Piovezan, T.C.; Mores, R.; Steinmetz, R.L.R.; Kunz, A. HYDROGEN SULFIDE REMOVAL IN BIOGAS USING A FULL-SCALE BIOTRICKLING FILTER: EVALUATING SPRAYING TIME AND NITRATE SOURCE. *Eng. Agríc.* **2024**, *44*, e20240032, doi:10.1590/1809-4430-eng.agric.v44e20240032/2024.
103. Capelli, L.; Bax, C.; Diaz, C.; Izquierdo, C.; Arias, R.; Seoane, N.S. *Review on Odour Pollution, Odour Measurement, Abatement Techniques*; H2020-SwafS-23-2017-789315; D-NOSES (Horizon 2020 Project), 2019;
104. Senatore, V.; Zarra, T.; Galang, M.G.; Oliva, G.; Buonerba, A.; Li, C.-W.; Belgiorno, V.; Naddeo, V. Full-Scale Odor Abatement Technologies in Wastewater Treatment Plants (WWTPs): A Review. *Water* **2021**, *13*, 3503, doi:10.3390/w13243503.
105. Wu, J.; Yang, J.; Wang, J.; Fang, L.; Fang, J. A Field-Scale Evaluation of the Removal of Odorous Gases by a Plant Material-Based Deodorant. *Front. Environ. Sci.* **2023**, *10*, 1073835, doi:10.3389/fenvs.2022.1073835.
106. Zhou, X.; Zhang, Q.; Huang, A. Evaluation of a Plant Material-Based Air Purifier for Removing H_2 S, NH_3 and Swine Manure Odour. *Environ. Technol.* **2012**, *33*, 2751–2756, doi:10.1080/09593330.2012.678888.
107. Ren, B.; Zhao, Y.; Lyczko, N.; Nzihou, A. Current Status and Outlook of Odor Removal Technologies in Wastewater Treatment Plant. *Waste Biomass Valorization* **2019**, *10*, 1443–1458, doi:10.1007/s12649-018-0384-9.
108. Conti, C.; Guarino, M.; Bacenetti, J. Measurements Techniques and Models to Assess Odor Annoyance: A Review. *Environ. Int.* **2020**, *134*, 105261, doi:10.1016/j.envint.2019.105261.
109. Giungato, P.; Di Gilio, A.; Palmisani, J.; Marzocca, A.; Mazzone, A.; Brattoli, M.; Giua, R.; De Gennaro, G. Synergistic Approaches for Odor Active Compounds Monitoring and Identification: State of the Art, Integration, Limits and Potentialities of Analytical and Sensorial Techniques. *TrAC Trends Anal. Chem.* **2018**, *107*, 116–129, doi:10.1016/j.trac.2018.07.019.
110. Muñoz, R.; Sivret, E.C.; Parcsi, G.; Lebrero, R.; Wang, X.; Suffet, I.H. (Mel); Stuetz, R.M. Monitoring Techniques for Odour Abatement Assessment. *Water Res.* **2010**, *44*, 5129–5149, doi:10.1016/j.watres.2010.06.013.
111. Kulig, A.; Szyłak-Szydłowski, M.; Wiśniewska, M. Application of Field Olfactometry to Monitor the Odour Impact of a Municipal Sewage System. *Energies* **2022**, *15*, 4015, doi:10.3390/en15114015.
112. Pawnuk, M.; Sówka, I.; Naddeo, V. The Use of Field Olfactometry in the Odor Assessment of a Selected Mechanical–Biological Municipal Waste Treatment Plant within the Boundaries of the Selected Facility—A Case Study. *Sustainability* **2023**, *15*, 7163, doi:10.3390/su15097163.
113. Motalebi Damuchali, A.; Guo, H. Evaluation of a Field Olfactometer in Odour Concentration Measurement. *Biosyst. Eng.* **2019**, *187*, 239–246, doi:10.1016/j.biosystemseng.2019.09.007.
114. Benzo, M.; Mantovani, A.; Pittarello, A. Measurement of Odour Concentration of Immissions Using a New Field Olfactometer and Markers Chemical Analysis. *Chem. Eng. Trans.* **2012**, *30*, 103–108, doi:10.3303/CET1230018.
115. Miroslaw Szydlowski Comparison of Two Types of Field Olfactometers for Assessing Odours in Laboratory and Field Tests. *Chem. Eng. Trans.* **2014**, *40*, 67–72, doi:10.3303/CET1440012.
116. Capelli, L.; Sironi, S.; Del Rosso, R. Odor Sampling: Techniques and Strategies for the Estimation of Odor Emission Rates from Different Source Types. *Sensors* **2013**, *13*, 938–955, doi:10.3390/s130100938.
117. Kasper, P.; Mannebeck, D.; Oxbøl, A.; Nygaard, J.; Hansen, M.; Feilberg, A. Effects of Dilution Systems in Olfactometry on the Recovery of Typical Livestock Odorants Determined by PTR-MS. *Sensors* **2017**, *17*, 1859, doi:10.3390/s17081859.
118. Zarra, T.; Reiser, M.; Naddeo, V.; Belgiorno, V.; Kranert, M. A Comparative and Critical Evaluation of Different Sampling Materials in the Measurement of Odour Concentration

by Dynamic Olfactometry. *Chem. Eng. Trans.* **2012**, *30*, 307–312, doi:10.3303/CET1230052.
119. Gebicki, J.; Byliński, H.; Namieśnik, J. Measurement Techniques for Assessing the Olfactory Impact of Municipal Sewage Treatment Plants. *Environ. Monit. Assess.* **2016**, *188*, 32, doi:10.1007/s10661-015-5024-2.
120. Sówka, I.; Miller, U.; Sobczyński, P. Dynamic Olfactometry and Modeling as Methods for the Assessment of Odor Impact of Public Utility Objects. *Environ. Prot. Eng.* **2016**, *42*, 143–152.
121. Zarra, T.; Naddeo, V.; Belgiorno, V.; Reiser, M.; Kranert, M. Odour Monitoring of Small Wastewater Treatment Plant Located in Sensitive Environment. *Water Sci. Technol.* **2008**, *58*, 89–94, doi:10.2166/wst.2008.330.
122. Klarenbeek, J.V.; Ogink, N.W.M.; Van Der Voet, H. Odor Measurements According to EN 13725: A Statistical Analysis of Variance Components. *Atmos. Environ.* **2014**, *86*, 9–15, doi:10.1016/j.atmosenv.2013.12.032.
123. Elst, T.V.; Delva, J. The European Standard Pren 16841-2 (Determination of Odour in Ambient Air by Using Field Inspection: Plume Method): A Review of 20 Year Experience with the Method in Belgium. *Chem. Eng. Trans.* **2016**, *54*, 175–180, doi:10.3303/CET1654030.
124. Miller, U.; Jońca, J.; Pommier, S.; Fau, P.; Fajerwerg, K.; Kahn, M.L.; Sówka, I. Comprehensive Approach to Monitoring and Managing Odour Impacts from Biowaste Treatment Facilities. *Adv. Sci. Technol. Res. J.* **2026**, *20*, 87–102, doi:10.12913/22998624/215438.
125. Jońca, J.; Bezyk, Y.; Miller, U.; Wróbel, M.; Arsen, A.; Szrek, J.; Muraszkowski, A.; Włóka, A.; Janicka, A.; Sówka, I. Holistic Approach to Odour Impact Assessment on the Basis of Three Waste Management Plants. *Waste Manag.* **2025**, *208*, 115156, doi:10.1016/j.wasman.2025.115156.
126. Meacham, A.; Gowans, P.; Bradley-Clarke, J.; Swearingen, A.; Lord, S. Effectiveness of Malodor-Reducing Ostomy Pouch Additives: An Assessment of Odor Intensity, Hedonic Tone, and Odor Character. *Cureus* **2024**, doi:10.7759/cureus.65172.
127. Sucker, K.; Both, R.; Bischoff, M.; Guski, R.; Winneke, G. Odor Frequency and Odor Annoyance. Part I: Assessment of Frequency, Intensity and Hedonic Tone of Environmental Odors in the Field. *Int. Arch. Occup. Environ. Health* **2008**, *81*, 671–682, doi:10.1007/s00420-007-0259-z.
128. Sucker, K.; Both, R.; Bischoff, M.; Guski, R.; Krämer, U.; Winneke, G. Odor Frequency and Odor Annoyance Part II: Dose–Response Associations and Their Modification by Hedonic Tone. *Int. Arch. Occup. Environ. Health* **2008**, *81*, 683–694, doi:10.1007/s00420-007-0262-4.
129. Mauro, F.; Borghesi, R. Using Citizen Science to Manage Odour Emissions in National IED Plants: A Systematic Review of the Scientific Literature. *Atmosphere* **2024**, *15*, 302, doi:10.3390/atmos15030302.
130. Oliva, G.; Cangialosi, F.; Grimaldi, M.; Fasolino, I.; Belgiorno, V.; Naddeo, V.; Zarra, T. Urban Odour Annoyance Management: An Advanced Embedded System for Real-Time Monitoring Enhanced by Citizen Science. *Case Stud. Chem. Environ. Eng.* **2024**, *9*, 100712, doi:10.1016/j.cscee.2024.100712.
131. Özkal, C.B. Analysis of Annual Citizen Odor Observation Records and Its Relationship with Meteorological Factors: Çorlu / Tekirdağ Case Study. *Atmos. Pollut. Res.* **2023**, *14*, 101734, doi:10.1016/j.apr.2023.101734.
132. Gavros, A.; Hsu, Y.-C.; Karatzas, K. Modelling Smell Events in Urban Pittsburgh with Machine and Deep Learning Techniques. *Atmosphere* **2024**, *15*, 731, doi:10.3390/atmos15060731.
133. Vasiliki, S.; Charikleia, K.; Stavros, V. A Citizen Science Approach to Address Odour Pollution in Greece. *Chem. Eng. Trans.* **2024**, *112*, 85–90, doi:10.3303/CET24112015.
134. Wiśniewska, M.; Szyłak-Szydłowski, M. The Impact of Objects with a Potential Odour Nuisance on the Life Comfort of the Urban Agglomeration Inhabitants. *Appl. Sci.* **2024**, *14*, 10708, doi:10.3390/app142210708.
135. Rincón, C.A.; De Guardia, A.; Couvert, A.; Wolbert, D.; Le Roux, S.; Soutrel, I.; Nunes, G. Odor Concentration (OC) Prediction Based on Odor Activity Values (OAVs) during Composting of Solid Wastes and Digestates. *Atmos. Environ.* **2019**, *201*, 1–12, doi:10.1016/j.atmosenv.2018.12.030.

136. Hayes, J.E.; Barczak, R.J.; “Mel” Suffet, I.; Stuetz, R.M. The Use of Gas Chromatography Combined with Chemical and Sensory Analysis to Evaluate Nuisance Odours in the Air and Water Environment. *Environ. Int.* **2023**, *180*, 108214, doi:10.1016/j.envint.2023.108214.
137. Pillai, S.M. A Comparative Performance Study Using Dynamic Headspace Sampling and Sorbent Tube Methods of Broiler Litter Odour. *Int. J. Environ. Agric. Res.* **2025**, *11*.
138. Brattoli, M.; Cisternino, E.; Dambruoso, P.; De Gennaro, G.; Giungato, P.; Mazzone, A.; Palmisani, J.; Tutino, M. Gas Chromatography Analysis with Olfactometric Detection (GC-O) as a Useful Methodology for Chemical Characterization of Odorous Compounds. *Sensors* **2013**, *13*, 16759–16800, doi:10.3390/s131216759.
139. Byliński, H.; Kolasińska, P.; Dymerski, T.; Gębicki, J.; Namieśnik, J. Determination of Odour Concentration by TD-GC×GC–TOF-MS and Field Olfactometry Techniques. *Monatshefte Für Chem. - Chem. Mon.* **2017**, *148*, 1651–1659, doi:10.1007/s00706-017-2023-8.
140. Gao, W.; Yang, X.; Zhu, X.; Jiao, R.; Zhao, S.; Yu, J.; Wang, D. Limitations of GC-QTOF-MS Technique in Identification of Odorous Compounds from Wastewater: The Application of GC-IMS as Supplement for Odor Profiling. *Atmosphere* **2021**, *12*, 265, doi:10.3390/atmos12020265.
141. Wu, C.; Liu, J.; Yan, L.; Chen, H.; Shao, H.; Meng, T. Assessment of Odor Activity Value Coefficient and Odor Contribution Based on Binary Interaction Effects in Waste Disposal Plant. *Atmos. Environ.* **2015**, *103*, 231–237, doi:10.1016/j.atmosenv.2014.12.045.
142. Pei, J.; Sun, L. Odor from Building Air Conditioners: Emission Characteristics, Odor Compounds and Influencing Factors. *Sustainability* **2023**, *15*, 1495, doi:10.3390/su15021495.
143. Yu, H.; Xie, T.; Xie, J.; Ai, L.; Tian, H. Characterization of Key Aroma Compounds in Chinese Rice Wine Using Gas Chromatography-Mass Spectrometry and Gas Chromatography-Olfactometry. *Food Chem.* **2019**, *293*, 8–14, doi:10.1016/j.foodchem.2019.03.071.
144. Kozicki, M. Identification of Olfactory Nuisance of Floor Products Containing Bitumens with the TD–GC–MS/O Method. *Materials* **2022**, *15*, 959, doi:10.3390/ma15030959.
145. Hochereau, C.; Bruchet, A. Design and Application of a GC-SNIFF/MS System for Solving Taste and Odour Episodes in Drinking Water. *Water Sci. Technol.* **2004**, *49*, 81–87, doi:10.2166/wst.2004.0540.
146. Bulliner, E.A.; Koziel, J.A.; Cai, L.; Wright, D. Characterization of Livestock Odors Using Steel Plates, Solid-Phase Microextraction, and Multidimensional Gas Chromatography–Mass Spectrometry–Olfactometry. *J. Air Waste Manag. Assoc.* **2006**, *56*, 1391–1403, doi:10.1080/10473289.2006.10464547.
147. Clausen, P.A.; Knudsen, H.N.; Larsen, K.; Kofoed-Sørensen, V.; Wolkoff, P.; Wilkins, C.K. Use of Thermal Desorption Gas Chromatography–Olfactometry/Mass Spectrometry for the Comparison of Identified and Unidentified Odor Active Compounds Emitted from Building Products Containing Linseed Oil. *J. Chromatogr. A* **2008**, *1210*, 203–211, doi:10.1016/j.chroma.2008.09.073.
148. Barczak, R.J.; Fisher, R.M.; Le-Minh, N.; Stuetz, R.M. Importance of 2,4,6-Trichloroanisole (TCA) as an Odorant in the Emissions from Anaerobically Stabilized Dewatered Biosolids. *Chemosphere* **2019**, *236*, 124340, doi:10.1016/j.chemosphere.2019.07.071.
149. Hanková, M.; Maturová, K.; Čížková, H. GC-MS/O for the Characterization of Odours from Cheese-Production Wastewater: A Case Study. *Water Sci. Technol.* **2020**, *82*, 2482–2490, doi:10.2166/wst.2020.513.
150. Sadowska-Rociek, A.; Kurdziel, M.; Szczepaniec-Cięciak, E.; Riesenmey, C.; Vaillant, H.; Batton-Hubert, M.; Piejko, K. Analysis of Odorous Compounds at Municipal Landfill Sites. *Waste Manag. Res. J. Sustain. Circ. Econ.* **2009**, *27*, 966–975, doi:10.1177/0734242X09334616.
151. Wang, C.; Li, J.; Wu, X.; Zhang, Y.; He, Z.; Zhang, Y.; Zhang, X.; Li, Q.; Huang, J.; Liu, Z. Pu-Erh Tea Unique Aroma: Volatile Components, Evaluation Methods and Metabolic Mechanism of Key Odor-Active Compounds. *Trends Food Sci. Technol.* **2022**, *124*, 25–37, doi:10.1016/j.tifs.2022.03.031.
152. J., B.R.; Hubert, B.; Tomasz, D.; Jacek, G.; Jacek, N. Odorous Vocs Identification from Ageing Dewatered Anaerobically Stabilised Biosolids from Polish Wwtp by Two-

Dimensional Gas Chromatography Couple with Time-of-Flight Mass Spectrometry. *Chem. Eng. Trans.* **2021**, *85*, 43–48, doi:10.3303/CET2185008.
153. Cheng, Y.; Li, G.; Wu, H.; Huang, L.; Wang, H. Identification of Light-Induced Key Off-Flavors in Ponkan Mandarin Juice Using MDGC-MS/O and GC–MS/PFPD. *J. Agric. Food Chem.* **2021**, *69*, 14259–14269, doi:10.1021/acs.jafc.1c05465.
154. Deller, Z.; Giustozzi, F.; Maniam, S. Predicting Odorous Emissions from Bitumen Collected at 13 Refineries: A Combined GC–MS and Supervised Learning Approach. *Fuel* **2024**, *364*, 131142, doi:10.1016/j.fuel.2024.131142.
155. Bouguerra, M.D.E.; Witkowski, B.; Gierczak, T.; Barczak, R.J. Degradation Kinetics of Common Odorants Emitted from WWTPs: A Methodological Approach for Estimating Half-Life Through Reactions with Hydroxyl Radicals. *Atmosphere* **2025**, *16*, 340, doi:10.3390/atmos16030340.
156. Jiang, Y.; Yao, Y.; Liu, H.; Zhang, S.; Bai, X.; Ma, X.; Wang, Y.; Ren, Q. Volatile Organic Compounds Conversion Pathways and Odor Gas Emission Characteristics in Chicken Manure Composting Process. *Front. Ecol. Evol.* **2023**, *11*, 1192132, doi:10.3389/fevo.2023.1192132.
157. Wang, M.; Chen, Y. Electronic Nose and Its Application in the Food Industry: A Review. *Eur. Food Res. Technol.* **2024**, *250*, 21–67, doi:10.1007/s00217-023-04381-z.
158. Zhai, Z.; Liu, Y.; Li, C.; Wang, D.; Wu, H. Electronic Noses: From Gas-Sensitive Components and Practical Applications to Data Processing. *Sensors* **2024**, *24*, 4806, doi:10.3390/s24154806.
159. Rabehi, A.; Helal, H.; Zappa, D.; Comini, E. Advancements and Prospects of Electronic Nose in Various Applications: A Comprehensive Review. *Appl. Sci.* **2024**, *14*, 4506, doi:10.3390/app14114506.
160. Wilson, A.D.; Baietto, M. Applications and Advances in Electronic-Nose Technologies. *Sensors* **2009**, *9*, 5099–5148, doi:10.3390/s90705099.
161. Gliszczyńska-Świgło, A.; Chmielewski, J. Electronic Nose as a Tool for Monitoring the Authenticity of Food. A Review. *Food Anal. Methods* **2017**, *10*, 1800–1816, doi:10.1007/s12161-016-0739-4.
162. Yu, Y.; Cao, X.; Li, C.; Zhou, M.; Liu, T.; Liu, J.; Zhang, L. A Review of Machine Learning-Assisted Gas Sensor Arrays in Medical Diagnosis. *Biosensors* **2025**, *15*, 548, doi:10.3390/bios15080548.
163. Patel, H.; Garrido Portilla, V.; Shneidman, A.V.; Movilli, J.; Alvarenga, J.; Dupré, C.; Aizenberg, M.; Murthy, V.N.; Tropsha, A.; Aizenberg, J. Design Principles From Natural Olfaction for Electronic Noses. *Adv. Sci.* **2025**, *12*, 2412669, doi:10.1002/advs.202412669.
164. Al-Dayyeni, W.S.; Al-Yousif, S.; Taher, M.M.; Al-Faouri, A.W.; Tahir, N.M.; Jaber, M.M.; Ghabban, F.; Najm, I.A.; Alfadli, I.M.; Ameerbakhsh, O.Z.; et al. A Review on Electronic Nose: Coherent Taxonomy, Classification, Motivations, Challenges, Recommendations and Datasets. *IEEE Access* **2021**, *9*, 88535–88551, doi:10.1109/ACCESS.2021.3090165.
165. Kim, C.; Lee, K.K.; Kang, M.S.; Shin, D.-M.; Oh, J.-W.; Lee, C.-S.; Han, D.-W. Artificial Olfactory Sensor Technology That Mimics the Olfactory Mechanism: A Comprehensive Review. *Biomater. Res.* **2022**, *26*, 40, doi:10.1186/s40824-022-00287-1.
166. Hu, W.; Wan, L.; Jian, Y.; Ren, C.; Jin, K.; Su, X.; Bai, X.; Haick, H.; Yao, M.; Wu, W. Electronic Noses: From Advanced Materials to Sensors Aided with Data Processing. *Adv. Mater. Technol.* **2019**, *4*, 1800488, doi:10.1002/admt.201800488.
167. Röck, F.; Barsan, N.; Weimar, U. Electronic Nose: Current Status and Future Trends. *Chem. Rev.* **2008**, *108*, 705–725, doi:10.1021/cr068121q.
168. Baldwin, E.A.; Bai, J.; Plotto, A.; Dea, S. Electronic Noses and Tongues: Applications for the Food and Pharmaceutical Industries. *Sensors* **2011**, *11*, 4744–4766, doi:10.3390/s110504744.
169. Mohd Ali, M.; Hashim, N.; Abd Aziz, S.; Lasekan, O. Principles and Recent Advances in Electronic Nose for Quality Inspection of Agricultural and Food Products. *Trends Food Sci. Technol.* **2020**, *99*, 1–10, doi:10.1016/j.tifs.2020.02.028.
170. Zhang, W.; Tang, W.; Wan, Z.; Fan, Z. Advanced Electronic Noses for Future Robotic Olfaction. *Npj Robot.* **2026**, *4*, 11, doi:10.1038/s44182-025-00071-y.
171. Wilson, A.D. Review of Electronic-Nose Technologies and Algorithms to Detect Hazardous Chemicals in the Environment. *Procedia Technol.* **2012**, *1*, 453–463, doi:10.1016/j.protcy.2012.02.101.

172. Cipriano, D.; Capelli, L. Evolution of Electronic Noses from Research Objects to Engineered Environmental Odour Monitoring Systems: A Review of Standardization Approaches. *Biosensors* **2019**, *9*, 75, doi:10.3390/bios9020075.
173. Karakaya, D.; Ulucan, O.; Turkan, M. Electronic Nose and Its Applications: A Survey. *Int. J. Autom. Comput.* **2020**, *17*, 179–209, doi:10.1007/s11633-019-1212-9.
174. Liu, T.; Guo, L.; Wang, M.; Su, C.; Wang, D.; Dong, H.; Chen, J.; Wu, W. Review on Algorithm Design in Electronic Noses: Challenges, Status, and Trends. *Intell. Comput.* **2023**, *2*, 0012, doi:10.34133/icomputing.0012.
175. Gębicki, J.; Dymerski, T.; Rutkowski, S. Identification of Odor of Volatile Organic Compounds Using Classical Sensory Analysis and Electronic Nose Technique. *Environ. Prot. Eng.* **2014**, *40*, doi:10.37190/epe140108.
176. Esfahani, S.; Tiele, A.; Agbroko, S.O.; Covington, J.A. Development of a Tuneable NDIR Optical Electronic Nose. *Sensors* **2020**, *20*, 6875, doi:10.3390/s20236875.
177. Arshak, K.; Moore, E.; Lyons, G.M.; Harris, J.; Clifford, S. A Review of Gas Sensors Employed in Electronic Nose Applications. *Sens. Rev.* **2004**, *24*, 181–198, doi:10.1108/02602280410525977.
178. James, D.; Scott, S.M.; Ali, Z.; O'Hare, W.T. Chemical Sensors for Electronic Nose Systems. *Microchim. Acta* **2005**, *149*, 1–17, doi:10.1007/s00604-004-0291-6.
179. Berna, A. Metal Oxide Sensors for Electronic Noses and Their Application to Food Analysis. *Sensors* **2010**, *10*, 3882–3910, doi:10.3390/s100403882.
180. John, A.T.; Murugappan, K.; Nisbet, D.R.; Tricoli, A. An Outlook of Recent Advances in Chemiresistive Sensor-Based Electronic Nose Systems for Food Quality and Environmental Monitoring. *Sensors* **2021**, *21*, 2271, doi:10.3390/s21072271.
181. Sierra-Padilla, A.; García-Guzmán, J.J.; López-Iglesias, D.; Palacios-Santander, J.M.; Cubillana-Aguilera, L. E-Tongues/Noses Based on Conducting Polymers and Composite Materials: Expanding the Possibilities in Complex Analytical Sensing. *Sensors* **2021**, *21*, 4976, doi:10.3390/s21154976.
182. Wojnowski, W.; Majchrzak, T.; Dymerski, T.; Gębicki, J.; Namieśnik, J. Portable Electronic Nose Based on Electrochemical Sensors for Food Quality Assessment. *Sensors* **2017**, *17*, 2715, doi:10.3390/s17122715.
183. Gutierrez-Osuna, R. Pattern Analysis for Machine Olfaction: A Review. *IEEE Sens. J.* **2002**, *2*, 189–202, doi:10.1109/JSEN.2002.800688.
184. Wörner, J.; Eimler, J.; Pein-Hackelbusch, M. Long-Term Drift Behavior in Metal Oxide Gas Sensor Arrays: A One-Year Dataset from an Electronic Nose. *Sci. Data* **2025**, *12*, 1628, doi:10.1038/s41597-025-05993-8.
185. Scott, S.M.; James, D.; Ali, Z. Data Analysis for Electronic Nose Systems. *Microchim. Acta* **2006**, *156*, 183–207, doi:10.1007/s00604-006-0623-9.
186. Efendi, Y.; Naba, A.; Wardoyo, A.Y.P. Optimizing Electronic Nose Performance for Detecting Coconut Sap Preservatives: A Comparative Analysis of Feature Extraction and Machine Learning Techniques. *Trends Sci.* **2025**, *23*, doi:10.48048/tis.2026.11628.
187. Lin, J.; Zhan, X. Sensor-Drift Compensation in Electronic-Nose-Based Gas Recognition Using Knowledge Distillation. *Informatics* **2026**, *13*, 15, doi:10.3390/informatics13010015.
188. Kombo, K.O.; Ihsan, N.; Syahputra, T.S.; Hidayat, S.N.; Puspita, M.; Wahyono; Roto, R.; Triyana, K. Enhancing Classification Rate of Electronic Nose System and Piecewise Feature Extraction Method to Classify Black Tea with Superior Quality. *Sci. Afr.* **2024**, *24*, e02153, doi:10.1016/j.sciaf.2024.e02153.
189. Senge, J.M.; Kaltenecker, F.; Krupitzer, C. Integrating Sensor Data, Laboratory Analysis, and Computer Vision in Machine Learning-Driven E-Nose Systems for Predicting Tomato Shelf Life. *Chemosensors* **2025**, *13*, 255, doi:10.3390/chemosensors13070255.
190. Li, M.; Wu, C.; Wang, Z.; Wu, Z.; Huang, W.; Chen, J.; Yu, K.; Wen, T.; Yin, H.; Wang, Z. Enhanced Gas Classification in Electronic Nose Systems Using an SMOTE-Augmented Machine Learning Framework. *Sensors* **2026**, *26*, 714, doi:10.3390/s26020714.
191. Lin, Y.; Shi, J.; Xia, W.; Zhou, M.; Gao, Y. A Mixed Gas Component Identification and Concentration Estimation Method for Unbalanced Gas Sensor Array Samples. *Sensors* **2025**, *25*, 6254, doi:10.3390/s25196254.
192. Zaki Dizaji, H.; Adibzadeh, A.; Aghili Nategh, N. Application of E-Nose Technique to Predict Sugarcane Syrup Quality Based on Purity and Refined Sugar Percentage. *J. Food Sci. Technol.* **2021**, *58*, 4149–4156, doi:10.1007/s13197-020-04879-4.

193. Aguilera, T.; Lozano, J.; Paredes, J.A.; Álvarez, F.J.; Suárez, J.I. Electronic Nose Based on Independent Component Analysis Combined with Partial Least Squares and Artificial Neural Networks for Wine Prediction. *Sensors* **2012**, *12*, 8055–8072, doi:10.3390/s120608055.
194. Khorramifar, A.; Rasekh, M.; Karami, H.; Covington, J.A.; Derakhshani, S.M.; Ramos, J.; Gancarz, M. Application of MOS Gas Sensors Coupled with Chemometrics Methods to Predict the Amount of Sugar and Carbohydrates in Potatoes. *Molecules* **2022**, *27*, 3508, doi:10.3390/molecules27113508.
195. Tatli, S.; Mirzaee-Ghaleh, E.; Rabbani, H.; Karami, H.; Wilson, A.D. Prediction of Residual NPK Levels in Crop Fruits by Electronic-Nose VOC Analysis Following Application of Multiple Fertilizer Rates. *Appl. Sci.* **2022**, *12*, 11263, doi:10.3390/app122111263.
196. Rahman, K.S.; Salehin, M.M.; Roy, R.; Swarna, J.B.; Rakib, Md.R.I.; Saha, C.K.; Rahman, A. Prediction of Mango Quality during Ripening Stage Using MQ-Based Electronic Nose and Multiple Linear Regression. *Smart Agric. Technol.* **2024**, *9*, 100558, doi:10.1016/j.atech.2024.100558.
197. Muñoz-Castells, R.; Modesti, M.; Moreno-García, J.; Catini, A.; Capuano, R.; Di Natale, C.; Bellincontro, A.; Moreno, J. Application of an Electronic Nose to the Prediction of Odorant Series in Wines Obtained with Saccharomyces or Non-Saccharomyces Yeast Strains. *Molecules* **2025**, *30*, 1584, doi:10.3390/molecules30071584.
198. Wang, J.; Wang, W.; Xu, W.; An, H.; Ma, Q.; Sun, J.; Wang, J. Fusing Hyperspectral Imaging and Electronic Nose Data to Predict Moisture Content in Penaeus Vannamei during Solar Drying. *Front. Nutr.* **2024**, *11*, 1220131, doi:10.3389/fnut.2024.1220131.
199. Dennler, N.; Stark, E.; Collaku, S.; Larson, L.; van Schaik, A.; Schmuker, M.; Crimaldi, J.; Güntner, A.T.; True, A. Odour Sensing in Turbulent Plumes with High-Speed Electronic Nose and Non-Invasive Ground Truth 2026.
200. Romain, A.C.; Godefroid, D.; Kuske, M.; Nicolas, J. Monitoring the Exhaust Air of a Compost Pile as a Process Variable with an E-Nose. *Sens. Actuators B Chem.* **2005**, *106*, 29–35, doi:10.1016/j.snb.2004.05.033.
201. López, R.; Giráldez, I.; Palma, A.; Jesús Díaz, M. Assessment of Compost Maturity by Using an Electronic Nose. *Waste Manag.* **2016**, *48*, 174–180, doi:10.1016/j.wasman.2015.09.039.
202. Moufid, M.; Bouchikhi, B.; Tiebe, C.; Bartholmai, M.; El Bari, N. Assessment of Outdoor Odor Emissions from Polluted Sites Using Simultaneous Thermal Desorption-Gas Chromatography-Mass Spectrometry (TD-GC-MS), Electronic Nose in Conjunction with Advanced Multivariate Statistical Approaches. *Atmos. Environ.* **2021**, *256*, 118449, doi:10.1016/j.atmosenv.2021.118449.
203. Costa, A.; Maria Tangorra, F.; Zaninelli, M.; Oberti, R.; Guidobono Cavalchini, A.; Savoini, G.; Lazzari, M. Evaluating an E-Nose Ability to Detect Biogas Plant Efficiency: A Case Study. *Ital. J. Anim. Sci.* **2016**, *15*, 116–123, doi:10.1080/1828051X.2016.1147930.
204. Delgado-Rodríguez, M.; Ruiz-Montoya, M.; Giraldez, I.; López, R.; Madejón, E.; Díaz, M.J. Use of Electronic Nose and GC-MS in Detection and Monitoring Some VOC. *Atmos. Environ.* **2012**, *51*, 278–285, doi:10.1016/j.atmosenv.2012.01.006.
205. Gawande, T.; Deshmukh, R.; Deshmukh, S. Analysis of Outdoor Air Quality Using Low-Cost MEMS-Based Electronic Nose and Gas Analyzer With Multivariate Statistical Approach. *IEEE Embed. Syst. Lett.* **2025**, *17*, 18–21, doi:10.1109/LES.2024.3431214.
206. Lee, K.; Cho, I.; Kang, M.; Jeong, J.; Choi, M.; Woo, K.Y.; Yoon, K.-J.; Cho, Y.-H.; Park, I. Ultra-Low-Power E-Nose System Based on Multi-Micro-LED-Integrated, Nanostructured Gas Sensors and Deep Learning. *ACS Nano* **2023**, *17*, 539–551, doi:10.1021/acsnano.2c09314.
207. Giungato, P.; De Gennaro, G.; Barbieri, P.; Briguglio, S.; Amodio, M.; De Gennaro, L.; Lasigna, F. Improving Recognition of Odors in a Waste Management Plant by Using Electronic Noses with Different Technologies, Gas Chromatography–Mass Spectrometry/Olfactometry and Dynamic Olfactometry. *J. Clean. Prod.* **2016**, *133*, 1395–1402, doi:10.1016/j.jclepro.2016.05.148.
208. Zarra, T.; Galang, M.G.K.; Oliva, G.; Belgiorno, V. Smart Instrumental Odour Monitoring Station for the Efficient Odour Emission Management and Control in Wastewater Treatment Plants. *Chemosphere* **2022**, *309*, 136665, doi:10.1016/j.chemosphere.2022.136665.

209. Moufid, M.; Hofmann, M.; El Bari, N.; Tiebe, C.; Bartholmai, M.; Bouchikhi, B. Wastewater Monitoring by Means of E-Nose, VE-Tongue, TD-GC-MS, and SPME-GC-MS. *Talanta* **2021**, *221*, 121450, doi:10.1016/j.talanta.2020.121450.
210. Romero-Flores, A.; McConnell, L.L.; Hapeman, C.J.; Ramirez, M.; Torrents, A. Evaluation of an Electronic Nose for Odorant and Process Monitoring of Alkaline-Stabilized Biosolids Production. *Chemosphere* **2017**, *186*, 151–159, doi:10.1016/j.chemosphere.2017.07.135.
211. Zarra, T.; Reiser, M.; Naddeo, V.; Belgiorno, V.; Kranert, M. Odour Emissions Characterization from Wastewater Treatment Plants by Different Measurement Methods. *Chem. Eng. Trans.* **2014**, *40*, 37–42, doi:10.3303/CET1440007.
212. Prudenza, S.; Panzitta, A.; Bax, C.; Capelli, L. Electronic Nose for Real-Time Monitoring of Odour Emissions at a Wastewater Treatment Plant. *Chem. Eng. Trans.* **2022**, *95*, 169–174, doi:10.3303/CET2295029.
213. Gutiérrez, M.C.; Chica, A.F.; Martín, M.A.; Romain, A.-C. Compost Pile Monitoring Using Different Approaches: GC–MS, E-Nose and Dynamic Olfactometry. *Waste Biomass Valorization* **2014**, *5*, 469–479, doi:10.1007/s12649-013-9240-0.
214. Sohn, J.H.; Smith, R.; Yoong, E.; Leis, J.; Galvin, G. Quantification of Odours from Piggery Effluent Ponds Using an Electronic Nose and an Artificial Neural Network. *Biosyst. Eng.* **2003**, *86*, 399–410, doi:10.1016/j.biosystemseng.2003.09.003.
215. Sohn, J.H.; Hudson, N.; Gallagher, E.; Dunlop, M.; Zeller, L.; Atzeni, M. Implementation of an Electronic Nose for Continuous Odour Monitoring in a Poultry Shed. *Sens. Actuators B Chem.* **2008**, *133*, 60–69, doi:10.1016/j.snb.2008.01.053.
216. Stuetz, R.M.; Fenner, R.A.; Engin, G. Assessment of Odours from Sewage Treatment Works by an Electronic Nose, H2S Analysis and Olfactometry. *Water Res.* **1999**, *33*, 453–461, doi:10.1016/S0043-1354(98)00246-2.
217. Sironi, S.; Capelli, L.; Céntola, P.; Del Rosso, R. Development of a System for the Continuous Monitoring of Odours from a Composting Plant: Focus on Training, Data Processing and Results Validation Methods. *Sens. Actuators B Chem.* **2007**, *124*, 336–346, doi:10.1016/j.snb.2006.12.037.
218. Romain, A.-C.; Delva, J.; Nicolas, J. Complementary Approaches to Measure Environmental Odours Emitted by Landfill Areas. *Sens. Actuators B Chem.* **2008**, *131*, 18–23, doi:10.1016/j.snb.2007.12.005.
219. Romain, A.-C.; André, Ph.; Nicolas, J. Three Years Experiment with the Same Tin Oxide Sensor Arrays for the Identification of Malodorous Sources in the Environment. *Sens. Actuators B Chem.* **2002**, *84*, 271–277, doi:10.1016/S0925-4005(02)00036-9.
220. Gębicki, J.; Dymerski, T.; Namieśnik, J. Investigation of Air Quality beside a Municipal Landfill: The Fate of Malodour Compounds as a Model VOC. *Environments* **2017**, *4*, 7, doi:10.3390/environments4010007.
221. Sironi, S.; Capelli, L.; Céntola, P.; Del Rosso, R.; Il Grande, M. Continuous Monitoring of Odours from a Composting Plant Using Electronic Noses. *Waste Manag.* **2007**, *27*, 389–397, doi:10.1016/j.wasman.2006.01.029.
222. Oliva, G.; Zarra, T.; Pittoni, G.; Senatore, V.; Galang, M.G.; Castellani, M.; Belgiorno, V.; Naddeo, V. Next-Generation of Instrumental Odour Monitoring System (IOMS) for the Gaseous Emissions Control in Complex Industrial Plants. *Chemosphere* **2021**, *271*, 129768, doi:10.1016/j.chemosphere.2021.129768.
223. Zarra, T.; Galang, M.G.K.; Belgiorno, V.; Naddeo, V. Environmental Odour Quantification by IOMS: Parametric vs. Non-Parametric Prediction Techniques. *Chemosensors* **2021**, *9*, 183, doi:10.3390/chemosensors9070183.
224. Lotesoriere, B.J.; Bax, C.; Capelli, L. Electronic Nose for Odor Monitoring at a Landfill Fenceline: Training and Validation of a Model for Real-Time Odor Concentration Measurement. *Heliyon* **2024**, *10*, e31103, doi:10.1016/j.heliyon.2024.e31103.
225. Ratti, C.; Bax, C.; Lotesoriere, B.J.; Capelli, L. Real-Time Monitoring of Odour Emissions at the Fenceline of a Waste Treatment Plant by Instrumental Odour Monitoring Systems: Focus on Training Methods. *Sensors* **2024**, *24*, 3506, doi:10.3390/s24113506.
226. Bax, C.; Lotesoriere, B.; Laura, C. Real-Time Monitoring of Odour Concentration at a Landfill Fenceline: Performance Verification in the Field. *Chem. Eng. Trans.* **2021**, *85*, 19–24, doi:10.3303/CET2185004.
227. Prudenza, S.; Bax, C.; Capelli, L. Real-Time Monitoring of Odour Concentration at the Inlet of an Abatement System by IOMS. *Chem. Eng. Trans.* **2024**, *112*, 139–144, doi:10.3303/CET24112024.

228. Prudenza, S.; Bax, C.; Capelli, L.C.L. Real-Time Monitoring of Odour Concentration at Emission Sources by IOMS: Comparison of Different Regression Models. In Proceedings of the 2024 IEEE International Symposium on Olfaction and Electronic Nose (ISOEN); IEEE: Grapevine, TX, USA, May 12 2024; pp. 1–4.
229. Prudenza, S.; Bax, C.; Capelli, L. OT5.73 - Continuous Monitoring of Odour Concentration at the Inlet of a Scrubber with an E-Nose: Focus on the Management of Interferences. In Proceedings of the Lectures; AMA Service GmbH, Von-Münchhausen-Str. 49, 31515 Wunstorf: Debrecen (Hungary), 2024; pp. 101–102.
230. Rybarczyk, P.; Szulczyński, B.; Gębicki, J. Simultaneous Removal of Hexane and Ethanol from Air in a Biotrickling Filter—Process Performance and Monitoring Using Electronic Nose. *Sustainability* **2020**, *12*, 387, doi:10.3390/su12010387.
231. Szulczyński, B.; Rybarczyk, P.; Gospodarek, M.; Gębicki, J. Biotrickling Filtration of N-Butanol Vapors: Process Monitoring Using Electronic Nose and Artificial Neural Network. *Monatshefte Für Chem. - Chem. Mon.* **2019**, *150*, 1667–1673, doi:10.1007/s00706-019-02456-w.
232. Szulczyński, B.; Rybarczyk, P.; Gębicki, J. Monitoring of N-Butanol Vapors Biofiltration Process Using an Electronic Nose Combined with Calibration Models. *Monatshefte Für Chem. - Chem. Mon.* **2018**, *149*, 1693–1699, doi:10.1007/s00706-018-2243-6.
233. Szulczyński, B.; Gębicki, J.; Namieśnik, J. Monitoring and Efficiency Assessment of Biofilter Air Deodorization Using Electronic Nose Prototype. *Chem. Pap.* **2018**, *72*, 527–532, doi:10.1007/s11696-017-0310-9.
234. Cangialosi, F.; Fornaro, A. Advancements in Instrumental Odour Monitoring System from Stationary Emission Sources. *Chem. Eng. Trans.* **2024**, *112*, 103–108, doi:10.3303/CET24112018.
235. López, R.; Cabeza, I.O.; Giráldez, I.; Díaz, M.J. Biofiltration of Composting Gases Using Different Municipal Solid Waste-Pruning Residue Composts: Monitoring by Using an Electronic Nose. *Bioresour. Technol.* **2011**, *102*, 7984–7993, doi:10.1016/j.biortech.2011.05.085.
236. Cabeza, I.O.; López, R.; Giraldez, I.; Stuetz, R.M.; Díaz, M.J. Biofiltration of α-Pinene Vapours Using Municipal Solid Waste (MSW) – Pruning Residues (P) Composts as Packing Materials. *Chem. Eng. J.* **2013**, *233*, 149–158, doi:10.1016/j.cej.2013.08.032.
237. Rybarczyk, P.; Szulczyński, B.; Gospodarek, M.; Gębicki, J. Effects of N-Butanol Presence, Inlet Loading, Empty Bed Residence Time and Starvation Periods on the Performance of a Biotrickling Filter Removing Cyclohexane Vapors from Air. *Chem. Pap.* **2020**, *74*, 1039–1047, doi:10.1007/s11696-019-00943-2.
238. Sohn, J.H.; Dunlop, M.; Hudson, N.; Kim, T.I.; Yoo, Y.H. Non-Specific Conducting Polymer-Based Array Capable of Monitoring Odour Emissions from a Biofiltration System in a Piggery Building. *Sens. Actuators B Chem.* **2009**, *135*, 455–464, doi:10.1016/j.snb.2008.10.007.
239. Liang, Z.; Wang, J.; Zhang, Y.; Han, C.; Ma, S.; Chen, J.; Li, G.; An, T. Removal of Volatile Organic Compounds (VOCs) Emitted from a Textile Dyeing Wastewater Treatment Plant and the Attenuation of Respiratory Health Risks Using a Pilot-Scale Biofilter. *J. Clean. Prod.* **2020**, *253*, 120019, doi:10.1016/j.jclepro.2020.120019.
240. Hassanalian, M.; Abdelkefi, A. Classifications, Applications, and Design Challenges of Drones: A Review. *Prog. Aerosp. Sci.* **2017**, *91*, 99–131, doi:10.1016/j.paerosci.2017.04.003.
241. Filkin, T.; Sliusar, N.; Ritzkowski, M.; Huber-Humer, M. Unmanned Aerial Vehicles for Operational Monitoring of Landfills. *Drones* **2021**, *5*, 125, doi:10.3390/drones5040125.
242. Hossain, K.; Villebro, F.; Forchhammer, S. UAV Image Analysis for Leakage Detection in District Heating Systems Using Machine Learning. *Pattern Recognit. Lett.* **2020**, *140*, 158–164, doi:10.1016/j.patrec.2020.05.024.
243. Tanda, G.; Balsi, M.; Fallavollita, P.; Chiarabini, V. A UAV-Based Thermal-Imaging Approach for the Monitoring of Urban Landfills. *Inventions* **2020**, *5*, 55, doi:10.3390/inventions5040055.
244. Burgués, J.; Esclapez, M.D.; Doñate, S.; Pastor, L.; Marco, S. Aerial Mapping of Odorous Gases in a Wastewater Treatment Plant Using a Small Drone. *Remote Sens.* **2021**, *13*, 1757, doi:10.3390/rs13091757.
245. Burgués, J.; Doñate, S.; Esclapez, M.D.; Saúco, L.; Marco, S. Characterization of Odour Emissions in a Wastewater Treatment Plant Using a Drone-Based Chemical Sensor System. *Sci. Total Environ.* **2022**, *846*, 157290, doi:10.1016/j.scitotenv.2022.157290.

246. Kim, E.; Lee, S.; Kim, J.; Kim, C.; Byun, Y.; Kim, H.; Lee, T. Pattern Recognition for Selective Odor Detection with Gas Sensor Arrays. *Sensors* **2012**, *12*, 16262–16273, doi:10.3390/s121216262.
247. Bretschneider, L.; Bollmann, S.; Houssin-Agbomson, D.; Shaw, J.; Howes, N.; Nguyen, L.; Robinson, R.; Helmore, J.; Lichtenstern, M.; Nwaboh, J.; et al. Concepts for Drone Based Pipeline Leak Detection. *Front. Robot. AI* **2024**, *11*, 1426206, doi:10.3389/frobt.2024.1426206.
248. Sonkar, S.K.; Kumar, P.; George, R.C.; Philip, D.; Ghosh, A.K. Detection and Estimation of Natural Gas Leakage Using UAV by Machine Learning Algorithms. *IEEE Sens. J.* **2022**, *22*, 8041–8049, doi:10.1109/JSEN.2022.3157872.
249. Arroyo, P.; Gómez-Suárez, J.; Herrero, J.L.; Lozano, J. Electrochemical Gas Sensing Module Combined with Unmanned Aerial Vehicles for Air Quality Monitoring. *Sens. Actuators B Chem.* **2022**, *364*, 131815, doi:10.1016/j.snb.2022.131815.
250. Fosco, D.; Molfetta, M.D.; Renzulli, P.; Notarnicola, B.; Carella, C.; Fedele, G. Innovative Drone-Based Methodology for Quantifying Methane Emissions from Landfills. *Waste Manag.* **2025**, *195*, 79–91, doi:10.1016/j.wasman.2025.01.033.
251. Montoya, J.M.; Olsson, A.; Martensson, S.-G.; Chilo, J. Drone Gas Concentration Measurement System for Landfills. In Proceedings of the 2020 IEEE International Instrumentation and Measurement Technology Conference (I2MTC); IEEE: Dubrovnik, Croatia, May 2020; pp. 1–5.
252. Hashim, M.; Ng, H.L.; Zakari, D.M.; Sani, D.A.; Chindo, M.M.; Hassan, N.; Azmy, M.M.; Pour, A.B. Mapping of Greenhouse Gas Concentration in Peninsular Malaysia Industrial Areas Using Unmanned Aerial Vehicle-Based Sniffer Sensor. *Remote Sens.* **2023**, *15*, 255, doi:10.3390/rs15010255.
253. Camarillo-Escobedo, R.; Flores, J.L.; Marin-Montoya, P.; García-Torales, G.; Camarillo-Escobedo, J.M. Smart Multi-Sensor System for Remote Air Quality Monitoring Using Unmanned Aerial Vehicle and LoRaWAN. *Sensors* **2022**, *22*, 1706, doi:10.3390/s22051706.
254. Abeywickrama, H.G.K.; Bajón-Fernández, Y.; Srinamasivayam, B.; Turner, D.; Rivas Casado, M. Development of a UAV Based Framework for CH4 Monitoring in Sludge Treatment Centres. *Remote Sens.* **2023**, *15*, 3704, doi:10.3390/rs15153704.
255. Andersen, T.; Vinkovic, K.; De Vries, M.; Kers, B.; Necki, J.; Swolkien, J.; Roiger, A.; Peters, W.; Chen, H. Quantifying Methane Emissions from Coal Mining Ventilation Shafts Using an Unmanned Aerial Vehicle (UAV)-Based Active AirCore System. *Atmos. Environ. X* **2021**, *12*, 100135, doi:10.1016/j.aeaoa.2021.100135.
256. Yong, H.; Allen, G.; Mcquilkin, J.; Ricketts, H.; Shaw, J.T. Lessons Learned from a UAV Survey and Methane Emissions Calculation at a UK Landfill. *Waste Manag.* **2024**, *180*, 47–54, doi:10.1016/j.wasman.2024.03.025.
257. Liu, S.; Yang, X.; Zhou, X. Development of a Low-Cost UAV-Based System for CH_4 Monitoring over Oil Fields. *Environ. Technol.* **2021**, *42*, 3154–3163, doi:10.1080/09593330.2020.1724199.
258. Liu, Y.; Paris, J.-D.; Vrekoussis, M.; Antoniou, P.; Constantinides, C.; Desservettaz, M.; Keleshis, C.; Laurent, O.; Leonidou, A.; Philippon, C.; et al. Improvements of a Low-Cost CO_2 Commercial Nondispersive near-Infrared (NDIR) Sensor for Unmanned Aerial Vehicle (UAV) Atmospheric Mapping Applications. *Atmos. Meas. Tech.* **2022**, *15*, 4431–4442, doi:10.5194/amt-15-4431-2022.
259. Yao Yao; Wei Shanlin; Zhang Honghui; Li Qiong Application of Uav in Monitoring Chemical Pollutant Gases. *Chem. Eng. Trans.* **2018**, *67*, 583–588, doi:10.3303/CET1867098.
260. Singh, S.S.; Themvinah, A.S.; Sharma, T.S.; Katrimsha Tarao, D.; Shougaijam, B.; Singh, T.C.; Bigensana Singh, R.K. Real-Time Monitoring of Atmospheric Air Pollutants Using Sensor Integrated UAV. In Proceedings of the 2024 International Conference on Electrical Electronics and Computing Technologies (ICEECT); IEEE: Greater Noida, India, August 29 2024; pp. 1–6.
261. Nicolas, J.; Cerisier, C.; Delva, J.; Romain, A.C. Potential of a Network of Electronic Noses to Assess in Real Time the Odour Annoyance in the Environment of a Compost Facility. *Chem. Eng. Trans.* **2012**, *30*, 133–138, doi:10.3303/CET1230023.
262. Mifsud, J.-C.; Ayouni, F. On Line Monitoring of Odour Emissions (OU) and Odour Sources Identification by Using a New Generation of IOMS Analyzers around an Animal Feed

Production Plant. In Proceedings of the 2024 IEEE International Symposium on Olfaction and Electronic Nose (ISOEN); IEEE: Grapevine, TX, USA, May 12 2024; pp. 1–3.
263. Dobrzyniewski, D.; Szulczyński, B.; Gębicki, J. Application of a Gas Sensor Array to Effectiveness Monitoring of Air Contaminated with Toluene Vapors Absorption Process. *J. Ecol. Eng.* **2022**, *23*, 269–282, doi:10.12911/22998993/152427.
264. Wolfrum, E.J.; Meglen, R.M.; Peterson, D.; Sluiter, J. Metal Oxide Sensor Arrays for the Detection, Differentiation, and Quantification of Volatile Organic Compounds at Sub-Parts-per-Million Concentration Levels. *Sens. Actuators B Chem.* **2006**, *115*, 322–329, doi:10.1016/j.snb.2005.09.026.
265. Szczurek, A.; Maciejewska, M.; Flisowska-Wiercik, B.; Bodzoj, Ł. Application of a Sensor System for Determining the Kind and Quantity of Two Component VOC Mixtures in Air after the Use of Solvents. *J. Environ. Monit.* **2009**, *11*, 1942, doi:10.1039/b907820g.
266. Singh, S.; S, S.; Poornima; Sreelekha, G.; Adak, C.; Shukla, R.P.; Kamble, V. Metal Oxide-Based Gas Sensor Array for the VOCs Analysis in Complex Mixtures Using Machine Learning 2023.
267. Dobrzyniewski, D.; Szulczyński, B.; Rybarczyk, P.; Gębicki, J. Process control of air stream deodorization from vapors of VOCs using a gas sensor matrix conducted in the biotrickling filter (BTF). *Arch. Environ. Prot.* **2023**, 85–94, doi:10.24425/aep.2023.145900.
268. Yu, G.; Wang, G.; Wang, S.; Yang, C.; Chen, H.; Zhu, Y.; Yu, L.; Li, J.; Kazemian, H. Performance Promotion and Its Mechanism for N-Hexane Removal in a Lab-Scale Biotrickling Filter with Reticular Polyurethane Sponge under Intermittent Spraying Mode. *Process Saf. Environ. Prot.* **2021**, *152*, 654–662, doi:10.1016/j.psep.2021.06.029.
269. Cheng, Y.; He, H.; Yang, C.; Yan, Z.; Zeng, G.; Qian, H. Effects of Anionic Surfactant on N-Hexane Removal in Biofilters. *Chemosphere* **2016**, *150*, 248–253, doi:10.1016/j.chemosphere.2016.02.027.
270. Salamanca, D.; Dobslaw, D.; Engesser, K.-H. Removal of Cyclohexane Gaseous Emissions Using a Biotrickling Filter System. *Chemosphere* **2017**, *176*, 97–107, doi:10.1016/j.chemosphere.2017.02.078.
271. Słupek, E.; Dobrzyniewski, D.; Makoś-Chełstowska, P.; Szulczyński, B.; Gębicki, J. Monitoring of Absorptive Model Biogas Purification Process Using Sensor Matrices and Gas Chromatography. *Measurement* **2025**, *239*, 115436, doi:10.1016/j.measurement.2024.115436.
272. Makoś-Chełstowska, P. VOCs Absorption from Gas Streams Using Deep Eutectic Solvents – A Review. *J. Hazard. Mater.* **2023**, *448*, 130957, doi:10.1016/j.jhazmat.2023.130957.
273. Moufawad, T.; Costa Gomes, M.; Fourmentin, S. Deep Eutectic Solvents as Absorbents for VOC and VOC Mixtures in Static and Dynamic Processes. *Chem. Eng. J.* **2022**, *448*, 137619, doi:10.1016/j.cej.2022.137619.
274. Gui, C.; Villarim, P.; Lei, Z.; Fourmentin, S. VOC Absorption in Supramolecular Deep Eutectic Solvents: Experiment and Molecular Dynamic Studies. *Chem. Eng. J.* **2024**, *481*, 148708, doi:10.1016/j.cej.2024.148708.
275. Han, J.; Li, H.; Cheng, J.; Ma, X.; Fu, Y. Advances in Metal Oxide Semiconductor Gas Sensor Arrays Based on Machine Learning Algorithms. *J. Mater. Chem. C* **2025**, *13*, 4285–4303, doi:10.1039/D4TC05220J.
276. Dobrzyniewski, D.; Szulczyński, B.; Gębicki, J. Determination of Odor Air Quality Index (OAQII) Using Gas Sensor Matrix. *Molecules* **2022**, *27*, 4180, doi:10.3390/molecules27134180.
277. Szyłak-Szydłowski, M.; Kos, W.; Tarakowski, R.; Tkaczyk, M.; Borowik, P. Assessment of Odour Emission During the Composting Process by Using Olfactory Methods and Gas Sensor Array Measurements. *Sensors* **2025**, *25*, 3153, doi:10.3390/s25103153.

List of Figures

Figure 1. Methods of odor analysis and their characterization in providing chemical information, sensory information, and potential for real-time odor monitoring. 14

Figure 2. Examples of osmophore groups of chemical compounds with their corresponding olfactory thresholds [43,44]. 16

Figure 3. The main sources of malodorous substance emissions in the environment. 22

Figure 4. Classification of methods for reducing odorous gas pollution. 28

Figure 5. Process flow diagram of an absorptive gas deodorization system comprising an absorption and desorption column. 30

Figure 6. Schematic representation of a traditional biofilter used for biological waste gas treatment. 32

Figure 7. Process flow diagram of a bioscrubber consisting of an absorption column and a bioreactor. 34

Figure 8. Process flow diagram of a biotrickling filter (BTF). 35

Figure 9. Odor emission reduction system based on aerosol misting technology (spraying installation and mist cannon). 37

Figure 10. General structure of the division of measurement methods used in the assessment of odor nuisance. 39

Figure 11. In-situ odor concentration measurement using the Nasal Ranger portable olfactometer. 42

Figure 12. Methods of sampling odor gases from point and surface sources for determining odor concentration by dynamic olfactometry. 44

Figure 13. A classification of odor in the form of an *odor wheel*, including the main odor groups and their descriptors. 45

Figure 14. Simplified schematic diagram of the GC-O system for identifying odorants. 49

Figure 15. Schematic comparison of the mechanism of odor perception in the human olfactory system and the process of odor analysis by e-nose. 52

Figure 16. Schematic representation of the structure and operating principle of a MOS-type sensor. 55

Figure 17. Schematic representation of the structure and operating principle of an EC gas sensor. 56

Figure 18. Schematic representation of the structure and operating principle of a photoionization detector. 57

Figure 19. Structure of data processing and identification obtained from e-noses. 59

Figure 20. Schematic diagram of the measurement setup for monitoring the absorption of toluene vapor. Adapted from [263], licensed by CC BY 4.0. 75

Figure 21. Structure of the pneumatic system (a) and general view of the gas sensor array prototype (b). Adapted from [263], licensed by CC BY 4.0. 76

Figure 22. Breakthrough curves of toluene (a) and acetone (b) during the absorption process. Points represent the mean values of the three replicate chromatographic analyses, and error bars indicate standard deviation (±SD). Adapted from [263], licensed by CC BY 4.0. 80

Figure 23. MLR calibration chart: toluene concentration determined by the model relative to GC-FID reference values. Reproduced from [263], licensed by CC BY 4.0. 81

Figure 24. Monitoring of the toluene absorption process: (a) inlet and outlet concentrations determined by GC-FID and MLR model; (b) absolute prediction errors; (c) absorptivity values determined from GC-FID and MLR results. Concentration values in panel (a) represent means of three replicate analyses, and error bars indicate standard deviations (±SD). Adapted from [288], licensed under CC BY 4.0. 82

Figure 25. Monitoring of toluene absorption in the presence of acetone: (a) inlet and outlet concentrations determined by GC-FID and MLR model; (b) absolute prediction errors; (c) absorptivity values determined from GC-FID and MLR results. Concentration values in panel (a) represent means of three replicate analyses, and error bars indicate standard deviations (±SD). Adapted from [288], licensed under CC BY 4.0. 84

Figure 26. Laboratory set-up for monitoring the biofiltration of n-hexane and cyclohexane in a BTF. Adapted from [267], licensed by CC BY-SA 4.0. 88

Figure 27. Structure of the pneumatic system (a) and general view of the gas sensor array prototype (b) used in the biofiltration process. Adapted from [267], licensed by CC BY-SA 4.0. 89

Figure 28. Structure of a generator for gas calibration mixtures with a sample humidification section. Adapted from [267], licensed by CC BY-SA 4.0. 91

Figure 29. Normalized responses of the gas sensor array to increasing concentrations of cyclohexane: (a) ΔS and (b) S_r, and n-hexane: (c) ΔS and (d) S_r. Points represent mean sensor responses at individual calibration concentrations, while lines connect consecutive concentration levels. Responses were normalized separately for each sensor signal using min–max scaling. 95

Figure 30. Pearson correlation coefficients between calibration concentration and sensor response characteristics (ΔS and S_r), temperature (T), and relative humidity (RH) for cyclohexane and n-hexane. Bar length and colour represent the magnitude and direction of Pearson's correlation coefficient (r). Asterisks indicate statistical significance after Benjamini–Hochberg correction (* $0.01 \leq p_{BH} < 0.05$, ** $0.001\ p_{BH} < 0.01$, *** $p_{BH} < 0.001$). 96

Figure 31. Calibration plots of the gas sensor array predictive models for cyclohexane: (a) MLR and (b) PCR, and n-hexane: (c) MLR and (d) PCR. Points represent concentrations predicted by the models versus reference GC-FID values. Solid lines indicate linear fits, while dashed lines represent the 1:1 agreement line. Adapted from [267], licensed by CC BY-SA 4.0. 98

Figure 32. Mean residuals of calibration model predictions for cyclohexane: (a) MLR and (b) PCR, and n-hexane: (c) MLR and (d) PCR. Points represent mean residuals, while error bars indicate ±SD for repeated measurements. The dashed horizontal line denotes zero residual. 99

Figure 33. Changes in removal efficiency (RE) and inlet loading (IL) during the biotrickling filtration of cyclohexane (a) and n-hexane (b). RE values were determined using the reference GC-FID method and predicted by the gas sensor array with PCR and MLR models. Inlet loading is presented on the secondary y-axis. Dashed vertical lines indicate the boundaries between the three process stages. 101

Figure 34. A test setup for the quantitative determination of acetone, toluene, and cyclohexane in a model biogas purification process. Adapted from [271], © 2024 Elsevier Ltd. 107

Figure 35. Structure of the pneumatic system (a) and general view of the gas sensor array prototype (b) used in the model biogas absorption process. Adapted from [271], © 2024 Elsevier Ltd. 108

Figure 36. Schematic diagram of the system for preparing calibration gas mixtures. Adapted from [271], © 2024 Elsevier Ltd. 111

Figure 37. Schematic of the measurement setup used to determine the effect of the absorbent on sensor signals and to determine the corrected baseline. Adapted from [271], © 2024 Elsevier Ltd. 112

Figure 38. Comparison of reference concentrations determined by GC-FID with concentrations predicted using MLR and PCR models for acetone (a, b), cyclohexane (c, d), and toluene (e, f). The dashed line represents perfect agreement between reference and predicted values (1:1), while solid lines indicate linear fits for the respective models. Adapted from [271], © 2024 Elsevier Ltd. 119

Figure 39. Distribution of residuals for MLR and PCR calibration models developed for acetone (a, b), cyclohexane (c, d), and toluene (e, f). Residuals were calculated as the difference between predicted and reference concentrations. The dashed horizontal line indicates zero residual. 121

Figure 40. Evolution of absorptivity during model biogas purification monitored by GC-FID and the gas sensor array with MLR and PCR models. Toluene: (a, b), acetone: (c, d), cyclohexane: (e, f). Genosorb: (a, c, e), OA:NA (1:1): (b, d, f). Reproduced from [271], © 2024 Elsevier Ltd. 122

Figure 41. P-B comparison of GC and gas sensor array results obtained using MLR and PCR models for acetone (a, b), cyclohexane (c, d) , and toluene (e, f) removal with Genosorb. Black line - regression fit, red line - identity line, blue dashed lines - 95% confidence limits. Adopted from [271], © 2024 Elsevier Ltd. 125

Figure 42. P-B comparison of GC and gas sensor array results obtained using MLR and PCR models for acetone (a, b), cyclohexane (c, d), and toluene (e, f) removal with OA:NA (1:1). Black line - regression fit, red line - identity line, blue dashed lines - 95% confidence limits. Adopted from [271], © 2024 Elsevier Ltd. 126

Figure 43. Bland-Altman comparison of GC and gas sensor array results obtained using MLR and PCR models for acetone (a, b), cyclohexane (c, d), and toluene (e, f) removal with Genosorb. Solid line - mean difference, dashed lines - mean ± 1.96 SD. Adopted from [271], © 2024 Elsevier Ltd. 129

Figure 44. Bland-Altman comparison of GC and gas sensor array results obtained using MLR and PCR models for acetone (a, b), cyclohexane (c, d), and toluene (e, f) removal with OA:NA (1:1). Solid line - mean difference, dashed lines - mean ± 1.96 SD. Adopted from [271], © 2024 Elsevier Ltd. 130

Figure 45. Study site location: (a) boundary of the Waste Utilization Facility Ltd. in Gdańsk, (b) enlarged view of the active landfill cell selected for the UAV measurements. 135

Figure 46. The DJI Phantom 4 Pro mobile UAV measurement platform in operational conditions: (a) the device on the launch platform prepared for data collection, (b) the drone during a measurement flight over the landfill site, (c) monitoring in the immediate vicinity of the degassing well. 136

Figure 47. Architecture and technical implementation of the measurement module: (a) view of the actual electronic system integrated with the sensor array, (b) block diagram showing the internal architecture and signal flow from the sensors to the data recording system. 136

Figure 48. Situation plan of the research area over the active landfill cell: visualization of the UAV measurement flight trajectory with the marked operational area and the location of the points (P1–P9) where gas samples were collected for analysis using the dynamic olfactometry method. 137

Figure 49. Generating a regular grid of spatial data in QGIS: visualization of the conversion of a concentration raster into a set of points with a resolution of 0.5 m², constituting the input for estimating odor concentration and odor emissions. 139

Figure 50. Gas sampling from the landfill cell surface: application of a flux chamber (0.5 m^2 area) to obtain landfill gas samples for reference olfactometric analyses. 140

Figure 51. Characteristics of the metrological conditions of the measurement campaigns: (a) metrological station used to record atmospheric parameters, (b) wind rose showing the distribution of wind directions and speeds, consulting a metrological input for modeling odor dispersion. 144

Figure 52. Reconstructed gas concentration fields (TIN interpolation from UAV flights) overlaid on point based dynamic olfactometry measurement results: (a) H_2S, (b) NH_3, (c) CH_4, (d) CO_2, (e) VOCs. 146

Figure 53. Comparison of measured and predicted values obtained using the developed calibration models: (a) logarithmically transformed odor concentration $\log(C_{od})$, (b) odor concentration expressed in ou_e/m^3, (c) odor emission expressed in ou_e/s. The dashed line represents the 1:1 relationship, whereas the solid line indicates the linear regression between measured and predicted values. 148

Figure 54. Residual analysis for the developed calibration models: (a) logarithmically transformed odor concentration $\log(C_{od})$, (b) odor concentration expressed in ou_e/m^3, (c) odor emission expressed in ou_e/s. Residuals were calculated as predicted minus measured values. The dashed horizontal line indicates zero residual, whereas the solid line represents the linear trend of residuals. 149

Figure 55. Spatial maps of the distribution of odor parameters across the active area of the landfill cell, determined using the PLS model: (a) odor concentration (ou_e/m^3), (b) odor emission (ou_e/s). 151

Figure 56. Isolines of average odor concentration in the surface layer (z = 1.5 m) obtained from the dispersion modeling of Gaussian plumes (OperatFB): (a) emission scenario based on reference dynamic olfactometry, (b) emission scenario based on UAV-PLS prediction model. 153

Figure 57. Comparison of results from the dynamic olfactometric scenario (DO) and the UAV-PLS model: (a) absolute difference in odor concentration as a function of distance from the geometric center of the source, (b) relationship between concentrations determined by both methods. 154

Figure 58. Location and place of research: (a) a map showing the location of the MTP, (b) the compost screening site where a gas sensor array (sensor BOX-3 XXXX) was installed. Adapted from [276], licensed by CC BY 4.0. 158

Figure 59. Design characteristics and location of the sensor BOX-3 XXXX: (a) view of the device installed at the compost screening site at the WTP, (b) interior of the device with the visible set of gas sensors. 159

Figure 60. Reference measurements in the field conditions: the panelist team during the determination of odor concentration using Nasal Ranger field olfactometers in the immediate vicinity of the device. 161

Figure 61. The $OAQI_l$ operational model: integrating chemical signals with human perception to objectify odor nuisance assessment. Adapted from [276], licensed by CC BY 4.0. 161

Figure 62. Calibration relationships between odor concentrations determined by field olfactometry and values predicted by the gas sensor array using models based on S_{max} signal features: (a) Model 1, (b) Model 2, (c) Model 3, and (d) Model 5. Adapted from [276], licensed by CC BY 4.0. 165

Figure 63. Calibration relationships between odor concentrations determined by field olfactometry and values predicted by the gas sensor array using models based on S_{dB} signal features: (a) Model 1, (b) Model 2, (c) Model 3, and (d) Model 4, (e) Model 5. Adapted from [276], licensed by CC BY 4.0. 166

Figure 64. Mean prediction residuals with standard deviations for odor concentration models based on S_{max} (a) and S_{dB}(b). Points represent mean residuals at individual odor concentration levels, and error bars indicate ±SD. The dashed horizontal line denotes zero residual. 167

Figure 65. Validation of odor concentration prediction models based on S_{max} signal features: (a) Model 1, (b) Model 2, (c) Model 3, and (d) Model 5. Colored areas correspond to the $OAQI_I$ class ranges, dashed lines indicate the boundaries between classes, and the solid line represents the 1:1 relationship. Red symbols indicate cases in which the predicted odor concentration was assigned to a different $OAQI_I$ class than the reference value. Adapted from [276], licensed by CC BY 4.0. 168

Figure 66. Validation of odor concentration prediction models based on S_{dB} signal features: (a) Model 1, (b) Model 2, (c) Model 3, and (d) Model 4, (e) Model 5. Colored areas correspond to the $OAQI_I$ class ranges, dashed lines indicate the boundaries between classes, and the solid line represents the 1:1 relationship. Red symbols indicate cases in which the predicted odor concentration was assigned to a different $OAQI_I$ class than the reference value. Adapted from [276], licensed by CC BY 4.0. 170

Figure 67. Temporal variation in odor concentration predicted by Model 2 based on S_{max} and Model 5 based on S_{dB} during field monitoring. Reference values obtained by field olfactometry are shown as individual points. Colored background areas represent the $OAQI_I$ class ranges, while dashed horizontal lines indicate the boundaries between classes. Adapted from [276], licensed by CC BY 4.0. 172

Figure 68. Bland-Altman analysis of agreement between odor concentrations predicted by the mathematical models and field olfactometry: (a) Model 2 based on S_{max} and (b) Model 5 based on S_{dB}. The solid line represents the mean difference (Bias), dashed lines indicate the 95% limits of agreement (Bias$\pm$1.96 SD), and the dotted line denotes zero difference. 174

Figure 69. Arrangement of elements of the IOMSN: strategic location of measuring devices (sensor BOX-3 XXXX) in the operational zones of the MSWTP, against the background of the main emission sources, including landfill cells, composting areas and logistic infrastructure. 179

Figure 70. Selected odor monitoring devices (sensor BOX-3 XXXX) during a field calibration campaign: photos document how devices were installed in operational conditions. 180

Figure 71. Distribution of S_{dB} signal values recorded by individual gas sensors in seven sensorboxes: (a) s2176, (b) s2715, (c) s3965, (d) s3968, (e) s4077, (f) s4088, and (g) s4095. Boxes represent the interquartile range, the horizontal line denotes the median, whiskers indicate the data range excluding outliers, and individual points represent outlying observations. 184

Figure 72. Scatterplot matrices and Pearson correlation coefficients between the signals of five gas sensors in seven sensorboxes: (a) s2176, (b) s2715, (c) s3965, (d) s3968, (e) s4077, (f) s4088, and (g) s4095. 185

Figure 73. Calibration plots comparing actual and predicted odor concentrations for seven sensorboxes: (a) s2176, (b) s2715, (c) s3965, (d) s3968, (e) s4077, (f) s4088, and (g) s4095. Dashed lines indicate the 1:1 relationship and solid lines the linear regression. 187

Figure 74. Evolution of model performance during successive calibration stages for seven measuring devices, assessed using RMSE and the coefficient of determination (R^2). 188

Figure 75. SENSORBOX s3968 model performance and validation: (a) Timeline of predicted odor concentrations for Calibration III and corresponding field olfactometric measurements (validation campaigns). The solid line represents model predictions, red dots indicate field measurements, and vertical dashed lines mark changes in model calibration. (b) Comparison of measured and predicted odor concentrations for successive model validations (Calibrations I–III). The dashed $y = x$ line indicates perfect agreement between measured and predicted values. Background shading represents odor concentration classes used to assess classification performance. R^2, RMSE, and Accordance values demonstrate the improvement in model performance across successive calibrations. 190

Figure 76. Model performance across three validation stages for seven sensorboxes. Bars represent RMSE, the black line represents R^2, and percentages above the bars indicate Accordance (bar colors denote the relative Accordance level within each sensorbox). 192

Figure 77. The IOMSN system's user interface in the mobile app: a spatial representation of the locations of seven monitoring devices on a map of the MSWTP, with automatic classification of odor nuisance based on the $OAQI_I$ index. 193

Figure 78. A consolidated summary of the weekly time-series data for predicted odor concentrations (ou/m^3) continuously recorded by all monitoring devices in the IOMSN. 194

List of Tables

Table 1. Summary of the advantages and disadvantages of deodorization methods. 38

Table 2. Latest projects and application examples of citizen science in odor nuisance monitoring. 47

Table 3. Selected applications of GC methods in the analysis of odorous emissions from various sources. 50

Table 4. A review of studies on the use of e-noses in monitoring odor air quality, in which instrumental techniques were used as reference or complementary methods. 62

Table 5. A review of studies on the use of e-noses in monitoring odor air quality, in which sensory techniques were used as reference or complementary methods. 63

Table 6. A review of studies on the use of e-noses in monitoring deodorization processes. 65

Table 7. Deployment of UAV-mounted gas sensor arrays for industrial odor air quality monitoring. 67

Table 8. Parameters of the chromatographic analysis used for the quantitative determination of toluene. 75

Table 9. Parameters of gas sensors used for monitoring the absorption of toluene vapor from the air stream. 76

Table 10. Operating parameters of the BTF system during each stage of the experiment. 90

Table 11. Calibration performance metrics of MLR and PCR models for cyclohexane and n-hexane. 99

Table 12. RMSE values between the removal efficiency (RE) determined by the GC-FID method and the values determined by the MLR and PCR models in individual biofiltration stages and for the entire process. 103

Table 13. Selected physicochemical properties of absorbents used to remove acetone, toluene, and cyclohexane from a model biogas stream. 107

Table 14. Summary of parameters and statistical criteria used to assess the quality of calibration and validation of the gas sensor array. 114

Table 15. Statistical parameters of MLR and PCR calibration models developed to predict acetone, cyclohexane and toluene concentrations. Reproduced from [271], © 2024 Elsevier Ltd. 118

Table 16. RMSE values for process monitoring results using MLR and PCR models versus GC-FID. Adopted from [271], © 2024 Elsevier Ltd. 123

Table 17. P-B regression parameters for the comparison of sensor array and GC-FID results during absorption experiments. 127

Table 18. Bland-Altman agreement parameters for the comparison of gas sensor array and GC-FID results during absorption experiments. 131

Table 19. Technical specifications and detection profile of the gas sensors used in the array. 135

Table 20. Olfactometric parameters (C_{od} and OER) determined using the dynamic olfactometry method (EN 13725) at reference points on the active surface of the landfill cell. 145

Table 21. Statistical parameters describing the agreement between measured and PLS predicted values for the developed calibration models. 147

Table 22. A comparison of the predicted odor concentrations Cod (ou_e/m^3) at receptor points P1 - P10 for the olfactometric scenario (DO) and the UAV-PLS model, along with the absolute difference in concentrations as a function of distance from the geometric center of the source. 152

Table 23. Basic parameters of the gas sensors used in the sensor BOX-3 XXXX. 159

Table 24. The four-level $OAQI_I$ scale: a classification of odor nuisance based on OI, HT and odor concentration ranges. 162

Table 25. Validation performance of odor concentration prediction models developed using S_{max} and S_{dB} signal features. Adapted from [276], licensed by CC BY 4.0. 171

Table 26. Quantitative comparison of odor concentrations predicted by the selected sensor-based models with field olfactometry. 174

Table 27. Evolution of the structural parameters (a, b) of the hybrid model and the degree of representativeness of the PC1 in subsequent stages of the multi-season calibration of the IOMSN. 186

Table 28. The effect of seasonal variations in training data on model fit statistics (R^2 and RMSE) for seven measurement devices. 189

Table 29. A summary of predictive performance metrics (R^2, RMSE, Accordance) for seven IOMSN network measuring devices at various stages of long-term validation. 191

Scientific achievements

A list of scientific papers, including bibliographic data that uniquely identifies each work:

1. Słupek, E., **Dobrzyniewski, D.,** Makoś-Chełstowska, P., Szulczyński, B., Gębicki, J.; (2025); *Monitoring of absorptive model biogas purification process using sensor matrices and gas chromatography*; MEASUREMENT; 239; https://doi.org/10.1016/j.measurement.2024.115436

   IF: 6.1, Quartile: Q1, MNiSW: 200

2. Rybarczyk, P., Cichon, K., Kucharska, K., **Dobrzyniewski, D.,** Szulczyński, B., Gębicki, J.; (2024); *Packing Incubation and Addition of Rot Fungi Extracts Improve BTEX Elimination from Air in Biotrickling Filters*; MOLECULES, 29(18); https://doi.org/10.3390/molecules29184431

   IF: 4.6, Quartile: Q2, MNiSW: 140

3. Konopacka-Łyskawa, D., Amibo, T., **Dobrzyniewski, D.,** Łapiński, M.S.; (2023); *Improving carbon dioxide capture in aqueous ammonia solutions by fine SiO2 particles*; Chemical and Process Engineering: New Frontiers, 44(e16); https://doi.org/10.24425/cpe.2023.146718

   IF: 0.5, Quartile: Q4, MNiSW: 100

4. **Dobrzyniewski, D.,** Szulczyński, B., Rybarczyk, P., Gębicki, J.; (2023); *Process control of air stream deodorization from vapors of VOCs using a gas sensor matrix conducted in the biotrickling filter (BTF)*; ARCHIVES OF ENVIRONMENTAL PROTECTION, 49, 85–94; https://doi.org/10.24425/aep.2023.145900

   IF: 1.4, , Quartile: Q4, MNiSW: 100

5. Rybarczyk, P., Szulczyński, B., **Dobrzyniewski, D.,** Kucharska, K., Gębicki, J.; (2023); *Removal of cyclohexane vapors from air in biotrickling filters: Effects of gas mixture composition and circular economy approach*; CHEMICAL AND PROCESS ENGINEERING: NEW FRONTIERS, 44(4); https://doi.org/10.24425/cpe.2023.147399

   IF: 0.5, Quartile: Q4, MNiSW: 100

6. **Dobrzyniewski, D.,** Szulczyński, B., Gębicki, J.; (2022); *Application of a Gas Sensor Array to Effectiveness Monitoring of Air Contaminated with Toluene Vapors Absorption Process*; JOURNAL OF ECOLOGICAL ENGINEERING, 23(10), 269–282; https://doi.org/10.12911/22998993/152427

   IF: 1.3, Quartile: Q4, MNiSW: 70

7. **Dobrzyniewski, D.,** Szulczyński, B., Gębicki, J.; (2022); *Determination of Odor Air Quality Index (OAQII) Using Gas Sensor Matrix*; MOLECULES, 27(13); https://doi.org/10.3390/molecules27134180

   IF: 4.6, Quartile: Q2, MNiSW: 140

8. Makoś-Chełstowska, P., Słupek, E., Kramarz, A., **Dobrzyniewski, D.,** Szulczyński, B., Gębicki, J.; (2022); *Green monoterpenes based deep eutectic solvents for effective BTEX absorption from biogas*; CHEMICAL ENGINEERING RESEARCH AND DESIGN, 188, 179–196; https://doi.org/10.1016/j.cherd.2022.09.047

   IF: 3.9, Quartile: Q2, MNiSW: 140

9. Wasilewski, T., Szulczyński, B., **Dobrzyniewski, D.,** Jakubaszek, W., Gębicki, J., Kamysz, W.; (2022); *Development and Assessment of Regeneration Methods for Peptide-Based QCM Biosensors in VOCs Analysis Applications*; BIOSENSORS, 12(5); https://doi.org/10.3390/bios12050309

   IF: 5.4, Quartile: Q1, MNiSW: 70

10. Czaplicka, N., **Dobrzyniewski, D.,** Dudziak, S., Jiang, C., Konopacka-Łyskawa, D.; (2022); *Improvement of CO2 absorption and inhibition of NH3 escape during CaCO3 precipitation in the presence of selected alcohols and polyols;* Journal of CO2 Utilization, 62; 102085; https://doi.org/10.1016/j.jcou.2022.102085

IF: 7.7, Quartile: Q1, MNiSW: 140

11. **Dobrzyniewski, D.,** Szulczyński, B., Dymerski, T., Gębicki, J.; (2021); *Development of gas sensor array for methane reforming process monitoring*; SENSORS, 21(15); https://doi.org/10.3390/s21154983

IF: 3.8, Quartile: Q2, MNiSW: 100

12. Słupek, E., Makoś, P., **Dobrzyniewski, D.,** Szulczyński, B., Gębicki, J.; (2020); *Process control of biogas purification using electronic nose*; CHEMICAL ENGINEERING TRANSACTIONS, 82, 427–432; https://doi.org/10.3303/CET2082072

IF: 1.5, Quartile: Q3, MNiSW: 20

Total Impact Factor: 41.3
Total MNiSW Points: 1320

A list of chapters in academic monographs, including bibliographic information that uniquely identifies each work:

1. Gębicki, J., Szulczyński, B., **Dobrzyniewski, D.;** (2025); *The use of instrumental measurements to assess the quality of atmospheric air in terms of odors*; In *Comprehensive Analytical Chemistry*, Elsevier B.V., 157–180; https://doi.org/10.1016/bs.coac.2024.11.005
2. Rybarczyk, P., Szulczyński, B., **Dobrzyniewski, D.,** Gębicki, J.; (2022); *Metody poprawy skuteczności oczyszczania powietrza zanieczyszczonego hydrofobowymi lotnymi związkami organicznymi w biofiltrach ze złożem zraszanym;* In *Przepływy wielofazowe i operacje mechaniczne inżynierii procesowej,* Wydawnictwo Politechniki Gdańskiej, 82-87; http://www.pg.edu.pl/wydawnictwo/katalog

Participation in scientific conferences/symposia/meetings:

1. **Dobrzyniewski, D.,** Szulczyński, B., Czaplicka, N., Gębicki J.; (2026); *An integrated approach to estimate odor emission from landfill using unmanned aerial vehicles (UAV) and multidimensional modeling* (poster)*; 25th Polish Conference of Chemical and Process Engineering OKICHIP25* (Kraków, Poland, 20-23 September 2026)
2. **Dobrzyniewski, D.,** Słupek, E., Kucharska, K., Szulczyński, B., Gębicki J.; (2026); *Implementation of gas sensor arrays for monitoring the effectiveness of absorption treatment of fermentation gases (poster);* 28th International Congress of Chemical and Process Engineering CHISA 2026 (Prague, Czech Republic, 23-27 August 2026)
3. **Dobrzyniewski, D.,** Słupek, E., Makoś-Chełstowska, P., Szulczyński, B., Gębicki J.; (2024); *Monitoring the process of absorption airflow purification using gas sensor array and gas chromatography (poster);* XIIth Scientific Conference Air Protection in Theory and Practice (Zakopane, Poland, 15-18 October 2024)
4. **Dobrzyniewski, D.,** Szulczyński, B., Gębicki, J.; (2023); *Monitoring of odorous air quality and identification of sources of landfill gas emission from a municipal landfill using an unmanned aerial vehicle (UAV) (poster);* XLVII International Scientific and Technical Seminar “Chemistry for Agriculture” (Karpacz, Poland, 26-29 November 2023)
5. **Dobrzyniewski, D.,** Szulczyński, B., Gębicki, J.; (2023); *An Unmanned Aerial Vehicle (UAV) designed to monitor landfill gas emission using gas sensors (poster);* 13th Conference on Interdisciplinary problems in Environmental Protection and Engineering EKODOK 2023 (Boguszów-Gorce, Poland, 19-21 June 2023)

6. **Dobrzyniewski, D.,** Szulczyński, B., Gębicki, J.; (2022); *Monitoring odorous air quality during compost screening process (poster);* XLVI International Scientific and Technical Seminar "Chemistry for Agriculture" (Karpacz, Poland, 20-23 November 2022)
7. **Dobrzyniewski, D.,** Szulczyński, B., Gębicki, J.; (2022); *The application of gas sensor array to monitor the deodorization process by the absorption method (poster);* 12th Conference on Interdisciplinary problems in Environmental Protection and Engineering EKODOK 2022 (Boguszów-Gorce, Poland, 06-08 June 2022)
8. **Dobrzyniewski, D.,** Szulczyński, B., Rybarczyk, P., Gębicki, J.; (2022); *Assessment of the efficiency of deodorization process of air stream contaminated with hydrophobic compounds in a biotrickling filter (BTF) using instrumental techniques and gas sensor array (poster);* 48th International Conference of the Slovak Society of Chemical Engineering and Membrane Conference PERMEA 2022 (Tatranske Matliare, Slovakia, 23-26 May 2022)
9. **Dobrzyniewski, D.,** Szulczyński, B., Gębicki, J.; (2021); *Using a gas sensor array for monitoring the biogas purification process (poster);* XLV International Scientific and Technical Seminar "Chemistry for Agriculture" (Karpacz, Poland, 21-24 November 2021)
10. **Dobrzyniewski, D.,** Słupek, E., Szulczyński, B., Gębicki, J.; (2021); *Process control of biogas purification using electronic nose and gas chromatography (poster);* 3rd Symposium Air Quality and Health (Wrocław, Poland, 12-14 May 2021)
11. Szulczyński, B., **Dobrzyniewski, D.,** Słupek, E., Rybarczyk, P., Gębicki, J.; (2021); *Kontrola procesowa usuwania związków uciążliwych zapachowo ze strumienia powietrza za pomocą technik instrumentalnych (poster);* XV Konferencja Naukowa POL-EMIS 2021 Aktualne trendy w ochronie powietrza i klimatu – kontrola monitoring, prognozowanie i ograniczenie emisji (Wrocław, Poland, 29-31 March 2021)

Scientific projects:

1.	Project title	Modułowy Miernik do Ciągłego Monitorowania Związków Odorowych
	Source of founding	European Regional Development Fund (ERDF), European Funds for a Modern Economy 2021-2027 (FENG)
	Project No./Acronym	26/1/2025/IDUB/02.05/FENG
	Principal Investigator	Ph.D., Asst. Prof. Bartosz Szulczyński
	Role	Project Team Member / Researcher
2.	Project title	Laptops and Lighthouses
	Source of founding	European Territorial Cooperation (Interreg South Baltic Programme 2021 – 2027)
	Project No./Acronym	STHB.03.01-IP.01-0003/25 (LAL)
	Partners	Municipality of Landskrona Kiviks Museum Nature Bornholm Gdańsk University of Technology EUCC Klaipeda Municipality of Palanga
	Principal Investigator	Ph.D., Asst. Prof. Andrzej Rogala
	Role	Project Team Member / Researcher (01.2026 – present)
3.	Project title	South Baltic E-mobility Enabling Services
	Source of founding	European Territorial Cooperation (Interreg South Baltic Programme 2021 – 2027)
	Project No./Acronym	STHB.01.01-IP.01-0010/23 (SBEES)

	Partners	Industrial Development Centre South (Sweden) Klaipeda University (Lithuania) Gdańsk University of Technology (Poland) Ostfalia University of Technology (Germany) Chargex AB (Sweden) Green Power Denmark Technical University of Denmark Municipality of Gdynia (Poland) University of Applied Science Stralsund (Germany) Malmö municipality Parkerings AB (Sweden)
	Principal Investigator	Ph.D., Asst. Prof. Piotr Rybarczyk
	Role	Project Team Member / Researcher (01.2026 – present)
4.	Project title	Studia 5.0. Programy studiów dla kluczowych branż krajowego przemysłu
	Source of founding	European Social Fund Plus (ESF+) under the European Funds for Social Development 2021-2027 (FERS) programme
	Project No./Acronym	FERS.01.05-IP.08-0027/23-00
	Principal Investigator	Mariusz Kaczmarek, Ph.D, D.Sc, University professor
	Role	Academic Teacher (01.11.2025 – 28.02.2026)
5.	Project title	Management of bio fraction waste for two-stage biohydrogen production with simultaneous treatment of gaseous streams with green solvents
	Source of founding	National Science Center (NCN)
	Project No./Acronym	UMO-2021/41/B/ST8/02395 / OPUS 21
	Principal Investigator	Jacek Gębicki, Ph.D, D.Sc, University professor
	Role	Young Scientist

Statutory grants (Faculty of Chemistry GUT):

1. **Mini-grant** subsidy from the fund supporting the development of young academics in 2021 at Gdańsk University of Technology, *Evaluation of the effectiveness of the deodorization process for air contaminated with hydrophobic compounds carried out in biotrickling filter (BTF) using instrumental technique and electronic nose*
2. **Mini-grant** subsidy from the fund supporting the development of young academics in 2022 at Gdańsk University of Technology, *Instrumentalization for measuring basic odor characteristics using a gas sensor array for continuous monitoring of the air stream deodorization process*
3. **Mini-grant** subsidy from the fund supporting the development of young academics in 2023 at Gdańsk University of Technology, *Unmanned aerial vehicle (UAV-drone) designed to monitor landfill gas emission using gas sensors*

Awards and Distinctions:

1. NAWA scholarship for the best foreign and Polish doctoral students carrying out doctoral projects in international cooperation, *Polish National Agency for Academic Exchange (NAWA) / Gdańsk University of Technology Doctoral School,* 2022/2023, Awarded as part of the “Gdańsk Tech Doctoral School Closer to Europe” within the NAWA STER Scholarship – Internationalization of Doctoral School Programme
2. FRANCIUM Supporting Outstanding Doctoral Candidates, *Excellence Initiative – Research University (IDUB),* Awarded 2 times (01.10.2022-01.09.2023, 01.10.2023-01.09.2024)

Academic Employment:

1. **Research and Teaching Assistant**
   Department of Process Engineering and Chemical Technology, Faculty of Chemistry, Gdańsk University of Technology (October 2025 – present)
2. **Technical Assistant**
   Department of Process Engineering and Chemical Technology, Faculty of Chemistry, Gdańsk University of Technology (February 2024 – October 2025)

Teaching Activities:

1.	Course:	Automatics and control of technical processes
	Field of study:	Green Technologies (WCh PG)
2.	Course:	Modelowanie Procesów Technologicznych
	Field of study:	Technologia Chemiczna (WCh PG)
3.	Course:	Automatyka i kontrola procesów technologicznych
	Field of study:	Zielone Technologie (WCh PG)
4.	Course:	Technologia wytwarzania paliw odnawialnych i alternatywnych
	Field of study:	Inżynieria odzysku surowców i energii (WILiŚ PG)
5.	Course:	Technologie Ochrony Powietrza
	Field of study:	Technologia Chemiczna (WCh)
6.	Course:	Automatyka i pomiary wielkości fizykochemicznych
	Field of study:	Technologia Chemiczna (WCh)
7.	Course:	Automation and sensor systems
	Field of study:	Green Technologies (WCh PG)
8.	Course:	Komputerowe wspomaganie projektowania
	Field of study:	Zielone Technologie (WCh PG)

Other scientific activities:

1. Organization of the Baltic Science Festival; (2023-2026); *Environmental Chemical Engineering: Building a Green Future* and *How do magical substances help clean up the environment;* Gdańsk University of Technology, Faculty of Chemistry, Department of Process Engineering and Chemical Technology
2. Assistance in organizing demonstration classes for high school students from Tczew who visited the Faculty of Chemistry at Gdańsk University of Technology on June 5th 2025. The classes included a guided tour of the Faculty of Chemistry and experiments related to solutions and separation methods (filtration, TLC chromatography, and adsorption of dye solutions)
3. Performing odor air quality measurements at WCR Jarocin using field olfactometry and dynamic olfactometry on the following dates: 27-29 May 2025
4. Air sampling from point source emitters to assess odor nuisance using dynamic olfactometry and evaluation of odor air quality in the surroundings of the poultry farms in Kąty and Kopytów on the following dates: 16-18 March 2025
5. Calibration and validation of odor air quality meters (model sensor BOX3-SE) using the field olfactometry technique at the innovative biogas plant in Brody on the following dates: 13 December 2024; 14 May 2025

6. Cooperation with the Municipal Solid Waste Treatment Plant in Gdańsk (ZUT Gdańsk) to assess odorous air quality at the site, which includes: periodic olfactometric measurements (field olfactometry and dynamic olfactometry), calibration and validation of odor air quality meters (model sensor BOX-3 SE), and periodic testing of waste morphology
7. Cooperation with the municipal landfill “Eko-Dolina” in Łężyce to assess odorous air quality at the site, which includes: periodic olfactometric measurements and periodic testing of waste morphology
8. Performance of olfactometric measurements and calibration/validation of the odor air quality meters (model sensor BOX-3 SE) using the field olfactometry technique at the site of ZUO International in Kunowice (Słubice) on the following dates: 25-26 April 2024; 23-24 May 2024, 12 December 2024
9. Conducting olfactometric measurements at the site of the waste alternative fuel production facility in Zawiercie using field olfactometry on the following dates: 18-19 April 2024; 13 May 2025
10. Carrying out olfactometric measurements with the use of field olfactometers, as well as carrying out scientific and research expertise on the occurrence of odor nuisance in the reclaimed areas in Świerkocin on the following dates: 16-17 October 2023
11. Preparation of a scientific and technical expert opinion on the occurrence of odor nuisance from the active ballast waste quarters of the Waste Management Plant “Eko-Mazury” in Ełk using the field olfactometry technique on the following dates: 23-24 March 2023; 18-19 September 2023
12. Performing olfactometric measurements (field olfactometry) as part of commissioned work at the Agricultural Biogas Plant in Mursa (Grochów Szlachecki) and calibration and validation of odor air quality meters (model sensor BOX-3 SE) using field olfactometry at the following dates: 09-10 February 2023; 07 March 2023; 10 March 2023.
13. Performing olfactometric measurements (field olfactometry) as part of commissioned work at the Bitumen (asphalt) plant in Krapkowice on the following dates: 26-27 January 2023
14. Performing olfactometric measurements (field olfactometry) as part of commissioned work at the Combined Heat and Power Plant FORTUM Zabrze and calibration and validation of odor air quality meters (model sensor BOX-3 SE) using field olfactometry on the following dates: 23-24 November 2022; 12 May 2025
15. Performing olfactometric measurements (field olfactometry) as part of commissioned work at the Agricultural Biogas Plant in Tragamin on the following dates: 18-19 November 2022
16. Performing olfactometric measurements (field olfactometry) as part of commissioned work at the Municipal Treatment Plant in Pruszków on the following dates: 14-16 December 2021; 18-19 May 2022; 28-29 June 2022
17. Performing olfactometric measurements (field olfactometry) as part of commissioned work at the Poznań University of Life Sciences on the following dates: 11-12 May 2022; 24 October 2022; 12 December 2022; 19 December 2022; 19 January 2023; 03 March 2023; 07 March 2023

Copyrights and permissions

Article:	Application of a Gas Sensor Array to Effectiveness Monitoring of Air Contaminated with Toluene Vapors Absorption Process
Authors:	**Dobrzyniewski D.***, Szulczyński B., Gębicki J.
Published:	*Journal of Ecological Engineering* **2022,** 23(10), 269-282
DOI:	10.12911/22998993/152427.
License:	The content is available under CC BY 4.0
Copyright statement:	Available

Request for written confirmation of permission to reuse material in a doctoral dissertation

Podsumuj tę wiadomość e-mail

Journal of Ecological Engineering<office@jeeng.net>
Do: Dominik Dobrzyniewski
Wt, 1.09.2026 13:05

Nie potrzebna jest zgoda do reprodukcji fragmentów pracy.
Autorzy zachowują prawa autorskie i pełne prawa wydawnicze bez ograniczeń.
Artykuł może być rozpowszechniany lub ponownie wykorzystywany w dowolnych celach, pod warunkiem prawidłowego cytowania autora i oryginalnego źródła.

Editorial Office

...

Odpowiedz | Prześlij dalej

Dominik Dobrzyniewski
Do: Journal of Ecological Engineering <office@jeeng.net>
Wt, 1.09.2026 12:34

Dear Editorial Office,

I am writing to kindly follow up on my request below regarding written permission to reproduce and adapt selected material from article mentioned below in my doctoral dissertation.

I understand that the Editor-in-Chief may have been unavailable, and I would be very grateful if you could let me know whether my request could now by considered.

Thank you very much for your time and assistance.

Best regards,
Dominik Dobrzyniewski
Department of Process Engineering and Chemical Technology,
Faculty of Chemistry,
Gdańsk University of Technology,
Gabriela Narutowicza 11/12 Street,
80-233 Gdańsk, Poland

Article:	Process control of air stream deodorization from vapors of VOCs using a gas sensor matrix conducted in the biotrickling filter (BTF)
Authors:	**Dobrzyniewski D.***, Szulczyński B., Rybarczyk P., Gębicki J.
Published:	*Archives of Environmental Protection,* **2023,** 49(2), 85-94
DOI:	10.24425/aep.2023.145900
License:	The content is available under CC BY-SA 4.0
Copyright statement:	Available

ODP: Request for written confirmation of permission to reuse material in a doctoral dissertation

---

Od Czesława Rosik-Dulewska <czeslawa.dulewska@ipispan.edu.pl>
Data Wt, 21.07.2026 10:59
Do Dominik Dobrzyniewski <dominik.dobrzyniewski@pg.edu.pl>
DW Jerzy Szdzuj <jerzy.szdzuj@ipispan.edu.pl>

Dominik Dobrzyniewski
Department of Process Engineering and Chemical Technology,
Faculty of Chemistry,
Gdańsk University of Technology,

I confirm posibility reproduce and adapt figures, tables and selected parts of the article in your doctoral dissertation, including its printed version and electronic version deposited in the institutional repository.
Very important: The original publication must will be fully cited and reproduced materials must will be identified as licensed under CC BY-SA 4.0.

Editor in Chief
Prof. Dr. Sc. Eng. Czesława Rosik-Dulewska
Ordinary Member of the Polish Academy of Sciences
Deputy Dean of the Faculty of Technical Sciences of the Polish Academy of Sciences
Member, European Academy of Sciences and Arts
Commission for Ethics in Science Polish Academy of Sciences
Chairman of the Scientific Council Institute of Environmental Engineering Polish Academy of Sciences
Chairman of the Scientific Council The Institute for Ecology of Industrial Areas

Institut of Environmental Engineering Polish Academy of Sciences
ul. Skłodowskiej-Curie 34,
41-819 Zabrze,
tel. 48 32 2717040
czeslawa.dulewska@ipispan.edu.pl
www.ipis.pan.pl

Article:	Monitoring of absorptive model biogas purification process using sensor matrices and gas chromatography
Authors:	Słupek E., **Dobrzyniewski D.**, Makoś-Chełstowska P., Szulczyński B., Gębicki J.
Published:	*Measurement* **2025**, 239, 11436
DOI:	10.1016/j.measurement.2024.115436
License:	The original article was published by © 2024 Elsevier Ltd
Copyright statement:	Available

Re: Request for written confirmation of reuse in doctoral dissertation [260720-019761]

Od Permissions Helpdesk <permissionshelpdesk@elsevier.com>
Data Wt, 21.07.2026 06:55
Do Dominik Dobrzyniewski <dominik.dobrzyniewski@pg.edu.pl>

Dear Dr. Dobrzyniewski,

Thank you for contacting us.

As an Elsevier journal author, you retain the right to Include the article in a thesis or dissertation (provided that this is not to be published commercially) whether in full or in part, subject to proper acknowledgment; see https://www.elsevier.com/about/policies/copyright for more information. As this is a retained right, no written permission from Elsevier is necessary.

As outlined in our permissions licenses, this extends to the posting to your university's digital repository of the thesis provided that if you include the published journal article (PJA) version, it is embedded in your thesis only and not separately downloadable.

Thank you.

Note:

As the author of the article, you are entitled to adapt article as per your requirement permission is not required.

Thomas Rexson Yesudoss
Permission Helpdesk
ELSEVIER
For queries on permission processes, please refer to FAQ. For guidance on applying for permissions and filling the permission log, please refer here



Monitoring of absorptive model biogas purification process using sensor matrices and gas chromatography

Author:
Edyta Słupek,Dominik Dobrzyniewski,Patrycja Makoś-Chełstowska,Bartosz Szulczyński,Jacek Gębicki

Publication: Measurement
Publisher: Elsevier
Date: 15 January 2025

© 2024 Published by Elsevier Ltd.

Quick Price Estimate

This service provides permission for reuse only. If you do not have a copy of the content, you may be able to purchase a copy using RightsLink as an additional transaction. Simply select 'I would like to.....' 'Purchase this content'.

Unclear about who you are?

Please note that, as the author of this Elsevier article, you retain the right to include it in a thesis or dissertation, provided it is not published commercially. Permission is not required, but please ensure that you reference the journal as the original source. For more information on this and on your other retained rights, please visit: https://www.elsevier.com/about/our-business/policies/copyright#Author-rights

I would like to...	reuse in a thesis/dissertation	I am the author of this Elsevier article...	Yes
I would like to use...	full article	I will be translating...	No
Circulation	5	My currency is...	EUR - €
My format is...	both print and electronic		

This reuse is free of charge and does not require a license. Please print this page for your records.

✓PRICE: 0.00 EUR

CONTINUE

Publisher Terms and Conditions

To request permission for a type of use not listed, please contact Elsevier Global Rights Department.

Are you the author of this Elsevier journal article?

© 2026 Copyright - All Rights Reserved | Copyright Clearance Center, Inc. | Privacy statement | Data Security and Privacy | For California Residents | Terms and Conditions Comments? We would like to hear from you. E-mail us at customercare@copyright.com

Article:	Determination of Odor Air Quality Index ($OAQI_I$) Using Gas Sensor Matrix
Authors:	**Dobrzyniewski D.***, Szulczyński B., Gębicki J.
Published:	*Molecules* **2022**, 27(13), 40180
DOI:	10.3390/molecules27134180
License:	The content is available under CC BY 4.0
Copyright statement:	Available

Re: Request for written confirmation of permission to reuse material in a doctoral dissertation

---

Od Molecules Editorial Office <molecules@mdpi.com>
Data Wt, 21.07.2026 05:53
Do Dominik Dobrzyniewski <dominik.dobrzyniewski@pg.edu.pl>

Dear Dr. Dominik Dobrzyniewski,

Thank you very much for your e-mail.

According to the MDPI Open Access Information and Policy, no special permission is required to reuse all or part of articles published by MDPI, including figures and tables.
MDPI | Open Access Information

Please feel free to reuse your article published by MDPI. And wish all the best of your doctoral dissertation.

Kind regards,
Cheryl Han
Managing Editor, MDPI
Molecules (http://www.mdpi.com/journal/molecules)

New Impact Factor of /Molecules/ (2025): 5.1

**Subscribe Alert and Keep Updated about Molecules:
https://www.mdpi.com/journal/molecules/toc-alert/

**Follow us on Twitter @Molecules_MDPI and LinkedIn "Molecules MDPI"

**Special Issue Proposal - Open for Application
https://www.mdpi.com/journalproposal/sendproposalspecialissue/molecules

---
Disclaimer: The information and files contained in this message are confidential and intended solely for the use of the individual or entity to whom they are addressed. If you have received this message in error, please notify me and delete this message from your system. You may not copy this message in its entirety or in part, or disclose its contents to anyone.